SCHOOL OF ENGINEERING SCIENCES
DEPARTMENT of MECHANICAL ENGINEERING

Biomedical Sensor for Transcutaneous Oxygen Measurements Using Thick Film Technology

By

YU-ZHI (LIZA) LAM

A thesis submitted for the degree of
Doctor of Philosophy

UNIVERSITY OF SOUTHAMPTON
2003

This thesis is the result of original work done wholly by myself whilst I was registered for postgraduate candidature within the Department of Mechanical Engineering, School of Engineering Sciences at the University of Southampton.

Yu-Zhi (Liza) Lam

UNIVERSITY OF SOUTHAMPTON
SCHOOL OF ENGINEERING SCIENCES

Doctor of Philosophy

Biomedical Sensor for Transcutaneous Oxygen Measurements Using Thick Film Technology

ABSTRACT

by Yu-Zhi (Liza) Lam

The measurement of the partial pressure of oxygen in arterial blood is essential for the analysis of a patient's respiratory condition. There are several commercially available methods and systems to measure this parameter transcutaneously. However, they tend to be cumbersome and costly. To overcome the disadvantages presented, a new type of sensor for transcutaneous blood gas measurement was investigated, employing thick film technology, which is an excellent technique to produce sensors in bulk, as it is cost effective and easy for reproducible fabrication.

This thesis describes the application of thick film technology to the investigation and production of these sensors, which are small in size and readily disposable. Such advantages are greatly welcomed from the medical point of view. The devices under investigation were based on amperometry. Gold electrodes were printed on an alumina substrate and covered with a layer of electrolyte gel and then finally, with a membrane. An external silver/silver chloride reference electrode was also employed in this electrochemical cell set-up. The project also involved several electronic circuits to support the transcutaneous oxygen measurement. The main studies were concentrated on the materials employed as the electrolyte and membrane. Investigations were carried out to evaluate the performance of these devices in atmospheric and hydrated environment as well as under the influences of different temperatures. Detailed discussions of the results were presented and future work for the project is identified.

The novel contributions towards this research work were categorized into two major modules. Firstly, in the heating module, a single element taking both the roles of a heating element and a feedback temperature sensor was employed for the wheatstone bridge circuit configuration to regulate the transcutaneous temperature. In addition, the oxygen sensing module included

studies on the effectiveness of using Nafion polyelectrolytes to achieve amperometric measurements for transcutaneous oxygen monitoring. From the experimental results, the most promising choice for the thick film transcutaneous oxygen sensor was the prototype with Nafion as the electrolyte and PTFE as the membrane. The disposable prototype produced results achieving low manufacturing cost of approximately £1 and was able to make continuous measurement of up to 46 hours. It proved to be compact, non-biohazardous and portable with a good degree of user-friendliness. It also provided accurate and reproducible measurements of not more than 3% error.

Thorough intensive research activities were carried out to overcome all existing problems in order to achieve the objectives of the research project. With more than 70% of the specifications being met, the positive results had presented a successful design for the fundamental version of the disposable transcutaneous oxygen sensor employing thick film fabrication processes.

CONTENTS

LIST OF FIGURES

LIST OF TABLES

ACKNOWLEDGEMENTS

I would like to express my deepest gratitude to my supervisor, Dr John K. Atkinson for his help, advice and enthusiasm. He has also been most approachable and encouraging throughout the course of my work.

Special mention of appreciation also goes out to Prof. R. Allen (Institute of Sound and Vibration Research) and Dr M. Hall (Senior Consultant for Neonatal Intensive Care Unit in Princess Anne Hospital) for their kind encouragement and sound advice. I would also like to thank Dr Russell P. Sion for his kind guidance, which proves helpful to the progress of my work.

Deeply appreciated the kind help from Mr C. S. Toh (Chemistry Department) for putting up with my questions on the topic of Electrochemistry and Polymers as well as Mr K. S. Tan (Surface Engineering group) for his guidance in obtaining the photographs from the optical microscope to determine material thickness. It was also a great pleasure to work with Mr J. Bilek (Socrates student) on the heating module. I would also take this opportunity to thank my colleagues and friends namely Dr Gary Zhang, Mrs Gloria Webb, Dr Arnaud Gac and Miss Yulan Zheng for creating a wonderful and cohesive environment at the Thick Film Unit.

Last but not least, many thanks to all that have helped me in one way or another throughout the course of my research. This project was funded by the School of Engineering Sciences, University of Southampton.

SYMBOL DEFINITIONS

A	Absorbance
A_i	Square roots of oxygen diffusion rate (i denoting layer type)
C	Concentration of oxygen (mol cm^{-3})
c_{bulk}	Oxygen concentration in bulk material (mol cm^{-3})
C_{dl}	Double layer capacitance (F)
c_e	Oxygen concentration in electrolyte (mol cm^{-3})
CE	Counter electrode
c_m	Oxygen concentration in membrane (mol cm^{-3})
D	Depth of adsorbing layer (m)
D_E	Diffusion coefficient of electrolyte (m^2 s^{-1})
D_L	Diffusion coefficient of liquid (m^2 s^{-1})
D_M	Diffusion coefficient of membrane (m^2 s^{-1})
e^-	Electron
E	Electrolyte layer
E_{IN}	Applied potentiostat potential (V)
E_{OUT}	Measured potential output of potentiostat (V)
GE	Guard electrode
H	Transient characteristic
I	Transmitted light intensity (candela)
I	Current (A or μA)
I_0	Incident light intensity (candela)
iR	Current within the potentiostat multiply by resistance (V)
k_B	Boltzmann's constant (joules.$kelvin^{-1}$)
K_i	Time constant in i layer
$K_{m \rightarrow bulk}$	Distribution coefficient from membrane to bulk material
$K_{m \rightarrow e}$	Distribution coefficient from membrane to electrolyte
k_s	Standard heterogeneous electron transfer rate constant
k_x	Oxygen permeability in x layer (m kg s^{-2} A^{-2})
L	Liquid layer
l_i	Length of layer i (m)
L_i	Ratio of diffusional resistance of layer i and the membrane

M	Membrane layer
N	Intensity of oxygen flux
N	Number of molecules in a mole
N_s	Steady state oxygen flux intensity
p_i	Partial pressure of oxygen in i layer
P_O	Partial pressure of oxygen (mmHg)
r	Radius of particle or molecule (m)
R	Gas constant
R_{CE}	Solution resistance between counter and reference electrode (Ω)
RE	Reference electrode
R_i	Diffusional resistance of layer i to oxygen transport (Ω)
R_{UN}	Uncompensated resistance between reference and working electrode (Ω)
R_x	Output resistance of potentiostat (Ω)
S_i	Ratio of L_i and A_i at i layer
T	Absolute temperature (K)
WE	Working electrode
v	Viscosity of the solvent (m N^2 s)
ε	Extinction coefficient
ϕ	Activity energy (J)
σ	Conductivity (S m^{-1})
σ_O	Conductivity at 0 °K (S m^{-1})
υ	Voltammeter sweep rate (V s^{-1})

GLOSSARY OF TERMS

Al_2O_3	Aluminum oxide
Ag	Silver
AgCl	Silver chloride
Ag / AgCl	Silver-Silver chloride
AgPd	Silver Palladium
Amperometric	Current measuring
Anion	Negatively charged ion
Anode	Positively charged electrode where oxidation occurs
Au	Gold
CA	Cellulose Acetate
Ca^+	Calcium ion
Cathode	Negatively charged electrode where reduction occurs
Cation	Positively charged ion
Cl	Chloride molecule
Cl^-	Chloride ion
CO_2	Carbon dioxide
d.c.	Direct current
GPIB	General purpose interface bus
H^+	Hydrogen ion
H_2	Hydrogen molecule
H_2O	Water molecule
H_2O_2	Hydrogen peroxide
InSb	Indium-antimony
IR	Infrared
K^+	Potassium ion
KCl	Potassium chloride
ΔKCl	Change in potassium chloride level
KNO_3	Potassium nitrate
Na^+	Sodium ion
NaCl	Sodium chloride
NO_3^-	Nitrate ion

$\Delta NaCl$	Change in sodium chloride level
O_2	Oxygen molecule
OH^-	Hydroxyl ion
P_aCO_2	Partial pressure of carbon dioxide in artery
P_aO_2	Partial pressure of oxygen in artery
PEO	Polyethylene oxide
pH	Measure of acidity or alkalinity
ΔpH	Change of acidity or alkalinity
PT100	Resistive thermistor
PTFE	Polytetrafluoroethylene
$P_{tc}CO_2$	Partial pressure of transcutaneous carbon dioxide
$P_{tc}O_2$	Partial pressure of transcutaneous oxygen
PVC	Polyvinyl chloride
R^2	Regression coefficient
SO_3^-	Sulphate ion
TCR	Temperature coefficient of resistance
THF	Tetrahydrofuran

Chapter 1 Introduction

1.1 Project Background

Healthcare and medical services have always played important roles in part and parcel of daily lives. In recent years, the need and demand for better and more economical medical equipment have been on the increase. In order to achieve such improvements, medical professionals and biomedical engineers often work hand-in-hand to carry out many research projects, which cover a whole range of medical applications. One such project of particular interest involves the monitoring and measuring of blood gas levels in arterial blood.

The measurement of partial pressures of two main gases namely oxygen and carbon dioxide in the arterial blood is essential for doctors to monitor the respiratory conditions of patients, in particular the preterm neonates who are undergoing surgery or experiencing respiratory difficulties. Sufficient delivery of oxygen to all the pulmonary and circulatory functions must be ensured when treating patients particularly critically ill ones. The intention of partial pressure of oxygen (P_aO_2) monitoring is to prevent a deficiency in the amount of oxygen reaching the body tissues, which is known as tissue hypoxia [1]. In the event of having too little oxygen, irreversible damage could be done to the body's most sensitive organs such as the brain and heart. Blood oxygen levels are important as the monitored results also reflect the possible damage due to an excess of oxygen in the body system, which is termed hyperoxia [1]. Exposure to excessive oxygen can cause retinal vasoconstriction and impaired cerebral blood flow [2]. Oxidative damage from free radical generation may also occur in other tissues.

The level of carbon dioxide is also very important as it indicates the status of the central and cerebral ventilation [1]. In the cases for babies, when there is an acute decrease in partial pressure of carbon dioxide (P_aCO_2), blood flow to the brain is reduced (cerebral ischaemia) and this possibly leads to severe periventricular cyst formation and cerebral palsy. At the other extreme, excess carbon dioxide could lead to high risk of germinal layer hemorrhage or profuse bleeding in the blood vessels [3]. These adverse effects due to changes in the blood gas levels take place very quickly, usually in a matter of several minutes and often, the

consequences prove to be fatal. Hence, continuous monitoring of P_aO_2 and P_aCO_2 levels are crucial in order for doctors to be aware of the patient's current medical condition.

Currently, there are three main methods of measuring blood gas levels commonly used in clinical practice. One of the techniques is the conventional method of extracting a blood sample from the patient and analyzing it using a commercial blood gas analyzer. Although this technique gives very precise and accurate diagnosis, it often exhibits several disadvantages such as placing unnecessary physical stress on the patient during the blood sampling procedures. In addition, the analyses and measurements for gas partial pressure can only be made momentarily using this method. The effective results often exhibit large variations from the actual on-going situation. In other words, continuous monitoring is not possible for this clinical evaluation. To overcome these disadvantages, the method of transcutaneous blood gas monitoring and measurement was introduced in the early 1970s [3]. More recently, oximetry which measures oxygen saturation, has become more widely available as it is easy to employ but has the drawback of less accurate measurement [4]. These methods will be further elaborated on in Chapter 2.

Due to the advantageous noninvasive feature of transcutaneous blood gas monitoring, it has constantly been the focus of many doctors and biomedical engineers to improve the existing commercial systems to achieve more effective measurements. Multi-disciplinary engineering has been involved to develop many different types of transcutaneous blood gas systems based on various technologies such as amperometry and optical means. In current measuring procedures, the sensors come in contact with the patients' skin surface via a detachable membrane. Hence the sensors are required to be prepared and sterilized before they can be used again for the following measurement. After each application, these used membranes are removed and new ones are placed manually. The electrolytes within the sensors are replenished after approximately 4 to 6 hours of continuous usage. Generally, existing commercial transcutaneous blood gas systems currently available in hospitals and clinics adopt such maintenance practices. These prove to be inefficient and cumbersome, as the replacement and alignment of the membranes must be carried out properly in order for the sensor to function effectively. Improvements have been made to ease this procedure such as screwing in the membrane instead of stretching and aligning the membrane over the sensor tip [5]. However, several disadvantages such as trapping air bubbles while replacing the membranes, still persist. These air bubbles usually contribute to erroneous measurements.

Hence, there is a need for a new type of sensor that does away with all the cumbersome membrane replacement procedure.

Thick film technology is a mature manufacturing technique used to fabricate large volumes of devices at low cost [6]. It has evolved since the 1950s from being able to produce replacements or alternatives to printed circuit boards to the current state-of-the-art densely packed semiconductor hybrid devices. Electrochemical sensors fabricated using thick film technology are deemed suitable for transcutaneous blood gas measurement, as they are compact in size, low cost and easy to fabricate in bulk. Thorough and intensive research has been carried out on both existing and new materials employed for the chemical composition and design of these sensors. This is essential so that more accurate and desirable measurement results of blood gas levels can be achieved. Experiments are subsequently being carried out to investigate the behaviour of the sensors under atmospheric, hydrated and clinical conditions.

1.2 Objectives and Scope of the Thesis

The main objective of this research project is to apply thick film technology to the fabrication of transcutaneous blood gas measurement/monitoring sensors in order to achieve better and more economical alternatives to existing commercial systems. Chapter 2 of this thesis begins by presenting an overview of the medical instruments which are currently used in hospitals and clinics for transcutaneous blood gas monitoring. This is followed by a brief explanation of the correlation between the partial pressure of oxygen in arterial blood and the corresponding transcutaneous measurement. The working principle of the intended sensor is based on amperometry of an electrochemical Clark cell [7] and a detailed breakdown study of the different materials employed for the electrodes, electrolytes and membranes is also addressed in Chapter 2. An overview of thick film technology is also made available to highlight the sensor development. In-house fabrication of the thick film sensors was carried out to produce various types of sensors economically for tests and evaluations.

The ideal blood gas sensor should cater for the measurements of the partial pressure of transcutaneous oxygen ($P_{tc}O_2$), the partial pressure of transcutaneous carbon dioxide ($P_{tc}CO_2$), the pH levels and more recently of immense interest, the level of nitric oxide. However for

initial studies, the main investigations involved in this project were focused only on the measurement of partial pressure of transcutaneous oxygen ($P_{tc}O_2$) levels. Oxygen sensor prototypes were printed in-house in order to evaluate and understand the sensors in more detail. The fabrication procedures of these sensors using the technique of thick film printing are presented in Chapter 3. The sensors require the support of electronics modules for effective operation and measurement. The design and construction of the electronics aspects such as the potentiostat circuit and heater circuit module are further elaborated on also.

In view of enhancing the geometrical layout as well as the electrolyte and membrane materials, preliminary theoretical modeling on the effects of diffusion rates is evaluated in Chapter 4. This technique facilitates the initial understanding of sensor design and enables improvements to be implemented easily. A one-dimensional diffusion model based on the four-electron stoichiometry of the oxygen cathode reaction [8] was employed and it involved simple mathematical evaluations based on several valid assumptions.

Chapter 5 covers a series of experiments, which focus individually on the effects of different parameters on the sensors. Different types of electrolytes and membranes are investigated under the influences of temperature, humidity changes and the levels of biasing voltage to the electrochemical sensors. A comprehensive discussion is presented in Chapter 6 to evaluate the results obtained from these experiments. In addition, a closer look is taken at the problems encountered to explain the validity of these results. Studies were also carried out to understand the effects of different salt concentrations and pH levels on the overall measured output. Finally, conclusions are drawn from all the investigations and some future work is also suggested to branch out the research topic into different possible avenues.

1.3 Specifications of Sensor Prototype

Much emphasis and effort is placed in the design and development of a novel transcutaneous oxygen sensor prototype as opposed to the existing systems. In general, the ideal sensor prototype should possess the following specifications.

(a) *Low cost*

Each prototype should cost approximately €1.25 as compared to the existing

sensor, which requires consumables equivalent to €2.50. The prices would reduce as the product volume per batch increases.

(b) *Use for longer period of time*

Each prototype should be capable of making continuous measurements for up to 30 hours without replacement as compared to replenishing and maintaining the existing sensor every 3 to 4 hours.

(c) *Power consumption*

The electronics modules include the potentiostat and the heating controller circuit. Generally, both circuits have been designed to adopt ±12V d.c. voltage supply. A relatively large amount of current (0.15 A) is drawn from the supply in order to power up the heating element. Ideally, the electronic modules should be supported by power supplies from both a.c. mains with appropriate transformers for normal on-site operation as well as rechargeable high-powered batteries for backup purposes.

(d) *Portable / Light weight*

As the sensor is to be attached onto the surface of the patient's skin, it has to be light weight and cause no hindrance. The patient may be moved about and having a sensor that is portable proves to be helpful.

(e) *Compact*

To cater for measurements on babies as well as grown-ups, the sensor needs to be physically small. Hence, considerations for the design must be given towards compactness in order to fit the whole oxygen monitoring module onto a limited amount of working area.

(f) *Disposable*

Currently, reusable transcutaneous sensors require constant maintenance and

sterilization. These procedures proved to be relatively time consuming and expensive. If the sensor is made disposable, it enhances cost effectiveness and also maintains a high standard of hygiene within the hospital environment.

(g) *Non-biohazardous*

The application of the sensor requires a high standard of safety since it comes in direct contact with the patient. There must not be any biohazardous electrochemical by-products during the reactions.

(h) *Accurate*

Each sensor type usually produces a unique and calibrated set of readings. It is important that medical doctors are informed of the relative changes in partial pressure of oxygen in the arterial blood in order to determine the status of the respiratory system. Thus, the corresponding absolute value is not essential, which relieves the need for extremely high accuracy in the sensor. Using the general specifications of existing commercial transcutaneous monitoring systems, the level of errors allowed should not be more than 5%. Hence, a reasonable sensitivity magnitude of the sensor would be approximately 1 μA / mmHg.

(i) *Quick response*

Each sensor should respond quickly to possible variations in oxygen levels, ideally reaching steady state measurements within 1 second. This proves to be necessary for continuous monitoring.

(j) *User-friendly*

Within a complex working environment such as the surgery rooms in a hospital, equipment is connected to the patients for the recording of different medical parameters. The daily maintenance and application of the equipment is carried out by the medical staff, who are often very busy and not technically trained. Hence, a high degree of user-friendliness is greatly encouraged. This allows hassle-free usage, which eventually leads to better efficiency.

(k) *Easy to integrate and implement*

The sensor design should be compatible with future upgrading and also conform to standard operating conditions such as voltage supply for possible integration into a larger general system.

In an attempt to satisfy these basic specifications for the desired new sensor design, thick film technology has been employed to explore the possibilities.

1.4 Contribution of the Research

This research project integrates the knowledge from different disciplines to develop a transcutaneous blood gas sensor. The technique of transcutaneous measurement and thick film technology are fairly mature. These aspects are applied to assist in the investigation of producing a new electrolyte material that is printable by means of thick film technology. The prototype also displays good accuracy and reliability in its measurement. The final sensor will then be presented to medical practitioners as a novel and cost effective biomedical instrument.

Chapter 2 Literature Review

2.1 Blood Gas Monitoring

The measurement of partial pressures of oxygen (P_aO_2) and carbon dioxide (P_aCO_2) in arterial blood is essential for monitoring the conditions of patients, especially premature or newborn babies who are suffering from respiratory difficulties. The typical value of P_aO_2 in the blood stream is approximately 75 to 100 mmHg for normal healthy human beings. The need for oxygen monitoring in pediatric and adult intensive care units is constantly required. Results from blood gas pressure monitoring could be used to denote disconnection due to failed oesophageal intubation more rapidly. This may prevent considerable periods of hypoxia, which often result in permanent brain dysfunction [9]. In addition, dangerous changes in oxygen concentration in the inspired gas may also indicate intrapulmonary shunting as well as other disturbances of ventilation and perfusion. In many cases, acute episodes such as pulmonary oedema [10], collapse and tension pneumothorax [11] could prove to be fatal. Another important application for monitoring the oxygen level is to control the anesthesia treatment for patients undergoing surgery [12]. There are several methods currently available in clinical practices to measure and monitor blood gases. These include blood sample analyzing via a blood gas analyzer, oximetry and transcutaneous blood monitoring. Generally, most of these systems can measure between a 20 mmHg and 500 mmHg partial pressure of oxygen.

For blood sample analysis, blood is extracted into a syringe, usually from an in-dwelling arterial or venous catheter or for babies, directly into a capillary tube from a heelprick. At times, if the blood is required to be kept prior to analysis, heparin is usually added to prevent coagulation. During the evaluation of the blood gas levels and ionic contents, the blood sample is injected into a commercial blood gas analyzer such as the CIBA CORNING 800 series [13]. The blood is fed into the system and flows through several chambers via fine capillary tubes. Each chamber houses a different type of membrane that is porous to the desired blood gas or ionic content under test. The chamber contains a measuring electrode and an aqueous electrolyte solution in an electrochemical cell set-up. The blood gases measured by this blood gas analyzer usually include the partial pressure of

oxygen (P_aO_2), the partial pressure of carbon dioxide (P_aCO_2) and the pH level. At the same time, the ionic contents such as potassium (K^+), sodium (Na^+), calcium (Ca^+) and chloride (Cl^-) are also reflected in the measured results. Often, these commercial blood gas analyzers also provide measurements of other useful parameters such as glucose and haematocrit levels. The main working principle for the blood gas level and ionic concentration measurements in each chamber of this analyzer is based on amperometry of an electrochemical cell. Figure 2.1 shows a general schematic representation of a typical two-electrode electrochemical cell. A fixed voltage is applied between the two electrodes of the cell. A current generated as a result of the oxidation or reduction reaction on the electrodes is measured. More detailed discussions on amperometry will be presented in section 2.3.

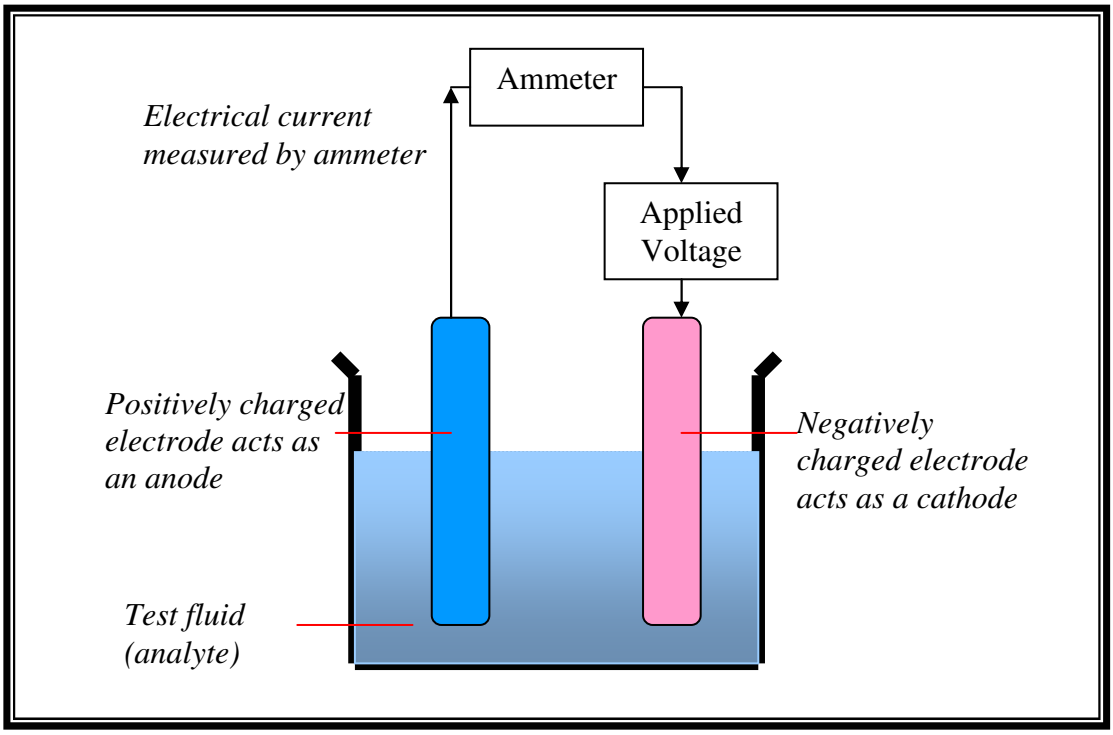

Figure 2.1: General Schematic Representation of an Electrochemical Cell Demonstrating Amperometry

There are also other types of blood gas analyzers that employ optical means of measurement. One such method uses absorption changes by the chemical compounds found in the blood, which are excited to a higher energy state when subjected to a laser light source. It is found that in many engineering fields such as computer and communication engineering, there is a common trend to divert from conventional methods to advanced optical measurement in order to gain significant improvements in terms of accuracy and stability.

Although the results obtained from the blood gas analyzers using sampled blood are accurate with respect to the contained arterial blood, they are neither real-time nor continuous. Hence, the measurements could prove useless in cases of emergencies where the condition of the patient must be monitored instantaneously to reflect his actual medical situation. With continuous monitoring, the doctors will be well informed of all parameters and hence the medical status of the patient. This enables diagnosis to be carried out more effectively. Another major disadvantage of these analyzers is cost. Each analyzer costing up to approximately £20,000 to £30,000. In addition, a conservative estimate of the daily consumables required to maintain the system in a hospital environment averages to approximately a few hundred pounds sterling, depending on the amount of use [13]. With such high expenditure, smaller medical centers and private practitioners could not afford to have such systems. To overcome most of these shortcomings, pulse oximetry [14] has been developed to measure the oxygen saturation continuously by using the differential light absorbency of two wavelengths of the light transmitted through the tissues. This simple, non-invasive technique is the brainchild of a Japanese bioengineer, Takuo Aoyogi [14].

In this measuring method, light passing through a living tissue, namely the ear or the finger will be partially absorbed by each constituent such as the skin pigments, tissue, cartilage, bone, arterial blood and venous blood. This is shown in the measurement setup in Figure 2.2. As further illustrated in Figure 2.3, the pulse oximeter measures the absorption of selected wavelengths of the light source that pass through the living tissue sample. For a given site, the absorption is constant except for the absorption from added blood volume due to arterial pulsations. This varying absorption is translated into a waveform at both red and infrared wavelengths. These absorbances (A) are additive and obey the Beer-Lambert law [14], given by Equation (2.1):

$$A = -log\,T = log\,\frac{I_0}{I} = \varepsilon DC \tag{2.1}$$

where I_0 and I are the incident and transmitted light intensities respectively, ε is the extinction coefficient, D is the depth of the absorbing layer and C is the concentration of oxygen. It can be observed that absorbance is directly proportional to the oxygen concentration.

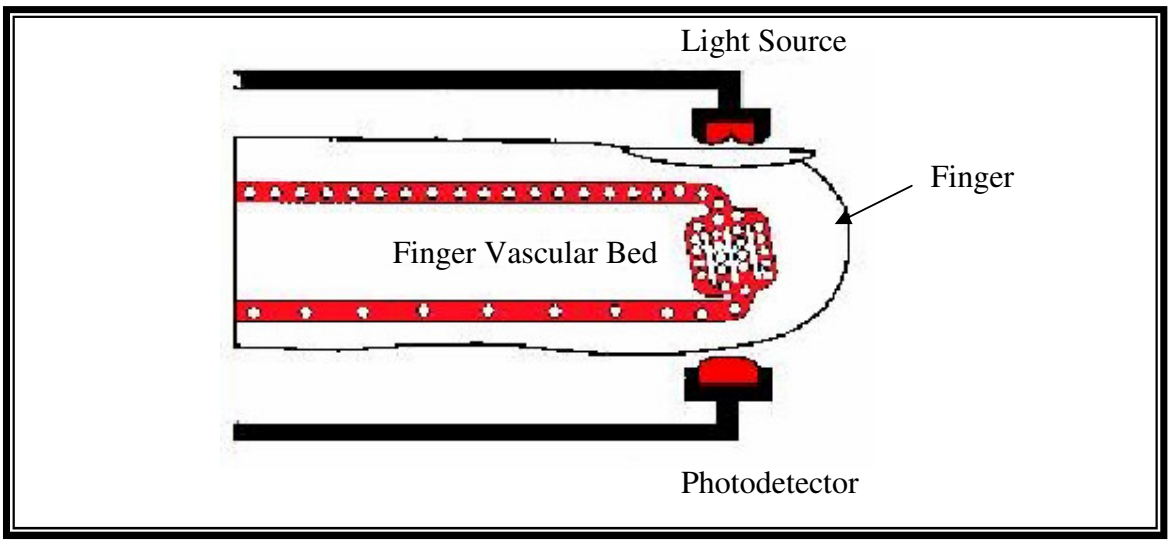

Figure 2.2: Measurement Set-up for Pulse Oximetry [14]

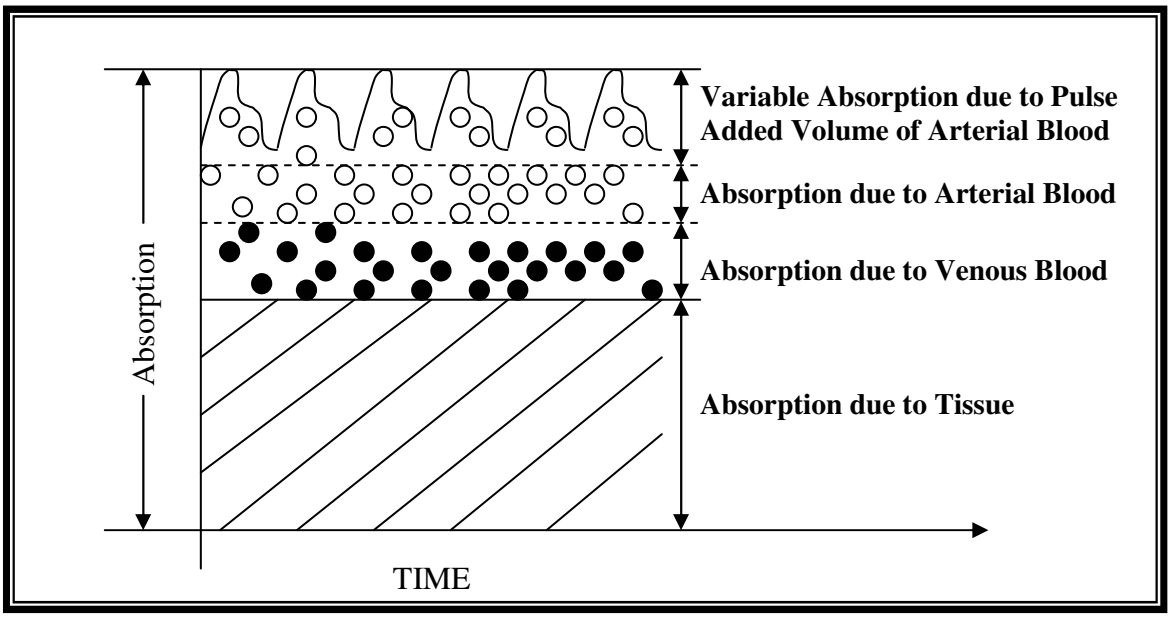

Figure 2.3: The Principle of Pulse Oximetry [14]

Pulse oximetry is employed to perform non-invasive and continuous measurement. In addition, it responds rapidly to significant desaturation and detects transient variations effectively. However, pulse oximeters are susceptible to movement artefacts [14] such as shivering, but this limitation does not reduce the need for the device. Roger A. Wolthuis *et al.* [15] developed a fibre optic oxygen sensor based on optical adsorption change for medical applications in 1992. The focus of his research was also based on the luminescence of chemical compounds in the blood upon excitation to a higher energy state. The luminescence

intensity could then be correlated to the partial pressure of oxygen. The sensor's viologen indicator becomes strongly absorbent after brief ultraviolet stimulation and then it returns to its original transparent state. The rate of the indicator returning back to the transparent state is proportional to the local oxygen concentration. Caution is practiced to avoid burns from prolonged skin contact in hypothermic or hypovolaemic patients. This technique however provides no information on the partial pressure of carbon dioxide (P_aCO_2).

A more comprehensive method of blood gas analysis could be achieved by employing transcutaneous monitoring. It provides continuous and reliable trend information on the body's ability to deliver oxygen to the tissue and respective organs via oxygenated blood. This technique also provides early warning on the onset of problems and reduces the need for blood sampling as required by the blood gas analyzers. The principles of transcutaneous monitoring are based on the fact that the elevation of skin temperature increases the cutaneous blood flow and hence the partial pressure of oxygen and carbon dioxide can be measured as the skin becomes permeable to gas diffusion [16].

2.2 Transcutaneous Blood Gas Monitoring

Transcutaneous monitoring of P_aO_2 and P_aCO_2 eliminates the need for the extraction of blood samples. Continuous monitoring enables sudden changes in the blood gas levels to be detected almost instantaneously. Generally, the analysis of a blood sample is only required when continuous monitoring justifies it for more accurate and absolute measurement results. It also provides early warning for sudden changes in the blood gas levels during monitoring. This advantage enables the medical staff to be informed of the patient's ongoing conditions so that proper attention and treatment can be given in time.

By increasing the temperature of the skin surface, the cutaneous blood flow is excited and causes the tissue to dilate. This increases blood flow, which subsequently causes the tissues in the desired area to be filled with arterial blood. At elevated temperature, the skin becomes permeable to gas diffusion as the pores expand. Therefore, the oxygen molecules in the blood diffuse through the tissue (epidermis layer) and reach the surface of the sensor. The oxygen molecules are allowed into the sensor's electrolyte and finally arrived to the electrode surface

where a redox reaction occurs. This way, transcutaneous oxygen measurements can be carried out.

In 1979, O. Lofgren *et al.* [17] carried out experiments to determine the effects of different electrode temperatures on the partial pressure for transcutaneous oxygen levels ($P_{tc}O_2$). It was found that the choice of electrode temperature is important, as a higher temperature is desirable to obtain adequate arterialization while a sufficiently low temperature is preferred in order to minimize the risk of burns on the skin surface. In short, a clever balance should be reached for optimum results. In their research analysis, a commercially available sensor from RADIOMETER [18] to measure $P_{tc}O_2$ from 42 °C to 46 °C was employed. The conclusions of their studies reflected that for this equipment, the percentage error for the measurements made between the desired temperature range is between ±1.5% (for normal healthy patients) to ±20% (for extreme hyperoxia or hypoxia cases). By performing repeated experiments, the optimal temperature of the electrode was estimated at an average of 44.5 °C. Each operating temperature varied slightly from one type of sensor to another due to the small differences in composition and construction. However, in general, a suitable temperature adopted for transcutaneous measurement is approximately 44 °C [19]. Although it is not a significantly high temperature, the skin of the patient especially babies may suffer mild blistering when subjected to long term monitoring. In order to minimize the negative effects, the sensor usually has its position changed after a continuous measurement of about 3 to 4 hours.

The measured transcutaneous results usually differ from those obtained by the blood sample tests. This difference is observed because the transcutaneous measurements are obtained from the gas tension underlying the skin tissues and not from the arterial gas tension. In other words, the transcutaneous oxygen level is under the influence of the blood flow to the skin and hence, oxygen is consumed in the subcutaneous tissue [1]. Gas tension in a liquid such as blood is equivalent to the partial pressure of the gas at the surface of the liquid at equilibrium. In 1981, D. W. Lubbers [20] worked out a theoretical model where transcutaneous blood gas level can be quantified with respect to the arterial blood gas concentration during maximum dilation of the local vasculature in the upper dermis.

Figure 2.4 depicts the layers of tissue and the skin structure through which oxygen diffuses in order for measurements to be made transcutaneously. As the skin of each individual person is

structured differently, the equation describing the relationship between $P_{tc}O_2$ and P_aO_2 is not entirely the same.

From Fenner's experiment [22], it was found that transcutaneous measurement appeared reliable but there were occurrences of inconsistencies in the relationship with respect to arterial measurement. A. Fenner *et al.* investigated the transcutaneous determination of arterial oxygen tension in 1975 on newborn infants. They tested two groups of infants during normoxia and hyperoxia using two different methods. The data of P_aO_2 and $P_{tc}O_2$ collected from the experiments ranged from 100 mmHg to 600mm Hg. Regression estimates were applied to the data obtained and it was observed that a linear relationship could be established between the transcutaneous blood gas level and the corresponding arterial blood gas level, with a gradient of approximately 1. This shows that $P_{tc}O_2$ is directly proportional to P_aO_2. Correlation and proper calibration ought to be performed in order to relate the transcutaneous measurements and their corresponding arterial values for individual cases.

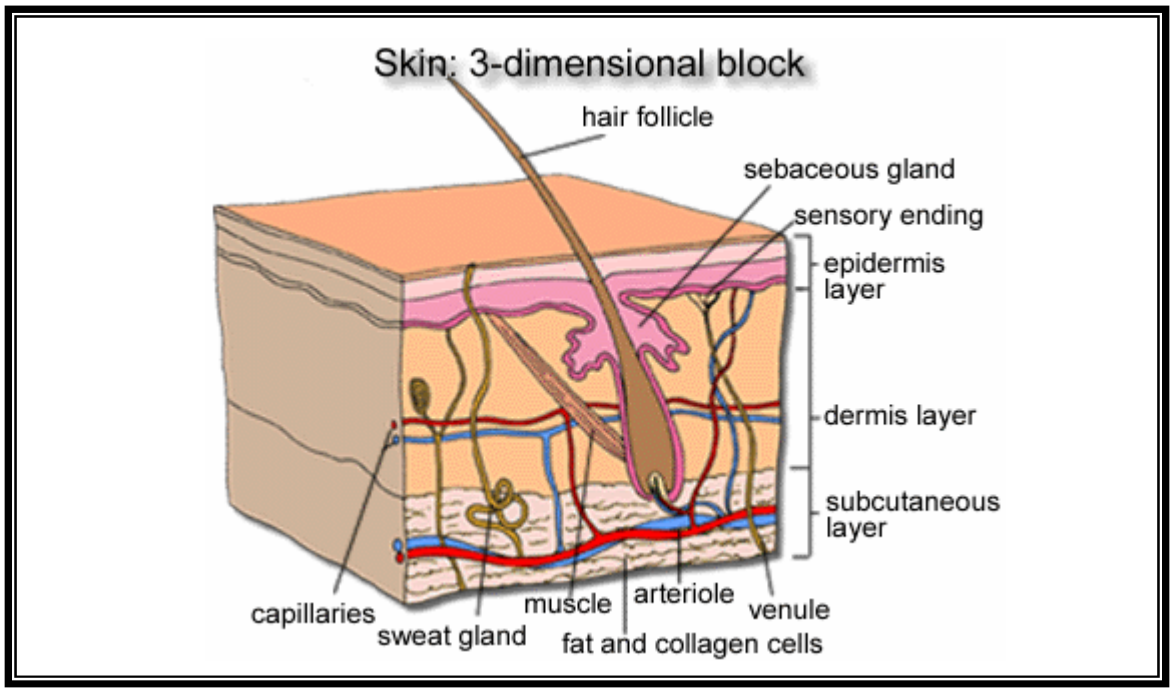

Figure 2.4: Layered Structure of Skin [21]

In 1991, Steven Keston *et al.* [9] characterized a transcutaneous monitoring system with healthy subjects who breathed various gas mixtures and the steady-state transcutaneous readings were compared to the simultaneous arterial blood gas analysis. Agreeing with Fenner's conclusion, the transcutaneous blood gas level is also found to be directly

proportional to the arterial blood gas level. Although a linear relationship was found, there was wide variability among the subjects under test. Transcutaneous measurements are problematic as they reflect both the arterial and tissue gas tensions, which are affected by capillary blood flow [23], cardiac output [24] and metabolic processes [25]. However, strong advantages such as easy application, patients comfort and fast responses prove to be more important than the existing problems. Hence, transcutaneous measurement is still welcomed by many medical professionals.

Currently, there are several commercial transcutaneous blood gas analyzers available and used in hospitals all over the world. The sensors are electrochemical cells based on the working principle of amperometry. An example of such equipment includes the TCM-3 model blood gas analyzer from Radiometer Copenhagen [18] as seen in Figure 2.5. It has good display panels and is very portable, which provides a high level of user-friendliness in aiding medical staff to carry out tests on patients. However, the TCM-3 blood gas analyzer possesses several disadvantages such as high cost in maintenance and replacement of consumables. In addition, for it to function efficiently over a longer monitoring period, saline has to be repeatedly applied to the surface of the sensor at intervals of 3 to 4 hours. This is carried out in order to replenish the depleted solvent in the sensor during the measurement so as to avoid sensor damage and inaccurate results.

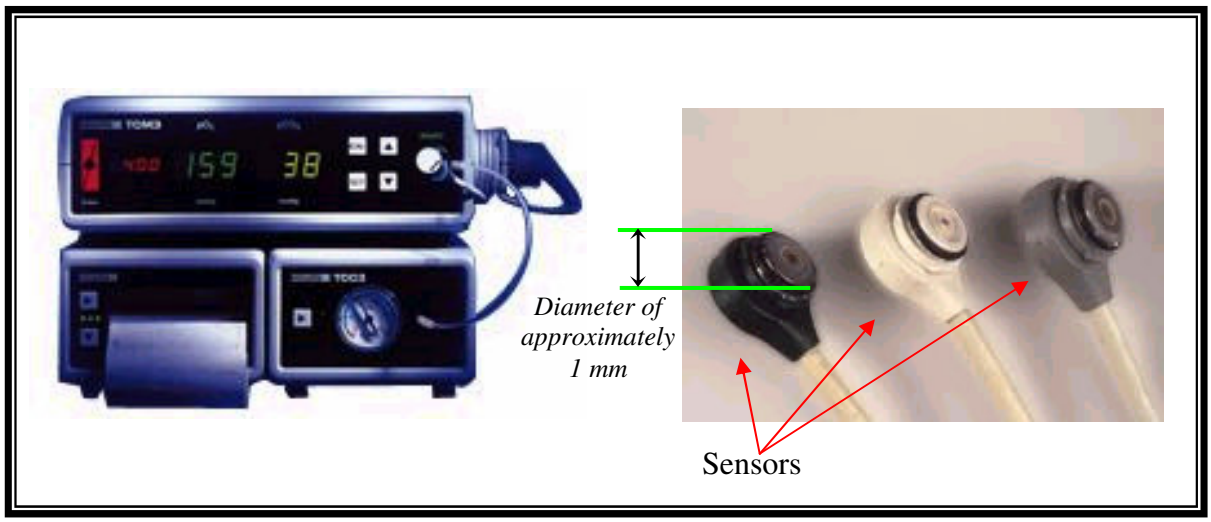

Figure 2.5: Commercial Transcutaneous Monitoring System from Radiometer [18]

Another example of the transcutaneous blood analyzer that is commercially available and works on amperometry measurement is the PO-550 from Sumitomo Electric [26]. Figure 2.6 briefly presents a block diagram of this monitoring system.

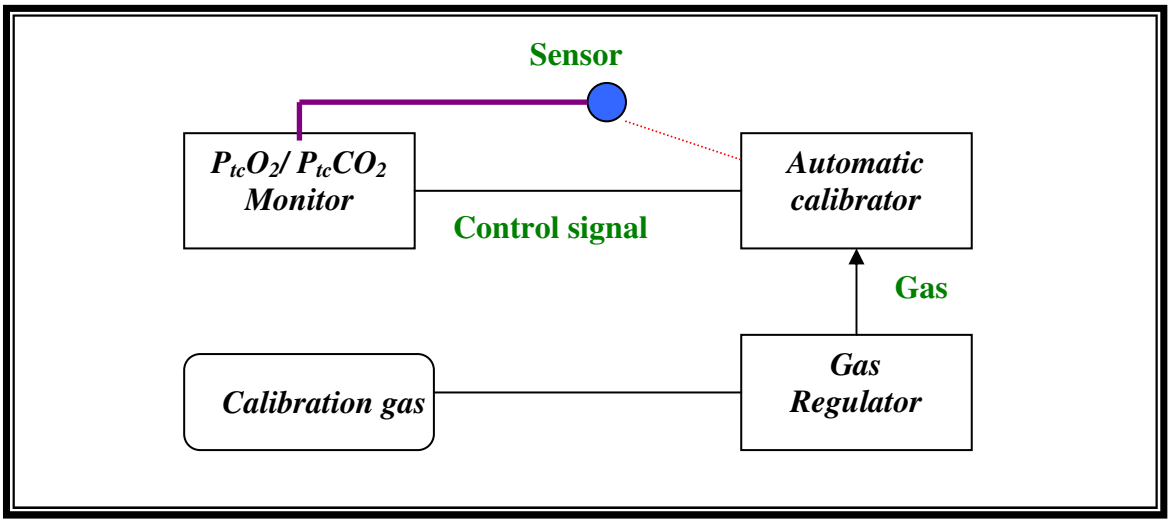

Figure 2.6: Block Diagram of PO-550 (Sumitomo) Monitoring System

It provides user-friendly features such as good printouts and simple operating procedures. This particular equipment is very useful as it combines the measurement of partial pressure of oxygen ($P_{tc}O_2$) and partial pressure of carbon dioxide ($P_{tc}CO_2$) using a single sensor. This breakthrough in technology has allowed convenience in measurement and is the key advantage of this equipment. However, there are several disadvantages in this system. Although they provide continuous, fast responding measurements, the sensors need to be prepared properly before use. The sensor in this system plays an important part of the measuring instrument and it has been manufactured and calibrated to give optimum results. Hence, it is costly and re-used after each measurement. The membrane is usually made of a disposable material that must be replaced for hygiene purposes. There are several procedures required to replace the membrane such as stretching the membrane over the sensor tip or tightening the membrane by screwing onto the sensor tip. In order to achieve good measurements, the membrane and sensor require good contact. The person carrying out this replacement requires some experience to replace the membrane properly. Improvements have been made over the years to ease this inconvenience so that inaccuracy in measurement due to improper fitting of the membrane has been minimized. Despite this, the idea of having a totally disposable sensor has always been welcomed by both medical and engineering

professionals. This new sensor must be cost effective, easy to manufacture, accurate and compact for making transcutaneous blood gas measurements.

After understanding the basic medical requirements of transcutaneous measurement, the design and working principles of the desired sensor from the engineering point of view can be reviewed.

2.3 Electrochemical Principles

The conventional method of analyzing blood samples is carried out by means of a Clark electrode, which was first discovered in 1956 by Dr Leland Clark [7]. In general, the typical oxygen sensor is an electrochemical Clark cell that comprises electrodes in contact with electrolytes. A suitable membrane is then placed over the cell to allow the desired gas to diffuse through. The working principle of the sensor is based on amperometry, which is affiliated to the oxygen reduction reaction of the electrochemical cell. The method of making transcutaneous measurements via a sensor requires the inclusion of an in-built heating device.

2.3.1 The Function of the Materials within a Clark Cell

In order to have a better appreciation of the working principles and sensor design, a fundamental understanding of electrochemistry and redox reactions is presented. Electrodes are defined as the solid electrical conductors where current enters or leaves the electrolytic cell. In a simple two-electrode electrochemical cell, one of the electrodes is made of a noble metal such as Platinum (Pt) or Gold (Au) as they are thermodynamically stable with respect to oxidation. In other words, these metals will not corrode under normal environmental conditions. The gold or platinum electrode is connected to the negative voltage potential for reduction of oxygen to occur. This electrode is known as the cathode. The other electrode is referred to as the anode and it is connected to the positive voltage potential for the oxidation half-reaction. When a potential of approximately -0.6V is applied across the two electrodes through a suitable electrolyte, a current proportional to the partial pressure of oxygen which diffused onto the surface of the electrodes will be produced [7, 27-79]. The Ag/AgCl anode acts as the reference electrode as it has a constant electrochemical potential when there is no current flow. Ag/AgCl reference electrodes have large hysteresis free reactions and can be

used at higher temperatures with low temperature coefficients. It is the best general purpose reference with a wide temperature range of -5 to +110°C [30].

At different biasing potentials, different reduction processes could occur [31]. The oxygen molecules are electrolyzed at the cathode by the following two-electron reactions:

$$O_2 + 2H_2O + 2e^- \longrightarrow H_2O_2 + 2OH^- \quad (2.2)$$

$$H_2O_2 + 2e^- \longrightarrow 2OH^- \quad (2.3)$$

The oxygen molecules reach the cathode via diffusion and reduce to hydroxyl ions and hydrogen peroxide components in the presence of H_2O provided by the electrolyte solution. Upon further reaction, the hydrogen peroxide reduces more to give another set of hydroxyl ions. The reaction tends to increase alkalinity in the medium. If an increase in pH takes place, a two-step mechanism of 2-electron reaction as described in Equations (2.2) and (2.3) will predominate. In more recent studies, Bianchi [32] found that in a solution where a high concentration of hydrogen peroxide was present, the oxygen reduced to hydroxyl ions directly in a four-electron mechanism given by:

$$O_2 + 2H_2O + 4e^- \longrightarrow 4OH^- \quad (2.4)$$

These reactions cause an electrolytic current to flow and the current is proportional to the oxygen concentration in the blood. This phenomenon can be observed from an output current vs input biasing voltage graph, called a voltammogram [31]. If the biasing voltage is further increased to beyond -1.5V, hydrogen evolution will occur via the following chemical equation:

$$2H_2O + 2e^- \longrightarrow H_2 + 2OH^- \quad (2.5)$$

The cyclic voltammograms give pictorial representations of all the reactions occurring at different input biasing potentials. In a two-electrode configuration, the electrolyte needs to be replenished in order to maintain charge balance. Generally for an Ag/AgCl anode, the reaction is given by:

$$4Ag + 4Cl^- \longrightarrow 4AgCl + 4e^- \quad (2.6)$$

The chloride ions are oxidized to provide the anode with electrons in order to complete the electrochemical circuit. Effectively, there is no net consumption or gain of electrons in this equilibrium situation.

2.3.2 The Function of Aqueous Salt Electrolytes and Membranes and their Materials

As the surface area of the silver electrode and the chloride (Cl^-) ion concentration is sufficiently large, the reaction does not affect the overall electrolytic current. A glass insulator is placed around the cathode wire to localize the oxygen sensitivity to an area very close to the point of contact. The electrodes are then placed in a well of electrolyte, which is usually of chloride ion bases such as sodium chloride (NaCl) or potassium chloride (KCl). The definition of an electrolyte is a chemical compound (salt, acid or base) that dissociates into electrically charged ions when dissolved in a solvent. In other words, the electrolyte becomes an electrically conductive medium upon ionization. In the event of this, any of the various ions, such as sodium, potassium, or chloride, are required by cells to regulate the electric charge and flow of water molecules across the cell. The resultant electrolyte solution is then an ionic conductor.

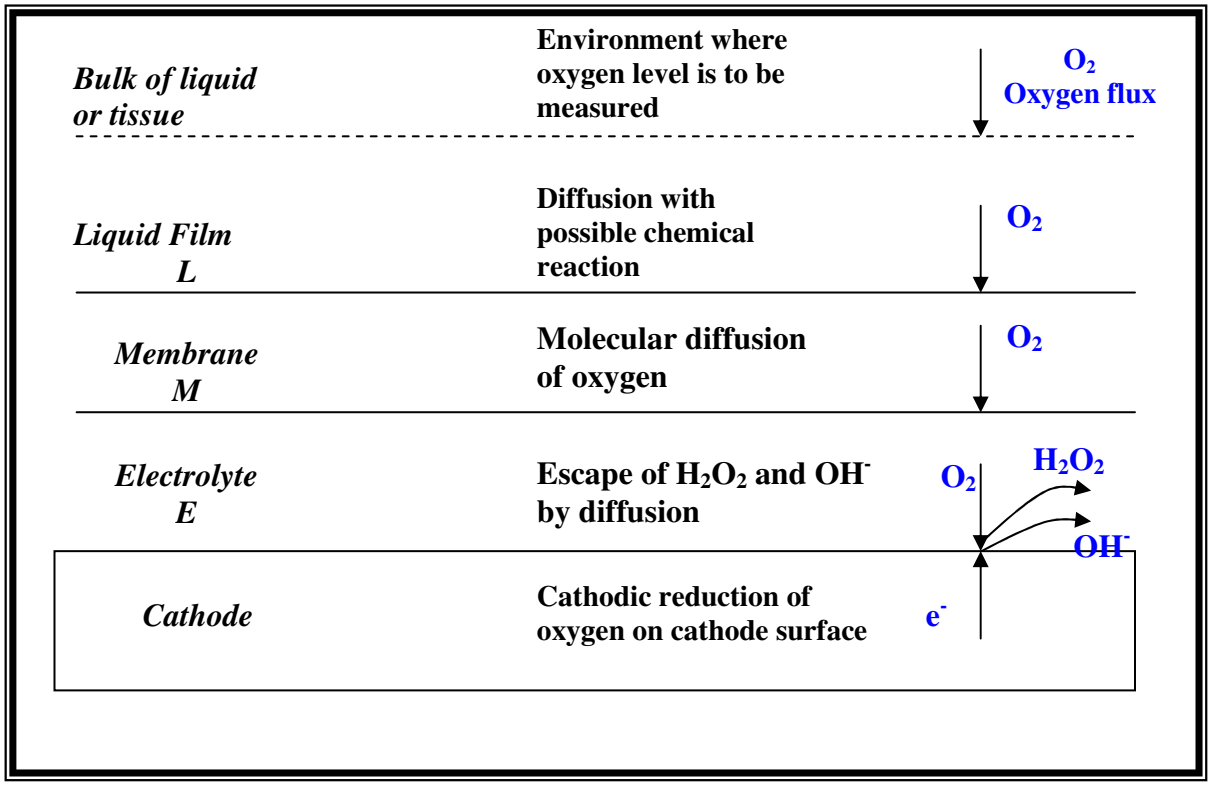

Figure 2.7: Diffusion Path of the Oxygen Molecule

The working principle of the electrolyte solution is to allow the substitution of hydroxyl ions from the cathodic reaction with the chloride ions within the electrolyte. Ionic conduction through the electrochemical cell will be carried out by these chloride ions. If there is an excess of hydroxyl ions, then the electrolyte will be depleted of chloride ions. Hence, there is a need for the electrolyte to be replenished. Another important function of the electrolyte material is to ensure transport control in the membrane. The electrolyte should be sufficiently thin, usually not thicker than the membrane.

The membrane is a thin layer of material that is porous to the desired measurand, in this case oxygen. The membrane is often necessary to control the amount of oxygen from the bulk material into the sensor. This is to avoid flooding the pores of the electrolyte which eventually prevents the ionic conduction process. If the membrane layer is too thin, it may not serve the purpose of controlling the ionic-exchange transport mechanism within the sensor. If too thick, the oxygen will have difficulty in diffusing through to the electrodes for the cathodic and anodic reaction for instantaneous response. Figure 2.7 illustrates the general overview of the electrochemical reaction and paths of the oxygen molecules at each interface.

2.3.3 Mass Transport of Oxygen in an Electrochemical Cell

The mass transport mechanism of oxygen relative to the cell is divided into three major regions, namely the thin electrolyte layer, the membrane and the bulk solution. Under the influence of a biasing voltage, the mass transport mechanism of oxygen from the electrode to the bulk material conforms to the Nernst Diffusion Layer model [32, 33] as illustrated in Figure 2.8. In the case of a stable and unchanging environment, the concentration of oxygen is constant in each region denoted by the dotted line. Upon the application of a biasing voltage potential across the two electrodes, the oxygen concentration in the bulk material (c_{bulk}) remains essentially the same. This is due to the large amount of bulk solution present, which leads to insignificant changes in oxygen concentration. This is usually known as the convective region. On the other hand, the oxygen concentration in the membrane (c_m) and the oxygen concentration in the electrolyte (c_e) will be subject to Fick's first law [31]. It states that the flux of any species through a plane parallel to the electrode surface is given by the product of the diffusion coefficient and the first derivative of the concentration with respect to its thickness.

Equation (2.7) shows the relationship between the concentration of oxygen in the membrane and bulk material via the distribution coefficient $K_{m->bulk}$. The distribution coefficient, otherwise known as the partition coefficient, describes the difference in concentration due to the different solubilities of oxygen in two different phases. Equation (2.8) relates the oxygen concentration between the membrane and electrolyte, governed by its respective distribution coefficient for oxygen ($K_{m->e}$).

$$c_m \quad \alpha \quad K_{m \rightarrow bulk} c_{bulk} \tag{2.7}$$

$$c_m \quad \alpha \quad K_{m \rightarrow e} c_e \tag{2.8}$$

If the partition coefficient for the three regions are considered to be unity depending on the nature of the materials, then levels *a* and *b* (found in Figure 2.8) will be zero. This means that at the thickness of x = *A*, the concentration of oxygen in the electrolyte and that of the membrane will be equal. Similarly, at x = *B*, the concentration of oxygen at the membrane is equivalent to that of the bulk solution.

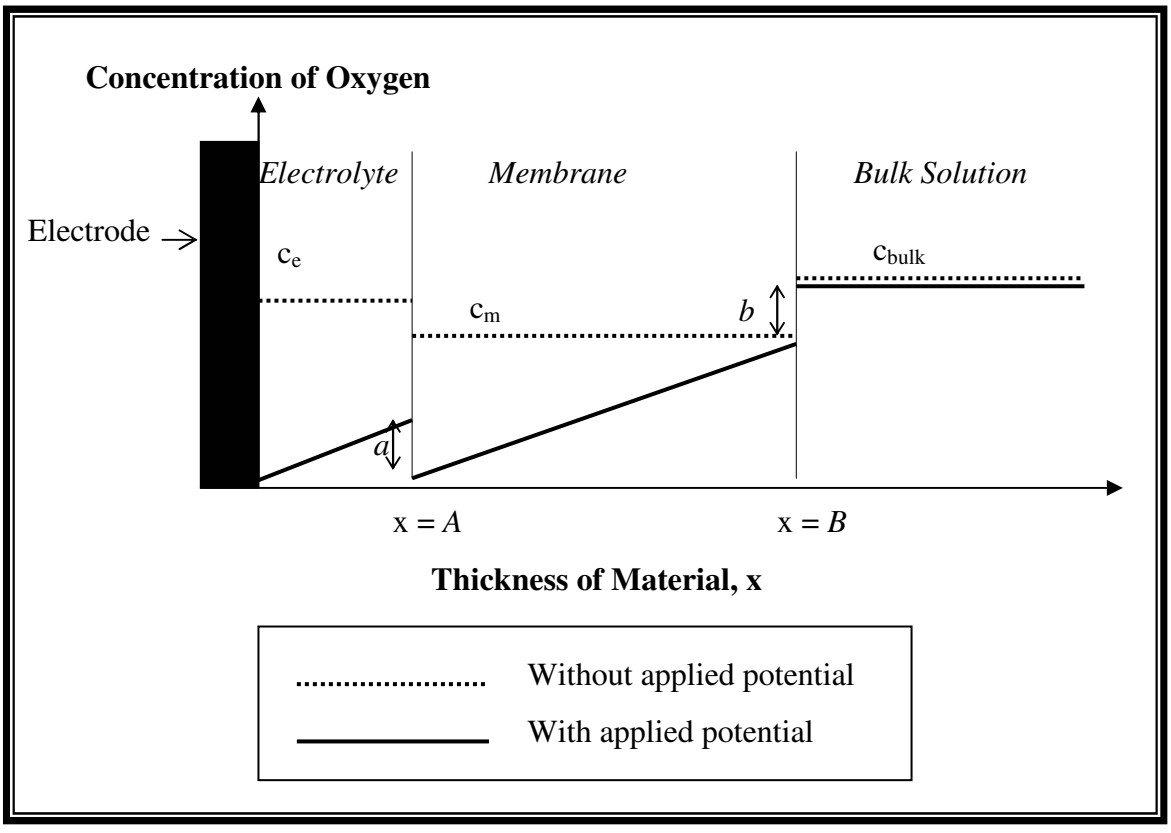

Figure 2.8: Nernst Diffusion Layer Model

When cyclic voltammetry is performed, the typical current to voltage relationship consists of current peaks in both the forward and reverse sweeps of the voltage potentials as shown in Figure 2.9. As the voltage potential increases beyond the current peak denoted by i_{pc} towards the switching point, the corresponding current levels decreased due to depletion of oxygen.

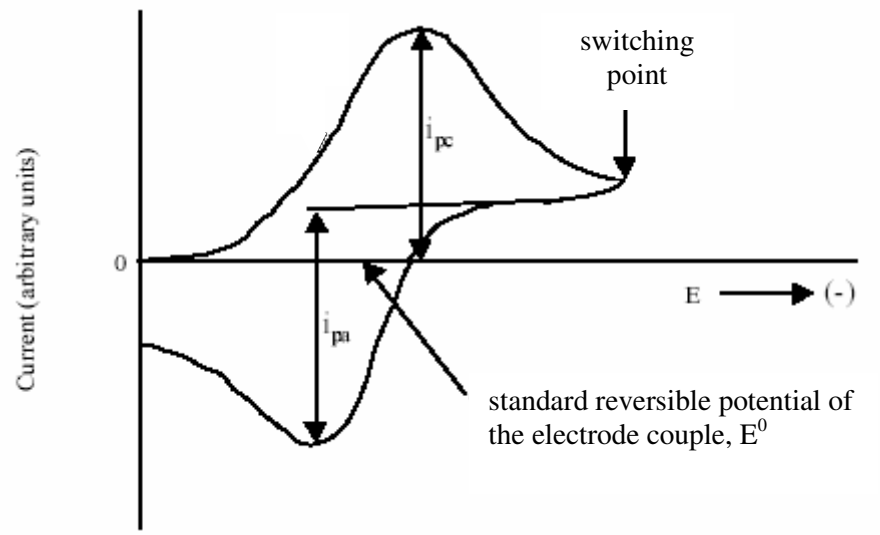

Figure 2.9: Typical Cyclic Voltammogram

In Figure 2.10 (a), the voltammogram reflects the response during an oxygen reduction reaction under a continuous supply of oxygen. The negative applied voltage increases at the cathode and this causes the corresponding current to increase initially and then subsequently saturate. This is observed because the reaction of oxygen at the cathode is very rapid but the rate of this reaction is limited by the diffusion of oxygen to the cathode surface. This is often referred to as the current diffusion limited plateau. As the negative bias voltage is further increased and this leads to a sudden increase in the current, which is mainly due to the reduction of water (H_2O) to hydrogen (H_2).

Figure 2.10 (b) shows that at a fixed bias voltage of approximately -0.7V, the current output of the electrode can be calibrated linearly with respect to the dissolved oxygen. Hence, current is proportional to the activity or equivalent partial pressure of dissolved oxygen. On the other hand, as the oxygen concentration increases outside the sensor, the flux of oxygen diffusing through the fluid boundary layer around the sensor via the membrane and arriving at the cathode increases thus causing more electrical current flow in the sensor's circuit. Generally, the output current obeys Fick's first law of diffusion.

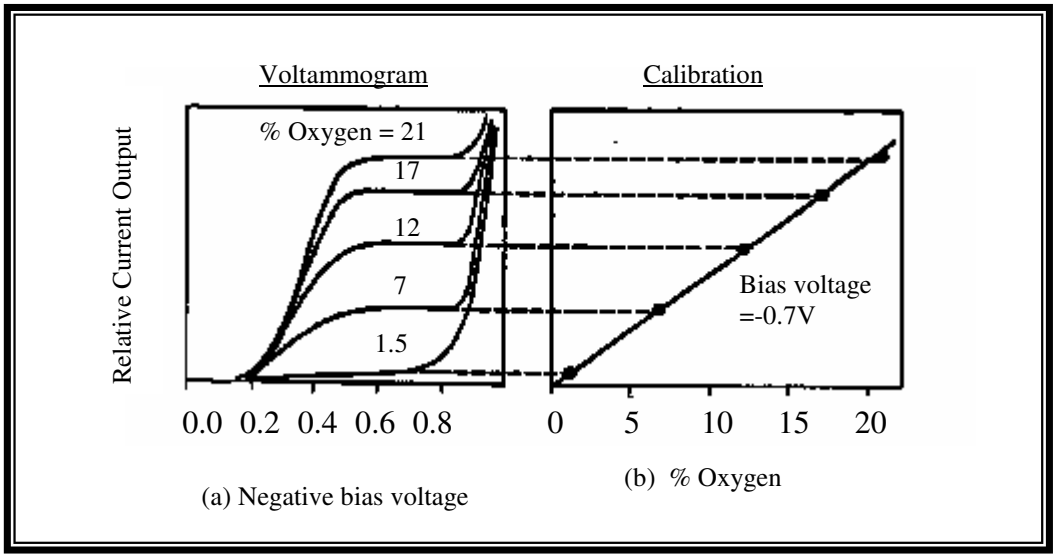

Figure 2.10 (a): Polarogram Depicting Current-to-Voltage Relationship at Different Oxygen Tensions;
(b) Calibration of Current to Oxygen at a Fixed Polarization Voltage [31]

2.3.4 Three-electrode Electrochemical Cell

The two-electrode system is simple and effective for amperometric measurement. If the material used for the anode is Ag/AgCl, then the electrolyte required should contain a massive amount of chloride ions. In addition to this, in the two-electrode system, the anode doubles up as the reference electrode. Hence, not only must the anode oxidize the ions, it must remain stable as all measurements are taken with respect to it. In view of this, a three-electrode system was introduced by Bard and Faulkner [34] to overcome the limitations posed. The working principle of this system is similar to that of the two-electrode system. It is based on amperometry but it requires a potentiostat for its operation. Chapter 3 will deal with the design of the potentiostat in greater detail.

The three electrodes involved are named the working electrode (WE), the counter electrode (CE) and the reference electrode (RE). The working electrode is equivalent to the cathode of the two-electrode system. It is made of a noble metal and its function is to reduce oxygen. The half-cell reaction at this electrode is given by [35]:

$$\frac{1}{2}O_2 + H_2O + 2e^- \rightarrow 2OH^- \qquad (2.9)$$

The counter electrode is analogous to the anode where oxidation takes place and provides the return path to complete the circuit. It is often made of the same material as the working electrode. The electrochemical half-cell reaction at the counter electrode is given by:

$$2OH^- \rightarrow \frac{1}{2}O_2 + H_2O + 2e^- \tag{2.10}$$

Oxygen is reduced to hydroxyl ions at the working electrode and the hydroxyl ions are oxidized at the counter electrode. From Equations (2.9) and (2.10), it is observed that there is no net consumption of oxygen or production of hydroxyl ions in this system. This is desirable as the electrolyte involved in this system will not experience any increase in alkalinity. In an ideal situation, the electrolyte will not experience any physical or chemical changes. In short, it will not be depleted of its ions in order to maintain charge balance. This relieves the restriction over the choice of electrolyte materials to provide the chloride ions required in the case of the two-electrode electrochemical cell.

The reference electrode is usually placed within the electrolyte so that it can be maintained at the desired polarizing voltage as the working electrode. The material for the reference electrode is usually Ag/AgCl. It does not participate electrochemically in the oxygen reduction process, hence it is not consumed. Due to these advantages of the three-electrode system, it was adopted for the development of the transcutaneous oxygen sensor.

2.4 Polymer Electrolytes

The materials used for the electrolyte have been studied in great depth for their suitability for application in the transcutaneous oxygen sensor. In Section 2.3.2, an introduction to salt electrolytes is given as part of the basic structure of a simple electrochemical cell. However, at elevated temperatures or for long term applications, the electrolyte solution will deplete and dehydrate, and hence require constant replenishing for continuous measurement. To overcome this impending problem, alternative electrolytes such as polymer electrolytes are explored. The requirements of these electrolyte include having an adequate level of ion conduction, electrochemical and thermal stability and the ability to form good interfacial contact with electrodes as well as compatibility with manufacturing technology [36]. Most

importantly, this electrolyte and the components formed during the reactions must be non-biohazardous for medical applications.

The working principle of the polymer electrolyte is based on ionic conduction. Low-field conduction in polymers frequently obeys the Arrhenius-type relationship [37] given by:

$$\sigma(T) = \sigma_0 \exp\left(-\frac{\phi}{k_B T}\right) \tag{2.11}$$

where σ_0 is the conductivity at temperature of 0 °K and ϕ is the activation energy. These two parameters are often experimentally determined and found to be constant over a relatively wide range of temperature. k_B is Boltzmann's constant and T is the temperature in °K.

The theory of ionic conduction involves the movement of ions through the ionic crystal. The concentration of charge carriers and their mobility is a function of temperature. In a polymer, the charge transport is classified into the different type of charge carriers namely ionic and electronic transport, which involve protons and holes respectively. The type of charge carriers that are mainly responsible for the conduction depends on the material's chemical and physical composition as well as the operating temperature and the frequency of the applied electric field. Other factors such as the electrode material and humidity conditions also play an influential role in the overall conduction. It is important to note that although ions are present in the polymer electrolyte for conduction, the constant ionic transport is based on the continuous formation of ions and their movements. These ions originate from the electrolytic reaction at the electrode surfaces. Intrinsic ionic conduction encompasses the dissociation of the main chain of the polymer structure in order to create cations or anions. Conversely, the ions involved in extrinsic ionic conduction are not part of the polymer electrolyte structure. They are impurities or dopants that percolate through the structure [37].

The materials that have been focused on for the current study include Nafion (by Dupont), AQ55S (by Eastman) and polyethylene oxide (PEO). These materials depend on ions traveling through the polymer electrolyte (or often abbreviated as polyelectrolyte) in order to achieve ionic conduction. The main objective to seek possible solutions to overcome the problem of electrolyte dehydration at approximately 44 °C for transcutaneous measurement

diverts the focus from aqueous salt electrolytes to polyelectrolytes. The dehydration process discourages the cathodic reaction and eventually lowers the level of ionic conductivity, which reduces the sensitivity and functionality of the sensor. There is a need to uncover other materials (usually polymer based) that possess suitable features for such application. In addition, there is increasing emphasis and interest in developing systems with polymer materials in many research fields such as fuel cells. This proves to be a relative new and suitable area that is worth exploring.

From initial test trials, Nafion 117 (available from Aldrich) displays promising potential as an nteresting and exciting polyelectrolyte material. Nafion [38] membranes are perfluorinated polymer membranes with good chemical, thermal and oxidative stability. Further it often acts as a solid electrolyte in contemporary fuel cells, and thus proves to be relevant in this search for a suitable electrolyte and membrane for the transcutaneous thick film oxygen sensor. Nafion is a trademark of Dupont with industrial medical and healthcare applications. Nafion consists of a hydrophobic tetrafluoroethylene backbone with pendant side chains of perfluorinated vinyl ethers that terminate with ion-exchange groups. It has the chemical structure given by formulae (2.12) [39].

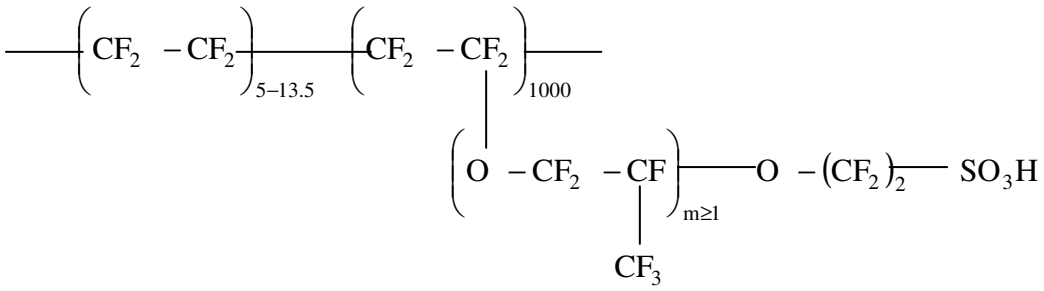

(2.12)

The commercial Nafion used for the sensors, comes in the form of a perflorinated hydrogen ion-exchange solution of 5% wt., mixed with lower aliphatic alcohol and 15% to 20% of water. Its working principle is simply based on having one hydrogen atom on the SO_3 part of the molecule detached in an hydrated environment, hence producing a free H^+ proton to hop between fixed SO_3^- sites on the Nafion backbone. This way, protons are exchanged within this electrolyte or more specifically polyanion, to create a form of ion conducting transportation mechanism.

AQ55S by Eastman [40] is known to be a polymer that possesses similar characteristics to Nafion. It has a glass transition temperature of 55 °C and an average molecular weight of approximately 14000. AQ55S is soluble in water, which is non-toxic and readily available. However, it then presents the disadvantages that the cured polymer can alter its characteristics upon interaction with water or even moisture from the atmosphere. Polyethylene oxide (PEO) is another candidate evaluated for its suitability as an electrolyte. formulae (2.13) is the chemical structure of a typical PEO with average molecular weight given by the y variable.

$$\begin{array}{l} \qquad\qquad\quad CH_3 \\ \qquad\qquad\quad | \\ HO\text{-}[\ CH_2\text{-}CH_2\text{-}O\ ]\text{-}[\ CH\text{-}CH_2\text{-}O\ ]_y\text{-}H \end{array} \tag{2.13}$$

Polyethylene oxide is made through high pressure processing. Polyethylene oxidizes in air at elevated temperature and it displays outstanding electrical insulating properties. Since it is a non-polar material, the dielectric constant is almost independent of frequency and temperature. There are several cases [41] where PEO is recommended as a polyelectrolyte.

Appendix A briefly describes the relationships between the current measured and the oxygen levels obtained from initial tests for the sensors employing AQ55S and PEO electrolytes. The results suggest that both screen-printed polyelectrolytes are not suitable for this application. On the other hand, the most responsive polyelectrolyte was found to be Nafion and it was hence used in all subsequent experiments.

2.5 Polymer Membranes

A membrane is required to control the amount of oxygen from the bulk material into the sensor. It also often serves as a filter to minimize the entry of undesired gases. In the experiments, some sensors were fabricated without the membrane layer while others are covered with cellulose acetate (CA), polytetrafluoroethylene (PTFE) or polyvinyl chloride (PVC).

The first membrane material, cellulose is one of many polymers found naturally and made from repeat units of glucose monomer. When acetic acid is added to cellulose, cellulose

acetate is produced and its structure is given in formulae (2.14). Cellulose acetate, CA (Sigma) is then dissolved in ethylene glycol diacetate (Fluka) in a weight ratio of 1:4 to form a printable ink. Approximately 24 hours of room temperature drying and curing is sufficient for continuous membrane formation. When damped, CA becomes porous to oxygen and acts as an effective membrane.

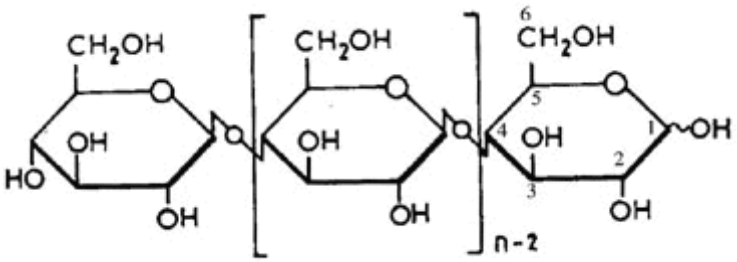

(2.14)

Polytetrafluoroethylene (PTFE) is a polymer made of a carbon backbone chain with two fluorine atoms attached to every carbon [42]. The single monomer unit is shown in formulae (2.15). PTFE is sprayed onto the surface of the substrate as a thin even membrane layer.

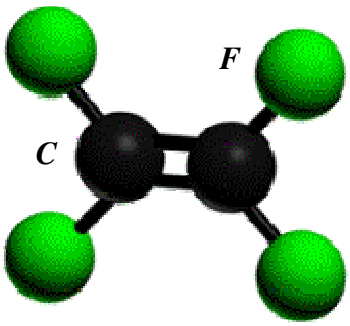

(2.15)

PVC is structurally a vinyl polymer where one of the hydrogen atoms is replaced with a chlorine atom at every other carbon atom in the backbone chain [43]. The single monomer unit formation as depicted in formulae (2.16) is possible due to the free radical polymerization of vinyl chloride. PVC powder from BDH is dissolved in commonly used room temperature organic solvents such as cyclohexanane or tetrahydrofuran (THF) to create printable ink.

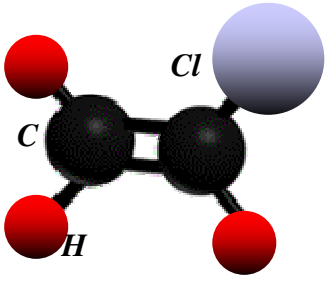

(2.16)

2.6 Thick Film Technology

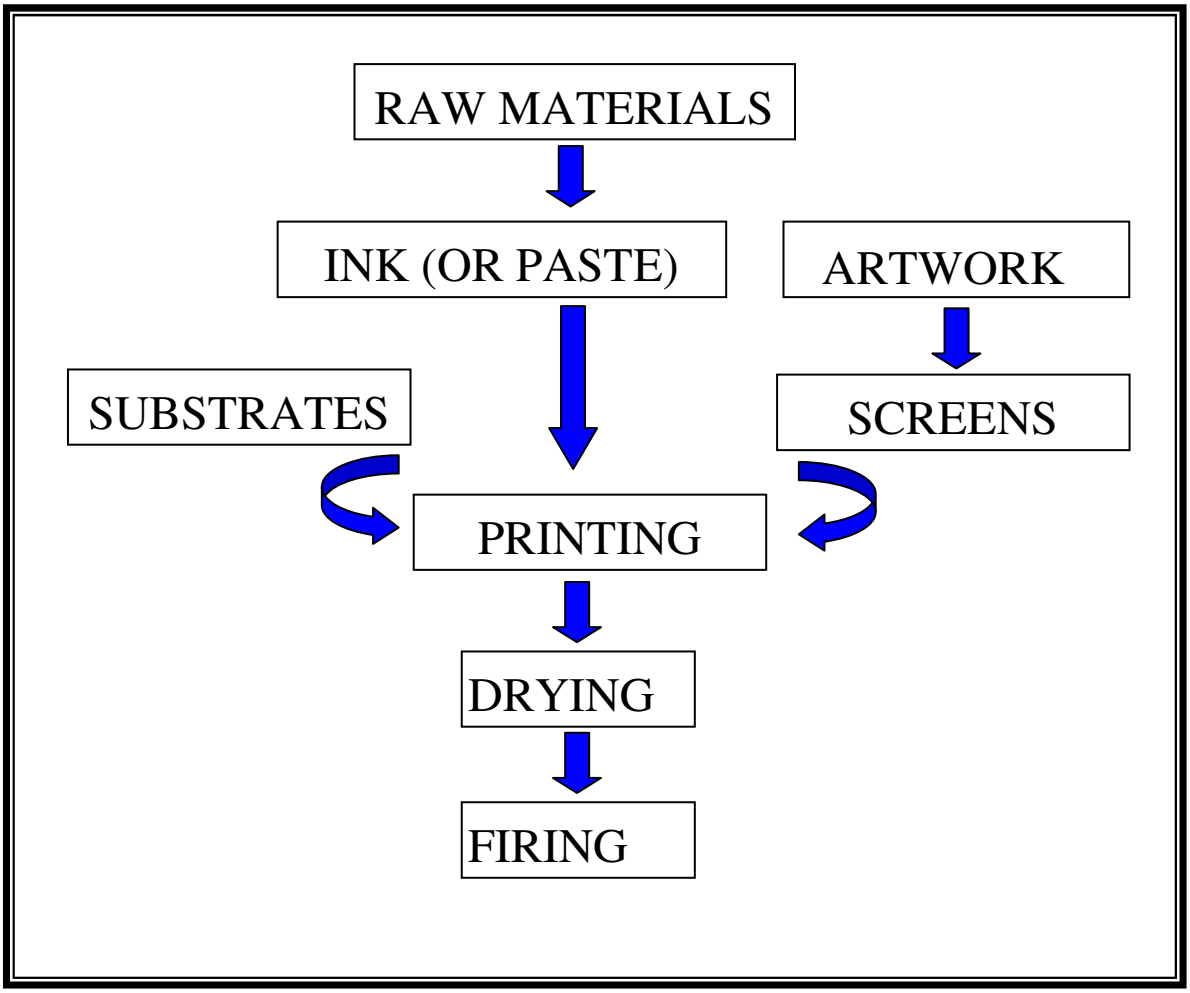

Figure 2.11: Block Diagram of Thick Film Fabrication

Thick film technology has evolved since the 1950s and has matured from being a mere replacement for printed circuit boards to the current sophisticated hybrid circuits. It is a high volume manufacturing technique that runs on low cost. Generally, thick film can be employed to fabricate three kinds of devices, namely hybrid circuits, physical sensors and electrochemical sensors based on the materials used in the ink. Therefore, the possibility of creating a disposable transcutaneous blood gas sensor via thick film technology is no longer hypothetical. Figure 2.11 depicts a block diagram describing the processes involved in thick film fabrication.

2.6.1 Raw Materials (Ink or Paste)

Each layer of the printed thick film device requires special inks (or pastes) to be deposited uniformly onto an insulating substrate. Different materials are used for different applications in the composition of the sensor. The in-house blood gas prototype developed as shown in Figure 2.12 has nine layers of different materials, each for a particular function.

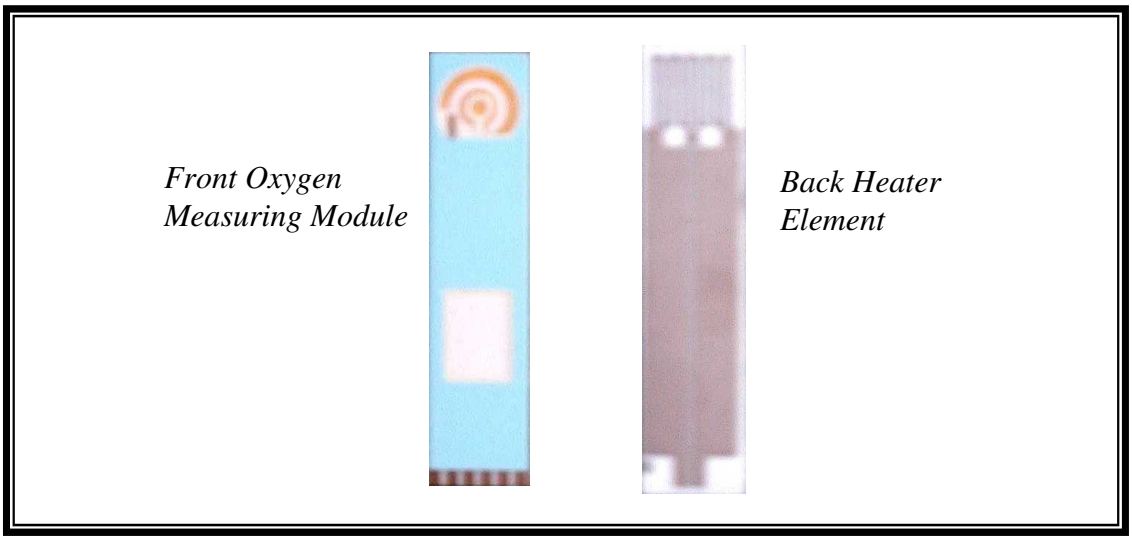

Figure 2.12: Thick Film (TF) Oxygen Sensor Prototype

The first layer of ink is silver palladium that is used for the soldering lead terminals. Wires can be soldered on these terminals and the sensor can be connected to external hardware circuits in order to carry out appropriate measurements. Platinum is then printed for the next layer as the heating element. It is then covered with a dielectric to electrically isolate the heater element from the oxygen sensor module. Within the sensor, electrical conductors are required to connect the electrochemical cell structure to the soldering terminals. Gold was selected as the ink for the conductors. Gold is a suitable metal for low noise applications and considered almost a perfect conductor. This advantage is crucial as the current flow within the electrochemical cell has amplitude in the order of micro-amperes. However, gold is too expensive to be used for all the conducting paths hence silver can be employed to supplement the less crucial paths. The choice of conductor materials is usually based on several considerations such as its resistivity, line definition, adhesion strength and resistance to migration under the influence of voltage gradients. The fifth layer is another dielectric layer (mainly containing glass) to act as electrical separation and isolation for overlapping

conductors. This enables the sensor design to be more compact instead of having spacious allocation laterally for each conductor track. The reference electrode is then printed with silver-silver chloride. The current flow in the electrochemical cell between the cathode and anode is established with the electrolyte layer. With the cell completed, the membrane is ready to be printed on top. The membrane chosen should allow oxygen ions to diffuse into the electrochemical cell in order for the reactions to take place. A final protective layer of dielectric is printed over the conductor tracks, exposing the area where the electrodes and electrolyte are printed, in order to prevent them from coming into contact with the conducting medium.

2.6.2 Screen Artwork

The artwork for the thick film devices is carefully designed in order to obtain optimum results by observing certain guidelines as shown in Appendix B. The screen material is usually either made of polyester or stainless steel. The method of screen fabrication involves the photopolymerisation of an ultraviolet sensitive emulsion [44].

Property	DIRECT	DIRECT/INDIRECT	INDIRECT
Ease of process	Relatively long	Intermediate	Simple, fast
Length of life	20000 prints	2000 to 3000 prints	200 to 300 prints
Definitions	Good	Good	Good
For prototypes	Very good	Good	Very Good
For mass production	Very good	Fair	Poor
Overall cost	Moderate	Cheap	Cheap (short run)

Table 2.1: Comparison Table for Different Screens [44]

There are three main methods of mesh pattern preparation namely direct, indirect, and the combination of both, which is denoted by direct/indirect. A simple and cheap screen such as indirect is made by exposing a pre-sensitised emulsion supported on a polyester backing sheet to an ultraviolet light source. The exposed areas, which are determined by the screen artwork, become hardened. The unexposed regions can then be removed by washing the whole screen with warm water.

A better screen that has good definition and longer shelf life is known as the direct screen. The technique employed for making the direct screen is to apply unsensitized emulsion onto the mesh in a paste form. The emulsion has to be laid evenly to give a smooth coat on the mesh. The emulsion in this case is sensitized in situ with ammonium dichromate solution. It is then exposed to an ultra-violet source and eventually developed using warm running water. The fabrication process of direct screens is significantly longer, hence it is not often used in prototype production.

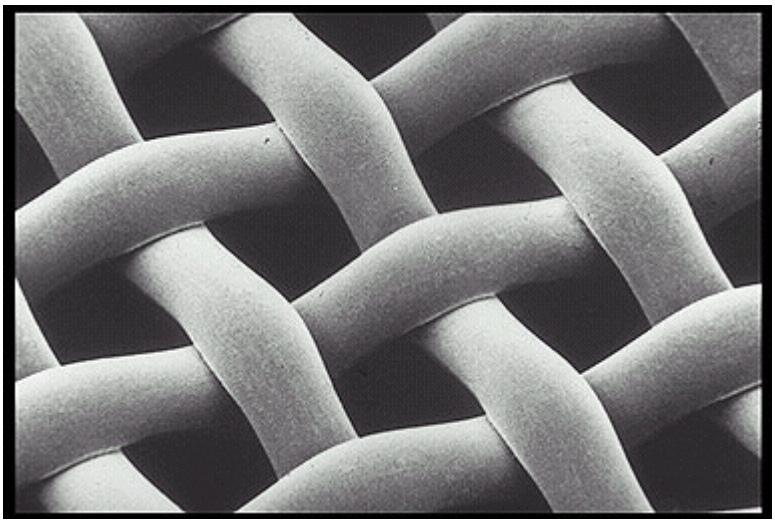

Figure 2.13: Microscopic View of the Mesh

As there are advantages to each type of screen, direct/indirect screen is also available and it takes on the best of both methods. The main difference of such screens from its two counterparts is that the method of making the screen is carried out by having unsensitized emulsion that is pre-laid or supplied on a double layer backing sheet. It is then sensitized in the same way as in the case for the direct screens. Table 2.1 compares the direct, indirect and direct/indirect screens with respect to their properties. Each screen is laid with a mesh and the size of the mesh will determine the definition of print. Figure 2.13 shows a microscopic view of the interlacing structure of a mesh.

2.6.3 Substrate

The substrate is an important part of any thick film structure. The material chosen should exhibit good electrical insulation properties and a high thermal conductivity for power dissipation. It has to withstand high temperatures of up to 1000 °C during the firing process. The substrate must be able to provide a strong and stable support in order to cater for printed components and attached devices. It also has to comply with dimensional tolerances required for consistently accurate screen printing. The uniformity of the substrate is also very important so as to minimize distortions such as bowing [45]. Hence, low surface roughness characteristics are desired.

The substrate needs to be chemically and physically compatible with the appropriate glaze components of the conductor and resistor compositions so that strong bonds between the thick film and the substrate can be established. As thick film technology is employed in mass production for cost effectiveness, the substrate has to be sufficiently reproducible to ensure that the inks printed on them are not affected by the differences in substrate composition, surface finish or physical properties. Currently, there are several materials suitable as substrates, namely barium titanate, titania, beryllia, glass and alumina. Although materials like beryllia display excellent potential as a good substrate [46], it proves to be too expensive. Furthermore, it gives lower strength and has handling problems despite its high thermal conductivity. Alumina [47] is usually chosen instead as its large grain size of up to 200 μm, proves to be advantageous. Alumina is a low cost ceramic material that is 96 % Al_2O_3. The electrical and dielectric properties generally improve with increasing purity.

2.6.4 Printing / Drying / Firing Processes

With the desired ink and the substrate chosen, the printing process can be carried out using a printing machine. There are five main parts to the printing machine that enables printing to be carried out in the mass production of thick film devices:

(a) Screen mounting
(b) Substrate holder
(c) Squeegee and its control mechanism

(d) Means of moving the substrate or the screen from the substrate loading to printing position

(e) Precise adjustment and alignment of the relative position between the screen and the substrate

Screen printing is one of the most matured forms of graphic art reproduction. Figure 2.14 shows the basic screen printing process. During the in-house fabrication of the sensor, the printing procedure is carried out on a DEK 1202 screen printer. The quality of prints for thick film is governed by the screen and machine variables. Firstly, screen variables that are determined during the fabrication of the screen include the mesh material, the mesh count, the mesh filament diameter as well as direction, the mesh weave, the mesh tension, the emulsion type and thickness, and the pattern direction. Machine variables also present equally important factors to printing good thick film devices. These include the squeegee attack angle, its hardness and edge shape. The squeegee's downward pressure and speed of motion can be controlled to give different effects in the print. The alignment of the squeegee, screen and substrate must be parallel. If these variables are not controlled properly, print faults such as ragged edges, smeared edges, incomplete patterns and uneven printing could occur and this leads to undesirable results [47].

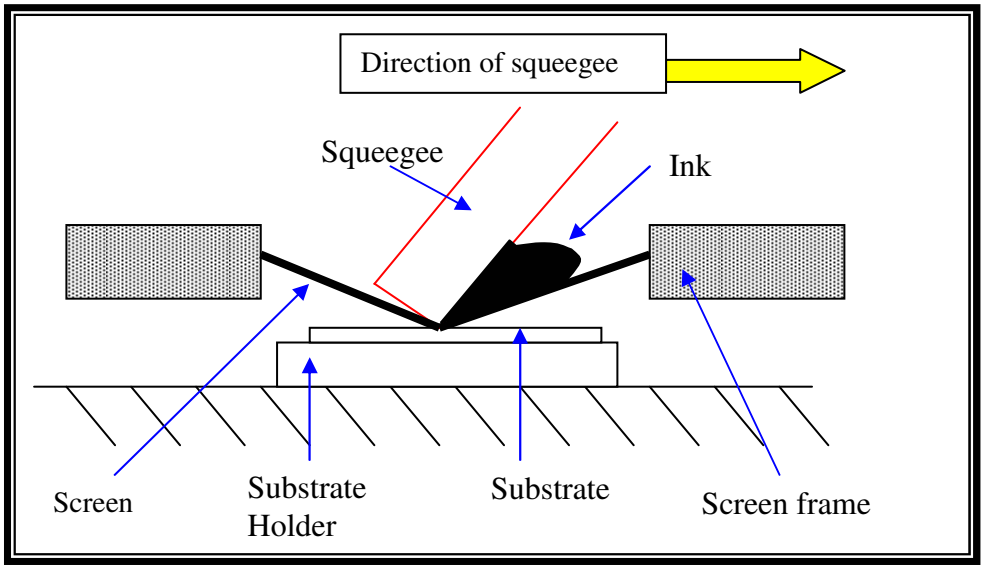

Figure 2.14: Basic Screen Printing Process

Different inks or pastes require different methods of curing. The printed ink on the substrate is initially laid down to level for approximately 10 to 15 minutes before it is dried in a DEK

1202 mini dryer. The next step involves the conductors being fired under high temperatures of approximately 850 °C to 1000 °C while dielectric layers undergo a different set of curing temperatures depending on the ink's specifications [45]. To carry out the firing process, the prototype is placed on a moving belt into a BTU 6-zone furnace with a temperature profile that peaks at 850 °C. This process binds the existing layer to the substrate permanently so that the next layer can be fabricated by repeating the whole procedure using the desired ink material. Most membrane layers do not need firing, hence simple drying or ambient curing is sufficient. Figure 2.15 gives a pictorial representation of the overall thick film process.

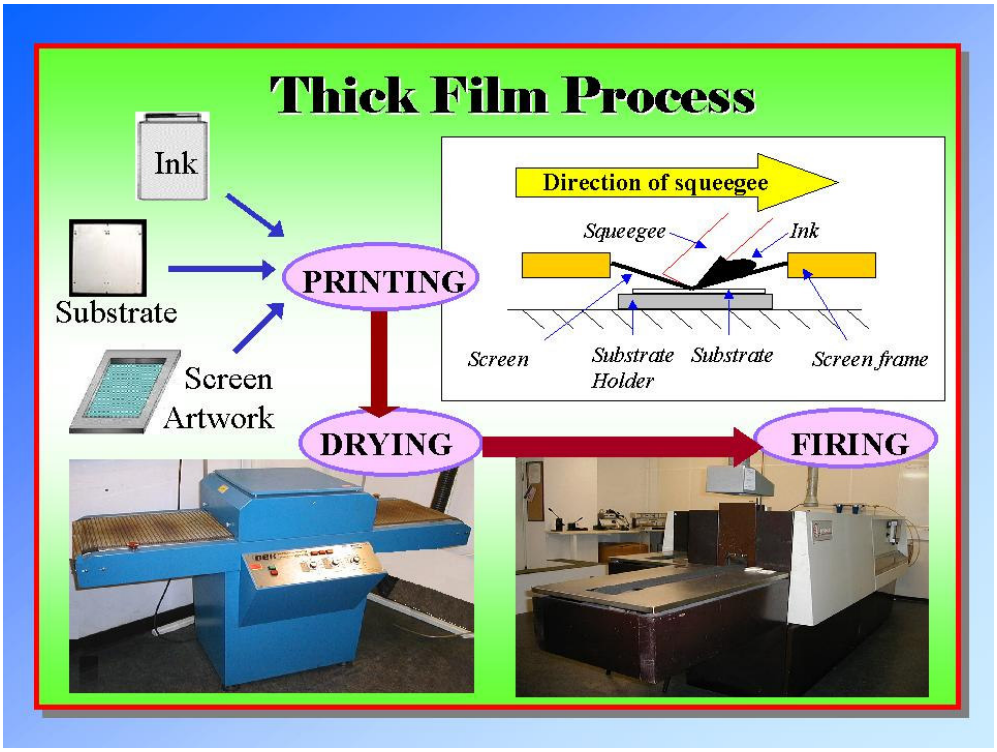

Figure 2.15: Overall Flow Diagram of Thick Film Process

When the thick film devices are fabricated, they are ready to be tested. Chapter 3 will present the sensor prototype design and the fabrication process.

Chapter 3 Sensor Fabrication and Design

3.1 Fabrication of Sensor Prototype

The general fabrication process of thick film sensors as described in Chapter 2 has been carried out to develop the blood gas sensor prototype in order to measure $P_{tc}O_2$. The low cost sensor design consisting of a heating module and an oxygen sensing module was constructed to achieve accuracy of at least 1 μA/mmHg and ideal fast response measurements of 1 sec. The first layer was the soldering terminal made from silver palladium (AgPd), printed onto a 0.635 mm thick 96% Al_2O_3 substrate, which is better known as alumina. Alumina has high thermal conductivity of approximately 35 W/m·°C and it is chemically inert to the printing process. This proves to be useful as the sensor will not produce undesirable chemical compounds, which may otherwise present possible biohazardous consequences. Figure 3.1(a) and (b) illustrate simple block diagrams on the construction of the different layers involved in fabricating the heater and oxygen sensing module of the prototype respectively.

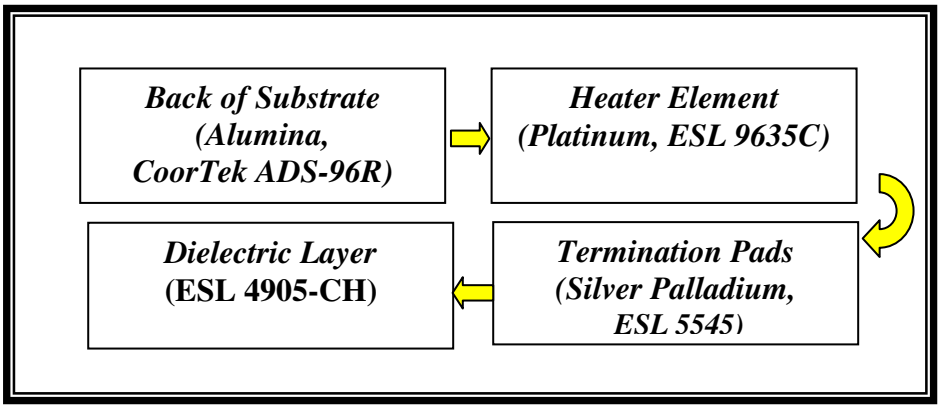

Figure 3.1(a): Thick Film Printing of the Layers Involved in the Fabrication of the Heater Module of Blood Gas Sensor Prototype

Platinum was the material selected for the heating element as it provided a good and stable resistance temperature coefficient (TCR) of 3850 ppm/°C for easy and effective manipulation of temperature control. Section 3.2 will describe the external heating circuit that has been designed to regulate the temperature of this heater element. In addition, the heating element design and some characteristic studies of the materials used have also been carried out experimentally.

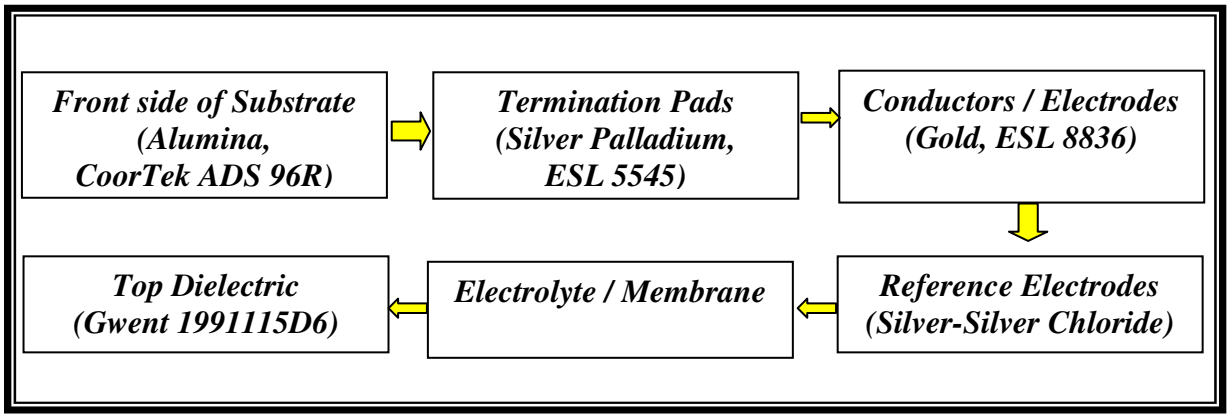

Figure 3.1(b): Thick Film Printing of the Layers Involved in the Fabrication of the Oxygen Sensing Module of the Blood Gas Sensor Prototype

The oxygen sensing module was printed on the front side of the substrate with silver palladium termination pads. Gold electrodes and conductors were required to connect the oxygen sensor layout to the termination pads for external access. Platinum electrodes are usually popular alternatives. However, gold displays several advantages over platinum as it is more resistant to impurity poisoning and minimal oxygen adsorption [8, 48, 49]. Furthermore, it possesses a higher overpotential for H_2O decomposition, which gives a broader range of diffusion limit for O_2 reduction. Although gold is not as good as platinum in terms of being an effective catalyst for hydrogen peroxide reduction, it is still very much preferred for the purpose of this sensor design.

To complete the three-electrode sensor, the reference electrode of silver-silver chloride (Ag/AgCl) was printed. The positioning and geometry of each electrode was optimised in such a way where there would be an even distribution of current and potential throughout the measurement region. In order to ensure that the current required by the working electrode (WE) was completely passed to the counter electrode (CE), circular instead of planar electrodes are employed with the CE having a larger area than the WE. In this case, the current density at the CE will be much lower than that of the WE. This was desirable as no significant polarisation would occur to contribute additional current in the measurement [28, 48, 49].

A supplementary conductor, known as the guard electrode (GE) was printed between the WE and CE. The guard was grounded to zero potential to ensure the minimum amount of

disturbance from laterally diffusing atmospheric oxygen during the transcutaneous oxygen measurement process. All atmospheric oxygen molecules from other directions should not be entertained in the measurement as they ought to be directed to the electrical ground potential. This will ensure the minimum amount of disturbance from atmospheric oxygen in order to obtain more accurate oxygen measurement only from the transcutaneous process as illustrated in Figure 3.2.

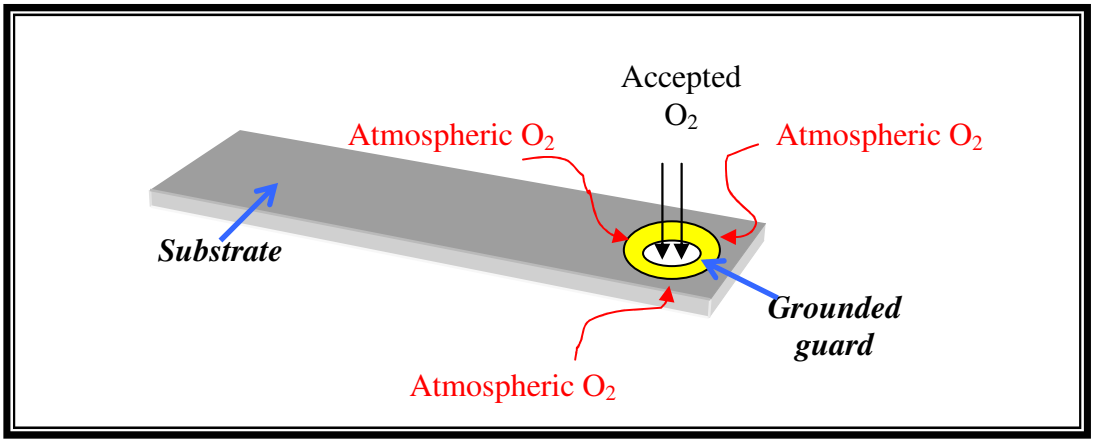

Figure 3.2: Effect of Grounded Guard on Oxygen Molecules

The next layer to be printed after the electrodes was the electrolyte. In the investigations, two main categories of electrolyte materials namely the aqueous salt and the polymer electrolytes were thoroughly studied. A three-electrode configuration adopted for the sensor layout eliminates the requirement of having a chloride-based electrolyte as needed in a two-electrode system with Ag/AgCl anode [28, 29]. 1.0 MOL potassium nitrate (KNO_3) gel was employed as the aqueous salt electrolyte because it was readily available and convenient to produce in-house. The gel was prepared by mixing one part of potassium nitrate powder (from Aldrich) and approximately two parts of gelatine into ten parts of de-ionized water. The solute and solvent were constantly stirred in a glass container, which was immersed in warm water. When completely dissolved, the gel was placed in the refrigerator for 24 hours before use.

The Nafion polymer electrolyte was investigated to explore its suitability in providing an ionic conduction path for the electrochemical oxygen sensor. Nafion was obtained in a liquid form with relatively low viscosity and this proved to be difficult for thick film printing as a non-uniform print was deposited onto the substrate through the screen mesh. Hence, in order

to add a relatively even layer of Nafion, the substrate with the printed electrodes was dipped into a solution of Nafion and left to dry in ambient conditions. Other attempts such as evaporating the sulphuric acid in the commercially obtained Nafion and doping with gelatine powder were explored in order to increase the viscosity.

The focus of this investigation includes the characterisation study of different electrolyte and membrane materials for application in a transcutaneous oxygen sensor. The effects of different temperature and environmental conditions on the chemical and physical properties were thoroughly investigated.

Using various sensors with either KNO_3 or Nafion as the electrolyte, several possible combinations with membrane materials were evaluated in search of interesting findings. Some sensors were fabricated without the membrane layer while others were covered with cellulose acetate (CA), polytetrafluoroethylene (PTFE), polyvinyl chloride (PVC) or Nafion. Finally, a top dielectric layer was printed to protect the conductors from exposure to atmospheric conditions.

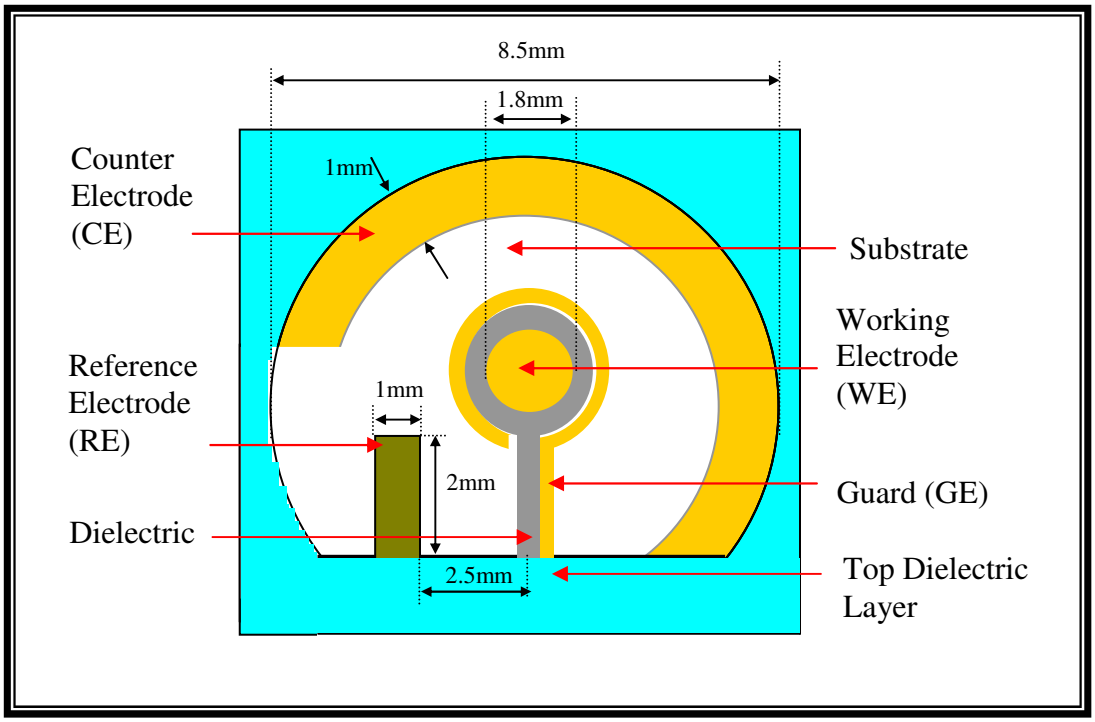

Figure 3.3: Schematic Layout of the Blood Gas Sensor Prototype

The electrochemical cell has the layout illustrated in Figure 3.3. The blood gas sensor prototype designed was a three-electrode electrochemical cell. The electrodes were connected

to an external measurement circuit, which is often referred to as the potentiostat. The reference electrode (RE), having high input impedance, and using non-polarizable material provided a fixed and stable potential with respect to time. The counter electrode (CE) acted as a current source required by the working electrode (WE) and provided a surface for a redox reaction to occur which balanced the one occurring at the WE. The electrolyte was printed over the whole area shown in Figure 3.3 and left in normal room conditions to be cured. Lastly, the membrane layer was applied and once dried, it was ready to be used in the experiments.

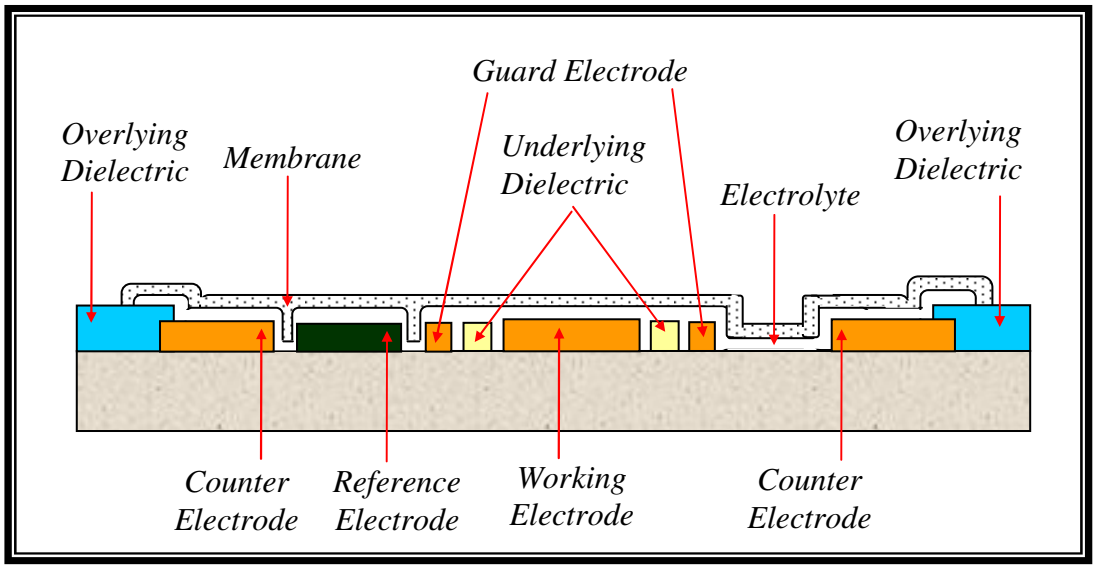

Figure 3.4: Schematic Diagram of the Cross-sectional Area of the Blood Gas Sensor Prototype

Figure 3.3 shows the sensor layout and Figure 3.4 describes its cross-sectional area. The working electrode (WE) was circular with an approximate diameter of 1.8 mm. It was surrounded by a 0.3mm wide gold guard electrode (GE), which served the purpose of minimising the influences of atmospheric oxygen on the transcutaneous measurment. In between the WE and GE, a 0.5 mm ring of underlying non-porous dielectric was printed to provide electrical isolation between the electrodes as well as preventing exposure to water. For even current distribution, the geometry of the prototype was designed to enclose the WE and GE with a wider (1 mm) gold counter electrode (CE). A larger CE as compared to the WE was encouraged so that no serious polarization should occur at CE [32, 48, 49]. Conforming to the requirements of compactness and miniaturization of the overall sensor, the area of each electrode was also designed to be sufficiently large so as to support minimum

current measurements in the order of microamperes. The printed Ag/AgCl reference electrode (RE) was positioned near CE and WE in this three-electrode configuration and it was in the form of a small (2 mm by 1 mm) rectangular block.

Different electrolyte and membrane materials took on different thicknesses during fabrication. The viscosity of the ink as well as the nature of the materials determined this parameter. The effects of membrane thickness were investigated and the findings are reported in Chapter 4.

3.2 Potentiostat

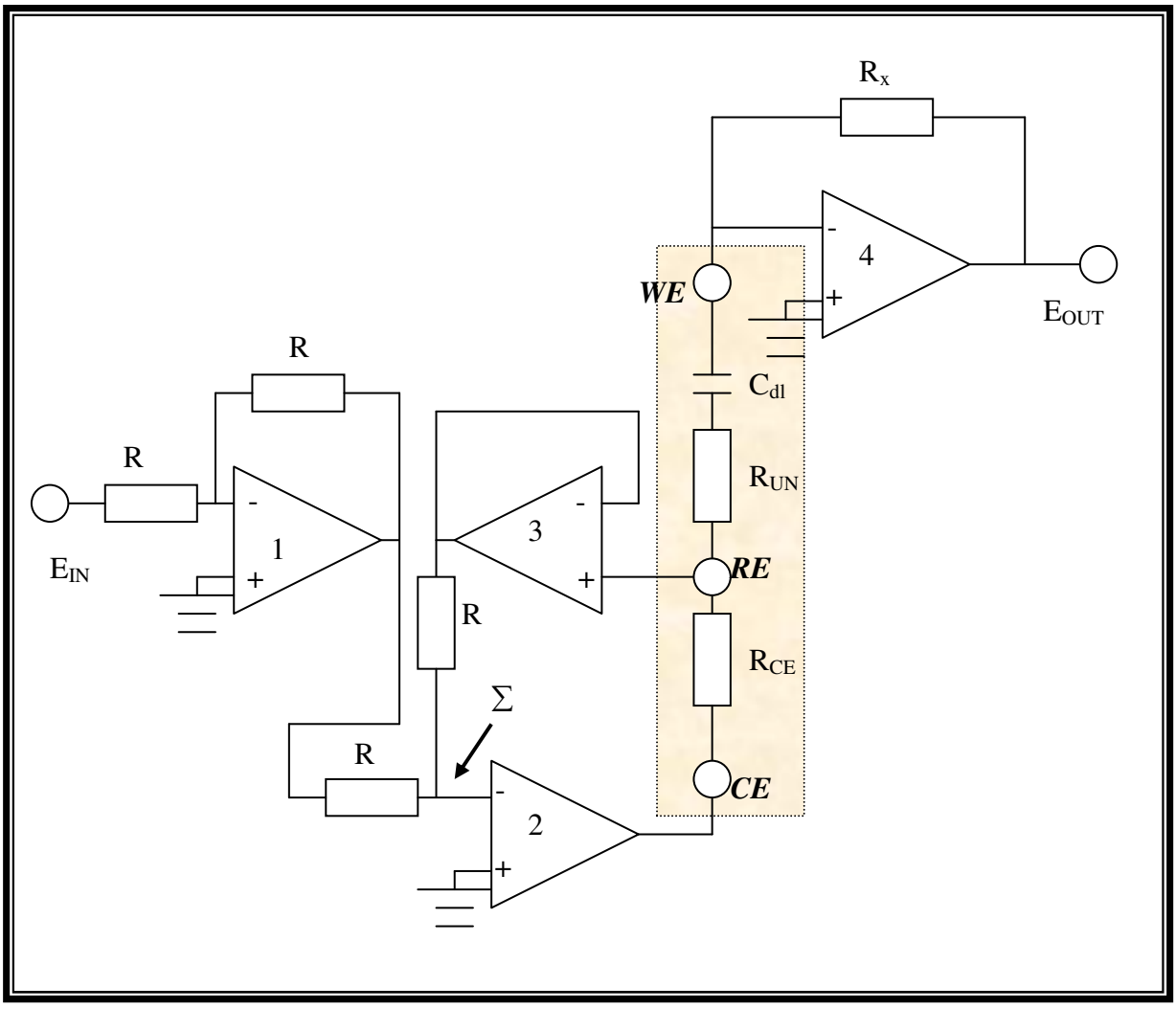

Figure 3.5: Functional Block of the Potentiostat Circuit

The potentiostat is a voltage feedback measurement circuit and Figure 3.5 shows a representation of the functional block. The shaded region depicts the electrical representation

of the three-electrode sensor. A resistance R_{CE} dominates the impedance effect along the current path between RE and CE. Between RE and WE, an uncompensated resistance (R_{UN}) and a series double layer capacitance (C_{dl}) are present. The resistance, R_{UN} is the intrinsic resistance contributed by the electrolytic path between RE and WE and it is present as long as the three-electrode configuration is laid out as shown in Figure 3.5 to form an electrical double layer.

The theory of the electrical double layer involves the charge distribution and electrical potentials that are the consequences of a charge separation [50]. Along any interface between two phases such as the electrodes and electrolyte solution, there is bound to be a segregation of positive and negative charges in the direction perpendicular to the phase boundary. The equilibrium established at the interface is not chemical since both phases do not have any common components. The set-up of RE and WE with an electrolyte solution in between is analogous to a parallel plate capacitor and this evolves to an electrostatic equilibrium. In the case where there is no external source applied at the electrodes, the charges within the electrolyte are still subjected to thermal motion. With this, a simple Helmholtz model as illustrated in Figure 3.6 is used to describe the electrical double layer.

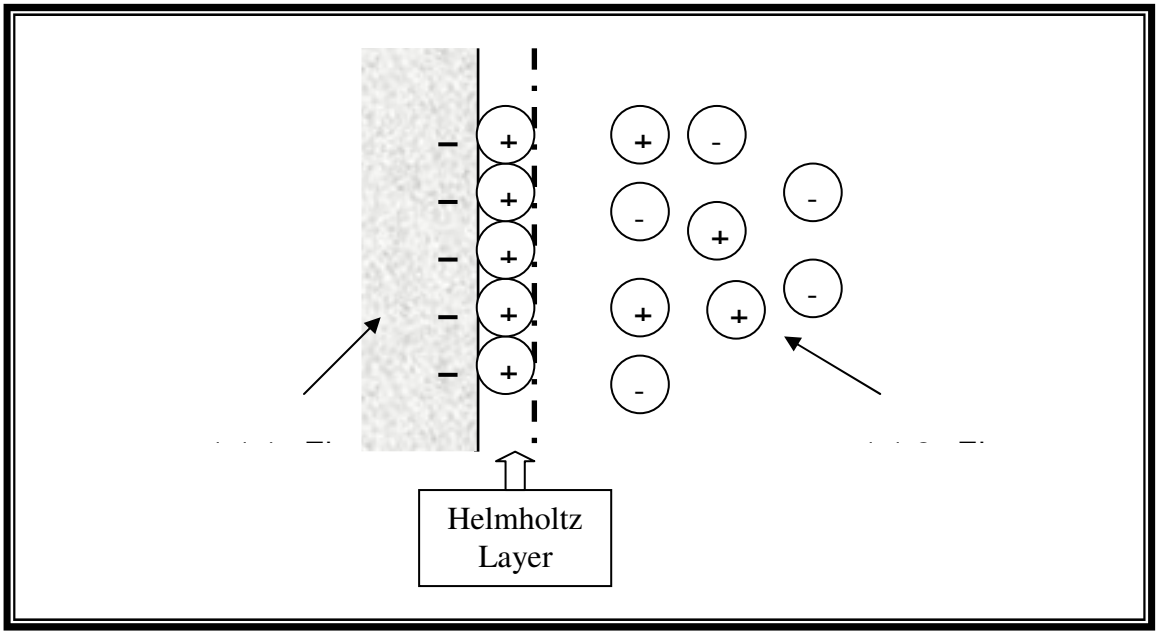

Figure 3.6: Helmholtz Layer Model of a Electrical Double Layer

In Figure 3.5, operational amplifier (Op-Amp) 2 provides a feedback loop and this drives the current between WE and CE. The output was hence adjusted to control the current flowing

through R_{CE} and R_{UN} so that the voltage potential at RE would be maintained at E_{IN}, despite having R_{CE} and R_{UN} fluctuating due to the changes in oxygen levels. The fluctuations were reflected in the shifts of the CE potential. E_{IN} was the input biasing voltage that was required to drive the performance of the sensor into the current diffusion plateau. The feedback loop also served the purpose of ensuring the input current drawn by the potentiostat would not be too large. E_{OUT} was measured and current (I) could be obtained from $\frac{E_{OUT}}{R_x}$. With the sensor connected to the potentiostat, experiments were carried out for practical measurements.

3.3 Heater Module

3.3.1 Heating Circuit

The heating circuit module was essential for transcutaneous measurement. The main objective of this module was to regulate the temperature of the heating element at the desired set point temperature (typically at 44 °C) despite changes in the environment. Initially for simplicity, the circuit was designed with two platinum elements where one was connected in a wheatstone bridge configuration for feedback monitoring of the current temperature and the other was connected at the output as the heating element. The concept of the circuit is shown in Figure 3.7 and basically provides the heating element with a current large enough to bring the temperature of the skin surface up to approximately 44 °C. The temperature of the sensor was meanwhile monitored by another platinum element on the same substrate as a feedback element. If there was a deviation from the set temperature, the wheatstone bridge would be unbalanced to give a non-zero output potential difference and this would be detected by a differential amplifier. It would then automatically increase its current output to elevate the temperature of the heating element. This way, the set temperature was regulated by this heating circuit module and its corresponding schematic is provided in Figure 3.8.

An improvement was then made on the initial design, which employed two platinum strips as shown in Figure 3.8 [51]. Only one strip was required for both the heating and feedback purposes. This design was achieved by introducing the platinum heater in a wheatstone bridge configuration that had the input point *A* of the bridge connected to the output path of a

18W power amplifier (TDA2030). The power amplifier was needed to heat up the platinum element to approximately 43 °C.

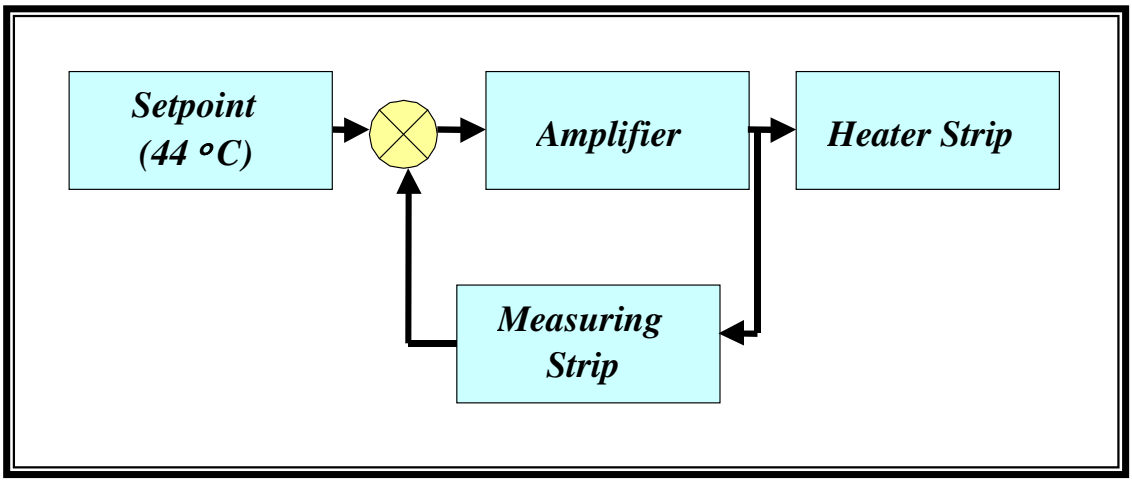

Figure 3.7: Block Diagram of the Heating Circuit

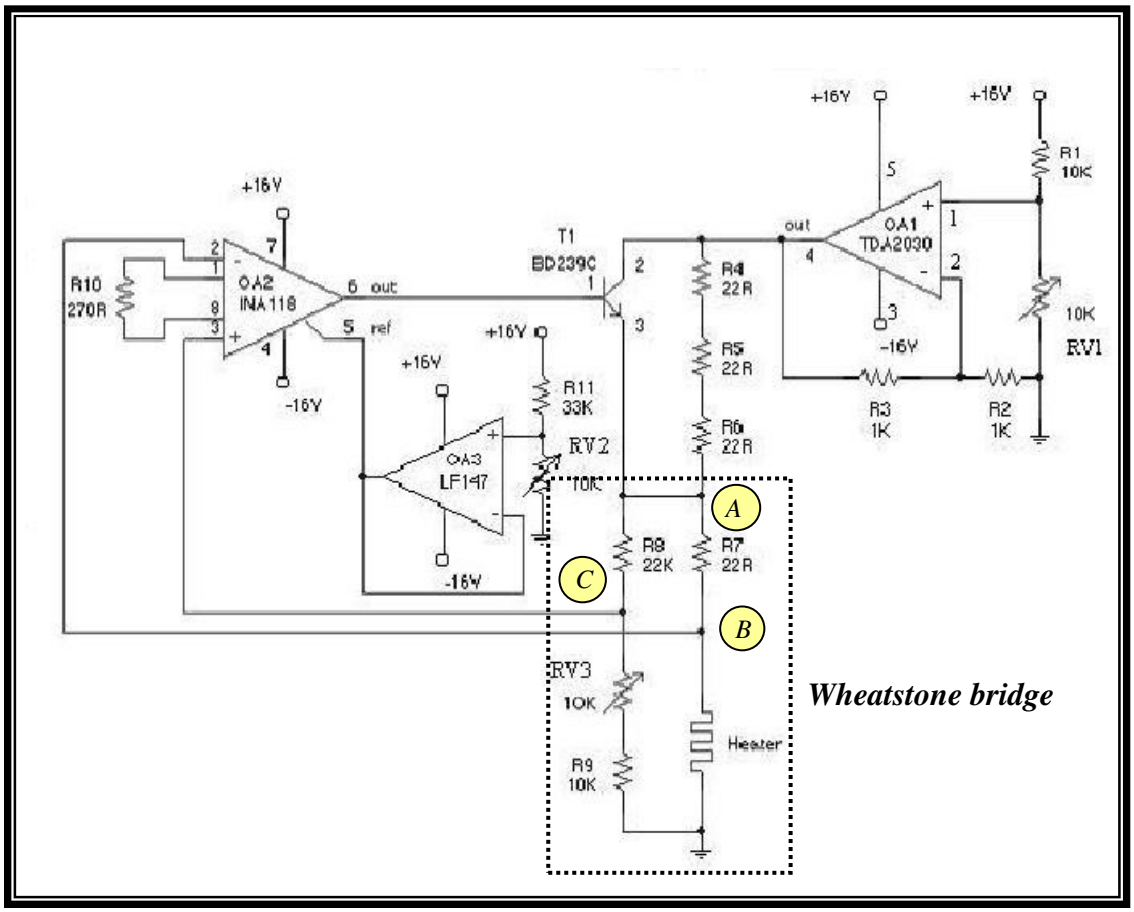

Figure 3.8: Heating Control Circuit using Single Heater Element

The operating point of the circuit depended mainly on two variables namely the gain and the reference voltage of the differential amplifier. The circuit allowed adjustment to be made to the supply voltage and the reference voltage. All resistors were soldered onto the PCB to ensure circuit stability from electrical noise.

The gain value controlled the speed at which the element heated up and this proved to be important for the long term stability of the circuit. The circuit would also respond almost instantaneously to any sudden change of conditions. With a resistor of 270Ω connected to pin 1 and 8 of the differential amplifier INA118, the gain was set to approximately 186.

The reference voltage of the differential amplifier played a significant role in determining the difference between the temperatures of the sensor before and after application onto the measured surface. If the reference voltage was set to a higher level, the difference in the temperatures would be lower. Hence, it would be appropriate to adjust the reference voltage as close as possible to the voltage on the Wheatstone bridge at 44°C. However, adjustment margins were given when carrying out the tuning in order to avoid over-heating of the sensor. The experiments were carried out with a reference voltage of 2V to demonstrate the circuit properties. Before tuning the circuit, the resistance of the heater was known.

Point *A* acted as a summing junction for another electrical path involving a switching transistor (BD 239C) that provided the fine tuning capability of the overall circuit. The switch would be activated by a comparator (INA 118) if the output points *B* and *C* of the wheatstone bridge are not balanced. The operational amplifier (LF 147) was to provide an electrically isolated reference voltage level to the comparator. The variable resistor (RV3) was used to adjust the required resistance value so as to match the resistance of the heater element at 44 °C. Conceptually, this circuit would provide a basic current level to bring the temperature of the heating element to approximately 43°C. The switching transistor will then add current through the element to increase the temperature to 44 °C. When changes in the surrounding temperature were encountered, the switching transistor would respond correspondingly to maintain the temperature at 44 °C by allowing a different amount of current to the summing junction *A*.

This way, the element was regulated at the desired transcutaneous temperature despite the possible adverse variation in surrounding temperature.

3.3.2 Heater Element

A cermet platinum ink (Part Number: ESL-5545) was employed to print the elements with a low resistivity value of approximately 60 mΩ per square (mΩ/□) to 80 mΩ/□. This ink was provided by Electro-Science Laboratories, and would be suitable for thermometer, heater and sensor designs. The relationship between the resistance and temperature is documented and known to be linear over a wide range of –50 °C to 500 °C [52]. Figure 3.9 shows an example of the heater element layout which is designed to have a resistance of approximately 15 Ω. A microscopic view of the platinum heater strip is also enlarged to illustrate the microstructure of the material.

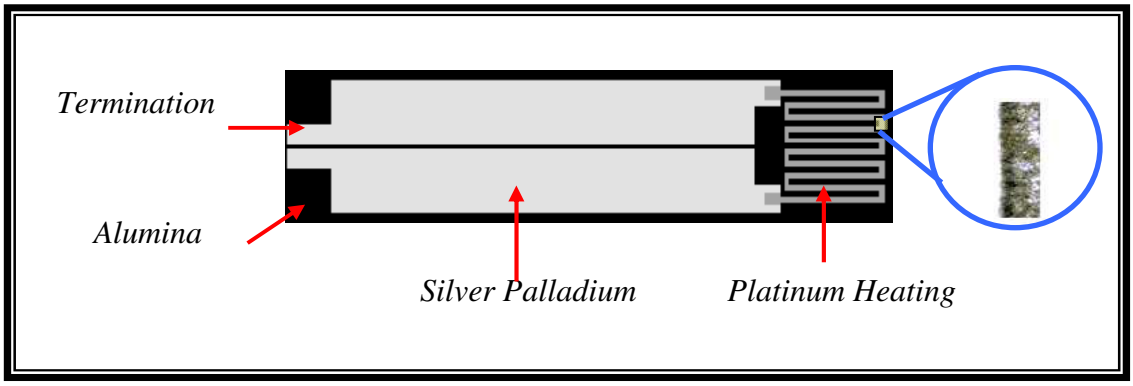

Figure 3.9: Heating Element

In practice, the total resistance of each sample measured at the termination pads was approximately 15 Ω to 18 Ω depending on the inconsistencies inherited during printing. These inconsistencies were usually caused by the inappropriate viscosity level of the ink prepared for printing and the thickness of the ink being deposited on the substrate. The effects of these differences were compensated by the proper calibration of the heating circuit with respect to each sensor.

Chapter 4 Theoretical Modeling for 1-Dimensional Diffusion

The main objectives of this chapter are to analyze the material's surface contour and thickness as well as focus on the effects of these parameters in a theoretical diffusion model prior to actual practical experiments.

4.1 Electrode Material and Structure

The oxygen sensing module of the prototype consisted of a gold working electrode (WE), counter electrode (CE), guard electrode (GE) and a silver/silver chloride reference electrode (RE). The gold material used was cermet ESL 8836, an economical choice usually employed for general purpose conductors on alumina. Figure 4.1 shows the microscopic view of the printed gold (ESL-8836) electrodes at (a) 50 times its original size and (b) 200 times its original size.

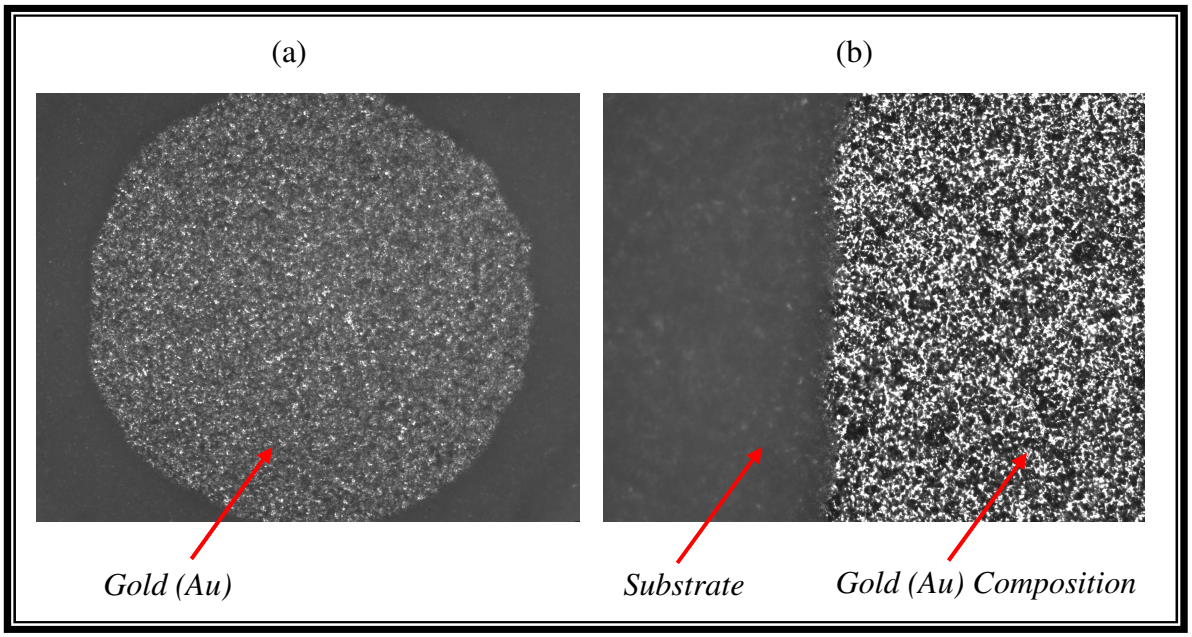

Figure 4.1: Gold (Au) Structure at (a) 50 times and (b) 200 Times its Original Size

From Figures 4.1 (a) and (b), it can be seen that the cermet gold ink has a densely bound grain structure following firing. It has a resistivity of approximately 6 mΩ/ and can remain stable at high temperature up to 150 °C.

Figure 4.2 illustrates the surface contour of the printed gold electrodes over a 1mm by 1.5mm area obtained using a confocal measurement technique that included a laser focus displacement meter from Keyence Corporation of America (LT series) and a motion controller from Newport Corporation (MM4006). Supporting Matlab programs were used to analyze the acquired data. The 3-dimensional representation of the gold surface depicts the printed layer as relatively homogenous and consistent. This suggests that the surface of the gold interfacing with the next layer of material would be maximized, which ought to facilitate redox reactions on the electrodes more effectively. In all the confocal measurements, the absolute values along the x-, y- and z-axes were arbitrarily allocated. The important information extracted from the reconstructed representation was the relative thickness of different layers.

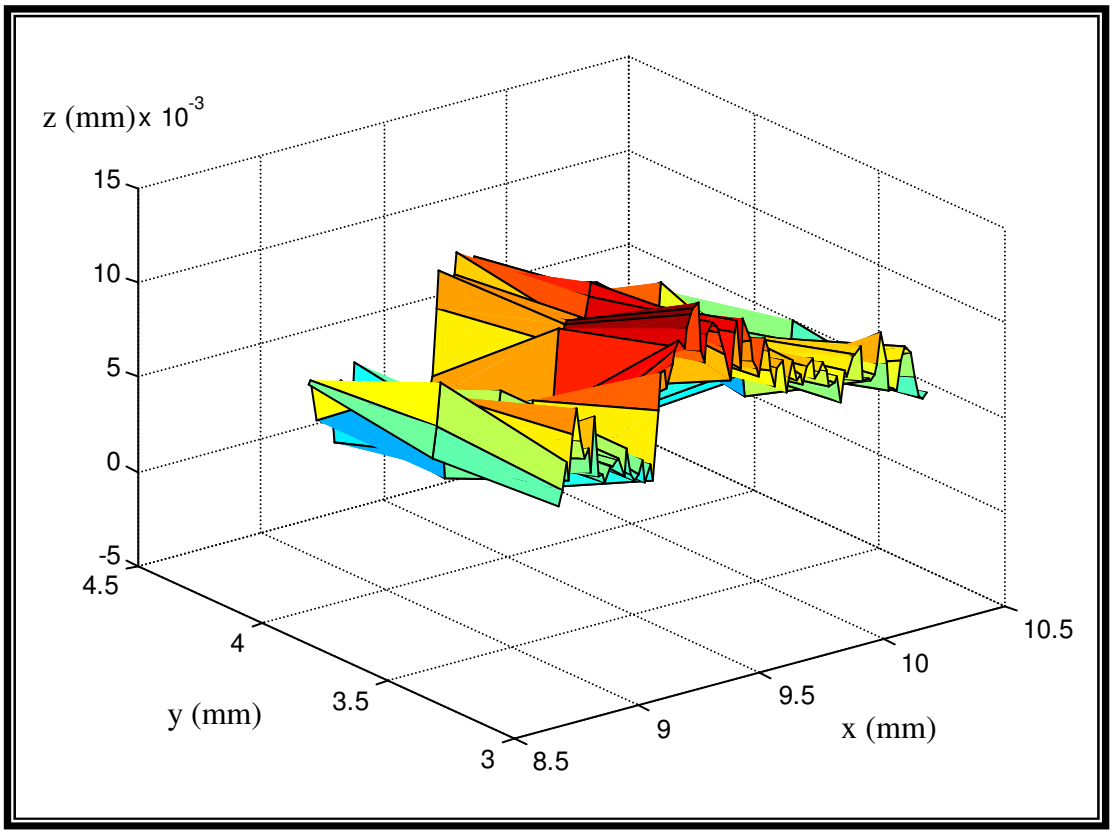

Figure 4.2: 3-D Surface Contour of Gold Electrodes

Figure 4.3 shows the corresponding 2-dimensional cross-sectional view where the thickness of the gold electrode is estimated at approximately 7 µm. It was observed that the surface appeared to be uneven at such high magnification especially at the edge of the printed electrode. Practically, this irregularity would not cause a significant amount of error in the overall current output since calibration would always be carried out prior to the measurements.

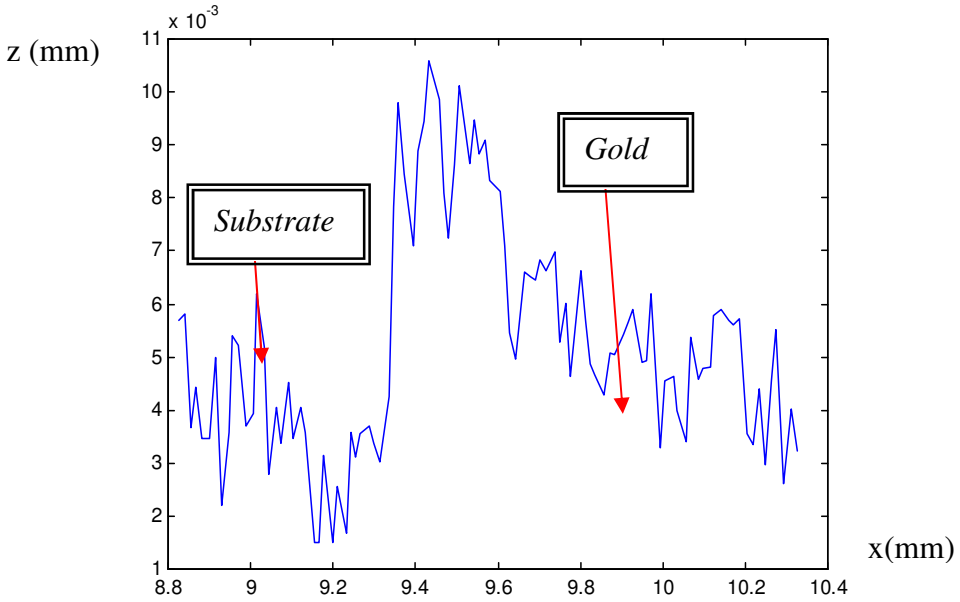

Figure 4.3: 2-D Cross-sectional Profile of Gold Electrodes

Figures 4.4 (a) and (b) illustrate the Ag/AgCl reference electrode structure at 50 and 200 times the original size respectively. The Ag/AgCl [53] ink was made from roll-milling silver chloride power (Aldrich 99%) and silver powder (Aldrich 99%) at the weight ratio of 2:1 using an Heraeus overglaze (IP9027) as the glassy binder. In Figure 4.4 (a), there is a dark shaded line near the middle of the diagram indicating an uneven surface probably due to the fact that there was an underlying printed layer of silver, which occupied a smaller area as compared to Ag/AgCl layer. Figure 4.4 (b) shows that the in-house roll-milled Ag/AgCl did not contain comparable sized particles and it seemed to be bound together in a random manner by the cured glassy binder.

The corresponding 2-dimensional and 3-dimensional representations of the surface contour are given in Figures 4.5 and 4.6 respectively. The thickness of Ag/AgCl was measured at

~20 µm. A gentle peak at the middle of the Ag/AgCl further confirmed the protrusion of the underlying Ag conductor.

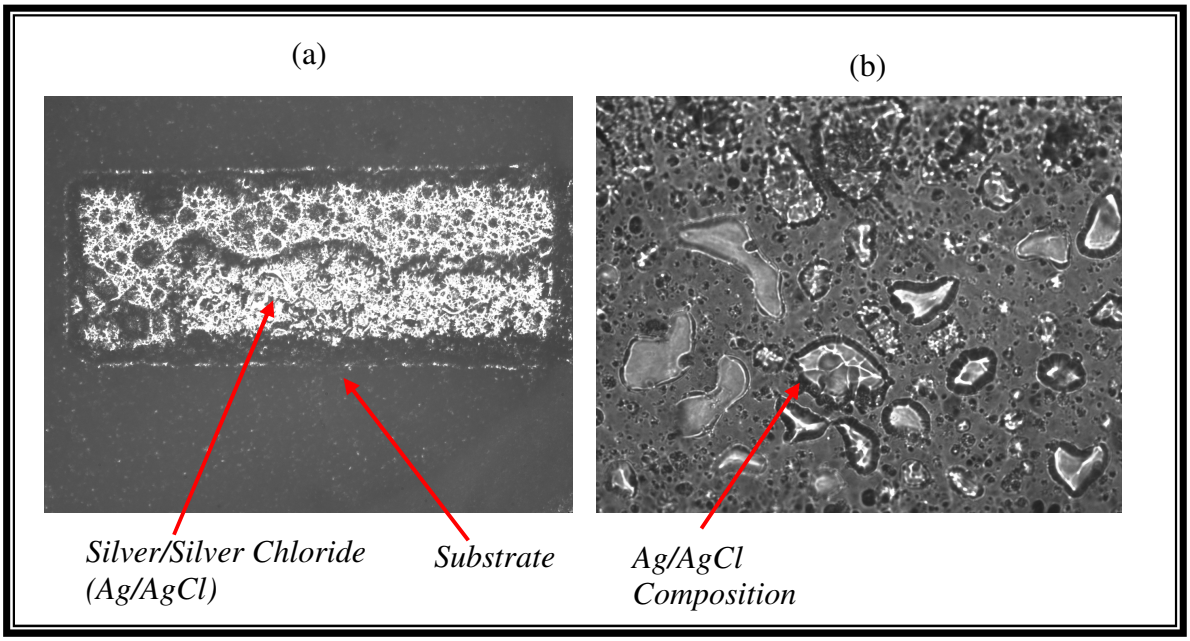

Figure 4.4: Silver/Silver Chloride (Ag/AgCl) Structure at (a) 50 times and (b) 200 Times its Original Size

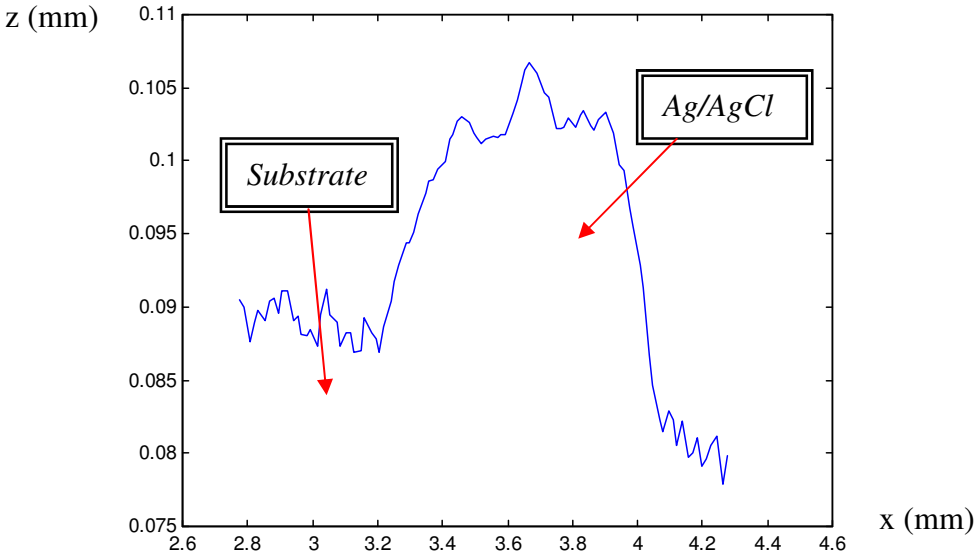

Figure 4.5: 2-D Cross-sectional Profile of Silver/Silver Chloride (Ag/AgCl) Reference Electrode

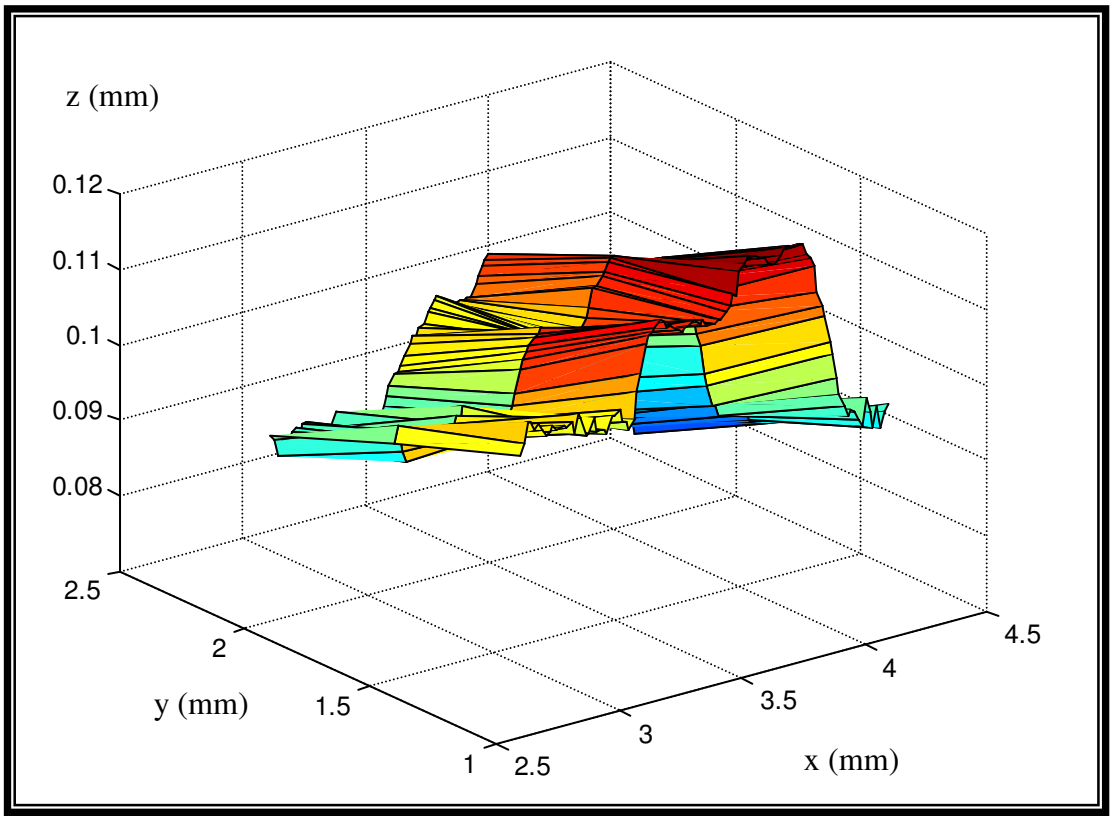

Figure 4.6: 3-D Surface Contour of Silver/Silver Chloride (Ag/AgCl) Reference Electrode

4.2 Electrolyte Material and Structure

Two different types of electrolyte materials were used in the experimental prototypes of the transcutaneous oxygen sensor. An aqueous salt electrolyte using potassium nitrate gel (KNO_3) was employed to provide ionic paths in order to complete the electrochemical cell. Figure 4.7 shows the microscopic view of the KNO_3 gel layer. It can be clearly seen that the KNO_3 gel when cured gave a lattice formation as shown in Figure 4.7(a). Although KNO_3 powder was dissolved in de-ionized water, the crystal structure remained intact when the material was kept dry. When hydrated, the electrolyte conveniently ionized to K^+ and NO_3^- to facilitate ionic conduction.

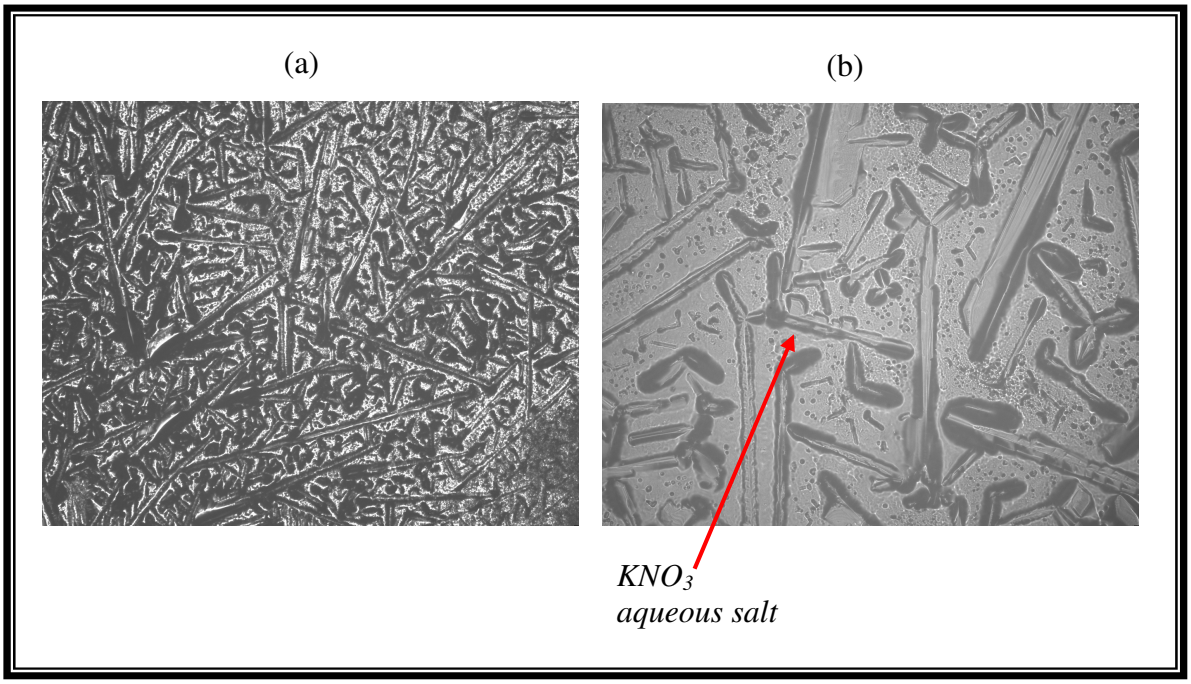

Figure 4.7: Potassium Nitrate (KNO_3) Structure at (a) 50 times and (b) 200 Times its Original Size

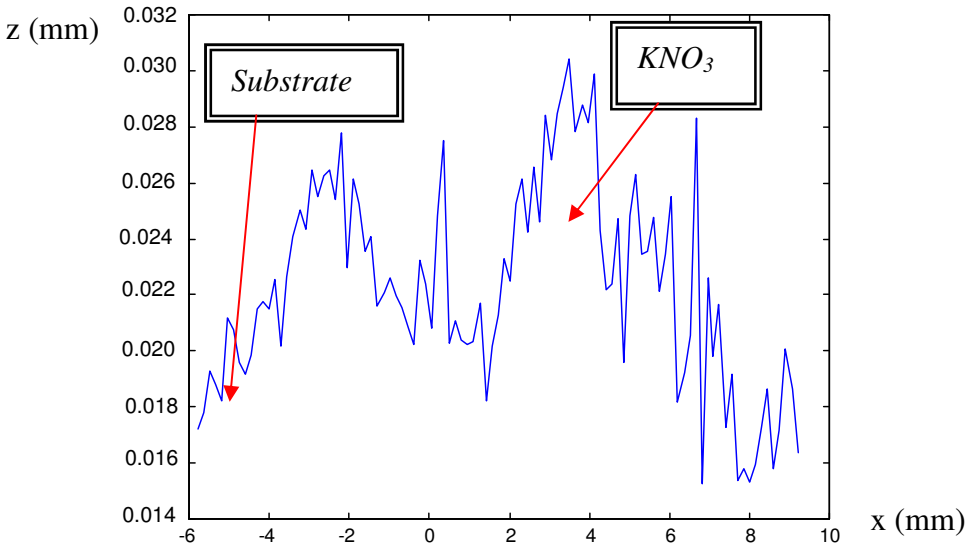

Figure 4.8: 2-D Cross-sectional Profile of Potassium Nitrate (KNO_3) Electrolyte Layer

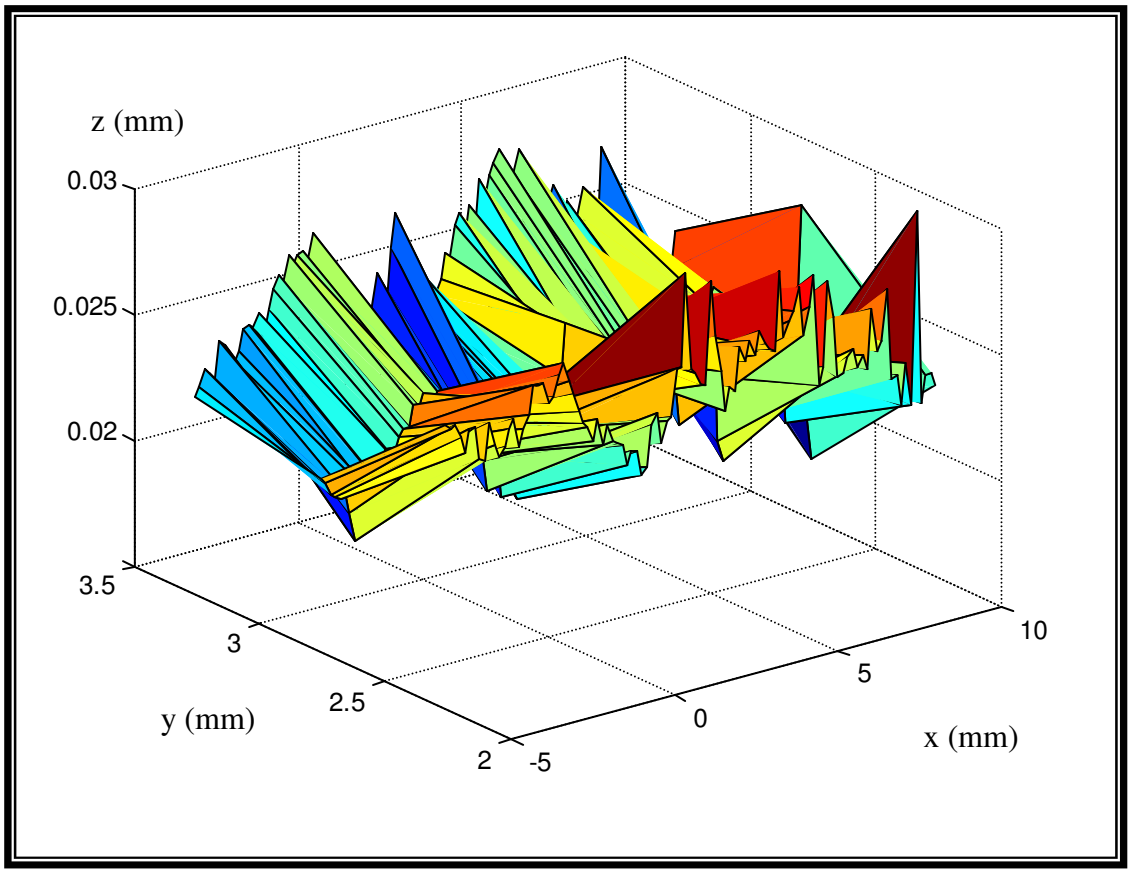

Figure 4.9: 3-D Surface Contour of Potassium Nitrate (KNO_3) Electrolyte Layer

A 2-dimensional representation of the surface contour is illustrated in Figure 4.8. The equivalent 3-D view is shown in Figure 4.9 where the 15 µm KNO_3 layer gives a slightly uneven surface contour, probably due to the crystalline KNO_3 structures contained within the gel as denoted in Figure 4.7. The thin layer proved to be essential because when oxygen diffused through the electrolyte to reach the electrode surface, the average current distribution would be effectively consistent over the whole surface area where the redox reaction would take place at an appropriate input biasing voltage, given a particular oxygen level.

Nafion was also adopted to extend the investigation into polymer electrolytes. Figure 4.10 shows the structure of dried Nafion on the alumina substrate. It can be seen that Nafion deposits a very thin layer onto the substrate. This observation would account for the overall lower current measured as compared to the measurement made using KNO_3 electrolyte

during the experiments. The thickness of the Nafion layer is estimated to be approximately 7 μm from Figure 4.11.

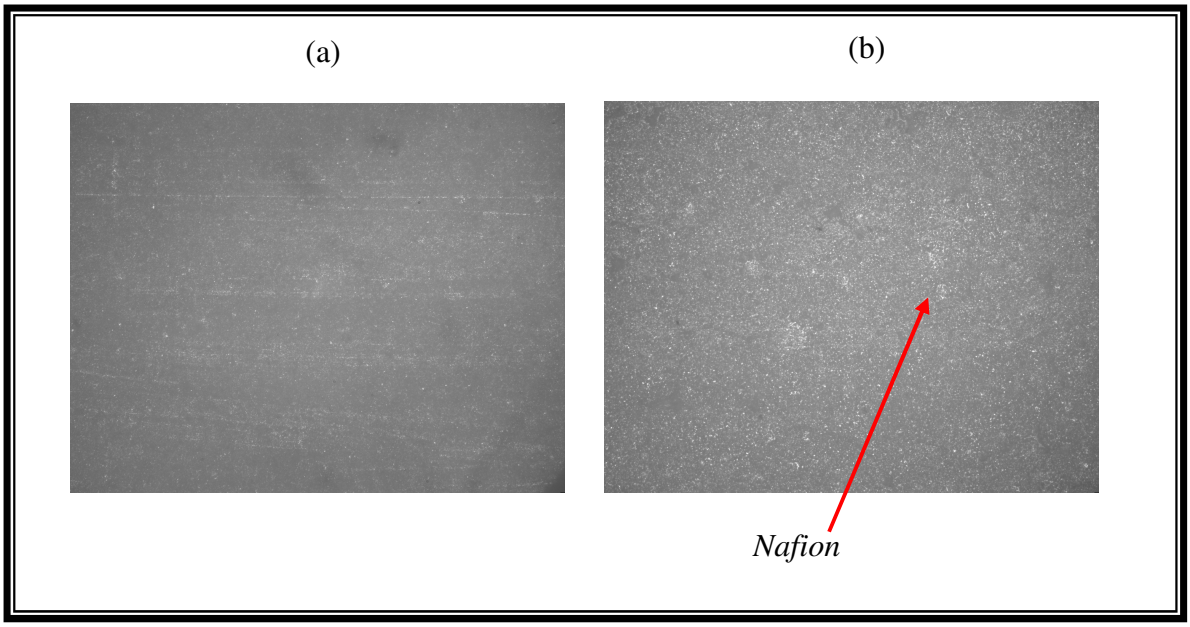

Figure 4.10: Nafion Structure at (a) 50 times and (b) 200 Times its Original Size

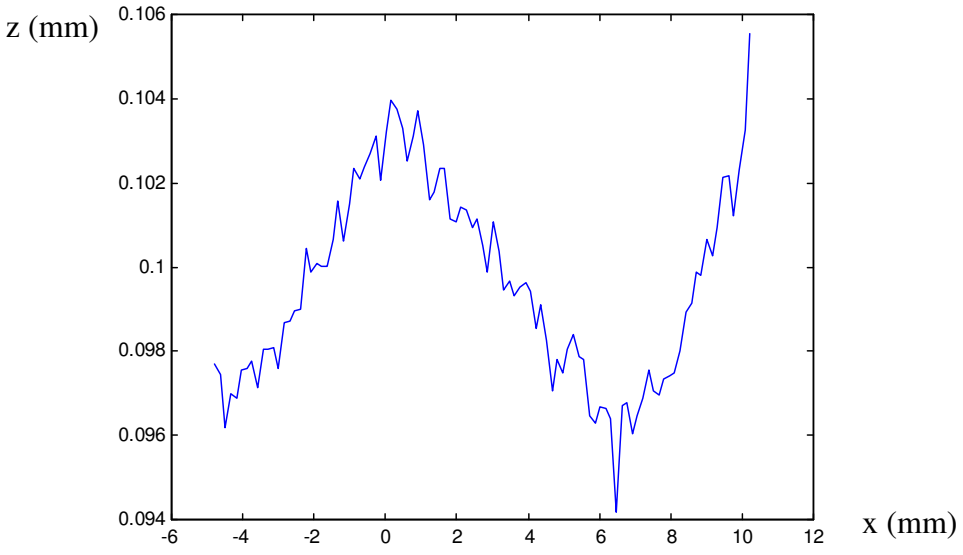

Figure 4.11: 2-D Cross-sectional Profile of Nafion Electrolyte / Membrane Layer

From Figure 4.12, one obvious advantage of employing Nafion as the electrolyte was the reduction of layer thickness in the final prototype. With further improvement made on Nafion,

the transcutaneous sensor could possibly migrate relatively easily from microscale to nanoscale technology.

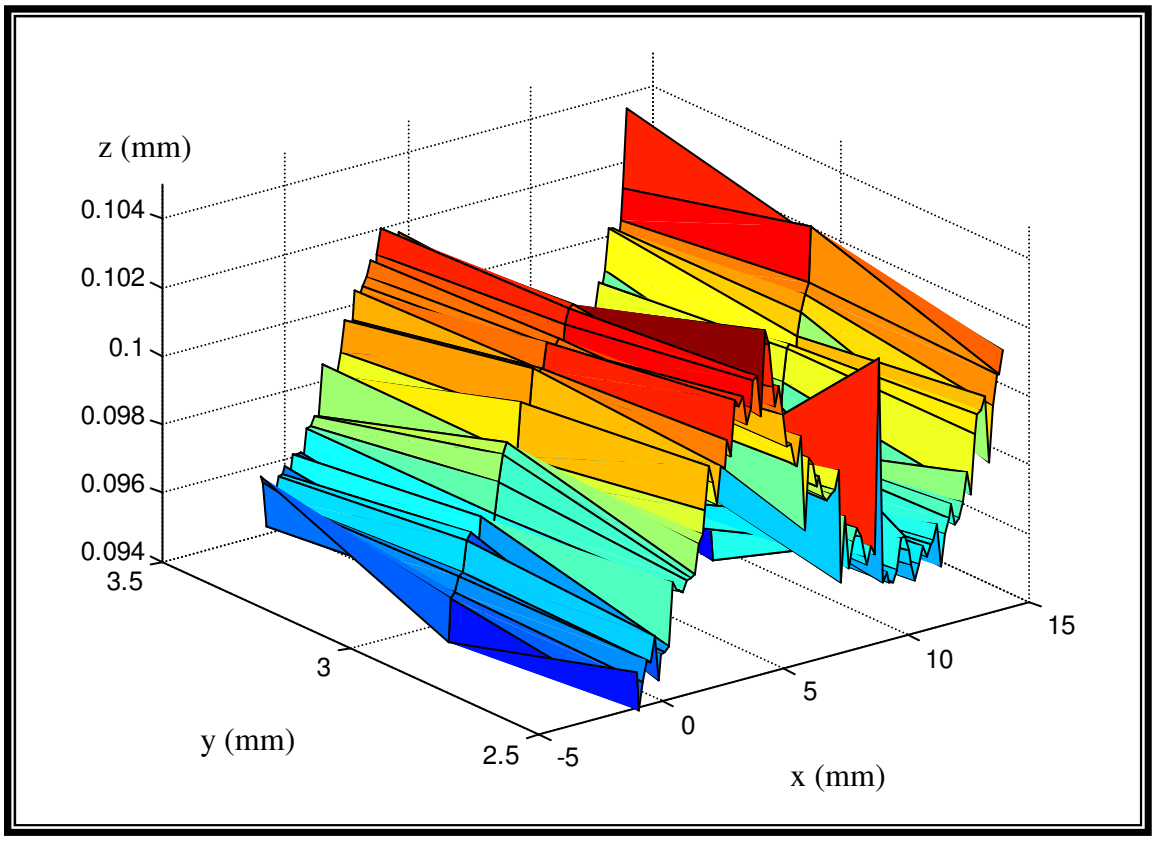

Figure 4.12: 3-D Surface Contour of Nafion Electrolyte / Membrane Layer

4.3 Membrane Material and Structure

Three main membrane materials namely cellulose acetate (CA), polyvinyl chloride (PVC) and polytetrafluoroethylene (PTFE) were studied. Firstly, a layer of CA was observed under a microscope and the results are presented in Figure 4.13. At 50 times the original size, CA appeared to form row structures in the direction of the printing action. It also provided pores, which seemed large enough for water molecules to percolate through.

Upon close magnification of 200 times, CA was observed to cure in a polygonal manner. From Figure 4.13 (b), the different shades of reflection suggested that the CA surface could develop several depths of contours. This hypothesis was further evaluated by using confocal measurement to re-construct the surface metrology as shown in Figure 4.14. An equivalent 2-dimensional representation is given in Figure 4.15 from which the thickness of the CA layer

can be estimated to be approximately 38 μm. From the profile representations, it was seen that the edge of the CA material with respect to the substrate experienced a gradual change in gradient. The inconsistency in surface smoothness was inherited from the screen printing process.

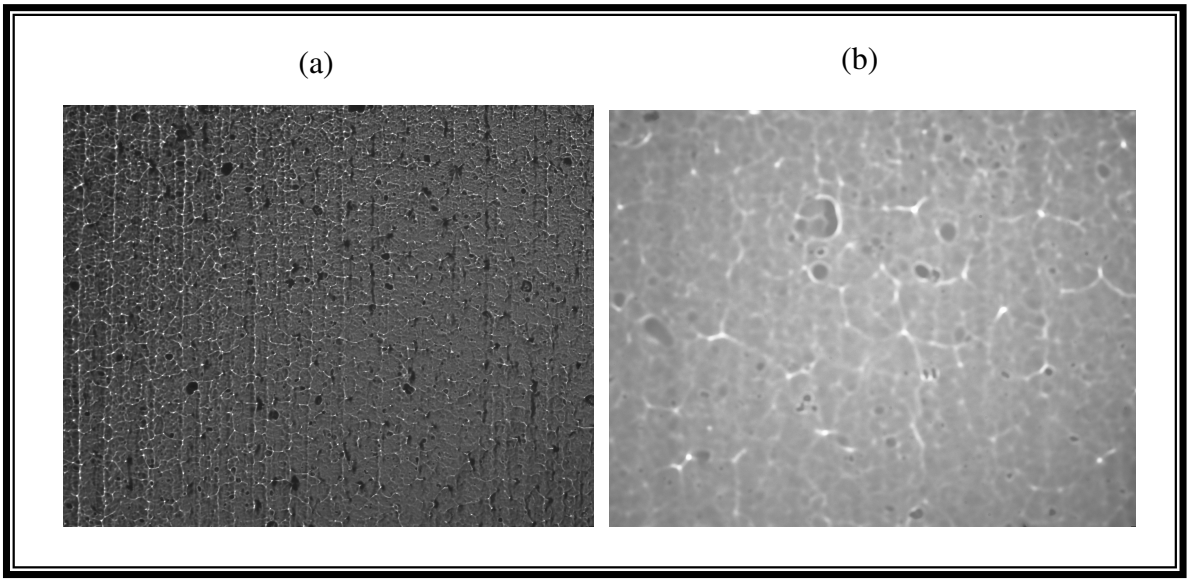

Figure 4.13: Cellulose Acetate (CA) Structure
at (a) 50 times and (b) 200 Times its Original Size

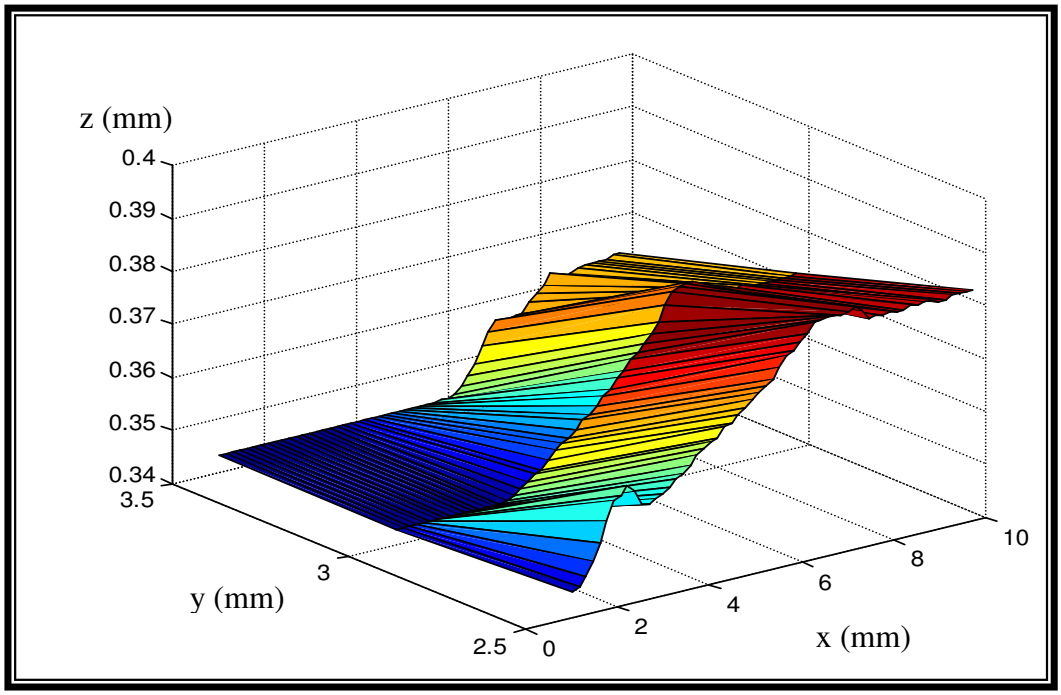

Figure 4.14: 3-D Surface Contour of Cellulose Acetate (CA) Membrane Layer

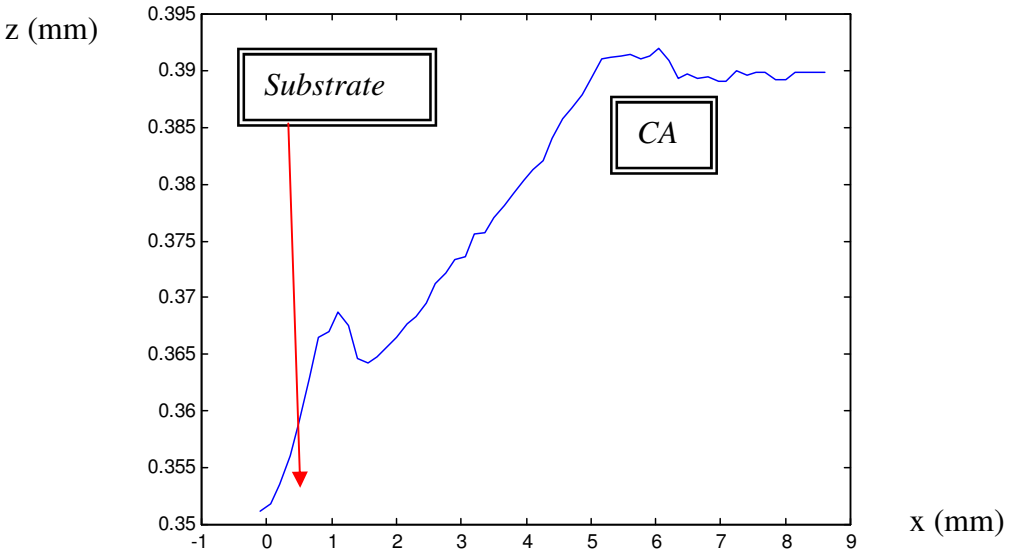

Figure 4.15: 2-D Cross-sectional Profile of Cellulose Acetate (CA) Membrane Layer

Polyvinyl chloride (PVC) powder was dissolved in cyclohexane to form a printable ink for thick film fabrication. When cured under ambient conditions, PVC formed a membrane layer over the substrate as seen enlarged in Figure 4.16.

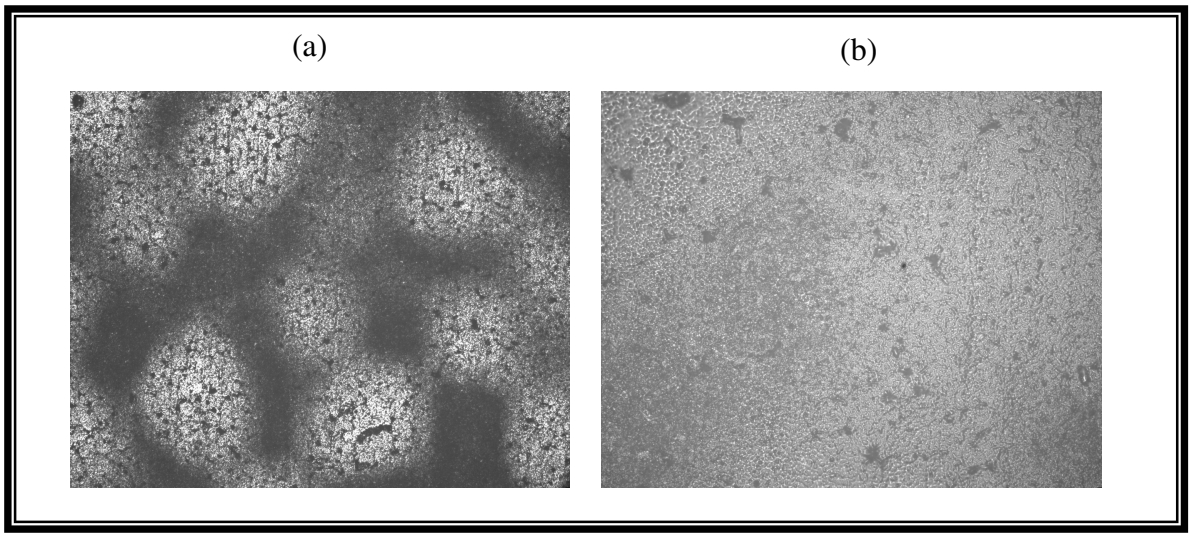

Figure 4.16: Polyvinyl Chloride (PVC) Structure at (a) 50 times and (b) 200 Times its Original Size

Figure 4.16 (a) shows that PVC forms patches throughout the measured area. It suggested that there was a high possibility of inconsistency in this material. Upon magnification of 200 times the original grain size as depicted in Figure 4.16 (b), it can be seen that within the

elliptical patches, PVC cured to produce a close knitted structure that enhanced its waterproof characteristic. Figures 4.17 and 4.18 illustrate the 2-dimensional and 3-dimensional surface contour of the PVC layer respectively. PVC appeared to finish more coarsely with a membrane thickness of approximately 7 μm and was deemed suitable for gas diffusion.

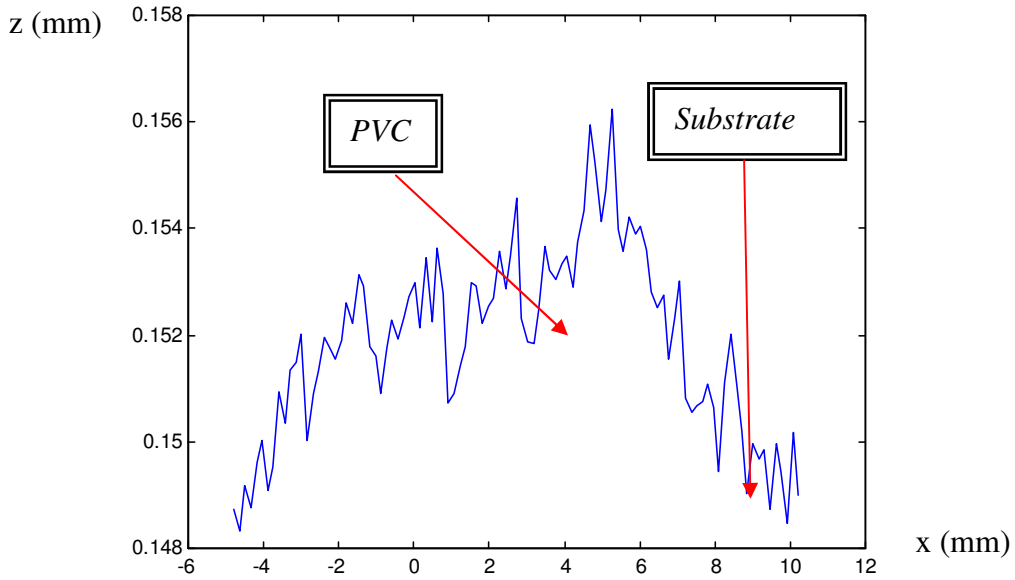

Figure 4.17: 2-D Cross-sectional Profile of Polyvinyl Chloride (PVC) Membrane Layer

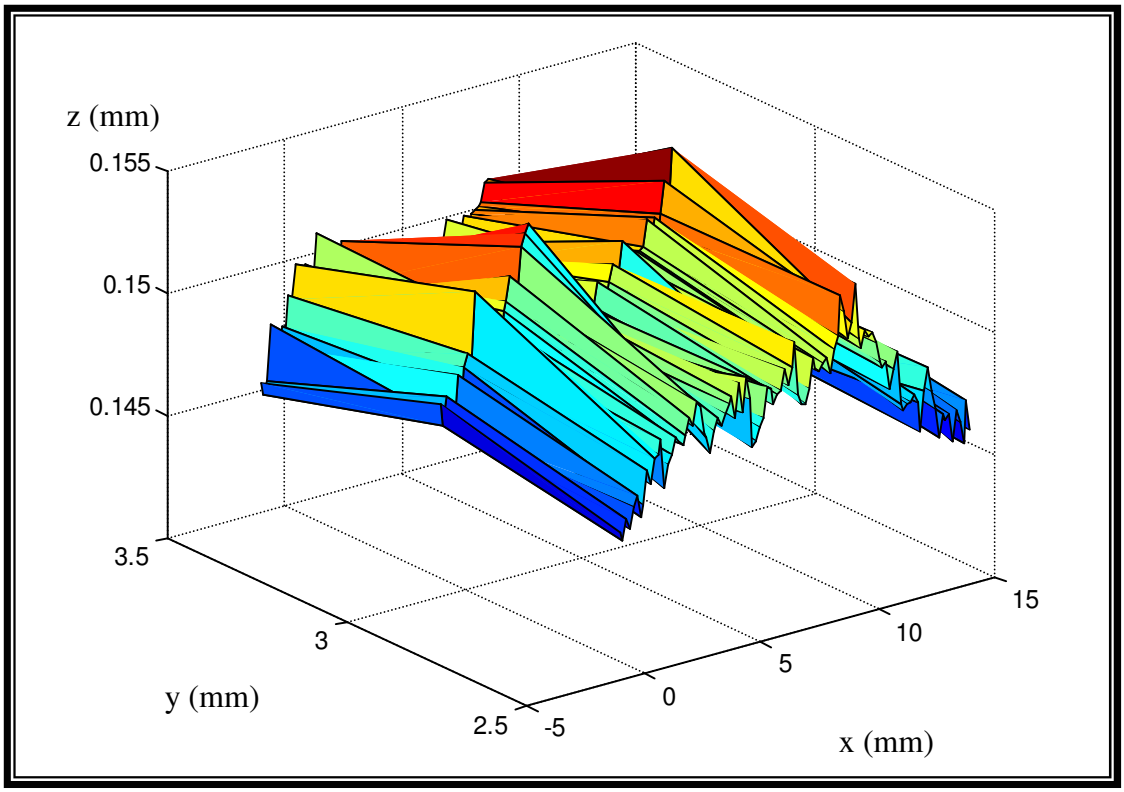

Figure 4.18: 3-D Surface Contour of Polyvinyl Chloride (PVC) Membrane Layer

The final material under investigation as a possible candidate as a membrane for the transcutaneous sensor was polytetrafluoroethylene (PTFE). Figure 4.19 presents the microscopic view of the surface structure.

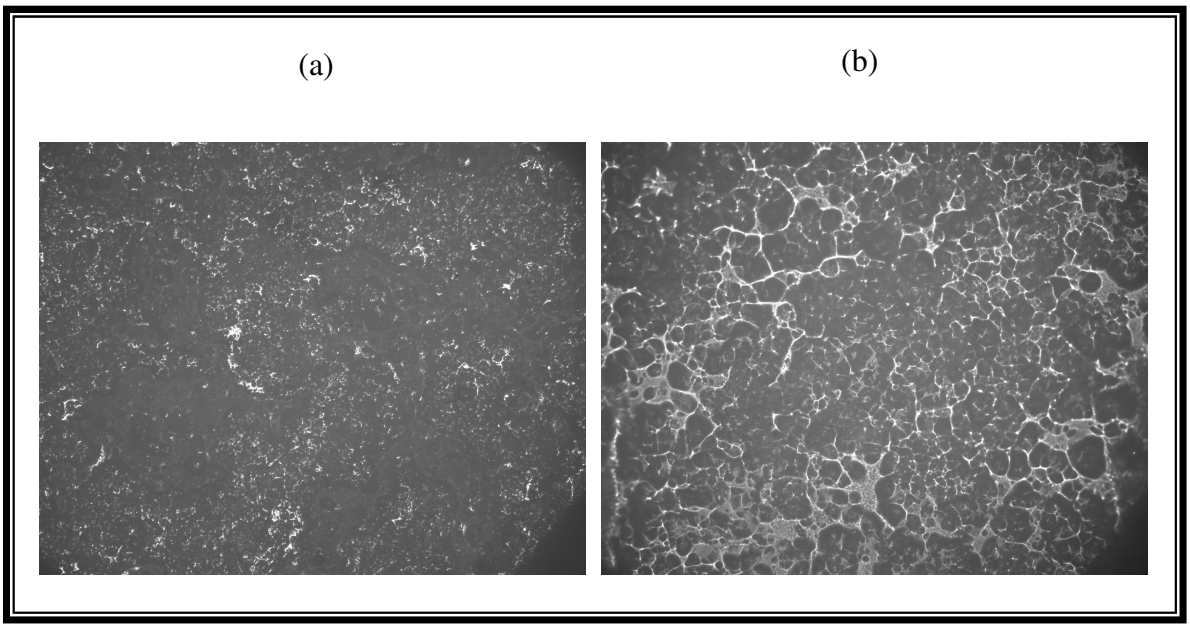

Figure 4.19: Polytetrafluoroethylene (PTFE)) Structure at (a) 50 times and (b) 200 Times its Original Size

The primary observation made from Figure 4.19 shows that the PTFE layer is relatively homogenous throughout the measured area. The 200 times enlargement, Figure 4.19(b) reveals that the binding arrangement allows visible pores for easy diffusion of gases. The surface contours in Figure 4.20 enforces this fact by illustrating the reconstruction of the PTFE layer more vividly. It also led to a detailed understanding of the membrane's performance during the subsequent experiments. The 2-dimensional cross-sectional view of the surface shown in Figure 4.21 allows the thickness of the PTFE layer to be determined at approximately 20 μm and this value is used in the theoretical model that analyzes the response time of the prototype. It was noticed that the surface contour was alternating between peaks and troughs as PTFE was sprayed onto the substrate, hence producing a relatively even-spaced array pattern. Deep troughs could also explain the possible high porosity of the membrane.

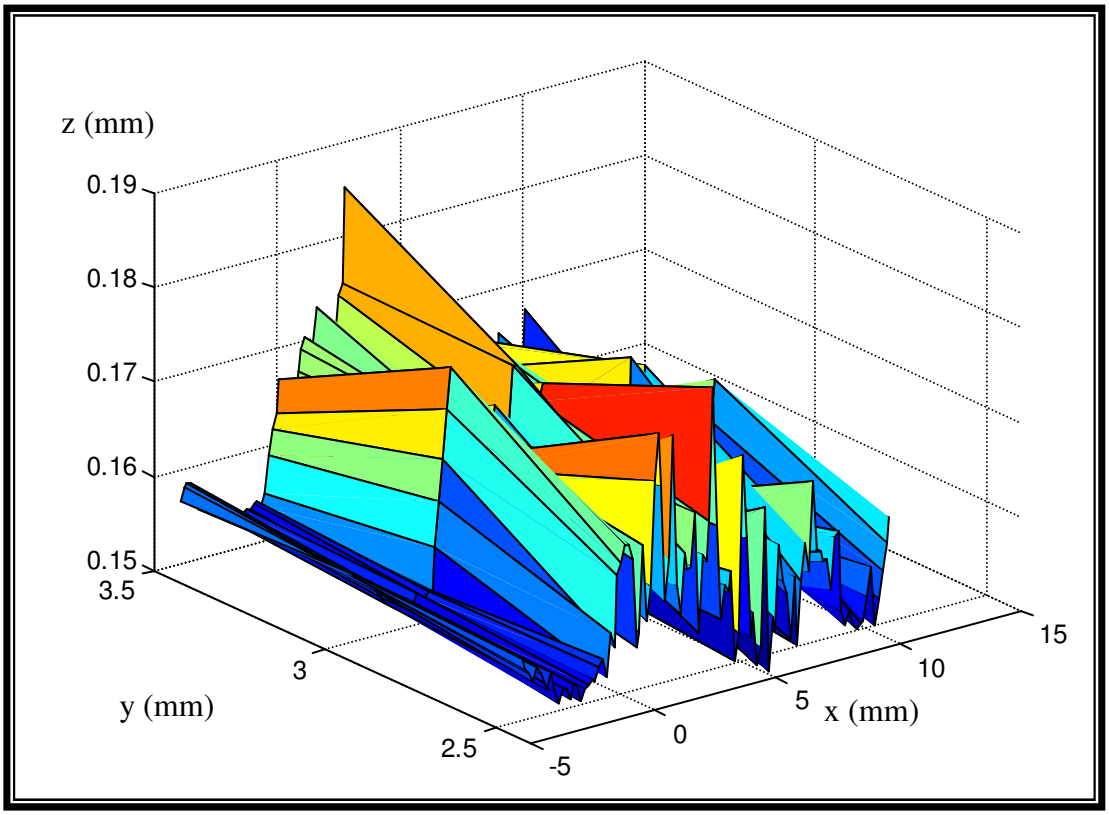

Figure 4.20: 3-D Surface Contour of PTFE Membrane Layer

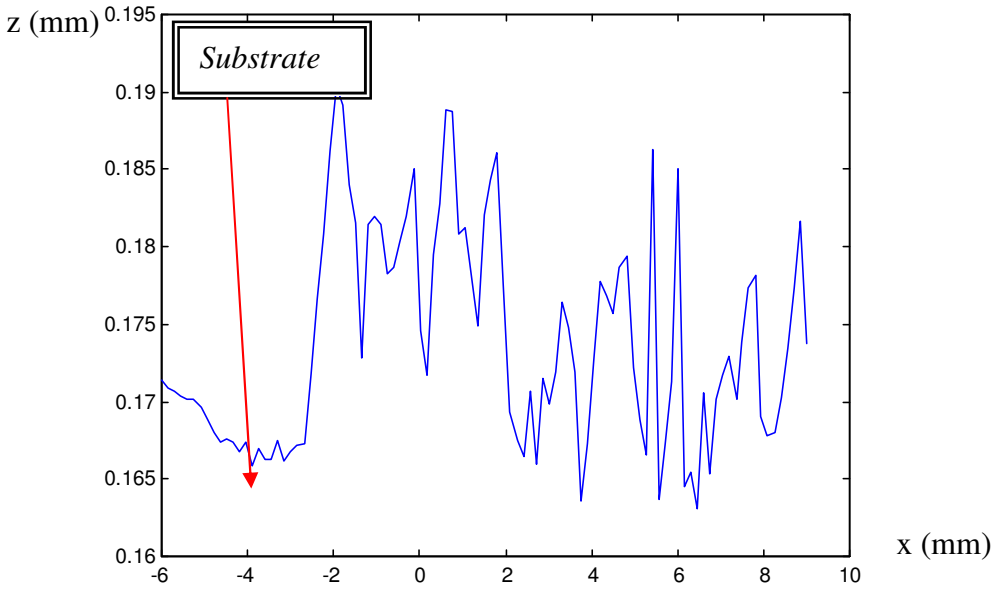

Figure 4.21: 2-D Cross-sectional Profile of PTFE Membrane Layer

4.4 Theoretical Modeling

The electrodes of an oxygen sensor were separated from external influences by means of employing a membrane that would be permeable to oxygen and other gases such as CO_2, Cl_2 and SO_2. This membrane ought to be impermeable to ions as well as other impurities present in the solution under test. In the absence of a membrane, the ions and impurities could interfere with the current signal, thus causing errors in determining the actual measurements. Impurities and ions would also tend to reduce the catalytic activity of the cathode. Hence, the presence of the membrane would be important and advantageous as it ensured reproducible conditions for oxygen transport towards the cathode. Different applications would determine the choice of materials based on the respective physical aspects such as thickness of the membrane layer.

A theoretical diffusion model encompassed a simple one-dimensional representation or alternatively a complex multi-dimensional equivalent. In the context of this research, only an estimation of the output current responses was required. Hence, a simple one-dimensional linear diffusion model was employed to investigate the transient and steady state response with respect to the variation in partial pressure of oxygen. Two basic types of cathode shapes namely spherical and planar were available for simple modeling purposes. The modeling equations were commenced with the general spherical cathode and the planar equivalent was a specified case of the spherical model [54] by limiting the radius of the electrode to infinity. A three layer planar model was suitable for actualizing the performance of the practical thick-film oxygen sensor prototype where side diffusion of oxygen was negligible.

The stoichiometric coefficient of the cathodic reduction of oxygen and the intensity of oxygen flux governed the current signal produced by the sensor prototype. This transformation method was based on the principle of superposition that included the use of convolution integral for the calculations. To begin modeling, the radial view of a spherical schematic and its different layers as shown in Figure 4.22 was defined.

The subscripts L, M and E denoted liquid film, membrane and electrolyte respectively. Liquid film was defined as a layer of external medium in contact with the membrane. This layer could be the conductive layer on the skin surface or sweat (containing KCl salt) or even some form of hydrated medium, which was present along the membrane-liquid film interface

in a practical application. However in the model, L was assumed to be negligible for simplicity and estimation purposes. Symbol r represented the radius and subscript O was the point of origin.

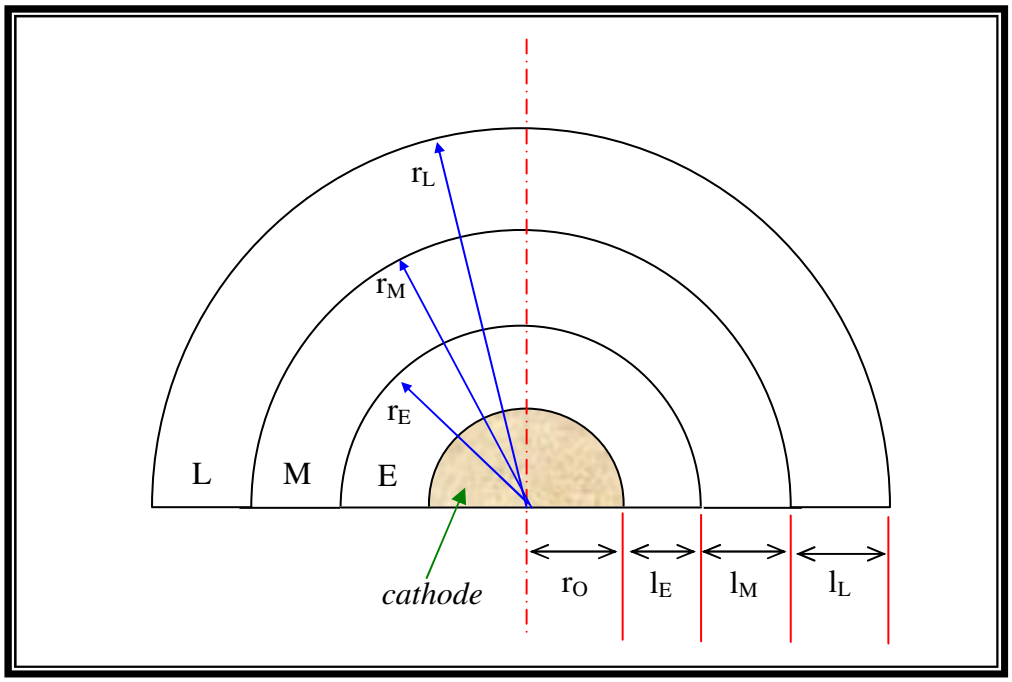

Figure 4.22 : Radial Schematic of Spherical Cathode

By combining Fick's first law of diffusion and the law for conservation of mass, Fick's 2nd law that related the change in concentration (C) with time (t) extended to include the 2nd derivative of concentration with respect to distance (x), as given by $\frac{\partial C}{\partial t} = D\frac{\partial^2 C}{\partial x^2}$. Converting the conventional Cartesian co-ordinates to the respective spherical co-ordinates, the following equations derived from Fick's 2nd law of diffusion [55] described the partial pressure of oxygen (p) across the layers, given that p was directly proportional to the concentration level (C).

$$\frac{\partial p_E}{\partial t} = D_E \frac{1}{r^2}\frac{\partial}{\partial r}\left(r^2 \frac{\partial p_E}{\partial r}\right) \tag{4.1}$$

$$\frac{\partial p_M}{\partial t} = D_M \frac{1}{r^2}\frac{\partial}{\partial r}\left(r^2 \frac{\partial p_M}{\partial r}\right) \tag{4.2}$$

$$\frac{\partial p_L}{\partial t} = D_L \frac{1}{r^2} \frac{\partial}{\partial r}\left(r^2 \frac{\partial p_L}{\partial r} \right) \tag{4.3}$$

D_X (where *x* is E, M, or L) is the diffusion coefficient of each type of material given by:

$$D_X = \frac{RT}{6\pi N v r_m} \tag{4.4}$$

where R is gas constant

T is absolute temperature

N is the number of molecules in a mole

v is the viscosity of the solvent

r_m is the radius of the particle or molecule

The initial conditions for Equations (4.1) to (4.3) are when $t = 0$, $p_E = p_M = 0$. The boundary conditions are:

$$r = r_O : \quad p_E = 0 \tag{4.5}$$

$$r = r_E : \quad p_E = p_M ; \quad k_E \frac{\partial p_E}{\partial r} = k_M \frac{\partial p_M}{\partial r} \tag{4.6}$$

$$r = r_M : \quad p_M = p_L ; \quad k_M \frac{\partial p_M}{\partial r} = k_L \frac{\partial p_L}{\partial r} \tag{4.7}$$

$$r = r_L : \quad p_L = P_{steady-state} \tag{4.8}$$

The symbol k_x (where *x* is E, M or L*)* denotes the respective oxygen permeability of the material. An explicit relationship for the intensity of oxygen flux, *N* to the cathode is governed by:

$$N(t) = -k_E \left(\frac{\partial p_E}{\partial r} \right) \tag{4.9}$$

By solving Equations (4.1) to (4.8) according to a method developed by Jaegar [56], *N*(t) was used to derive the solutions (4.10) to (4.13) to describe the performance of the sensor with respect to oxygen diffusion. Table 4.1 summarizes all denotations used in the evaluation. Using the respective equations and the values in Table 4.2, the values for sensor prototypes with KNO_3 or Nafion as the electrolyte and PTFE as the membrane were calculated.

Affiliation	***Equation***	***Value for Prototype***
Steady-state oxygen flux	$N_S = \lim_{t\to\infty} N(t)$	$N_{S(KNO_3)} = 1.71068\times10^{-6}$ $N_{S(NAFION)} = 1.30062\times10^{-6}$
Transient characteristic	$H = \frac{N}{N_S}$ for $\frac{p_S}{p_L} = 0$	Functional curve in Figures 4.23 and 4.24
Time constant (where *Di* = D_X is diffusion coefficient)	$K_i = \frac{D_i}{l_i^2}$	$K_M = 0.03125$
Square roots of oxygen diffusion rate in layer i and in the membrane	$A_i = \sqrt{\left(\frac{K_M}{K_i}\right)} = \frac{l_i\sqrt{D_M}}{l_M\sqrt{D_i}}$	$A_{E(KNO_3)} = 0.0419263$ $A_{E(NAFION)} = 0.0875$
Diffusional resistance of layer i to oxygen transport	$R_i = \frac{l_i}{k_i}$	$R_M = 6.85\times10^9$
Ratio of diffusional resistance of layer i and the membrane	$L_i = \frac{l_i k_M}{l_M k_i}$	$L_{E(KNO_3)} = 0.1095$ $L_{E(NAFION)} = 22.966$
Required parameter	$S_i = \frac{L_i}{A_i}$	$S_{E(KNO_3)} = 2.61173$ $S_{E(NAFION)} = 262.461$

Table 4.1: List of Denotations for Solutions to Planar Cathode Model

The steady-state oxygen flux was evaluated to give:

$$N_S = \frac{p_S}{R_M[1 + L_E]} \tag{4.10}$$

The transient characteristic presented in a general form was:

$$H(t) = 1 + 2(1 + L_E)\sum_{n=1}^{\infty}\frac{exp(-K_M\alpha_n^{\,2}t)}{Q(\alpha_n)} \tag{4.11}$$

where α_n were the positive roots of equation (4.12)

$$S_E cos\alpha \cdot sin\, A_E\alpha + sin\,\alpha \cdot cos\, A_E\alpha = 0 \tag{4.12}$$

and

$$Q(\alpha) = (1 + L_E)\ cos\alpha \cdot cos\, A_E\alpha - (A_E + S_E)\, sin\,\alpha \cdot sin\, A_E\alpha \tag{4.13}$$

Solutions (4.12) and (4.13) appeared relatively complex hence they were solved empirically using numerical methods to evaluate the unknown parameters. This was carried out with the aid of the *Mathematica* software [57], which allowed easy manipulation of complicated functions. Prior to performing the iterations, approximated values of all variables which were adopted from other literature resources and the dimensions of the sensor prototype are obtained as tabulated in Table 4.2, where k_i is the oxygen permeability (i is E or M), D_X is the diffusion coefficient (X is E or M), l_E is the radial length of the electrolyte and l_M is the radial length of the membrane.

Material	k_i ($mole.m^{-1}.sec^{-1}.Pa^{-1}$)	D_X (m^2/sec)	l_E (μm)	l_M (μm)
KNO_3 (E)	20×10^{-15} [58]	4×10^{-9} [59]	15	-
Nafion (E)	2.225×10^{-15} [60]	2×10^{-10} [61]	7	-
PTFE (M) [58]	2.92×10^{-15}	1.25×10^{-11}	-	20

Table 4.2: Summary of the Properties for Different Materials

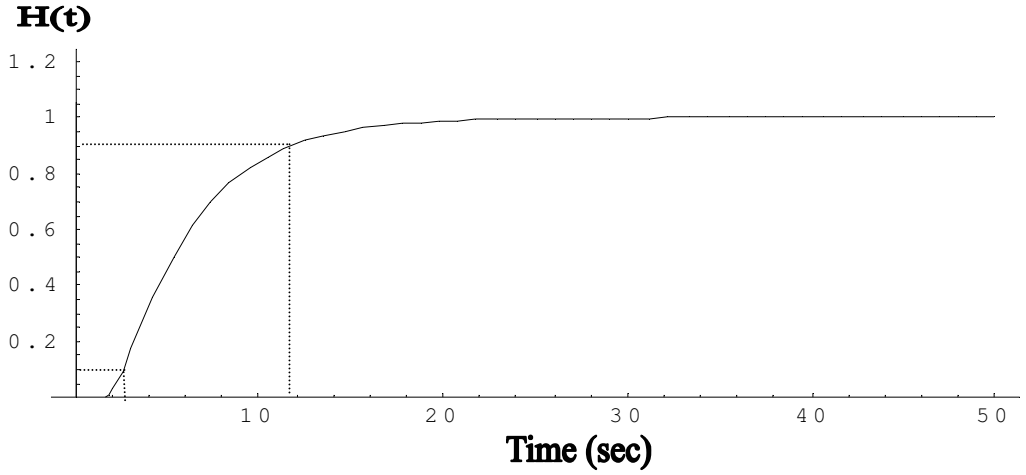

Figure 4.23: H(t) *Response Plot for Sensor with KNO_3 Electrolyte and PTFE Membrane*

The steps involved in evaluating the functions are elaborated in Appendix C. The transient plot of $H(t)$ for the sensor with KNO_3 as the electrolyte and PTFE as the membrane is shown in Figure 4.23. It could be observed that with the specified membrane thickness and different physical parameters such as diffusion coefficient, the settling time of the sensor was approximately 8.7 seconds. Settling time was defined as the time period between 10% and 90% of the steady state value. Using the same method of simulated analysis, the H(t) response plot of the sensor with Nafion as the electrolyte and PTFE as the membrane is evaluated as shown in Figures 4.24 respectively. The settling time was estimated at 14 seconds, which was considerably longer than that of the sensor with KNO_3 electrolyte.

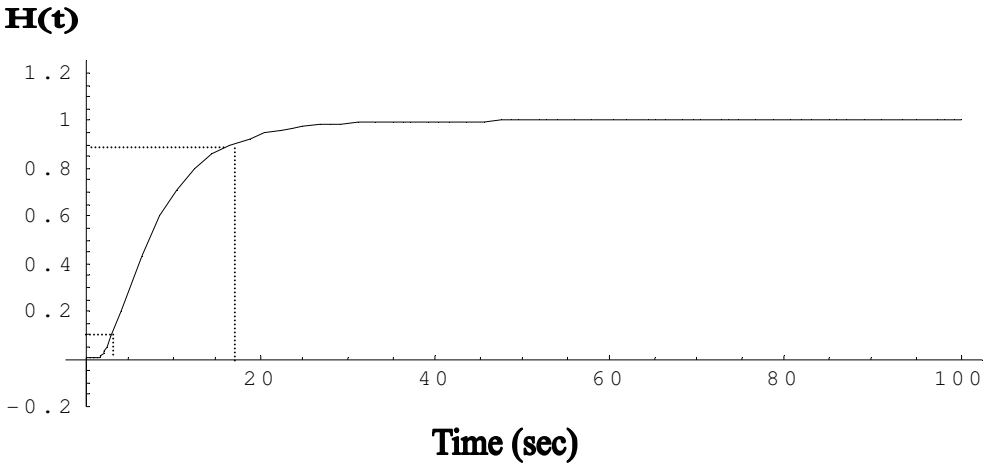

Figure 4.24: Function H(t) *Response Plot for Sensor with Nafion Electrolyte and PTFE Membrane*

From Table 4.2, it is observed that although the thickness of the KNO_3 membrane is double that of the Nafion membrane, it possesses a higher diffusion coefficient and oxygen permeability, which enables its response time to be relatively shorter. Using the graphical information provided from response plots similar to those in Figures 4.23 and 4.24, different materials and dimensions of electrolytes and membranes could be easily studied for material stability as well as sensor performance during the diffusion stages. With deeper understanding of the materials, various combinations could be used to develop prototypes that would improve response times as well as optimize the reduction in membrane sizes and eventually bring about more economical alternatives. Talbot *et al.* [63] also developed a dynamic model of oxygen transport for transcutaneous oxygen analysis. The model was complex as it took properties such as skin thickness and blood tension into considerations.

Although Talbot's mathematical representation was more comprehensive, the one dimensional diffusion model established by Linek was adopted for its simplicity.

Chapter 5 Investigations on Heater and Conditional Testing of Oxygen Sensing Module

5.1 Effects of Different Placements of Heater Element

The heater element on the substrate was printed using cermet platinum (ESL 5545). In the specification data sheet provided by ESL, it was found that this material was suitable as it possessed a temperature coefficient of resistance in the range of 3500 ± 200 ppm/°C. As the material changes its resistance linearly between the temperatures of -50 °C and +500 °C, cermet platinum is often used in designs of thermometer, heater and sensor applications.

5.1.1 Experimental Procedure

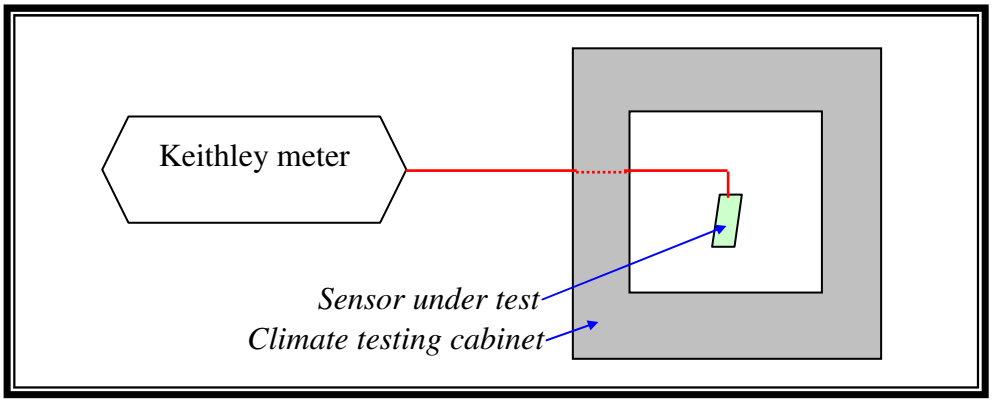

Figure 5.1 : Experimental Setup Using Climate Testing Cabinet

Figure 5.1 basically shows the experimental setup to determine the performance of the heater element. Each prototype is fabricated by printing the cermet platinum heater onto the alumina substrate, followed by a dielectric layer and different overlying membrane materials. These printed substrates were placed in a temperature chamber (Climatic testing cabinets, series SB, system Weiss) where the temperature was set to 15 °C, 30 °C and 45 °C on separate occasions. The respective resistances were then recorded using a Keithley 2001 multimeter. The investigations explored the effects of the heater element position, the overlying dielectric material employed as well as the membrane type on the temperature

stability of the sensor. Since the heater material was chosen possessing a linear temperature-resistance relationship, three point plots were sufficient to establish a series of well-defined correlations. Measurements were made for prototypes with:

(i) two different overlying dielectrics: Dupont 5704 (Dielectric 1) and ESL 4905-CH (Dielectric 2)

(ii) two different positions of heater element: underneath the oxygen sensor module and on the back of substrate

5.1.2 Resultant Relationship Plots between Resistance and Temperature

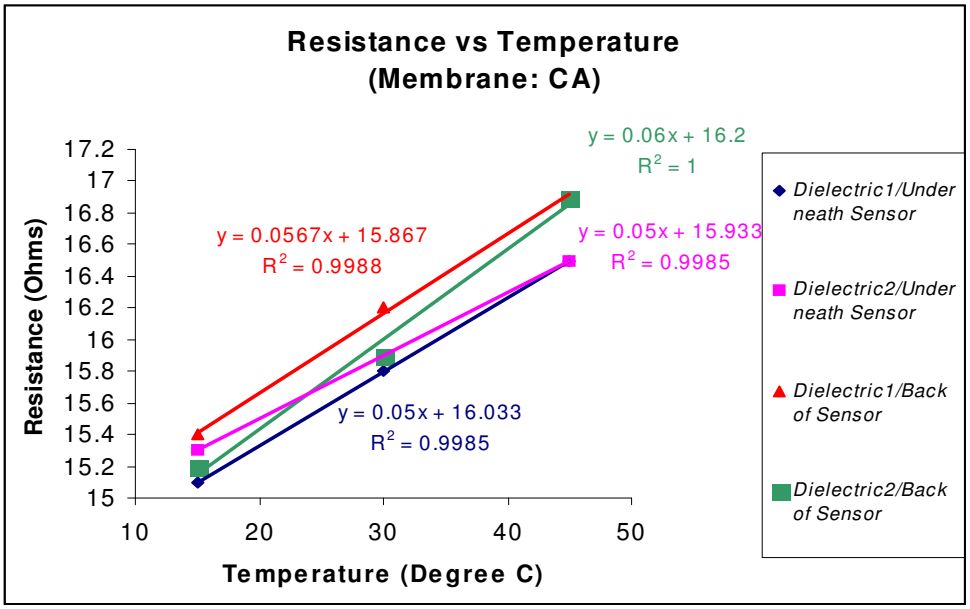

Figure 5.2: Graph of Resistance vs Temperature with Cellulose Acetate (CA) as the Membrane over the Oxygen Sensor

Figures 5.2, 5.3 and 5.4 depict the relationships between resistance and temperature for sensors employing CA, PTFE or PVC membranes respectively. The data regressed linearly and a governing equation was obtained for each heater element. This equation was then used to calibrate the resistance value to its corresponding temperature in future experiments. In other words, the corresponding resistance for each unit of temperature could be evaluated easily and accurately.

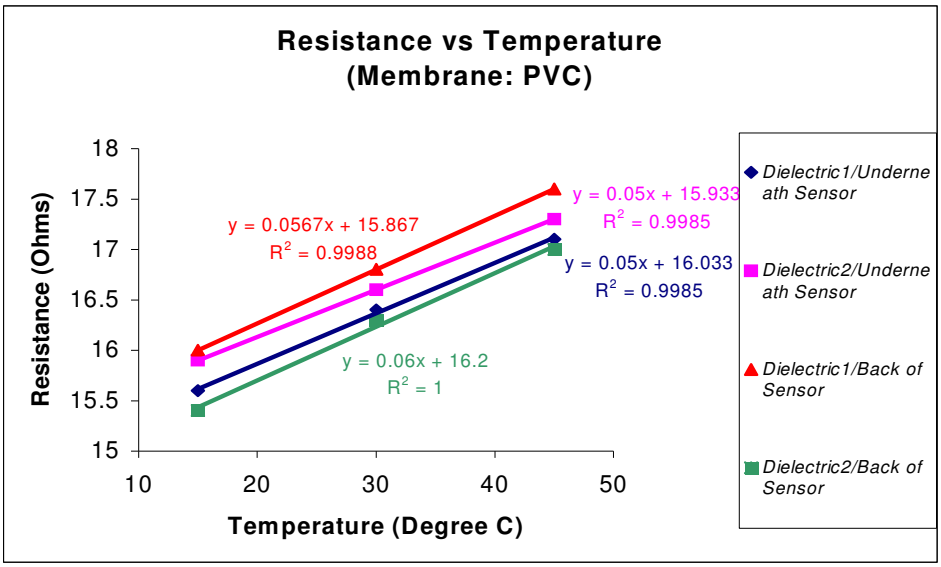

Figure 5.3: Graph of Resistance vs Temperature with PTFE as the Membrane over the Oxygen Sensor

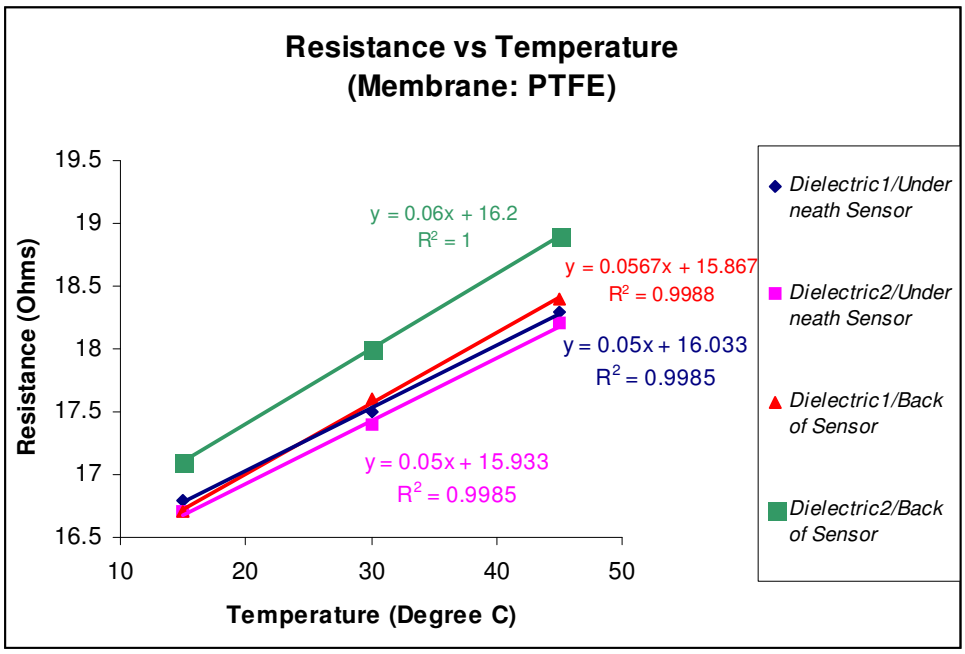

Figure 5.4: Graph of Resistance vs Temperature with Polyvinyl Chloride (PVC) as the Membrane over the Oxygen Sensor

5.1.3 Observations and Discussion

From the results obtained, it was concluded that the platinum heater element conformed to a linear relationship with the regression coefficient (R^2) larger than 0.9985 in every case. The gradients of each graph were found to be relatively consistent at approximately 0.05. The

results obtained did not vary significantly due to differences in the position of the heater element nor the material of the membrane. The only factor that perhaps influenced the choice of the heater position would be the ease and flexibility of carrying out the fabrication procedure. In view of this issue, the preferred heater position would be at the back of the substrate as it presented several advantages. Firstly, the oxygen module would be physically separated from the heater module altogether. If the heater module were printed underneath the oxygen module, the separating dielectric layer would be 'sandwiched' between two sets of conductors - the gold electrodes and the platinum heater element. In terms of practicality, a build up of charges known as the battery effect may occur and this could cause polarization at the electrodes, hence interfering with the actual measurements in the oxygen sensor module.

Secondly, there would be a higher possibility of uneven printing for the underlying dielectric layer, which would in turn cause difficulties in printing the overlying electrodes and successive layers. Thirdly, with the element printed at the back of the substrate, a more compact sensor layout could be designed for both modules since the overall available space would be effectively larger. Finally, the overall thickness of the printed sides would also be more balanced. Both types of dielectric materials employed presented similar regression equations. Thus, there would not be any preference made in the choice when developing the actual sensor prototype.

5.2 Stability of Heater Module

The objective of these experiments was to investigate the long-term stability of the heater module of the transcutaneous oxygen sensor. This parameter was primarily important to obtain reliable transcutaneous measurements at approximately 44 °C. A closed loop temperature control circuit, requiring the cermet platinum element to be attached within a feedback wheatstone bridge, was designed to achieve a high order of temperature stability and accuracy. This circuit shown in Figure 5.5 also ensured the temperature of the heater would not exceed 46 °C avoiding burning of the subject under test or fall below 42 °C where the transcutaneous measurement would encounter significant attenuation in output current levels.

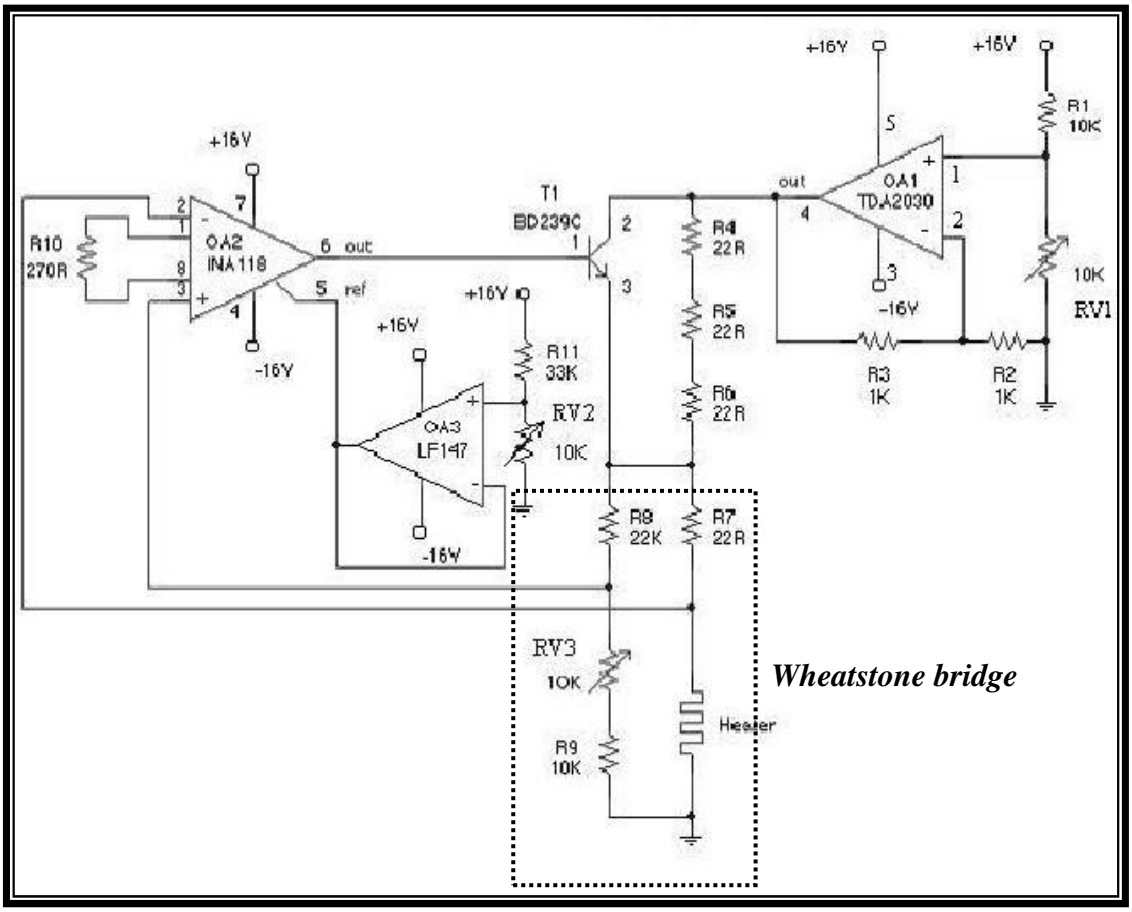

Figure 5.5: Heater Module Temperature Control Circuit

The heater elements were then connected to the heating circuit to investigate their stability and reliability over a period of time. The 10kΩ variable resistor (RV2) in the Wheatstone bridge as shown in Figure 5.5 was tuned with high accuracy of approximately ±5Ω.

5.2.1 Experimental Procedure

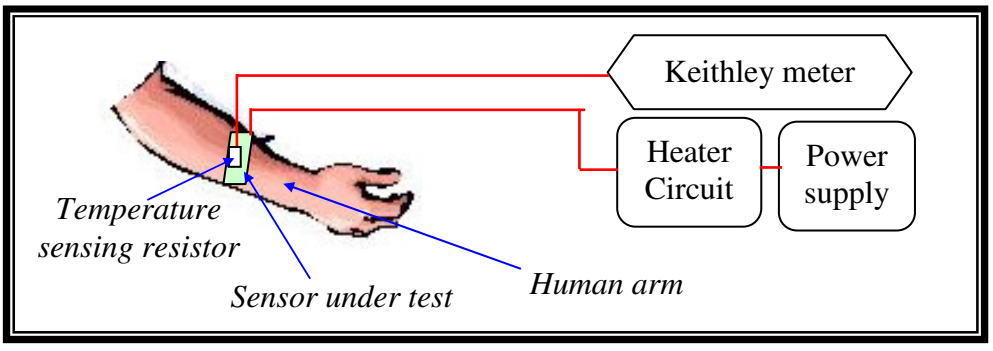

Figure 5.6: Experimental Setup for Long-term Stability Test

Figure 5.6 illustrates the experimental setup for testing the long-term stability of the heater module. Each prototype consists of a cermet platinum heater printed on an alumina substrate and it is connected to the heating control circuit as shown in Figure 5.5. The circuit is powered by the Thurbly PL320 dual power supply (K2 module). A temperature-sensing resistor (PT100) [63] is attached onto the prototype and connected to the Keithley 2001 multimeter in order to record the temperature of ongoing measurements. The first experiment was carried out with the prototype suspended, hence subjected to normal atmospheric conditions for approximately 5 minutes. After which, the heater element was placed onto the skin surface and the measurements were taken for the next 5 minutes. The circuit variables such as the tuning of the variable resistors were adjusted according to the requirements for transcutaneous measurements.

5.2.2 Observations and Discussion

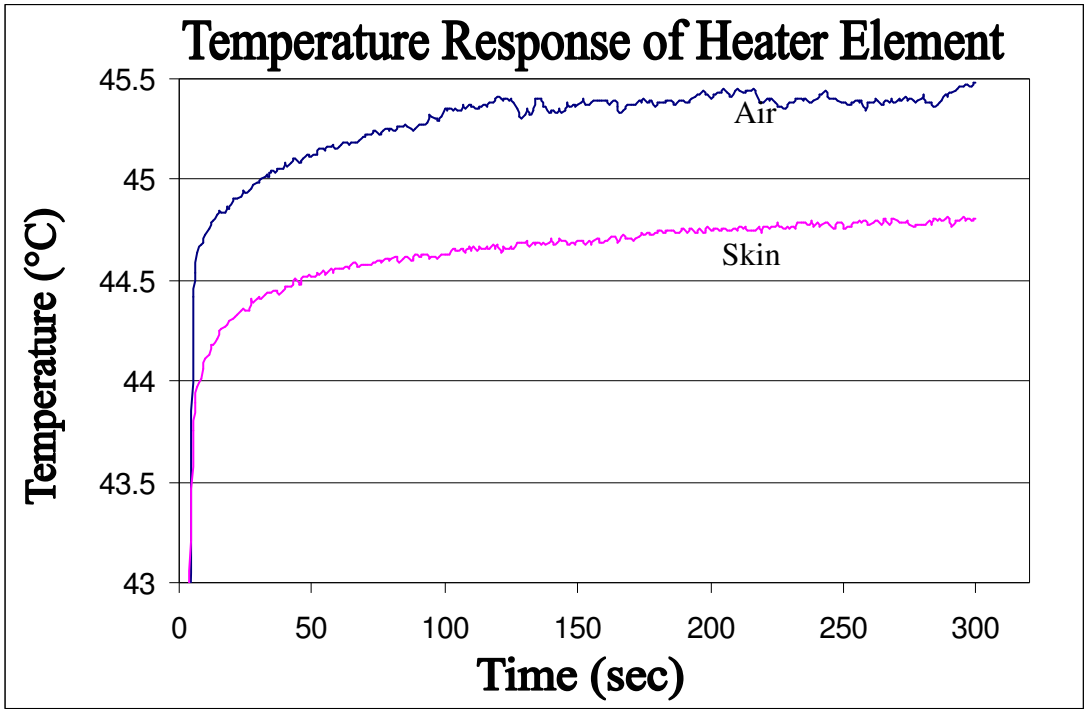

Figure 5.7: Temperature Response of Heater Element in Air and on Skin Surface

From the transient responses shown in Figure 5.7, it can be observed that the gradient for the plot with measurements made in air during the first 3 or 4 seconds is approximately 6°C per second. This occurred due to the sudden surge in current delivered to the element upon power

up. After approximately 5 seconds, the temperature increased gradually at a lower rate of 0.07°C per 10 seconds until the end of the first minute. During this period of time, the transistor (BD 239C) in the control circuit turned off and current to the element was only supplied by the path, consisting of the series resistors R4, R5 and R6 as shown in Figure 5.5. At the point where the transistor was just about to be turned on, the heater element experienced a relatively stable current of 110 to 130 mA. After 100 seconds, the temperature is approximately 45.3°C as shown in Figure 5.7.

In the temperature response plot where the element was placed on the skin surface, the temperature gradient during the first few seconds of the experiment was estimated at 2.5°C per second. During the subsequent 2 minutes, the gradient varied between 0.15°C and 0.25°C per minute. Further measurements for longer periods of time were not shown in Figure 5.7 as steady state responses could be observed after the first 5 minutes. More fluctuations were observed at the steady state response of the element when exposed to air as compared to that on the skin surface. This could be due to that fact that changes in ambient temperature varied more than the skin surface. The steady state temperature gave a maximum error of ±0.1°C. Other important factors to be considered were the position and placement of the heater on the skin. The pressure applied and the contact area with skin also contributed significantly to the measurements. If the contact area with the skin were not adequately large, the temperature characteristic would take on a response similar to that in air and the temperature of the heater would be higher.

The reference voltage and the gain of the differential amplifier were chosen based on several trials during prior test and tuning of the circuit. The value of the offset was adjusted based on experience gained during the measurements, as there would be a number of combinations to find an optimal operation point of the circuit efficiently. The value of the temperature would depend on the conditions of positioning the element in terms of applied pressure and contact area. Nevertheless, the temperature would not be kept lower than 43.5°C or higher than the temperature when the element was exposed in normal atmospheric conditions. It was essential for the temperature control circuit to ensure that the temperature was maintained at transcutaneous levels regardless of whether the element was placed on the skin surface or in air.

The main aim of the heating circuit was to regulate the temperature to the desired set value despite temperature and humidity changes in the environment. The temperature stability of the heater module would be considered as a very important specification in order to maintain proper and reliable transcutaneous measurements.

5.3 Transient Heater Measurement Using an Infrared Camera

The infrared (IR) camera from DeltaTerm, supported by the software DeltaVision v.16a was used for thermal stress analysis. The IR camera could be used to provide efficient full-field accurate verification of finite element models and non-destructive analysis. In addition, it has been employed in the evaluation of components produced by rapid prototyping technologies during the early stages of a design cycle [64].

Figure 5.8: DeltaTerm Infrared Camera

The IR camera as shown in Figure 5.8 contains a 128 by 128 array of detecting elements. Each element is made up of an Indium-Antimony (InSb) detector. Every element of the IR camera produces an electrical signal that is transferred to the computer and subsequently evaluated upon sensing the radiated light. The sensing detectors were cooled by liquid nitrogen through the whole measurement procedure. The system software DeltaVision v.16a could capture images at the minimum rate of one frame per second. This was sufficient to store images since the main aim of the experiment was to verify long term temperature distribution over the sensor surface.

5.3.1 Experimental Procedure

The heat distribution measurements were made on several different heater elements. All the samples consisted of a substrate with printed conductor lines and platinum heater element. Some of them had an additional coat of a blue dielectric layer (Gwent code number: D1991115D6). Finally, measurements were taken with the same sensors coated with a sprayed black matt paint from Hammerite Products Limited to avoid reflections from environmental light. Matt black spray paint was used for thermographic analysis because it was highly emissive (non-reflective) and brought about more comprehensive reconstruction of the captured image.

Each sample was connected to the heating circuit shown in Figure 5.5. Upon activation of the heating element, the temperature distribution of both the front and back of the substrate was compared. The back of the substrate was defined as the side where the heater element was not printed and used for measuring the temperature during the heating process. The front of the substrate would be the side with the heater element and hence this side would eventually experience the maximum temperature. The simultaneous images of both sides could not be captured by the DeltaTerm IR camera via its supporting software package (DeltaVision v.16a). Hence, the back was measured first, followed by the front. Some significant differences in accuracy were noted in the measurement. When the sensor was turned to the front and placed in front of the IR camera, the distance from the camera was changed slightly. The control of the distance factor was difficult because the sample was suspended in free air and could not be placed against any other supporting object. In the event of such inconsistencies, small variations in the temperature magnitude were expected and subsequently encountered. However, the temperature distribution remained very similar.

The measurements became more accurate when the measured object was placed closer to the IR camera because smaller areas with different temperature could be better observed and evaluated. The temperature was measured on the back surface using a resistive thermistor (PT100) [63] and the value was compared with the IR camera equivalent.

5.3.2 Results and Discussion

The resistance of the PT100 at the back of the heater element was found to have a temperature of 44.2 ± 0.2°C throughout the measurements. The transient analysis and the change in temperature distribution with respect to time were captured after the first minute (Figure 5.9) and the fifth minute of heating process (Figure 5.11).

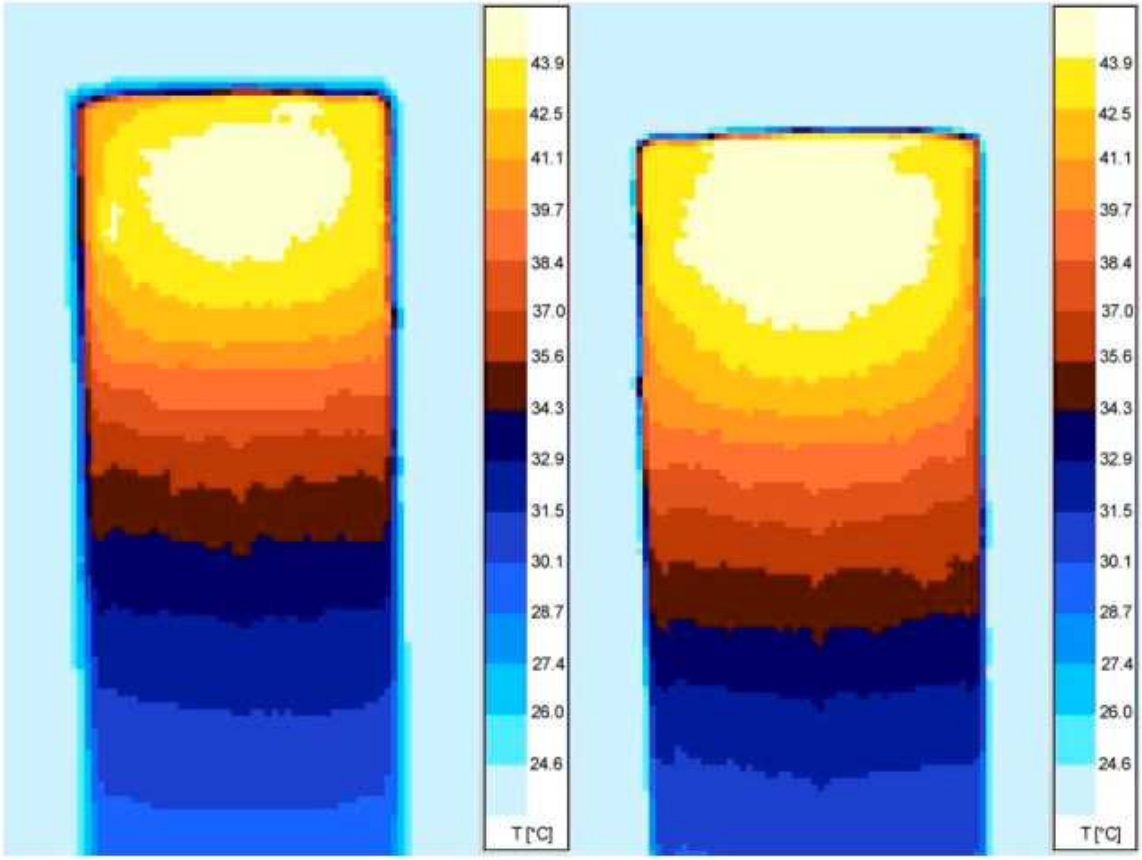

Figure 5.9: Temperature Distribution after 1 Minute, Front (Left) and Back (Right)

From Figure 5.9, it is observed that the back image appears bigger than the front equivalent. This was possibly caused by inaccurate positioning of the IR camera, with respect to the position of the sample. A more suitable comparison could be made by the visual presentation described in Figures 5.10 and 5.12 for the temperature distribution after 1 minute and 5 minutes respectively. These grid pictures were reconstructed using the digitized data output files from the DeltaVision software. Each colour code represented a change of 0.5 °C. The area of the heater was indicated within the 8.8mm by 8mm white rectangle and

grid lines were included for better graphical comparison. Each cross point of the grid corresponded to one detecting element in the IR camera.

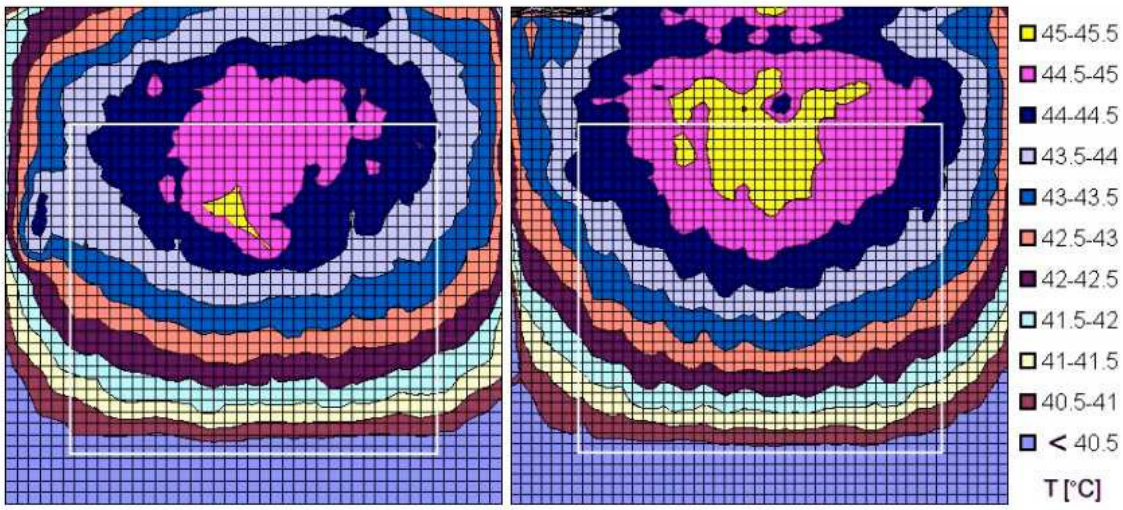

Figure 5.10: Reconstructed Digitized Images of Temperature Distribution after 1 minute, Front (Left) and Back (Right)

The images presenting the temperature distribution after 1 minute were adequate representations of the transient response of the element. After powering up the element for 5 minutes, it could be assumed that a stable steady state response as illustrated in Figure 5.11 was reached using the temperature control circuit in normal room temperature conditions. Images taken at 10 minutes and 30 minutes after powering up resembled the one after 5 minutes, hence validating the assumption. Low airflow speed could also cause the effect of asymmetrical temperature distribution.

In general, a better understanding of the temperature distribution over the substrate was achieved by these real-time pictorial representations. From the results obtained, it was found that temperature distribution within the skin contact area of the sensor reached relatively uniform and stable levels after an acceptable amount of time delay of approximately 1 or 2 minutes. With this, the heated sensor would be placed on the skin surface and this would increase its temperature to transcutaneous measurement levels.

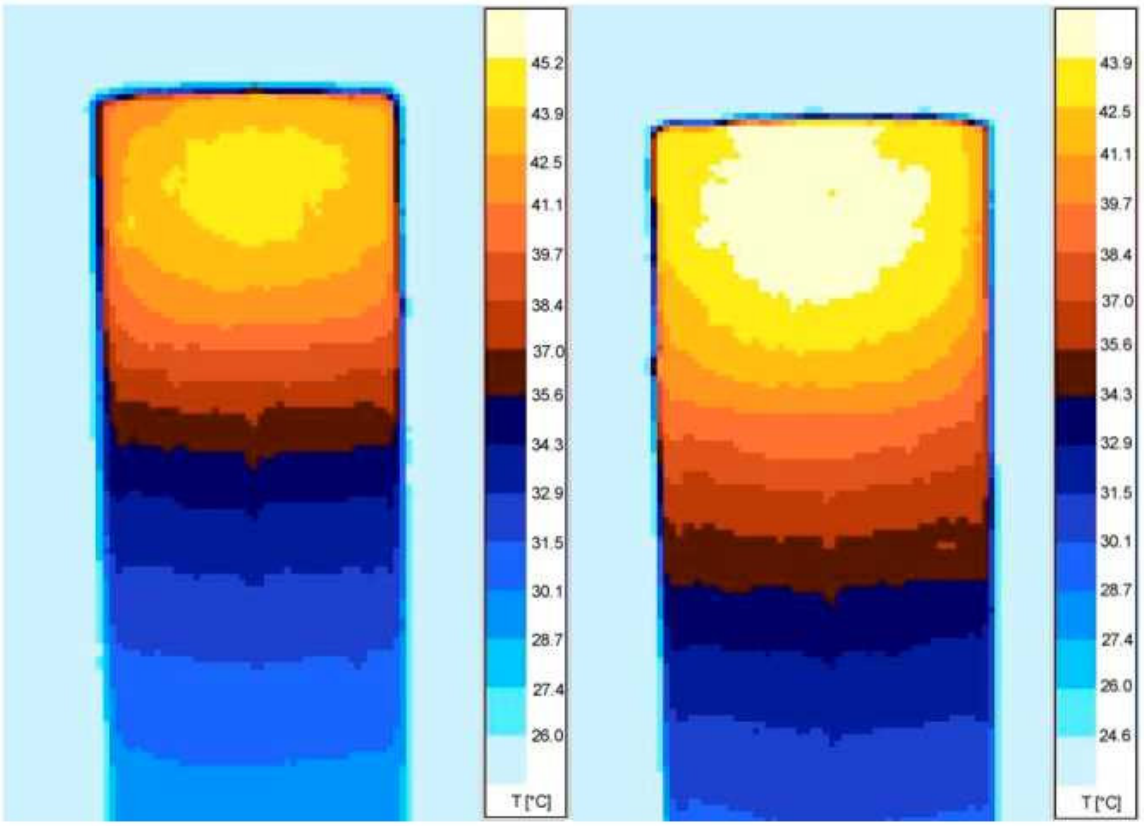

Figure 5.11: Temperature Distribution after 5 Mins, Front (Left) and Back (Right)

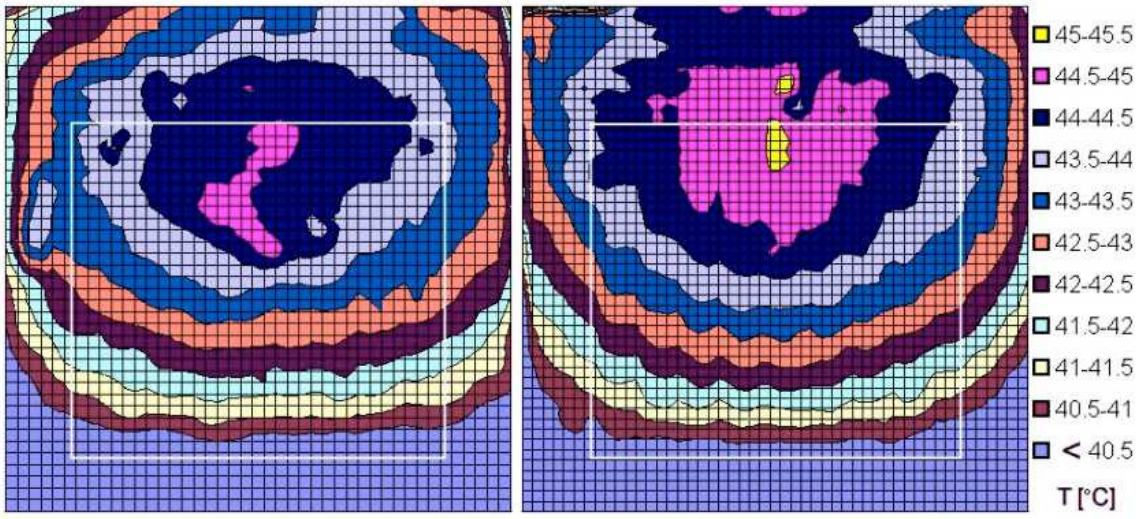

Figure 5.12: Reconstructed Digitized Images of Temperature Distribution after 5 Minutes, Front (Left) and Back (Right)

5.4 Sensor Fabrication

All the sensors were fabricated in-house with commercially available ink materials using a DEK Model 1202 screen printer. A heater element was firstly printed, on the back of the 0.635 mm thick alumina substrate. The substrate was then laid to dry in the DEK 1202 mini dryer at approximately 150 °C, subsequently it was fired in the BTU 6-zone furnace with a temperature profile that peaked at 850 °C. This process would bind the existing layer to the substrate permanently so that the next layer could be fabricated by repeating the whole procedure using the desired ink material.

The oxygen-sensing module was fabricated on the front of the substrate. It consisted of the soldering terminals fabricated using silver palladium (AgPd) ink (ESL-9635C), gold (ESL-8836) working and counter electrodes as well as a silver-silver chloride (Ag/AgCl) reference electrode to complete a three-electrode configuration. The Ag/AgCl ink [53] was made by roll-milling silver chloride power (Aldrich 99%) and silver powder (Aldrich 99%) with a ratio of 2:1 by weight using an Heraeus overglaze (IP9027) as the glassy binder.

In order to complete the 3-electrode electrochemical cell, a layer of KNO_3 electrolyte was employed. To adapt the aqueous salt electrolyte to the thick film fabrication process, 99% KNO_3 powder (Aldrich) was dissolved in AnalaR grade de-ionized water with gelatin powder (BDH Laboratory Supplies) with a weight ratio of 1:5. This electrolyte layer was cured and dried at room temperature for approximately 2 hours. In the presence of a solvent, the KNO_3 electrolyte gel would dissociate into K^+ and NO_3^- ions. These ions would interact with the surrounding solvent ions to form solvated ions. Under the influence of an externally applied electrical field, the solvated ions can move through the solution producing an ionic current [65]. The 3-electrode configuration was deemed suitable for such a medical application as it would avoid internal polarization of the RE and compensate for the *iR* cell drop [28, 34].

The sensors were fabricated with cellulose acetate (CA), polytetrafluoroethylene (PTFE), polyvinyl chloride (PVC) or Nafion as the membrane, which was often necessary to control the diffusion of oxygen from the bulk material into the sensor. All membranes were placed in a room temperature environment to cure for a minimum of two hours before proceeding to the next fabrication stage. Finally, a dielectric layer (Gwent code number: 1991115D6) was

printed using screen artwork which had an open window over the membrane. It was then dried in a Gallenkamp oven at 60 °C for one hour. The purpose of this layer served to give a waterproof protection layer to the bare conductors.

5.5 Voltammograms for Transcutaneous Measurement at 0% Oxygen

The transcutaneous oxygen sensor consisted of two major modules namely the heater module and the oxygen measurement module. Studies on the heater modules have been presented in Sections 5.1 to 5.3. It was found that the temperature control circuit produced viable and stable heating for performing transcutaneous measurement. The subsequent experiments were carried out focusing on investigations of the oxygen-sensing module, incorporating the heater module.

The electrodes of the sensor were required to be properly connected to the potentiostat so that it could be biased to the appropriate voltage potential for oxygen reduction at the working electrodes. The range of typical biasing potentials occurred between -0.5 V and -1.0 V with respect to Ag/AgCl reference electrode. An investigation was done to study the effects of making measurements employing different types of sensor prototypes at near 0% oxygen under low humidity or hydrated condition. The main aim of this experiment was to understand the sensors' behaviour at the initial state where theoretically no oxygen reduction should happen.

5.5.1 Experimental Procedure

Figure 5.13 shows the general setup for voltammetry experiments to trace the electrochemical activity of the sensor prototype during oxidation-reduction (redox) reactions. The resultant voltammogram would present the relationship between the output current measured and the input biasing voltage between WE and RE. The oxygen-sensing module of the sensor was connected to the potentiostat (Chapter 3.2) where the EG&G Princeton Applied Research polarographic analyzer stripping voltammeter (Model 264A) [66] supplied a ramped range of biasing voltages at a specified sweep rate. In order to make measurements at the transcutanous temperature, the heater module of the sensor was connected to the heating circuit (Section 5.2). The Thurbly PL320 dual power supply (K2 module) was

employed to provide ±12V supply to the components of both the potentiostat and temperature control circuit. A TESTPOINT [67] computer program was written to automate the data acquisition process at the output of the potentiostat via a Keithley 2001 digital multimeter, a General Purpose Interface Bus (GPIB) interface card and IEEE-488 bus. This program also controlled the Gossen flow valve control system (Model 5878) via a digital to analog (DAC) card for regulating the level of nitrogen and compressed air (both from BOC Gases Ltd) allowed into a glass container where the sensors under test were placed. The whole container was then submerged in a 8-litre Clifton constant temperature bath in order to minimize the influence of the surrounding temperature to the sensor. This was set to approximately 37 °C to follow the typical body temperature of a normal human being.

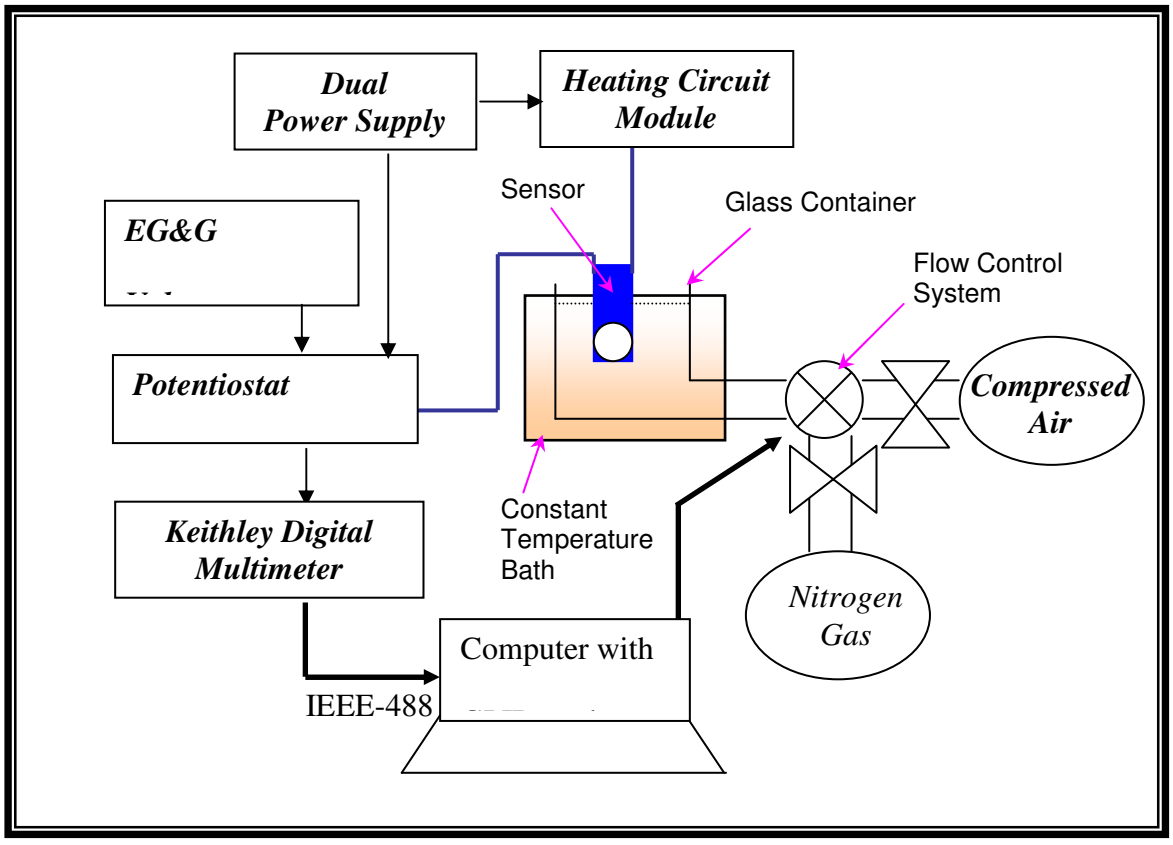

Figure 5.13: Experimental Setup for Voltammetry

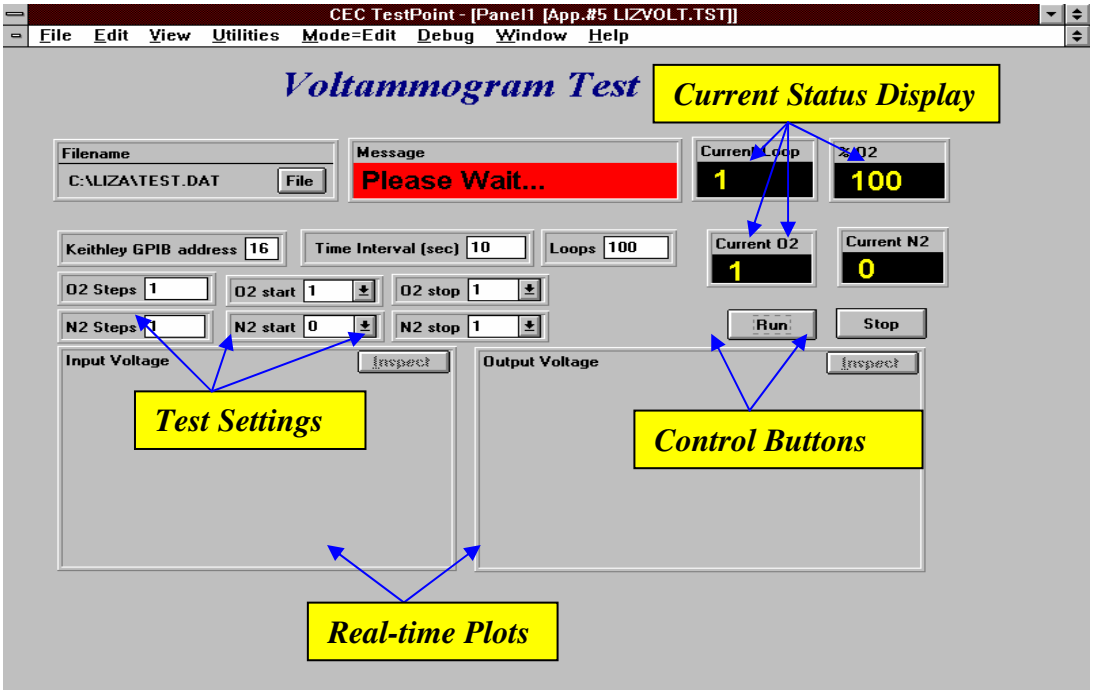

Figure 5.14: TESTPOINT Menu for Voltammogram

In this experiment, the TESTPOINT program controlled the flow system to allow 99.99% nitrogen, equivalent to ~0% oxygen into the enclosed beaker. Figure 5.14 illustrates the program display and the corresponding TESTPOINT codes are available in Appendix D. Initially, measurements were taken for the sensor suspended within the beaker at low humidity (ambient) conditions. When these were completed, the beaker was filled with de-ionized water through which ~100% nitrogen was bubbled.

5.5.2 Observations and Discussion

Figures 5.15 and 5.16 present the voltammograms obtained from sensors with a KNO_3 electrolyte, individually covered with CA, PVC or PTFE membranes under low humidity and hydrated conditions respectively. It was found that at low humidity, all sensors appeared to be non-operative throughout the whole biasing potential sweep. The current magnitude was low and this could be regarded as noise. When the sensors were immersed in de-ionized water, more positive responses were obtained as shown in Figure 5.16.

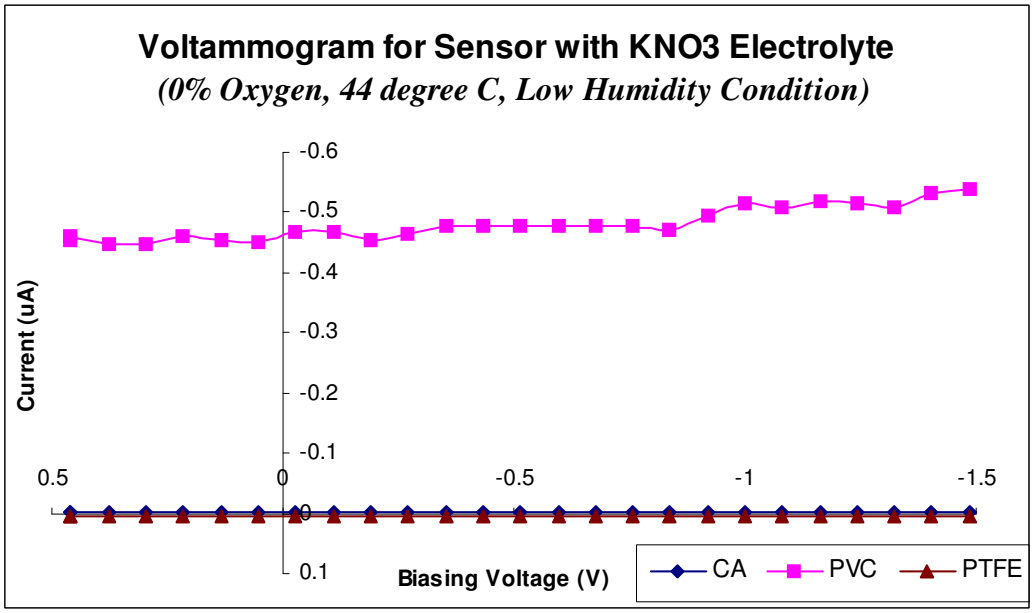

Figure 5.15: Voltammogram for KNO_3-based Sensor at 44℃, ~0% Oxygen and Low Humidity Conditions

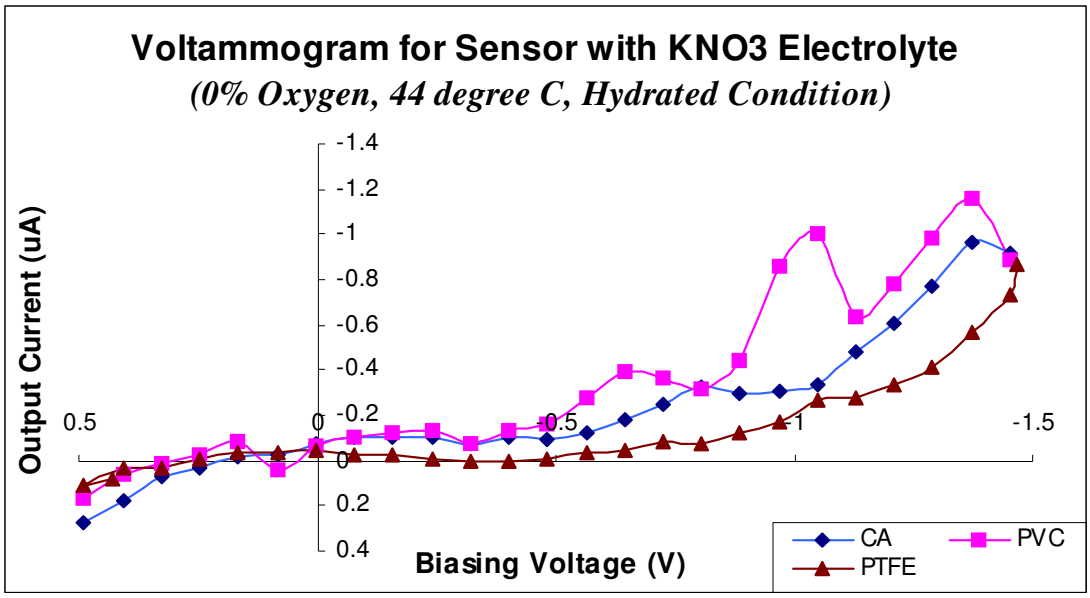

Figure 5.16: Voltammogram for KNO_3-based Sensor at 44℃, ~0% Oxygen and Hydrated Conditions

From Figure 5.16, it can be observed that the output currents increased gradually along the biasing potential of -0.6V and formed possible current diffusion limited plateaus between

approximately -0.6V to -0.8V, which could be due to the diffusion of small amount of oxygen. Within this region, the sensor with a PVC membrane recorded the largest current magnitude at -0.4μA. However, fluctuations were noted beyond -1.0V and the information thereafter was not relevant.

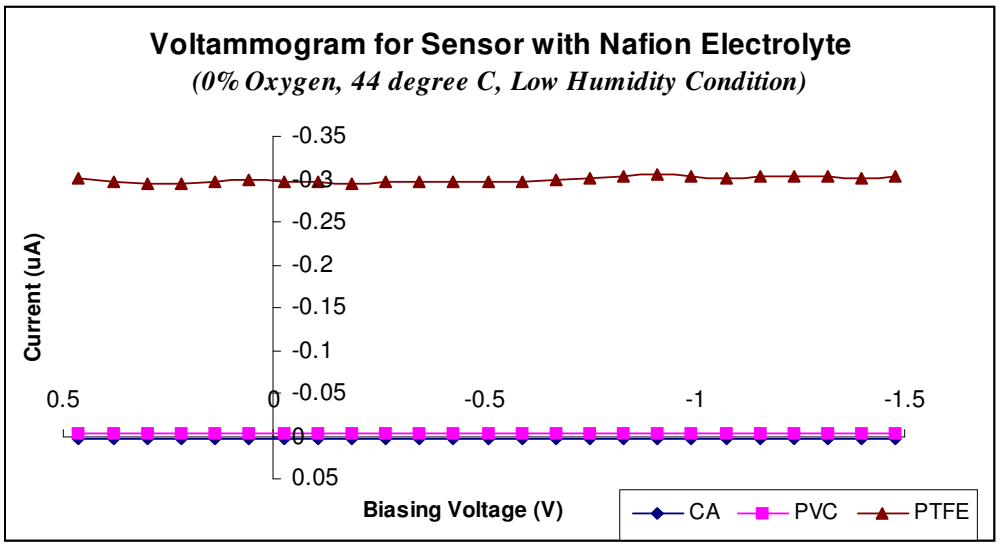

Figure 5.17: Voltammogram for Nafion-based Sensor at 44℃, ~0% Oxygen and Low Humidity Conditions

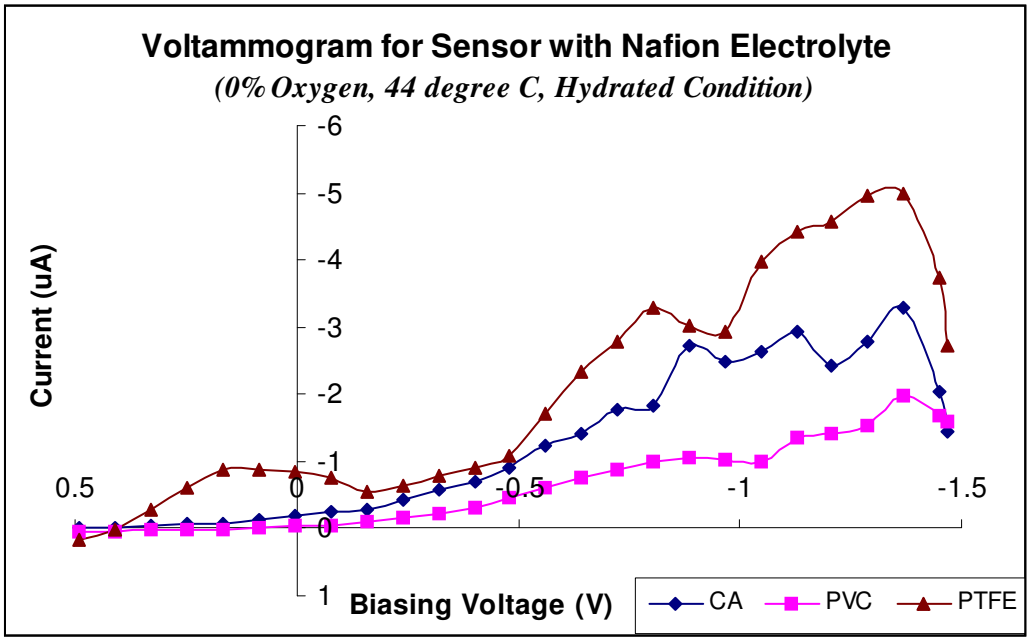

Figure 5.18: Voltammogram for Nafion-based Sensor at 44℃, ~0% Oxygen and Hydrated Condition

Figures 5.17 and 5.18 illustrate the results obtained from similar experiments with the exception of employing sensors with Nafion electrolyte for low humidity and hydrated conditions respectively. In a low humidity environment at 44 °C, the sensors did not respond as seen in the corresponding voltammograms. On the contrary, when the sensors were placed in de-ionized water, the performance of the sensors significantly improved to record current magnitudes as large as -2µA.

De-ionized water at room temperature often contained dissolved gases, which may percolate through these membranes. Although 100% nitrogen was pumped into the beaker to remove all traces of oxygen, this ideal situation may not have occurred and in turn caused some redox reaction at the working electrode. Ideally at 0% oxygen, the output current ought to be zero. However due to electrochemical drifts and offsets, zero output was often not possible. Further correlation was carried out to establish the relationship between output current and oxygen levels. The findings are presented in Chapter 6. From these experiments, it was also found that Nafion displayed potential for being a suitable alternative electrolyte. Hence, further studies were made to evaluate and compare the sensor with Nafion as its electrolyte with that of the KNO_3-based prototype.

5.6 Investigations on the Effects of Electrolyte Thickness for Nafion-based Prototype

The working principle of Nafion is based on ionic conduction in this amperometric technique for oxygen level measurement as elaborated on in Chapter 2.4. Oxygen diffused through the Nafion layer to reach the electrodes, where redox reactions would take place. The output current depended on several factors that may affect the reproduction of valid and accurate measurements. This study aimed to investigate one such factor namely the thickness of the Nafion electrolyte layer.

5.6.1 Experimental Procedure

The experimental set up was similar to that shown in Figure 5.13 (Section 5.5.1) with the exclusion of the EG&G voltammeter. Hence, the biasing voltage for the potentiostat is fixed at approximately -0.7V.

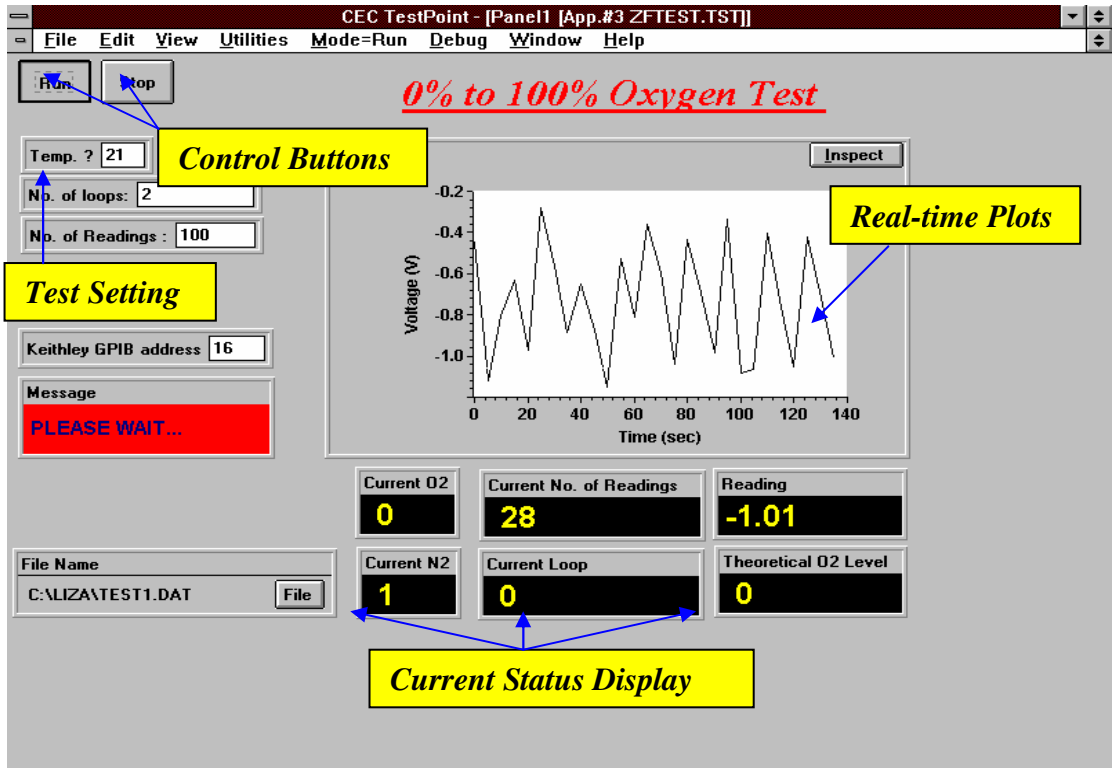

Figure 5.19: TESTPOINT Menu for Varying Oxygen Measurement

Each sensor was placed in the beaker where the concentration of air was regulated to desired levels for the measurements. This control was carried out by another TESTPOINT program given in Appendix D. It displayed the user interface menu as shown in Figure 5.19. The constant temperature bath maintained the gas temperature at approximately 37 °C. At each concentration level, the corresponding currents were recorded every 10 seconds over a 10-minute period.

5.6.2 Results and Discussion

An average current measurement was calculated at each concentration level for every individual sensor. The results were then plotted as shown in Figure 5.20 and it was found that

employing 2 to 3 layers of Nafion as the electrolyte displayed good responses. The output current also exhibited relatively good linearity with the change in oxygen level. The results for 1 layer of Nafion were not included as the measured current was fluctuating and comparable to noise levels. When the number of electrolyte layers increased more than 3, it appeared to be more difficult to distinguish the different levels of oxygen based on the current measured and this observation was supported by the low gradient value of the regressed relationship equation in Figure 5.20.

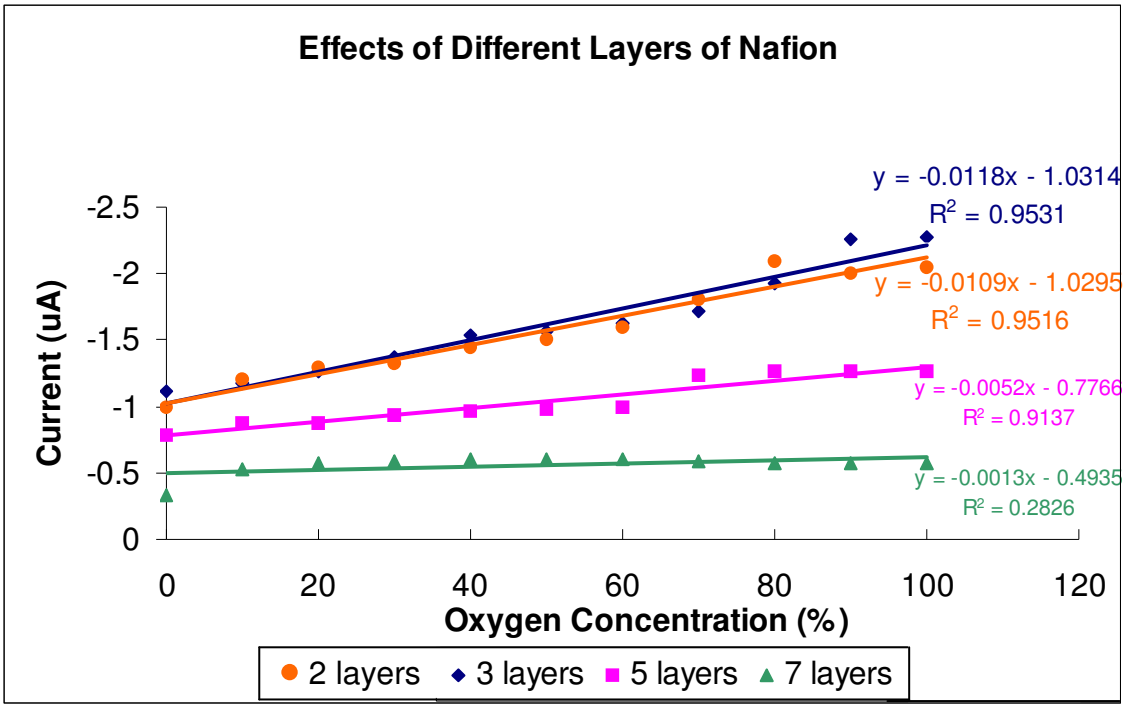

Figure 5.20: Current vs Oxygen Concentration Plot for Different Numbers of Nafion Layers

In order to achieve fast sensing responses during on-going instantaneous measurements, the electrolyte/membrane ought to be adequately thin as modelled in Chapter 4. On the other hand, the electrolyte also needed to provide sufficient ions for conduction so as to achieve measurable values that could be distinguished from noise. There would always be an appropriate electrolyte/membrane thickness where the output current magnitude as well as the response time of the sensor prototype would be optimized. In the case of Nafion, 2 layers would be most suitable as it could carry out measurable current levels in a more economical way.

5.7 Study of Sensor's Performance under Continuous Powering Conditions

An investigation on the oxygen measurement was carried out to evaluate the stability and reliability of the sensor. In a practical situation, this disposable sensor would be subjected to continuous usage over a long period of time, up to 30 or 40 hours before being replaced with a new one. It would be essential to understand the sensor's performance so that proper corrections and offsets could be made in order to obtain accurate measurements. As electrochemical redox reactions were involved for oxygen sensing, by-products as well as other impurities could be present and alter the original characteristic of the sensor. Furthermore, there could be depletion of electrolyte and wearing of the electrode surfaces that contributed to a less stable measurement as time went by.

5.7.1 Experimental Procedure

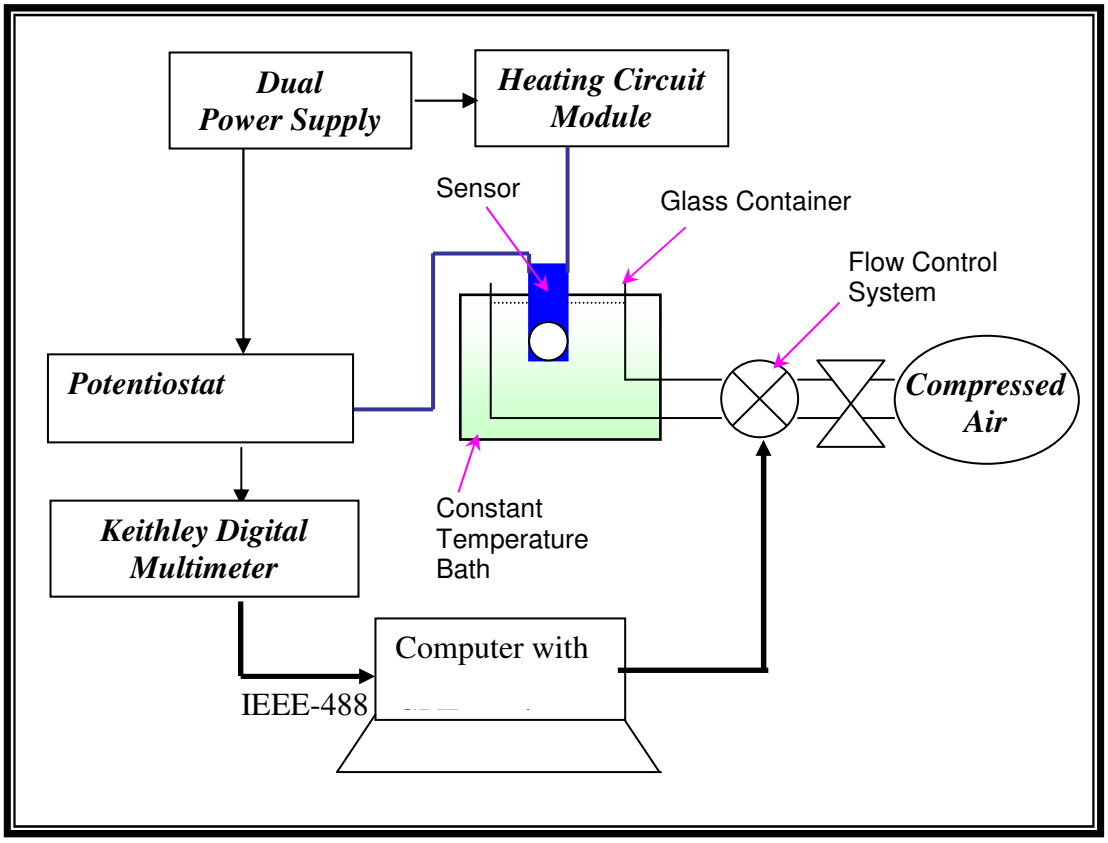

Figure 5.21: Experimental Setup for Stability Test of Sensor Prototype

Figure 5.21 shows the setup for this experiment. Each sensor used for this investigation is covered with KNO_3 electrolyte and either a CA, PVC or PTFE membrane. The heating

circuit module is connected to the heater element so that the sensor could be maintained at the transcutaneous measuring temperature.

The test involved exposing each type of sensor to 20% oxygen delivered from the compressed air cylinder (from BOC Gases Ltd) via the Gossen flow control system (Model 5878). The sensors were all immersed in de-ionized water and heated to 44 °C. The enclosed temperature was maintained at 37 °C using the 8-litre Clifton constant temperature bath. The reference voltage of the potentiostat was adjusted to -0.7V so that the sensor would operate within the current diffusion limited plateau. The Keithley 2001 multimeter recorded each measurement at intervals of 10 minutes for a total of 46 hours.

5.7.2 Results and Observations

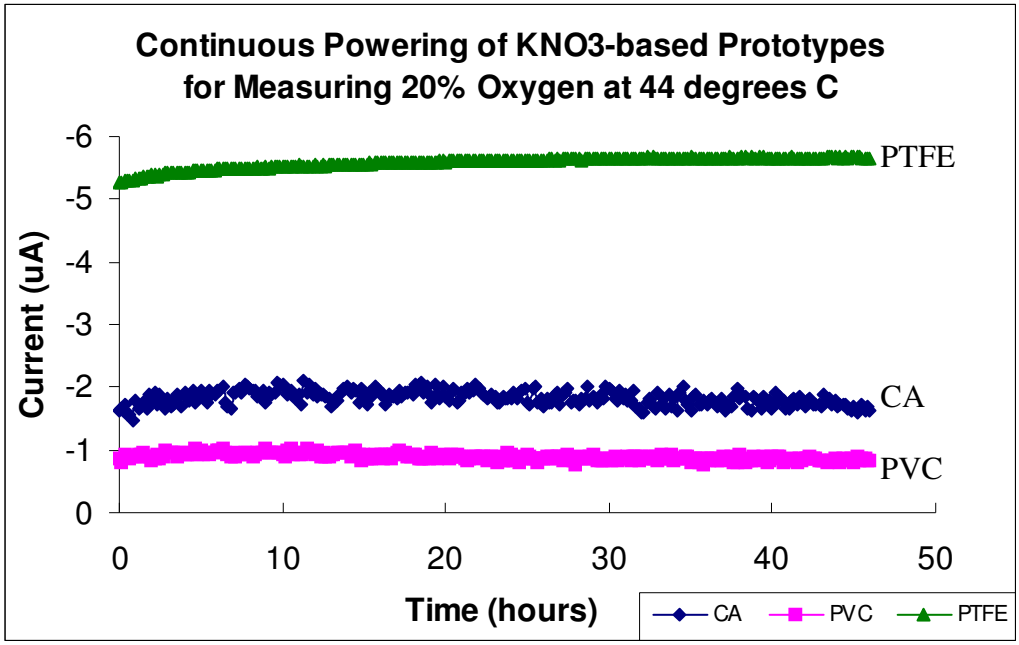

Figure 5.22: Results of KNO_3-based Sensor under Continuous, Long-term Measurement

From Figure 5.22, it can be observed that the sensor with KNO_3 electrolyte and a PTFE membrane produced the largest current magnitudes of approximately -5.2 µA. For the first 30 hours of continuous operation, the current magnitude increased gradually, then it somewhat stabilized for the rest of the experiment. The difference between the largest and smallest current magnitude obtained was about -0.2 µA, which presented relatively insignificant effects (3% to 4% deviation) towards the overall measurements. The results from the sensor

with a CA membrane appeared to fluctuate throughout the 46 hours of monitoring at -1.8 ± 0.3 µA, which would be equivalent to a deviation of approximately 17%. This percentage level is significantly large for an error margin. However, it was later found that each oxygen level could still be distinctive identified with current magnitudes larger than that of the estimated deviation. Hence, this generous margin was considered acceptable. The sensor with a PVC membrane recorded measurements at approximately -1 µA and the graph depicted a stable output over long-term measurement.

In Figure 5.23, the Nafion-based sensors appear to have a higher degree of long term stability when compared to the KNO_3-based sensors. The prototypes with Nafion as electrolyte generally made output current measurements at lower average magnitudes at approximately -3.85 µA, -3.25 µA and -3.15 µA for PTFE, CA and PVC membranes respectively. The sensors with the exception of CA-membrane prototypes presented relatively good long-term stability profiles. The deviation of the sensor with a CA membrane reduced to ±0.08 µA and the enlarged y-axis scale in Figure 5.23 shows that the output current tends to decrease as time increases.

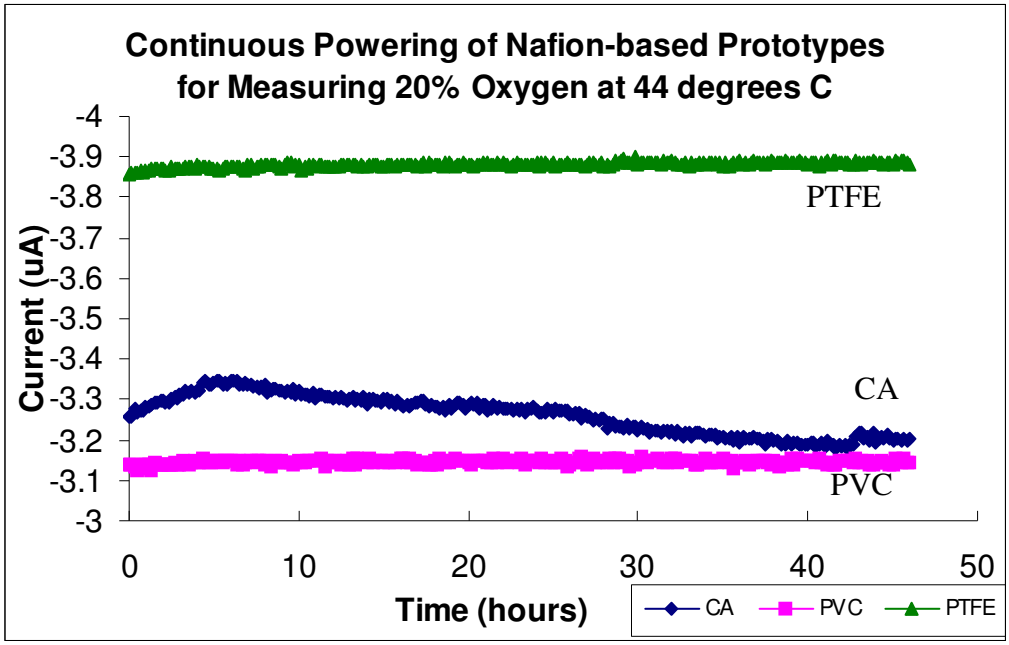

Figure 5.23: Results of Nafion-based Sensor under Continuous, Long-term Measurement

5.7.3 Discussion

In general, all six types of sensors performed well within specifications during the 46-hour procedure. Although the PVC-membrane sensors delivered the most stable measurements during the long-term experiment, they produced the lowest current magnitude levels. These two types of sensors remained almost unchanged in appearance from their original states except minor membrane peelings as shown in Figure 5.24. This could indicate the possibility of having long operating periods for PVC-membrane sensors. On the other hand, the sensors with a CA membrane gave measurements that fluctuated most. In addition, gradual decrements in output current magnitudes were observed and this could lead to more erroneous measurements if these types of sensors were used for continuous operation beyond 46 hours. At the end of the investigation, purplish residual stains probably due to gold electrode surface oxidation were also observed. The CA membrane was wrinkled and seemed to retain fluid, similar to a sponge. Physically, these sensors with CA membranes went through a total transformation, which could indicate the possibility of short-term operation only.

Finally, the sensors with PTFE membranes displayed relatively stable measurements with minimum deviations as well as large output current magnitudes. With these advantages, the effects of noise could easily be overcome and neglected. However, the used sensors may encounter some formation of hydroxides, which left specks of white residue underlying the PTFE membrane [68]. This is shown by the 'cloudy' layer depicted in Figure 5.24. Possible minor silver/silver chloride migration indicated by the smeared effects located around the reference electrode (RE) were also observed. In the long run, the sensors' operating stability would be questionable and deviations due to measured results exceeding the allowable 5% error which is specified by existing commercial transcutaneous systems would also be expected. Nonetheless, it would be not as crucial since an acceptable and economical lifetime of the disposable sensor for transcutaneous application was estimated at 30 hours.

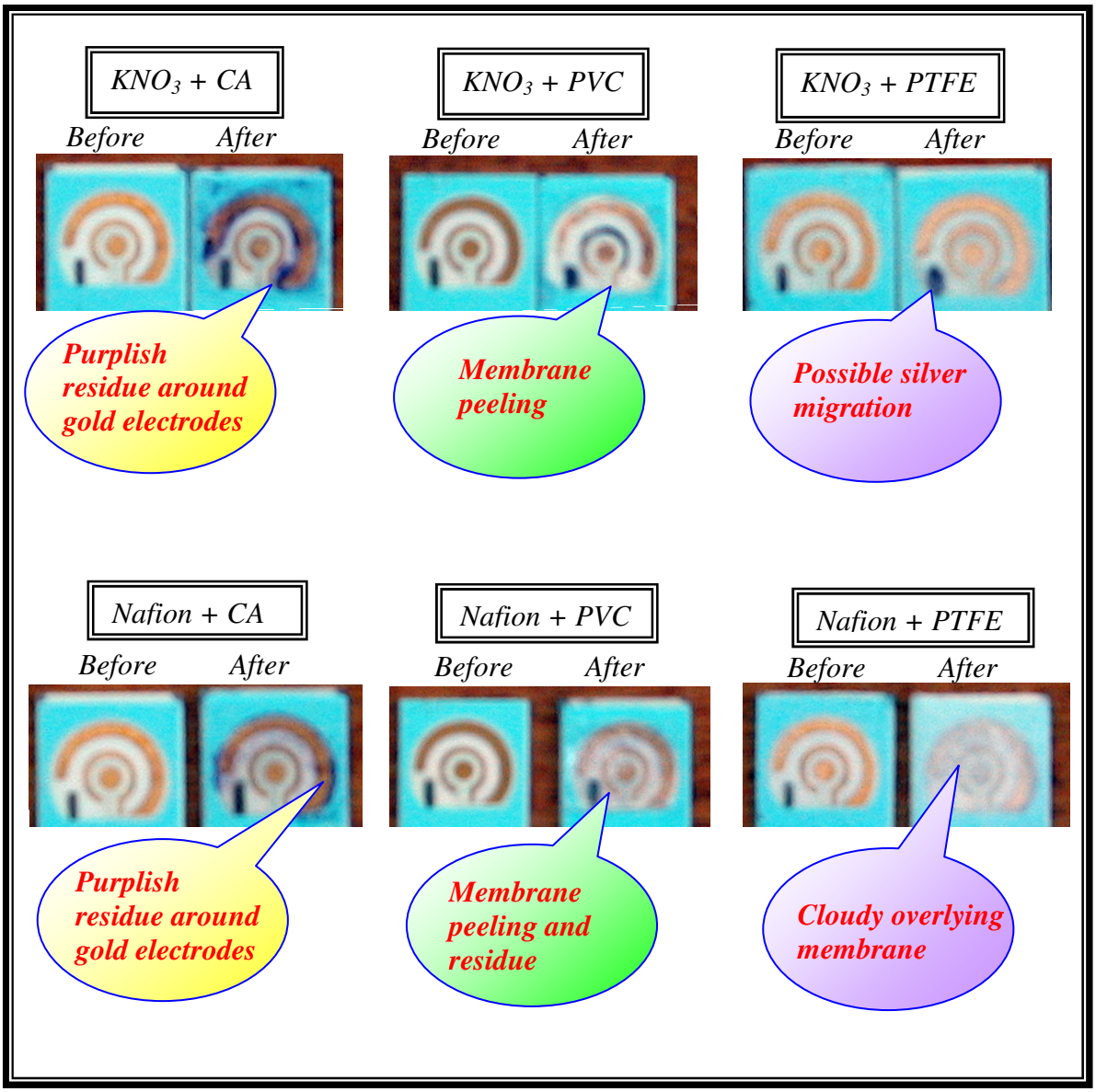

Figure 5.24: Prototype Samples after Long-term Continuous Powering

5.8 Transient Response of Oxygen Sensor at Transcutaneous Temperature

Based on the composition and design of the oxygen sensor, a theoretical model was established to estimate the transient and steady state response. The main objective of the model was to enable future designs to be made more easily and economically. In the model, two major aspects namely response time, often known as settling time, as well as the steady state response were investigated with respect to the material used. In order to validate the simple model described in Chapter 4, series of experiments were carried out on physical oxygen sensors to correlate and compare the corresponding parameters.

5.8.1 Experimental Procedure

The experimental setup as described in Section 5.7, shown in Figure 5.21 was used for this study. A TESTPOINT program was written to allow 0% oxygen (100% nitrogen) to enter the glass beaker filled with de-ionized water. The sensors were immersed in the de-ionized water, which was maintained at 37 °C. The sensors were also powered up to 44 °C and measurements were taken at intervals of 10 seconds. After approximately 750 seconds, 20% oxygen was allowed into the glass beaker.

5.8.2 Results and Observations

The transient responses of the sensors with KNO_3 and Nafion as electrolyte are illustrated in Figures 5.25 and 5.26 respectively. It could be observed that the change of output current level was most evident for the sensors with PTFE membranes. The regression from the point where 20% oxygen was introduced into the glass beaker to the point where a steady state level was attained assumed exponential functions. The flow rate of gas entering the 750ml beaker was approximately 12 litres/min. Hence, the time required to flush the beaker with 20% oxygen was estimated to be 3.75 sec. All the sensors under test are subjected to this consistent amount of time in the overall response. The relative performances of the sensors were compared and evaluated. Table 5.1 summarizes the settling time, which is defined as the time difference between 10% and 90% of the steady state value, required for each sensor.

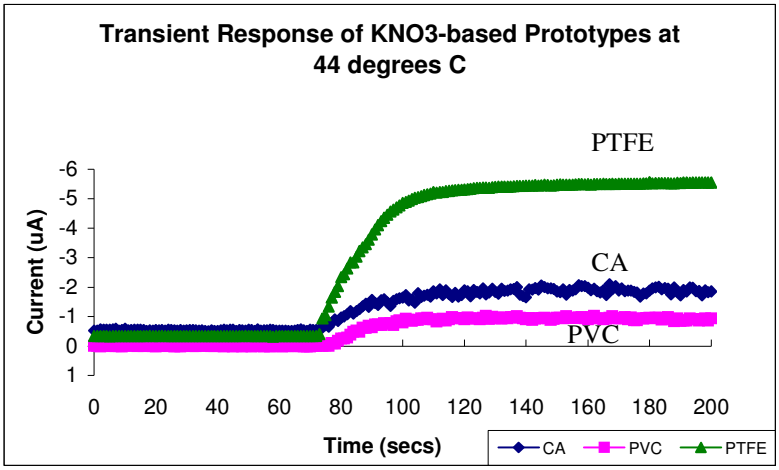

Figure 5.25: Transient Response of KNO_3-based Sensors at 44 °C

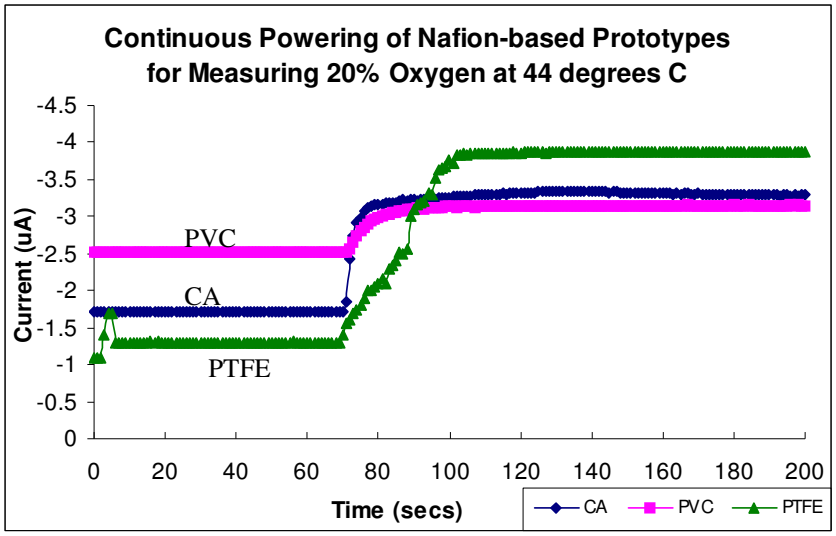

Figure 5.26: Transient Response of Nafion-based Sensors at 44 ℃

	Settling Time (seconds)		
Electrolyte \ Membrane	CA	PVC	PTFE
KNO_3	7	11	17
Nafion	5	11	20

Table 5.1: Settling Time for Transient Response of Sensor Prototypes

5.8.3 Discussions

In Chapter 4, the theoretical settling times for the sensors using KNO_3 / PTFE and Nafion / PTFE were calculated to be approximately 8.7 seconds and 14 seconds respectively. This was based on the one dimensional diffusion model employing planar electrodes with an overlying layer of electrolyte and membrane. Comparing the theoretical values with that of the experimental equivalent as shown in Table 5.1, it was found that the experimental settling time were approximately double the calculated values.

Many assumptions were made in the theoretical model in order to simplify the calculations. Parameters such as diffusion coefficients and oxygen permeability values took on fixed values from manufacturers' specification data sheets. These were usually typical values that

had a range of tolerances. In the evaluation of the models, typical values were chosen. However in actual fact, the true absolute value could have contributed to the differences in output measurements. Physical imperfections due to the fabrication process such as surface unevenness and the introduction of impurities also played important roles in the overall responses. These were all omitted from the theoretical model. Moreover, the influence of electrode geometry and sensor layout could also influence the diffusion rate of oxygen whereas the model only concentrated on a stand-alone cathode without the effects of other proximate electrodes.

The planar electrode model was adopted as an estimate to match the practical sensor. The model ignored the study of the fluid (L) layer (Chapter 4) but the experiments were carried out in an enclosed beaker filled with de-ionized water, hence layer L existed. One important issue to highlight was that the model did not include the effects of a transcutaneous measuring temperature of 44 °C. If all the assumptions were identified with quantifiable values, the theoretical model would closely match the data obtained from the experimental prototypes.

At elevated temperatures, the diffusion coefficient should be higher for the different materials. Hence, the settling time of the sensor ought to be shortened at 44 °C when compared to that at room temperature. However, this was not the case due to the assumptions made with respect to the calculated values. In hydrated conditions with KNO_3 as the electrolyte and a PTFE membrane, the sensor responded faster than the Nafion equivalent as it had a larger oxygen permeability value of 20×10^{-15} $mole.m^{-1}.sec^{-1}.Pa^{-1}$. This observation was supported by the theoretical calculations since the sensors with a KNO_3 electrolyte and PTFE membrane took on shorter response times (Chapter 4).

In conclusion, it was found that although the model assumed many factors, the assumptions were still acceptable to form a general trend to highlight the response and settling time of the sensors. This verified the validity of the model and also provided a gateway to carry out pseudo designs to improve responses of future prototypes.

5.9 Conclusions

The experiments in this chapter mainly focused on two major areas namely the heater module and the oxygen module. The investigation of the heater module included the verification of the linear resistance-temperature relationship for the cermet platinum heater element. It also revealed that the position and placement of the heater element on the substrate was not crucial to achieve accurate results. As the final practical sensor was targeted at being disposable, economical and accurate for transcutaneous oxygen measurement within a relatively reasonable period of effective operation, the long-term stability of output current was evaluated. It was found that the prototypes could sustain a stable temperature over 46 hours of continuous monitoring and this was sufficient from a practical point of view. Finally, from the images captured by the IR camera, it could be concluded that the temperature distribution produced by the heater element was relatively consistent. This proved that the substrate has good thermal conductivity and a measuring transcutaneous temperature could be achieved within approximately 5 minutes following powering up. In addition, the transcutaneous measuring temperature would remain relatively stable over a long period of time.

Initial investigations were carried out on the oxygen module to establish a better understanding of the oxygen sensor. Voltammograms of sensors with different electrolytes and membranes were produced for 0% oxygen measurement in a low humidity and dehydrated conditions. It was concluded that the sensors could not perform any measurement at a transcutaneous measuring temperature in a low humidity environment. Conversely once in the hydrated state, proper current diffusion limited plateaus formed. The measurement of 0% oxygen ought to correspond with zero current. However, offsets were observed for the prototypes but this could be easily overcome and compensated for using results obtained from prior calibrations made with known oxygen levels.

Nafion was the main polyelectrolyte material employed in the design to study its suitability as an alternative to aqueous salt electrolytes. Experiments were dedicated to study the effects of Nafion thickness on the output current measurement. The electrolyte layer should be substantially formed to provide sufficient ions for conduction. At the same time, this thickness factor should also allow a high oxygen diffusion rate. From the results obtained, 2 layers of Nafion would be ideal to optimize its functionality in the most economical way. The

oxygen level measurement over 46 hours was also carried out to observe the sensors' performance under continuous power. The results indicated that the variations from the average measured current were approximately 5.5% and identification of different oxygen levels was still possible even in the presence of such deviations.

The transient responses of the prototypes reflected the settling time towards a steady state response. Comparing the experimental and corresponding theoretical values calculated in Chapter 4, the general trend for both types of responses regressed to exponential approximations. In addition, the sensor with KNO_3 electrolyte and a PTFE membrane approached a steady state quicker than the sensor with Nafion electrolyte and PTFE membrane. Hence, the theoretical model could prove useful for developing future sensors, which may employ different and new materials in order to improve response times and other design aspects.

Chapter 6 Establishing Relationship between Oxygen Levels and Output Current

6.1 Sensors Employing KNO_3 Electrolyte

The disposable transcutaneous oxygen sensor was designed and fabricated in-house employing screen-printing methods so as to achieve cost effective and reliable production. The performances of different screen printed membrane materials were evaluated in both hydrated and dry test conditions using voltammetry and static experiments where the devices were subjected to different oxygen levels. This study explored the influences of temperature and humidity changes on the KNO_3-based sensors with different membrane materials.

6.1.1 Investigating the Effects of Different Voltammetric Sweep Rates

The sensor using KNO_3 electrolyte with CA membrane was subjected to a series of voltammetric experiments where the electrochemical activity was traced during oxidation-reduction (redox) reactions. The resultant voltammograms presented the relationship between the output current measured and the input biasing voltage between WE and RE.

6.1.1.1 Experimental Setup

The sensor was connected to the EG&G voltammeter where a ramped range of biasing voltages was applied at a specified sweep rate. A TESTPOINT computerized program was written to automate the data acquisition process via a Keithley 2000 series digital multimeter, a General Purpose Interface Bus (GPIB) interface card and IEEE-488 bus. This program also regulated the level of nitrogen and compressed air allowed into a glass container where the sensors under test were placed. The whole container was then submerged in a constant temperature bath in order to minimize the influence of the surrounding temperature to the sensor. This was set to approximately 37 °C to follow the typical body temperature of a normal human being. Figure 6.1 illustrates the experimental setup for obtaining voltammograms.

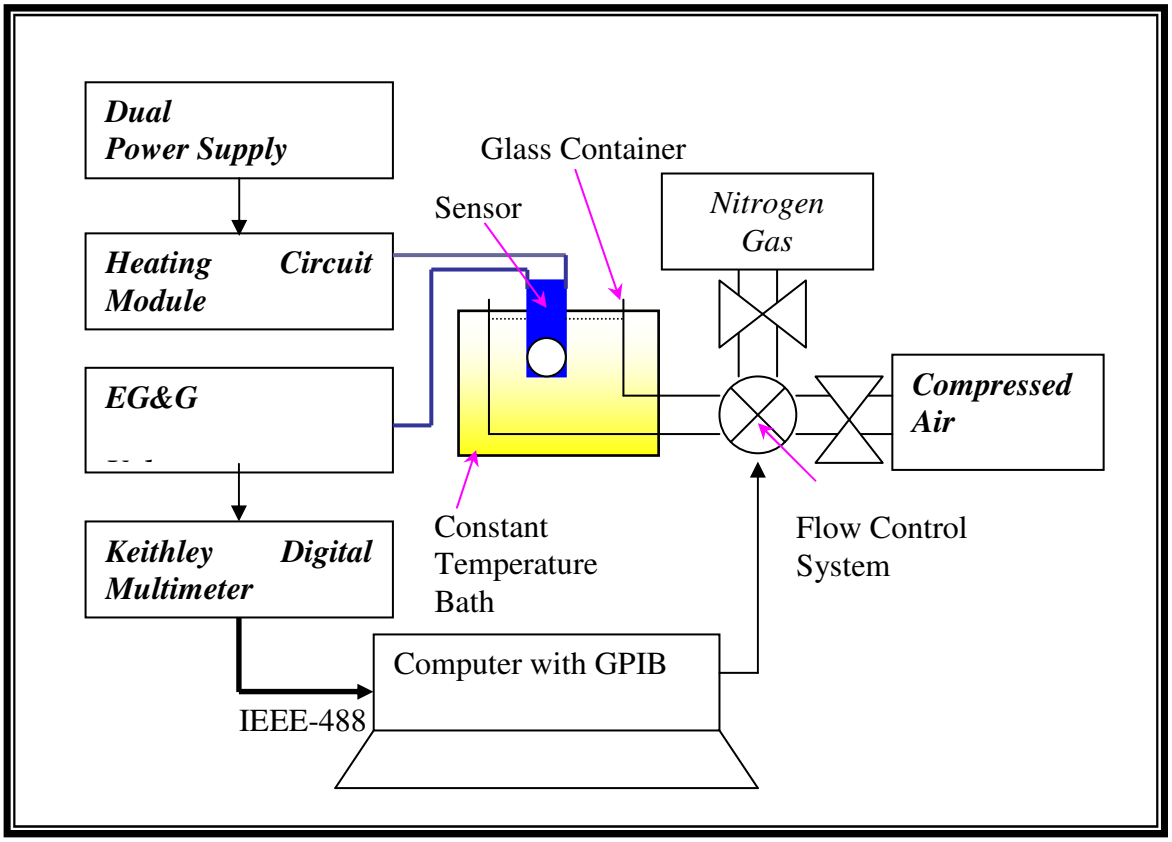

Figure 6.1: Experimental Set-up for Voltammogram

This experiment was carried out to determine the effects of different sweep rates, set by the EG&G voltammeter, on the output current of the sensor. The sensor temperature was initially set to approximately 25 °C under non-transcutaneous conditions. The sensor was suspended within the glass container, where the relative humidity was recorded at 68%. The aim of this temperature setting was to evaluate the sensors' performance under ambient atmospheric conditions as well as to ensure that the CA membrane would not completely dehydrate during the course of the experiment. The sensor was subjected to input biasing voltages between +0.5V and -1.5V across WE and RE at the sweep rate of 2mV/sec. The output current was measured via the Keithley meter and recorded at intervals of 10 seconds. The whole procedure was then repeated for the sweep rates of 10 mV/sec as well as 20 mV/sec.

6.1.1.2 Results of Voltammogram to Investigate the Effect of Different Sweep Rates

Figure 6.2 shows the voltammograms obtained from a sensor fabricated with KNO_3 electrolyte and CA membrane at different sweep rates of 2 mV/sec, 10 mV/sec and 20 mV/sec. The sensor is subjected to an environment of low humidity (58% relative humidity) with 20% oxygen at 25 °C. It is found that typical phenomena from redox reactions occur within the biasing potential range of +0.5V to -1.5V across WE and RE.

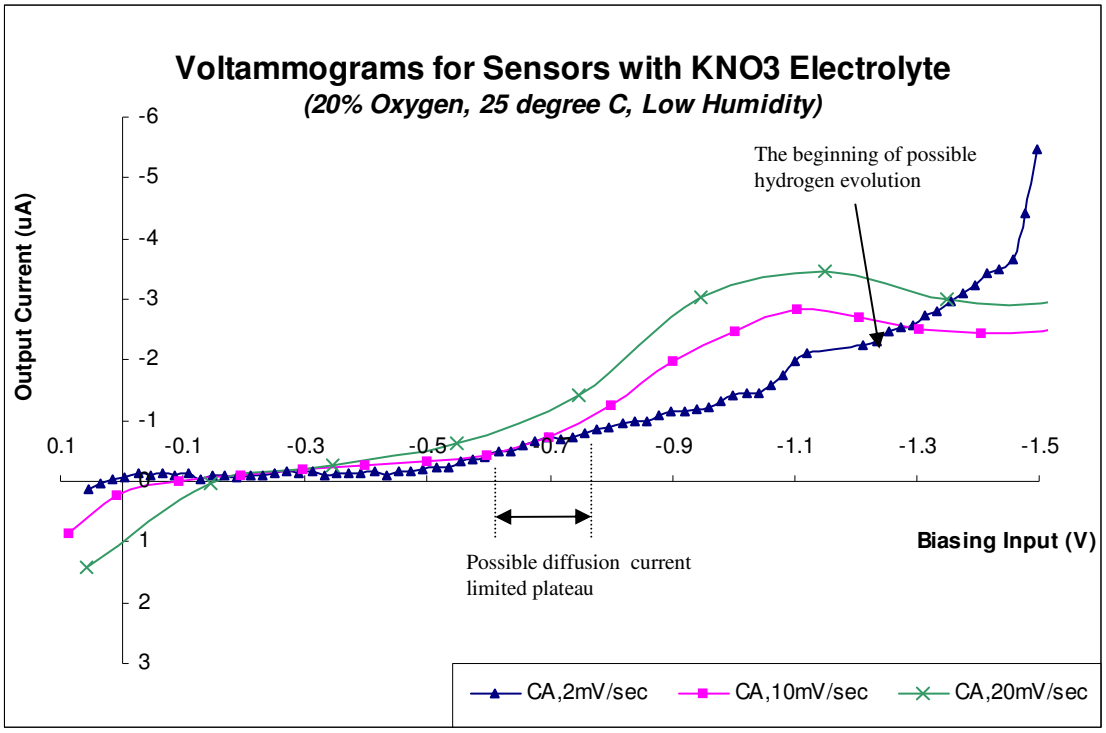

Figure 6.2: Voltammograms for Sensor with KNO_3 Electrolyte and CA Membrane under the Influence of Different Sweep Rates (at 25 °C in a Low Humidity Environment)

This redox system ought to remain in equilibrium throughout the potential scan [34], hence it would be denoted as reversible. Electron transfer kinetics would be sufficiently rapid to maintain the surface concentrations of oxidation and reduction as governed by the Nernst equation [32, 33]. The change of sweep rate from the EG&G voltammeter affected the absolute current output value. It was seen that as the sweep rate (ν) increased, the measured current took on larger absolute magnitudes. It also appeared that the curve given by ν at the 20mV/sec appeared to less noise fluctuations as compared to that at 2mV/sec. Reversibility depended on the relative values of the standard heterogeneous electron transfer rate constant (k_s) and ν [34]. Therefore, decreasing ν allowed more time for surface concentrations to be

adjusted to the new values required by the changing potential. With this, minute influences on the output current levels could be detected more readily.

6.1.1.3 Conclusions for the Effect of Different Sweep Rates

The voltammograms of the sensor with CA membrane was obtained at low humidity and room temperature of approximately 25°C using three different sweep rates of 2 mV/sec, 10 mV/sec and 20 mV/sec. From the results obtained, it was noted that the magnitudes of the current levels within individual possible diffusion current limited plateau increased as the sweep rates became larger. Agreeing with the theoretical finding of the Randles-Sevcik equation [34], the peak current was found to be directly proportional to the square root of sweep rate ($\nu^{1/2}$). Figure 6.3 shows the trends of the forward sweep responses for an ideal diffusion controlled cyclic voltammogram (reference to section 2.3.3) and the corresponding peak current vs $\nu^{1/}2$ relationship.

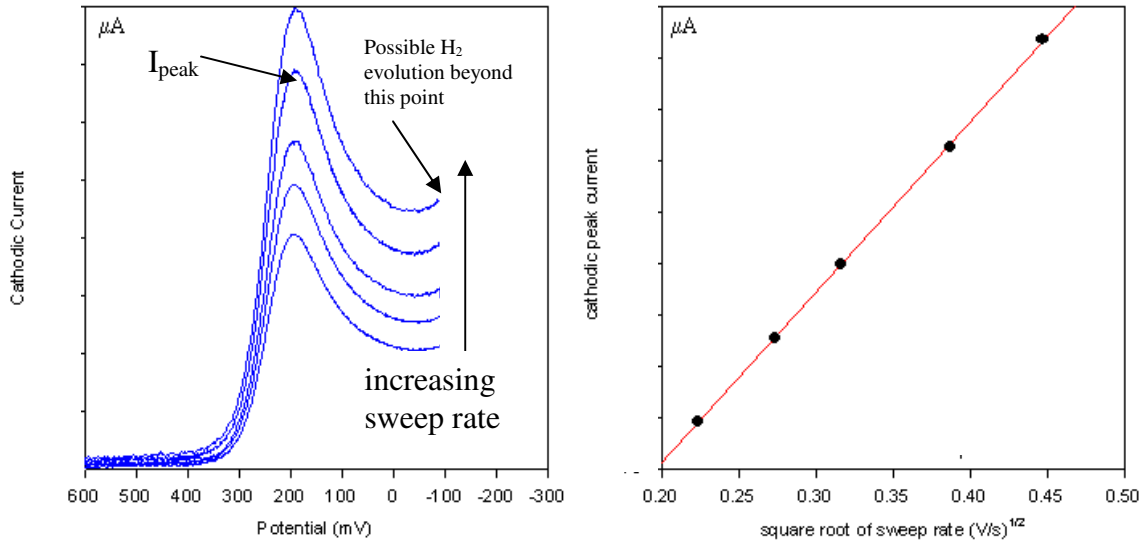

Figure 6.3: An Ideal Example of the Voltammetric Responses during Forward Sweep (Cathodic)

During a slow voltage sweep, the diffusion layer would extend much further from the electrode in comparison to a rapid sweep. This phenomenon resulted in having a flux at the electrode surface that was considerably smaller at slow sweep rates than it was at faster rates. Current being proportional to the flux towards the electrode would therefore be lower at slow

sweep rates and higher at faster sweep rates. The voltammogram given by the slower sweep rate displayed more fluctuations, which implied less estimation error at each biasing potential interval. This was adopted as it reflected more closely to the measurements made when a biasing potential was required from the potentiostat during static measurement.

With the effects of different sweep rates demonstrated, the optimum biasing potential of the sensor under low humidity test conditions at 25 °C was determined by the voltammograms to be at approximately -0.6V. This value is estimated at the start of the possible diffusion current limited plateau of the voltammogram at the sweep rate of 2 mV/sec as shown in Figure 6.2. The variable resistor in the potentiostat was adjusted to produce this voltage potential for the next experiment where the influences of humidity and temperature were studied.

6.1.2 Measurement of Oxygen Levels at Different Temperatures

This investigation identified the problems encountered by the sensor prototype at elevated temperature of typically 44 °C for transcutaneous measurement under low humidity conditions. Four sensor samples were prepared by employing KNO_3 gel electrolyte and CA membrane, while four others were covered with a PTFE membrane. Each individual sensor was connected to a potentiostat that was adjusted to a suitable biasing voltage for that type of sensor in order to drive the sensor into the diffusion limited current plateau. This potential was determined by the results obtained from prior voltammograms.

6.1.2.1 Experimental Setup

The output current measurement was recorded by the Keithley meter at intervals of 10 seconds. These sensors were initially exposed to a constant 0% oxygen level for 20 minutes in an unchanged environment, followed by a 20% oxygen level for the next 20 minutes as illustrated in the test pattern given by Figure 6.4. These measurements were carried out continuously for several cycles in order to verify the repeatability of the results.

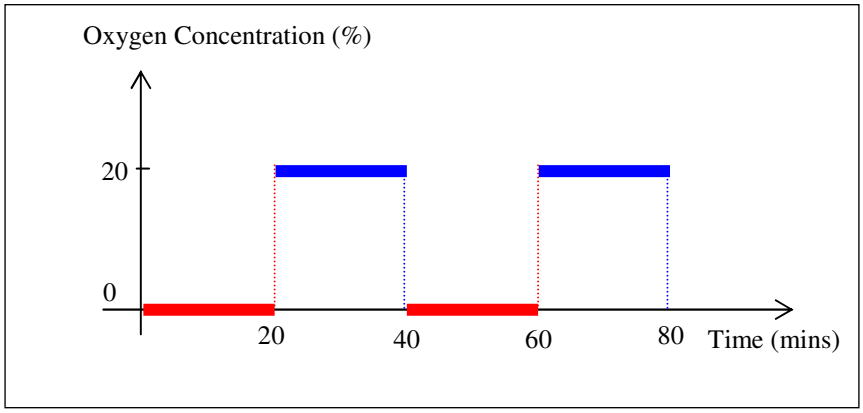

Figure 6.4: Test Pattern of Oxygen Level Inputs

Initially, both types of sensor were placed in the dry glass container with their respective platinum heaters powered to approximately 25 °C. The next set of tests involved the same measurements with the exception of changing the sensors' temperature to the transcutaneous temperature of 44 °C. When both sets of results under dry conditions were obtained, de-ionized water was added to the glass container so that the sensors' performances could be evaluated under hydrated conditions.

6.1.2.2 Comparison between Sensors' Performance in Normal Room and Transcutaneous Temperature

From the voltammograms illustrated in Figure 6.2, a biasing potential of -0.6V was chosen to operate the sensors for oxygen measurement at a normal room temperature of 25 °C as well as at the transcutaneous measuring temperature (44 °C). This potential was deemed suitable as it lay within the diffusion limited current plateau. It was essential for the biasing potential to be chosen within the diffusion limited current plateau so that even in the event of possible electrochemical drifts, the output current level would remain relatively stable and consistent when measuring a given oxygen level. The sensors employed for this experiment included previous units with CA membranes as well as newly fabricated PTFE-membrane prototypes. The sensors were required to detect oxygen set at two extreme levels, which were the minimum of 0% and maximum of 20%.

Membrane	***25 ℃***		***44 ℃***	
	Current at 0% O_2 (μA)	Current at 20% O_2 (μA)	Current At 0% O_2 (μA)	Current at 20% O_2 (μA)
CA (humid ≈ 58% RH)	-0.03	-0.72	0	0
CA (hydrated)	-0.06	-1.01	-0.15	-1.80
PTFE (humid ≈ 58% RH)	-0.03	-0.93	-0.02	-0.02
PTFE (hydrated)	-0.04	-0.95	-0.20	-1.60

Table 6.1: Output Steady-state Current for Sensors at Room and Transcutaneous Temperature

Table 6.1 summarizes the current measured for the sensors under different temperature and humidity conditions. The humid condition represented a relative humidity of 58%. At 25 °C, the sensors were effective and responded correspondingly to changes in oxygen levels. However, the sensor with sprayed-on PTFE membranes required a longer time to respond and detect changes in oxygen levels. This could be attributed to the fact that the physical thickness of CA and PTFE layers were different as well as the two materials having different diffusion coefficients and response times.

When the temperature was elevated to 44 °C, the sensors in low humidity completely failed to respond. They were then immersed in de-ionized water, still maintained at the transcutaneous measuring temperature for the next set of measurement. The response resumed with much higher current magnitudes as compared to the results obtained when the temperature of the sensor is at 25 °C. This trend of results was observed for both the sensors employing CA and PTFE as their respective membranes.

6.1.2.3 Conclusions on Sensor Performance in Normal Room and Transcutaneous Temperature

It was found that the sensors with CA or PTFE as their respective membranes were able to identify two distinct levels of oxygen namely 0% and 20% under both low and high humidity conditions at 25 °C. However when the temperature was elevated to 44 °C, the sensors could

only respond when fully hydrated in de-ionized water. At low humidity, the current magnitude was very small and the sensors failed to distinguish 0% from 20% oxygen.

For this biomedical application, elevated temperature was essential in order to allow the skin to be sufficiently porous for arterial oxygen to diffuse out onto the surface. However at 44 °C, the membrane materials experienced possible dryness and discontinuity of viable paths for oxygen to diffuse through. Conversely, should the membrane be subjected to a consistent level of dampness, the sensors could function effectively with only a slight decrease in current magnitudes.

6.1.3 Voltammograms for Sensors with Different Membranes for Transcutaneous Measurement

Each KNO_3-based sensor was coated with one of the four different membrane materials namely CA, PVC, PTFE or Nafion. The objective of this investigation was to determine the most suitable biasing potential from the diffusion limited current plateaus for the sensors performing transcutaneous measurement.

6.1.3.1 Experimental Setup

The experimental setup is depicted in Figure 6.1. All measurements were made with the sensor powered to 44 °C in a hydrated environment and exposed to a 20% oxygen level. The EG&G voltammeter was set to provide the biasing potential across WE and RE from +0.5V to -1.5V at 2mV/sec sweep rate.

6.1.3.2 Results and Discussion on Voltammogram for Sensors with Different Membrane Materials under Transcutaneous Conditions

From Figure 6.5, it is observed that there is a relatively leveled region with very low current output, which is comparable to noise between +0.5V to approximately -0.2V. The output current magnitude then increased significantly within the range of biasing voltage from -0.4V to approximately -0.6V. Beyond this point, a possible diffusion limited current plateau was found between -0.65V to -1.4V. The current magnitudes were much larger and the profile was relatively flat with the inclusion of some sudden peaks. These current peaks could be due

to undesirable contributions from impurities, which might have been introduced during the fabrication process [70].

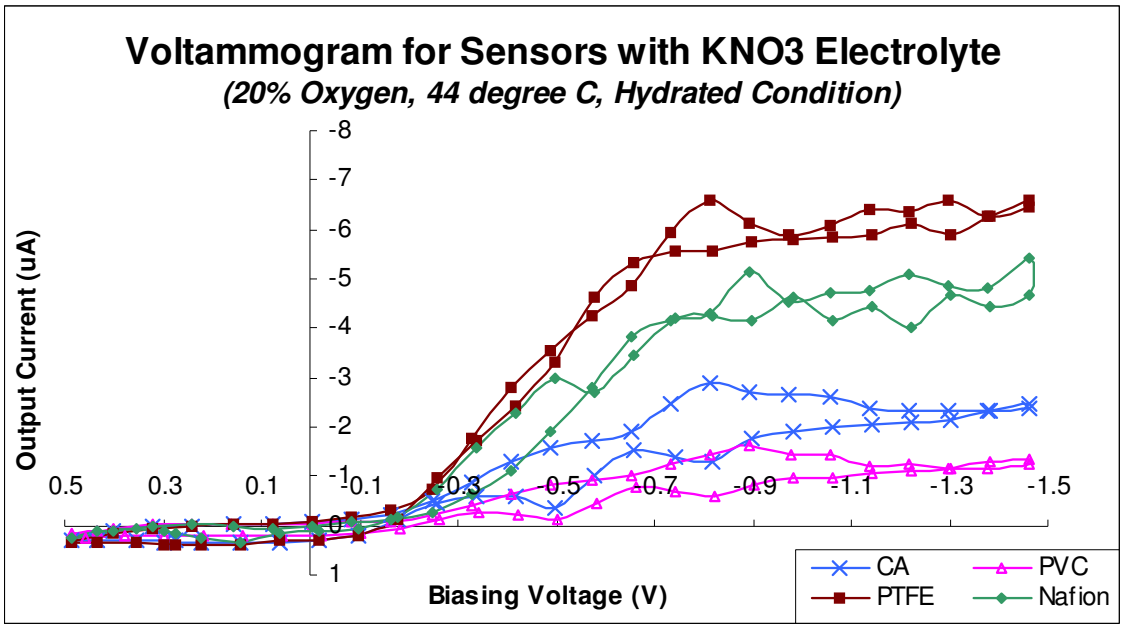

Figure 6.5: Voltammogram for Sensors with Different Membranes at 44 ℃

Although cyclic voltammetry was performed on the sensors to determine an optimum biasing potential, only the results from the forward sweep along the current diffusion limited plateau which correspond to cathodic reactions were taken into considerations. Generally, the hystersis became more evident at the region bounded by the current diffusion limited plateau for all the sensors under test. The biasing potential at which the sensors operated might differ slightly for different types of samples. Nonetheless, several samples of the same sensor type appeared to reproduce voltammograms depicting similar current diffusion limited plateaus. To conform to a most convenient common setting for the potentiostat, the most reasonable choice from the forward sweep of the voltammogram was selected at approximately -0.7V for the biasing potential at transcutaneous temperature.

By repeated experiments and inspecting the obtained voltammograms, -0.7V appeared to be statistically the minimum biasing potential possible in order to activate the sensors within the diffusion limited current plateau. This potential for transcutaneous measurement was not too distant from that given by the response at 25 °C where the potential was defined at -0.6V. From all the voltammograms shown in Figure 6.5, no evident oxygen or hydrogen evolution occurred within the experimental biasing potential sweep range.

The graphs obtained from the sensors with PVC, CA, Nafion and PTFE membranes all displayed similar trends of responses in terms of the region dedicated for current diffusion limiting. However, the current magnitude given by the sensor with a PVC membrane recorded the lowest value of approximately -0.8 μA at the biasing voltage of -0.7V. The CA-membrane sensor produced slightly higher currents of -1.6 μA. The sensors with Nafion and PTFE as the membrane responded with outputs as large as -4 μA and -6 μA respectively.

6.1.3.3 Conclusions for Sensors with Different Membrane Materials

To overcome the problem of sensors not responding at low humidity and transcutaneous temperature, all subsequent experiments to establish the relationship between output current and oxygen level were carried out under hydrated conditions. Two other new polymer materials namely PVC and Nafion were introduced to allow a basis for more comprehensive comparisons. The voltammogram for each individual sensor was obtained to determine its respective biasing potential in a fully hydrated environment at 44 °C. The most prominent observation is that the current magnitudes for different sensors were not the same. The possible region for the diffusion limited current plateau took on the range between -0.65V and -1.4V. A viable biasing potential for all four types of sensors narrowed down to -0.7V for measurements made under fully hydrated transcutaneous conditions.

6.1.4 Relationship between Output Current and Transcutaneous Oxygen Level

In these experiments, the relationships between the output current measured and its respective oxygen level were established for the sensors used in Section 6.1.3. Potentiostats were adjusted to appropriate biasing potentials that were determined from respective voltammograms.

6.1.4.1 Experimental Setup

The main experimental setup was similar to that as described in Section 6.1.2.1. The procedures involved having the sensors immersed in de-ionized water so as to keep the membrane hydrated at the transcutaneous temperature of 44 °C. With the aid of a new TESPOINT program, 100% nitrogen (equivalent to 0% oxygen) was initially allowed into the glass container via the gas inlet. Readings were taken at intervals of 40 seconds for

approximately 20 minutes. After which, the gas content in the glass container was varied to 4% oxygen, and the same measurement procedure was repeated. The oxygen level continued to increase to 20% in increments of 4%, then decrease from 20% to 0% at the same interval.

The final experiment involved the same set of sensors subjected to the same procedures but with the addition of a self-adhesive polymer membrane, known as Tegaderm (trademark from 3M). Tegaderm is basically polyurethane [71] and is used to mimic the porosity of the skin for transcutaneous measurement in a laboratory environment. It allows oxygen to diffuse but does not possess the other physical properties of skin, for example the electrical conductivity.

6.1.4.2 Establishing Relationship between Output Current and Transcutaneous Oxygen Level

Each sensor was biased at -0.7V across WE and RE via the potentiostat. Transcutaneous conditions were applied in this experiment and the sensors were subjected to increasing oxygen levels, which was alternated with brief exposure to of 100% nitrogen for re-initializing to a known reference level. Figure 6.6 illustrates the graphs obtained from these experiments.

It was noted that each level of oxygen was distinguished from another relatively clearly. By averaging the data obtained from measuring an unchanging oxygen level, good repeatability was found. The response time of the sensor detecting the change in oxygen levels was fast enough to be regarded as an instantaneous measurement. In the case of the sensor with a PTFE membrane, it was observed that the current measurements at 16% and 20% oxygen were fluctuating considerably despite the theoretically constant level of oxygen supplied. This may cause some discrepancy in determining the actual oxygen level. However in the practical application of transcutaneous measurement, it proved to be less crucial as these ranges of variations were well beyond the specifications for indicating a patient's normal condition, which is between 9% to 14% oxygen.

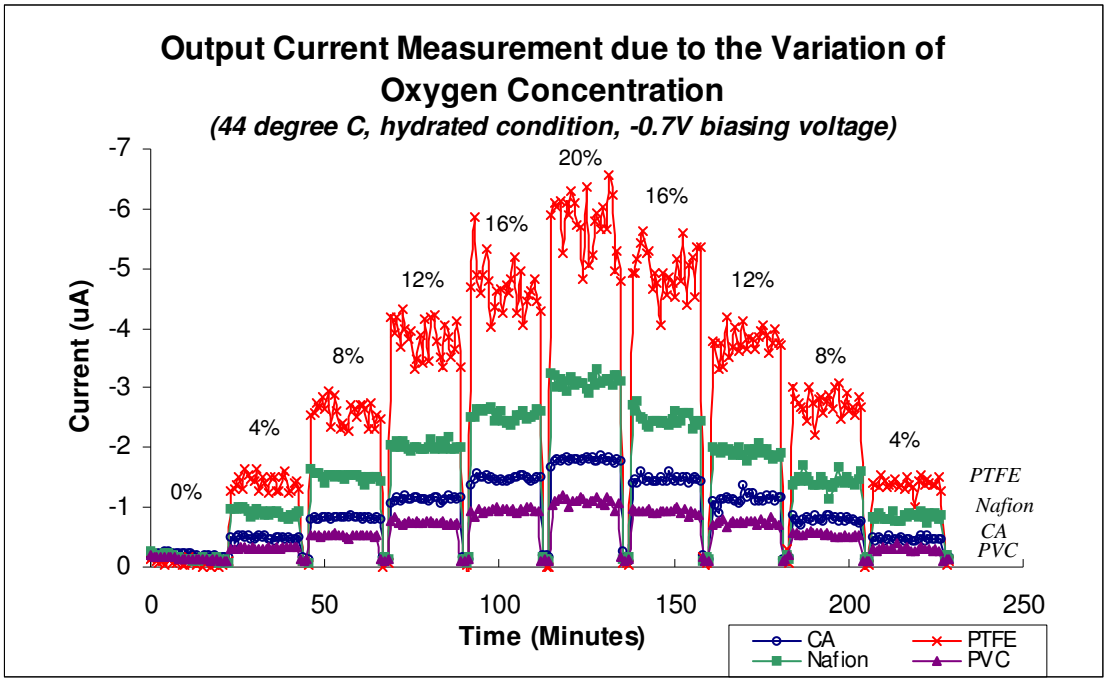

Figure 6.6: Current Outputs due to Change in Oxygen Levels at 44℃

Figure 6.7 illustrates the averaged results at individual oxygen levels obtained from Figure 6.6. The percentage oxygen was correlated to its respective partial pressure equivalent in mmHg through multiplication by a conversion factor of 7.8. This conversion factor was obtained by considering the ideal situation where normal atmospheric pressure was given by 780 mmHg with full (100%) oxygen content occupying only 20% of the total atmospheric pressure. It was found that all sensors produced linear relationships between the output current and oxygen level. PTFE and Nafion membrane sensors could identify the differences in oxygen level distinctly by the steeper gradients as shown in Figure 6.7. This indicated a large change in output current with respect to a small change in oxygen level. With this calibration graph, the corresponding oxygen level could be measured effectively.

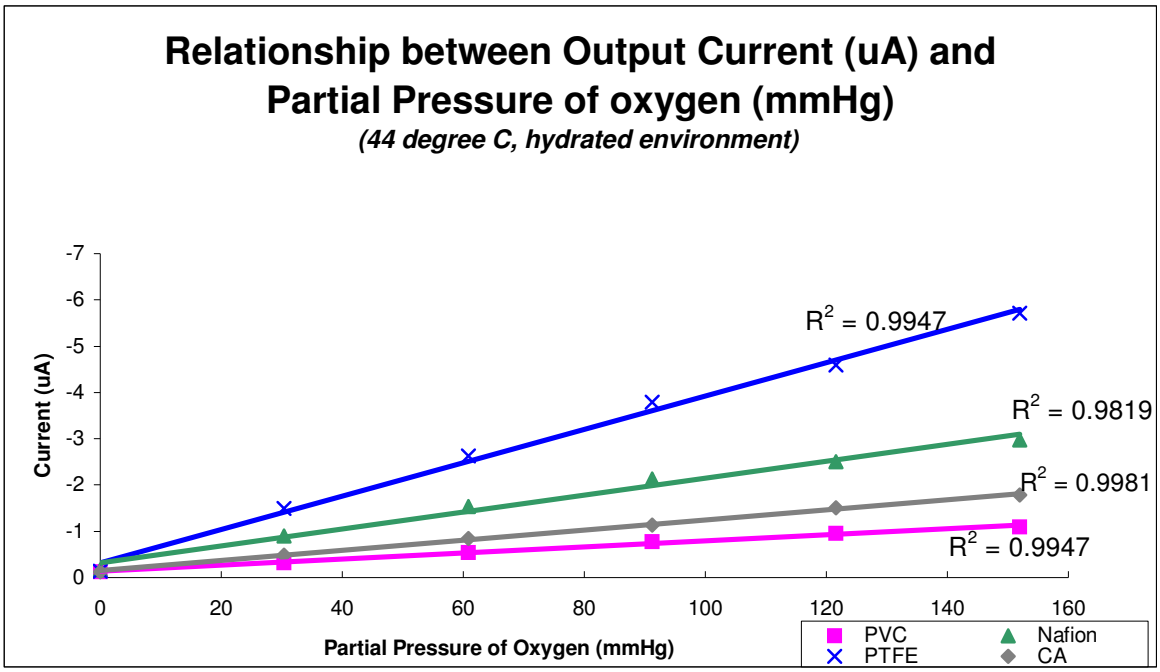

Figure 6.7: Graph to Correlate Output Current Measurement with Transcutaneous Partial Pressure of Oxygen

In order to create a real practical situation for transcutaneous measurement, a polymer (Tegaderm from 3M) with porosity similar to human skin was used to introduce an additional layer between the sensor membrane and the oxygen gas. The results in Figure 6.8 show that the different levels of oxygen could no longer be clearly defined by all four types of sensors. Significant decreases in current magnitudes were observed when the sensors were subjected to an initializing level of 0% oxygen at the beginning of the experiment. This reflected the slow response attributed to the additional layer of Tegaderm. Hence, the transient response time required to reach steady state levels was evidently much longer.

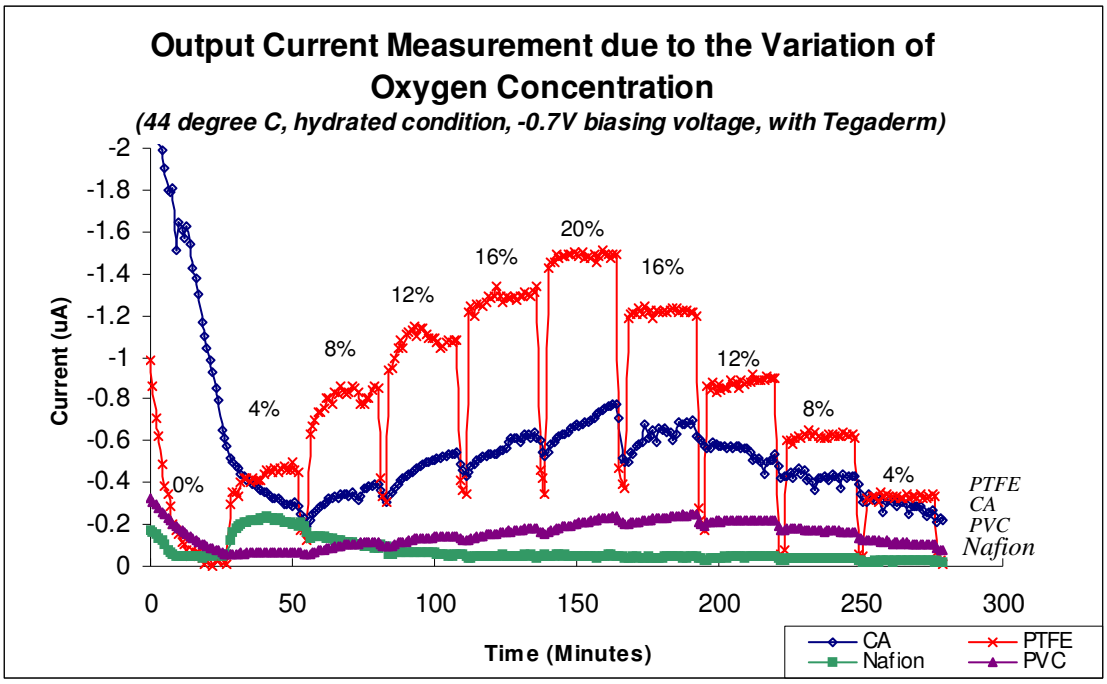

Figure 6.8: Measurement Made from Changing Oxygen Levels at 44℃ with the Use of Tegaderm

The sensor with PTFE as its membrane appeared to be fairly effective in distinguishing different oxygen levels despite more fluctuations. However at 20% oxygen, the current magnitude had changed significantly from approximately -5.8 μA to -1.5 μA. It was also noticed that the current measured at each brief interval of 0% oxygen (when re-initializing the sensor) did not return to the same value. The poor repeatability of current output at the same oxygen level on two separate occasions (once when oxygen level was increasing and the other when oxygen level was decreasing) is also observed from Figure 6.8. The sensor with Nafion as the membrane failed to respond after increasing the oxygen level beyond 4% in this experiment. Both CA and PVC membrane sensors also suffered from poor records of performance in terms of stability, repeatability and low current magnitude.

6.1.4.3 Conclusions on Establishing Relationship between Output Current and Transcutaneous Oxygen Level

With all the potentiostats adjusted to -0.7V, the main objective to correlate current with different oxygen levels was achieved as illustrated in Figure 6.6. Each sensor was able to track the changes in oxygen levels faithfully with relatively short response times. This was

ideal for continuous measurement where sudden variations could be detected almost instantaneously. The repeatability of measuring each oxygen level was shown to be well within satisfactory deviations of approximately ±3%. Generally, when the sensors were measuring a particular constant oxygen level, the fluctuations of output current measurements gave a mean standard deviation of approximately 0.2, low enough to be neglected for most cases. For the sensor with PTFE membrane, the fluctuations were more apparent with the maximum standard deviation of 0.5 when measuring beyond 16% oxygen levels. This error due to the fluctuation could be minimized by employing averaging methods in the data processing. Figure 6.7 presents the linear regression plot of the mean current obtained at particular oxygen level intervals. The relationships between the current (I in μA) and the partial pressure of oxygen (P_O in mmHg) for the sensors with different membranes as well as their respective regression coefficient (R^2) are listed in Table 6.2.

Membrane employed	***Output current equation***	***Regression coefficient***
PTFE	$I = -0.036P_O - 0.323$	0.9947
Nafion	$I = -0.0183P_O - 0.3128$	0.9819
CA	$I = -0.011P_O - 0.1463$	0.9947
PVC	$I = -0.0066P_O - 0.1341$	0.9981

Table 6.2: Correlation Equation for Output Current with Partial Pressure of Oxygen

The mathematical definition of parameter sensitivity [72] was given by the first-order derivative of the state variable (in this case being current, I) with respect to the value of a parameter of interest (i.e., partial pressure of oxygen). Hence, the sensitivity of the sensors could be evaluated by differentiating the output current equation. The results were the gradients of individual linear regression lines. The sensor with PTFE membrane displayed the highest sensitivity of -0.036 μA/mmHg, followed by the sensors with Nafion, CA and PVC membranes. The y-axis intercept value of the regression lines corresponded to the output current when the partial pressure of oxygen was zero. Ideally this value should be close to zero because in the absence of oxygen, there should not be any oxygen reducing reaction occurring, hence implying no output current. In practice, this y-axis intercept value

might be contributed to by offsets presented by the electronic circuit in the potentiostat and other supporting measuring equipment.

Several assumptions were not entirely valid due to restrictions imposed by apparatus and experimental factors. For example, to achieve 0% oxygen, although the glass container where the sensors were placed for test is filled with a continuous flow of 99% nitrogen, it might not completely seal. Atmospheric influences could affect the gas content within the container.

From the results, the sensor with a PTFE membrane displayed the largest initial current value of -0.323 μA under no influence by partial pressure of oxygen. One possible reason could be due to the fact that sprayed-on PTFE might have allowed oxygen as well as other chemical species or impurities to percolate through to the electrode surfaces and participate in the reduction process. In the case of the Nafion membrane, full hydration increased its conductivity by about 60% in a process known as conductivity relaxation [73, 74]. Once hydrated, the overall output current reached levels comparable to that of PTFE. Conductivity relaxation as opposed to dielectric relaxation is the re-orientation of electrical dipoles where the centers are not fixed. When Nafion is hydrated, the hydrogen ions become mobile hence, ionic conductivity increases with the free H^+ proton hopping from one SO_3 site to another through the electrolyte.

Although screen-printed membranes of CA and PVC performed poorest among all the sensors under test in terms of current magnitudes, they reflected good repeatability and stability upon activation. They also had relatively small y-axis intercept values at -0.146 μA and -0.134 μA respectively. CA was a water-porous material that permitted dissolved gases to percolate through the enlarged gaps within the hydrated material rather easily. PVC on the other hand was a waterproof material and the water molecules could only stay on the membrane surface. Dissolved gas diffused through these water molecules at the water-PVC interface, then through the membrane material before reaching the electrolyte. This mechanism greatly hindered the rate of oxygen reduction at the electrode surface and decreased the output current as observed from Figure 6.6.

In an attempt to realize the whole experimental setup as closely as possible to a practical situation, Tegaderm was attached in front of the sensors to imitate the presence of skin. This

way, the membrane and electrolyte would not be in direct contact with the de-ionized water. The results displayed in Figure 6.8 suggest that Tegaderm being a gas permeable waterproof material appeared to attenuate the amount of gas diffusion non-linearly. With an additional layer involved, diffusion of gas would naturally be decelerated. The sensors with PTFE and CA membranes managed to give reasonable current measurements despite having deteriorating repeatability due to the assumption that Tegaderm could have trapped uneven amounts of residual gas and water, which contributed negatively to the final result. Response times of the sensors were also seriously affected and distinct changes in oxygen levels could no longer be identified easily.

When Tegaderm was introduced in between the PVC membrane and de-ionized water, the sensor was practically deprived of any possible water-PVC interface. Such a configuration hindered the oxygen diffusion path more significantly and resulted in the poor responses obtained in Figure 6.8. An interesting observation was noted for several sensors with Nafion as a membrane. Initially, the sensors seemed to be able to follow the traces of oxygen level variation. However, after measuring approximately two different oxygen levels, they could not distinguish the changes happening in their surrounding. In order to verify such behaviour, more studies should be carried out.

6.1.5 Overall Conclusions on Sensors Employing KNO_3 Electrolyte

Thick film technology had been employed to fabricate the in-house transcutaneous oxygen sensor prototypes, which were subjected to several experiments and evaluations. The investigations included studies carried out on the influence of voltammetric sweep rates as well as the effects due to variations in temperature and humidity changes on the electrochemical sensors with KNO_3 electrolyte and different membrane materials.

In conclusion, these investigations had brought about a better understanding of different membrane materials employed in screen-printed sensors with aqueous salt-based (KNO_3) electrolyte. The choice of materials was considered crucial in realizing an optimum low cost design for a transcutaneous oxygen sensor. It was also found that although each sensor resulted in slightly different ranges of current diffusion limited plateaus, a general biasing potential of approximately -0.7V was adopted after subjecting several samples of KNO_3-based sensors to repeated trials.

The results obtained from the various experiments suggested that the sensors with PTFE and PVC membrane could be subjected to further transcutaneous tests, especially in clinical trials to justify their suitability in realizing a commercial prototype oxygen sensor.

6.2 Sensors Employing Nafion Polyelectrolyte

Due to the sensor operating at an elevated temperature of typically 44°C, a non-aqueous electrolyte was required to avoid problems related to rapid dehydration. Several different polymer electrolyte and membrane materials were evaluated in the study of the devices and their performances in both wet and dry test conditions were compared. Some encouraging results had been obtained with the sensors at both ambient and elevated temperatures but the humidity level of the test conditions proved to be an influential parameter. The investigations had greatly contributed towards the understanding of the materials' suitability in achieving a viable low cost sensor. This section presents the investigations gathered from the effects of temperature and humidity changes on the electrochemical sensors, which contained the polymer electrolyte, Nafion overlaid with different membrane materials.

6.2.1 Effects of Different Voltammetric Sweep Rates on Nafion-based Sensors

The influences of sweep rates set by the EG&G voltammeter on the output current were studied for in-house fabricated sensors employing Nafion as the polyelectrolyte with no other additional layer of membrane.

6.2.1.1 Experimental Setup and Procedure

Figure 6.9 describes the experimental setup for obtaining the voltammogram when the sensor was subjected to ramped input biasing voltages from +0.5V to -1.5V across WE and CE.

TESTPOINT software was employed to generate a computerized program to automate the data acquisition process via a Keithley 2000 series digital multimeter, a General Purpose Interface Bus (GPIB) interface card and a IEEE-488 bus. This program also controlled a digital-to-analog converter (DAC) card to regulate the nitrogen and compressed air valves. This allowed desired levels of oxygen to fill a glass beaker where the sensors were placed.

The whole beaker was then submerged into a constant temperature bath so as to minimize the influence posed by the surrounding temperature. The reference temperature of the bath was also set to the typical body temperature of a normal human at 37 °C. The heating controller circuit module was employed to elevate the temperature of the sensor to approximately 44 °C for transcutaneous measurement.

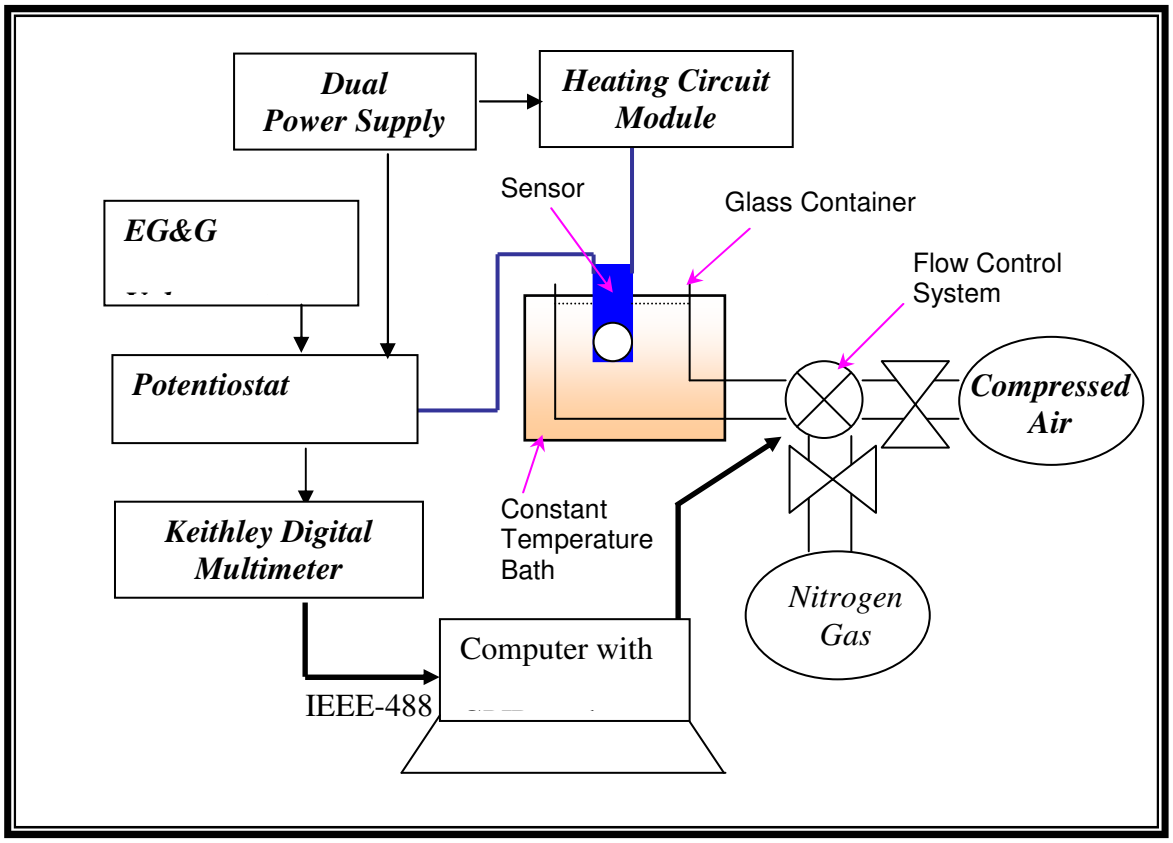

Figure 6.9: Experimental Set-up for Voltammogram

The output current was recorded at intervals of 10 seconds for sweep rates at 2 mV/sec, 10 mV/sec as well as 20 mV/sec. The results highlighted the characteristics of the sensor at different stages of operation.

6.2.1.2 Investigation on the Effect of Sweep Rate using Direct Voltammetry

Figure 6.10 shows the direct voltammograms obtained from the sensor prototype fabricated with Nafion electrolyte. The sensor was subjected to 20% oxygen level at 44 °C. From previous literature [69], the diffusion limited current plateau of general amperometric sensors usually occur within the biasing potential range of -0.2V to -1.0V with

respect to an Ag /AgCl reference across WE and CE. Hence for this experiment, the potential sweep was carried out from +0.1V to -2.0V. Possible hydrogen evolution could be identified beyond -1.7V where the output current suddenly surges to relatively large magnitudes. Meanwhile, a relatively flat diffusion limited current plateau was observed between -0.7V to -1.5V. Peaking was also observed at the start of this plateau and appeared to occur at larger input biasing potential magnitudes when the sweep rate was increased. From Figure 6.10, it appears that the graph given by sweep rate (ν) at 20mV/sec produces a much narrower plateau as compared to that at 2mV/sec. This outcome favoured the choice of employing the slowest possible sweep rate for investigative purposes.

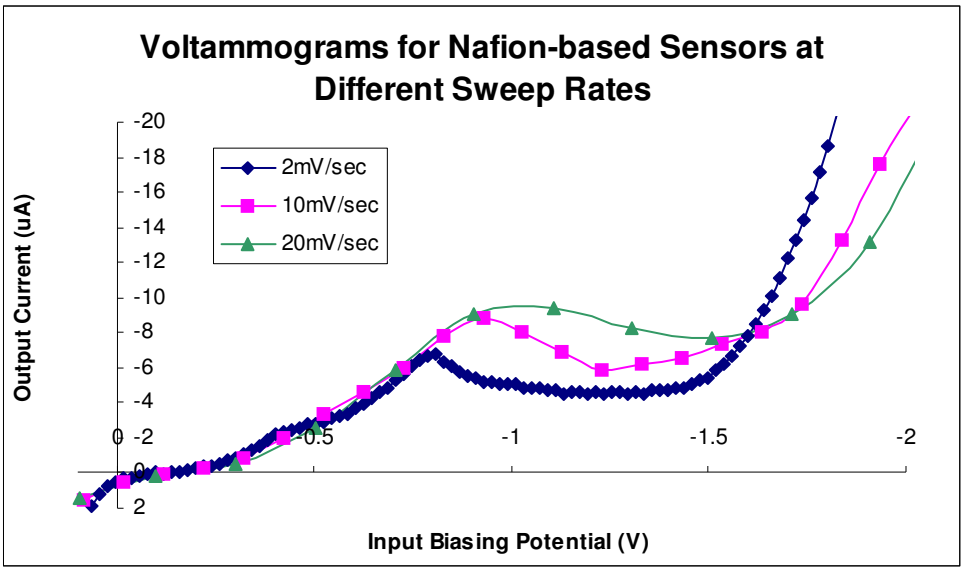

Figure 6.10: Voltammograms for Sensor with Nafion Electrolyte under the Influence of Different Sweep Rates (at 44 °C)

6.2.1.3 Conclusions on the Effect of Sweep Rate using Direct Voltammetry

Before evaluating the performances of prototypes under different test conditions, the effect of different sweep rate settings produced by the EG&G voltammeter on the measured current output via its internal potentiostat was studied. Voltammograms at fully hydrated and transcutaneous conditions of approximately 44°C were generated using three different sweep rates of 2 mV/sec, 10 mV/sec and 20 mV/sec. From the results obtained, the current magnitudes were found to increase, as sweep rates became larger. The outcome was similar to that of the experiment using KNO_3-based sensors as discussed in Section 6.1, therefore

both types of sensors exhibited similar characteristics. Current, being proportional to the flux towards the electrode surface [34], would hence be lower at slow sweep rates and higher at high sweep rates, which was observed from Figure 6.10.

6.2.2 Voltammograms for Transcutaneous Sensors with Different Membranes

This investigation included sensors employing Nafion polyelectrolyte without a membrane as well as those coated with three different membranes namely CA, PVC or PTFE.

6.2.2.1 Experimental Setup and Procedure

The effectiveness for the different materials to act as the membrane for the transcutaneous oxygen sensor was studied using the experimental setup as described in Figure 6.9 with the exception of including external potentiostats. All measurements were carried out with the sensors' temperature increased to 44 °C in a hydrated environment. They were exposed to a 20% oxygen level with the EG&G voltammeter providing the biasing potential across WE and CE from +0.5V to -1.5V at a fixed sweep rate of 2 mV/sec. The voltammograms were obtained by plotting the measured current against the input biasing potential.

6.2.2.2 Voltammograms of Sensors with Different Membrane Materials under Transcutaneous Conditions

Different polymer materials were coated on top of the electrolyte layer as a membrane to provide control over gas diffusion and prevent contamination from external impurities. In order to proceed with proper correlated measurements, suitable biasing potentials ought to be determined from the voltammogram of each sensor type, which should lie within the diffusion limited current plateau. The output current level should remain relatively consistent when measuring a fixed oxygen level even in the event of possible electrochemical drifts. The voltammograms of hydrated sensors employing no membrane, CA, PVC or PTFE as the membrane material are illustrated in Figure 6.11.

With the exception of the sample with a PVC membrane, most sensors gave near zero current outputs that were comparable to electrical circuit noise between +0.3V to approximately -0.2V. Beyond -0.2V biasing potential, all sensors experienced overall increases in current

magnitudes at different rates. In Figure 6.11, it is observed that the sensor without any membrane produced the largest current magnitudes averaging -7.3 µA along the possible diffusion limited current plateau of -0.7V to -1.0V. Two prominent peaks were also noted from the graph at -0.7V and -1.2V respectively. A relatively flat and long plateau from -0.5V to -0.95V was generated by the sensor using PTFE as its membrane. Its output current was at sizeable values of approximately -3.8 µA. The sensor with CA as the membrane experienced similar trends of electrochemical activities throughout the sweep as the former two sensors despite having comparatively small output current magnitudes. A minor peak occurred at -0.92V along the possible plateau of -0.7V to -1.1V. Such peaks could be attributed to impurities within the sensor material that were introduced during the fabrication process [70]. With repeated sweeps, some of these peaks disappeared depending on the state of the impurities throughout the reactions.

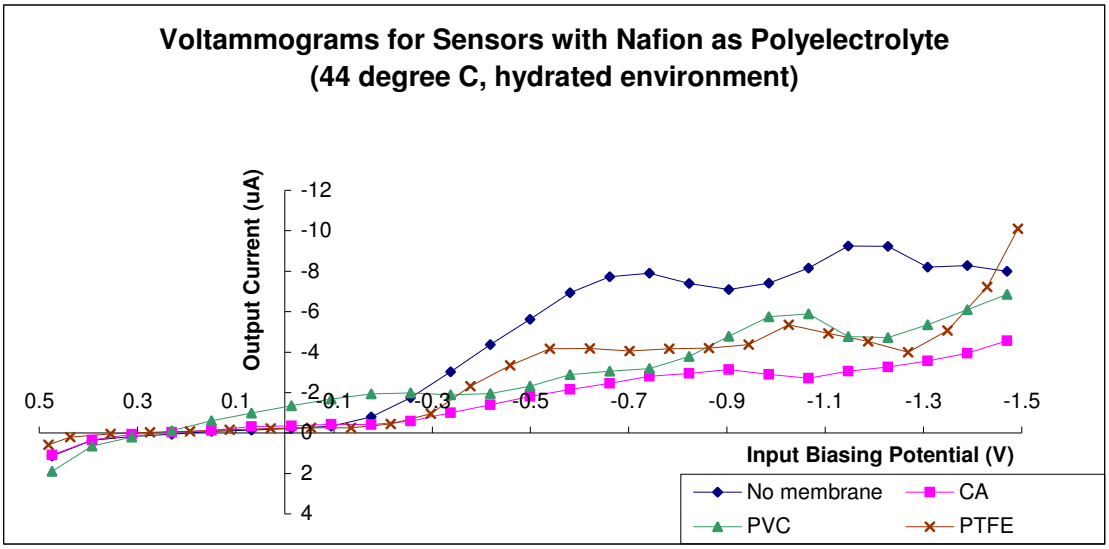

Figure 6.11: Voltammograms for Sensors with Different Membranes at 44 ℃ and 20% Oxygen

Some obvious differences were noted for the sensor with PVC as its membrane. Firstly, all absolute current magnitudes obtained from biasing potentials of 0V to -1.5V registered values larger than -1.5 µA. Two narrow current diffusion limited plateaus could be estimated in the ranges between -0.1V to -0.4V and -0.55V to -0.75V.

The biasing potential at which each sensor operates might differ for different sample types as indicated by individual voltammograms. The most reasonable choices for sensors with no membrane, CA, PVC and PTFE membrane were selected at approximately -0.75V, -0.9V, -0.75V and -0.8V respectively. By repeating the experiments and evaluating the corresponding voltammograms, these values were deemed statistically suitable as biasing potentials for operating the sensors within the current diffusion limited plateaus.

6.2.2.3 Conclusions on the Voltammetric Study on Nafion-based Sensors

Viable biasing potentials of the sensors with no membrane, CA, PVC and PTFE as their respective membranes were determined by individual voltammogram at approximately -0.75V, -0.9V, -0.75V and -0.8V. These values were obtained when the sensors were subjected to a hydrated environmental condition and 20% oxygen. These biasing potentials fell well within each region enclosed by the corresponding diffusion limited current plateaus. The PVC-membrane sensor presented an interesting voltammogram with two possible narrow diffusion limited current plateaus, while the rest of the prototypes only displayed one such plateau. One possible reason for this observation was that the oxygen molecules were reduced at the cathode by the following two-electron reactions within the diffusion limited current plateau derived from the PVC-membrane sensor:

$$O_2 + 2H_2O + 2e^- \longrightarrow H_2O_2 + 2OH^- \quad (6.1)$$

$$H_2O_2 + 2e^- \longrightarrow 2OH^- \quad (6.2)$$

The oxygen molecules reached the cathode via diffusion and reduced to hydroxyl ions and hydrogen peroxide components in the presence of water. Upon further reaction, the hydrogen peroxide is reduced to give another set of hydroxyl ions. The reaction would tend to produce alkalinity in the medium. If an increase in pH level should take place, a two-step mechanism of 2-electron reactions as described in Equations (6.1) and (6.2) would predominate and govern each of the possible diffusion limited current plateaus respectively. In more recent studies, Bianchi [32] found that in a solution where high concentration of hydrogen peroxide was present, the oxygen reduced to hydroxyl ions in a four-electron mechanism given by:

$$O_2 + 2H_2O + 4e^- \longrightarrow 4OH^- \quad (6.3)$$

In which case, only one apparent plateau would be detected in the voltammogram. This could appear to be the case encountered by the sensors with no membrane, CA and PTFE membranes.

6.2.3 Effects of Oxygen Level Measurement at Room Temperature and Transcutaneous Temperature

Previous experiments were carried out in fully hydrated conditions in order for ionization to occur conveniently. However, given the fact that transcutaneous measurement might be done on dry skin surfaces, the effect of different humidity levels ought to be evaluated. This simple experiment identified the complications arising from the elevated temperature of 44 °C for transcutaneous measurement. Four sensor samples coated with Nafion polyelectrolyte employed PVC as their membrane and four others used PTFE membrane. These sensors were involved in the monitoring of two extreme alternating constant levels of oxygen (0% and 20%) for a period of time in an unchanged environment.

6.2.3.1 Experimental Setup and Procedure

Individual potentiostats were adjusted accordingly to suitable biasing voltages in order to drive the sensor into the diffusion limited current plateau as determined by previous voltammograms presented in Section 6.2.2. The output current measurements were recorded by the Keithley multimeter at intervals of 10 seconds.

Both types of sensors were initially placed in a low humidity environment (estimated at 58% relative humidity) and their platinum heaters were powered to 25 °C. They were then exposed to 0% and 20% oxygen levels, each alternating for approximately 20 minutes. This process was carried out in recurring cycles to observe the repeatability. Upon completion, the whole procedure was repeated with the sensors heated to 44 °C. For the next part of this experiment, the sensors were immersed in de-ionized water and measurements were taken at both 25 °C and 44 °C.

6.2.3.2 Comparing Sensors' Performances in Normal Room and Transcutaneous Temperature under Different Levels of Humidity

The sensors with PVC or PTFE as their membranes were randomly chosen for this experiment. The voltammograms in Figure 6.11 show that the operating biasing potential could be determined at approximately -0.75V or -0.80V respectively. The sensors were subjected to two extreme oxygen levels at the minimum of 0% and maximum of 20% for a period of 20 minutes each. They were initially exposed to a low humidity environment (approximately 58% relative humidity) at normal room temperature of 25 °C. Upon completion, the measurements were taken at 44 °C. The whole procedure was then repeated with the sensors being fully hydrated in de-ionized water. The measured output currents under these different conditions are summarized in Table 6.3.

Membrane	***25 °C***		***44 °C***	
	Current at 0% O_2 (μA)	Current at 20% O_2 (μA)	Current at 0% O_2 (μA)	Current at 20% O_2 (μA)
PVC (humid ≈ 58% RH)	-0.360	-1.033	-0.034	-0.036
PVC (hydrated)	-0.564	-1.060	-0.014	-3.141
PTFE (humid ≈ 58% RH)	-0.158	-0.241	0.032	0.034
PTFE (hydrated)	-0.265	-0.350	-0.180	-4.011

Table 6.3: Output Steady-state Current for Nafion-based Sensors at Room and Transcutaneous Temperature

The results suggested that at approximately 25 °C, all sensors appeared to be effective and responded accordingly to changes in oxygen levels regardless of the humidity level. However, the sensor with sprayed-on PTFE membrane displayed larger current magnitudes as compared to that of the PVC membrane sensor. This could be attributed to physical parameters such as membrane thickness and the diffusion coefficient.

When the temperature was elevated to 44 °C, the sensors in low humidity completely failed to respond. At a fixed oxygen level, the low output current suggested random noises rather

than useful signals. Significant differences in the measured current were noticed for 0% and 20% oxygen levels when the sensors were hydrated in de-ionized water.

6.2.3.3 Conclusions on Nafion-based Sensors' Performances in Normal Room and Transcutaneous Temperature

Elevated temperature would be essential in this biomedical application to allow the skin to be sufficiently porous for arterial oxygen to diffuse through onto the surface. However at 44 °C, the membrane materials experienced dryness and may discontinue possible paths for oxygen diffusion. The sensors with PVC or PTFE as their respective membrane were able to identify two distinct levels of oxygen, namely 0% and 20% under both low humidity of approximately 58% relative humidity and hydrated condition at 25 °C. When the temperature was elevated to 44 °C, the sensors could only respond when fully hydrated in de-ionized water. Low humidity responses gave small noisy currents and the sensors fail to distinguish 0% from 20% oxygen. This test showed that effective transcutaneous measurement could only occur when some form of hydration was present.

6.2.4 Relationship between Output Current and Transcutaneous Oxygen Level

The ultimate objective of this research was to establish the relationship between the measured output current and its respective oxygen level for different types of sensor.

6.2.4.1 Experimental Procedure

The sensors used in Section 6.2.2 were all subjected to this experiment where a TESTPOINT program was written to control the different levels of oxygen by mixing appropriate proportions of nitrogen and compressed air. Initially, 100% nitrogen (equivalent to 0% oxygen) was allowed into the glass container via the gas inlet. The sensors were immersed in de-ionized water at 44 °C (transcutaneous temperature). Measurements were taken at 40 seconds intervals for approximately 20 minutes. After which, the gas content in the glass container was automatically varied to 4% oxygen, and the same measurement procedure was repeated. Prior to every change in oxygen level, the sensors were flushed with 0% oxygen to 're-initialize' themselves so as to avoid any contribution from residual reduction. Oxygen levels were increased from 0% to 20% in steps of 4%, it was then reversed by decreasing

from 20% to 0% at the same interval. Finally, the whole experiment was repeated with the same set of sensors having an additional layer of self-adhesive polymer membrane, known as Tegaderm.

6.2.4.2 Establishing the Relationship between Output Current and Transcutaneous Oxygen Level for Each Nafion-based Sensor Prototype

Figure 6.12 depicts the results obtained from the experiment to establish the relationship between output current and transcutaneous oxygen level. It was noted that each level of oxygen was distinguished from another very distinctly. Good repeatability when measuring the same level of oxygen on separate occasions was also observed. The response times of the sensors were adequately short to be regarded as instantaneous measurements.

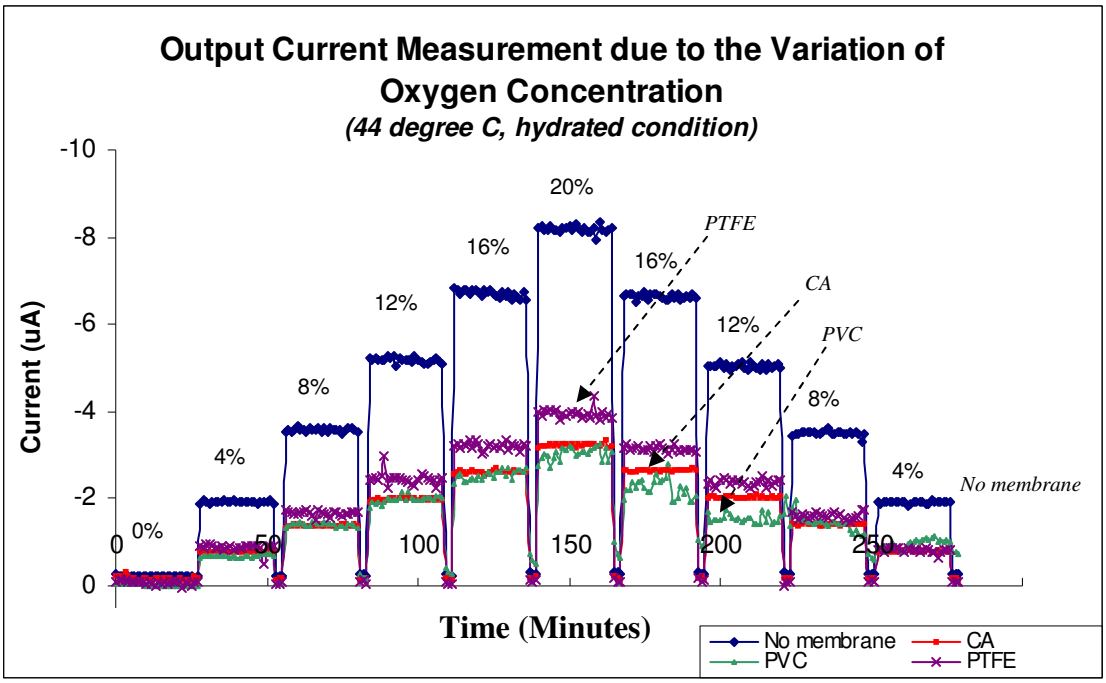

Figure 6.12: Current Outputs due to Change in Oxygen Levels at 44 ℃

For the case of the sensor with a PVC membrane, it was observed that the current measurements at 16% and 20% oxygen were fluctuating considerably despite the constant level of oxygen supplied. Comparatively poor repeatability was also discovered in this prototype, which often caused discrepancy in determining the actual oxygen level. To this point in the investigation, the sensor had already gone through a substantial amount of strain and stress that may have caused deterioration to its performance. Conversely, this might also

indicate the functional life span of the sensor. In the practical application of transcutaneous measurement, such ranges of variations would still be acceptable if the measurement would fall well within the specifications of indicating a patient's normal condition of approximately 9% to 14% oxygen [17]. Nonetheless, the reliability of the sensor would remain questionable.

The sensors with CA and PTFE membranes clearly displayed constant output currents at each oxygen level, although the latter tended to give slightly erroneous deviations at low oxygen levels when the time scale was between approximately 220 to 280 minutes as shown in Figure 6.12. A reassuring improvement was noted when these sensors obtained faithful output current reproduction after each re-initialization process where the sensor was flushed with nitrogen to prevent prior residual effects. The most encouraging measurement was found in the sensor without a membrane that gave large and distinct output current magnitudes to denote each corresponding oxygen level distinctly. The sensor also appeared to be responsive and sensitive with high ability to repeat measurements.

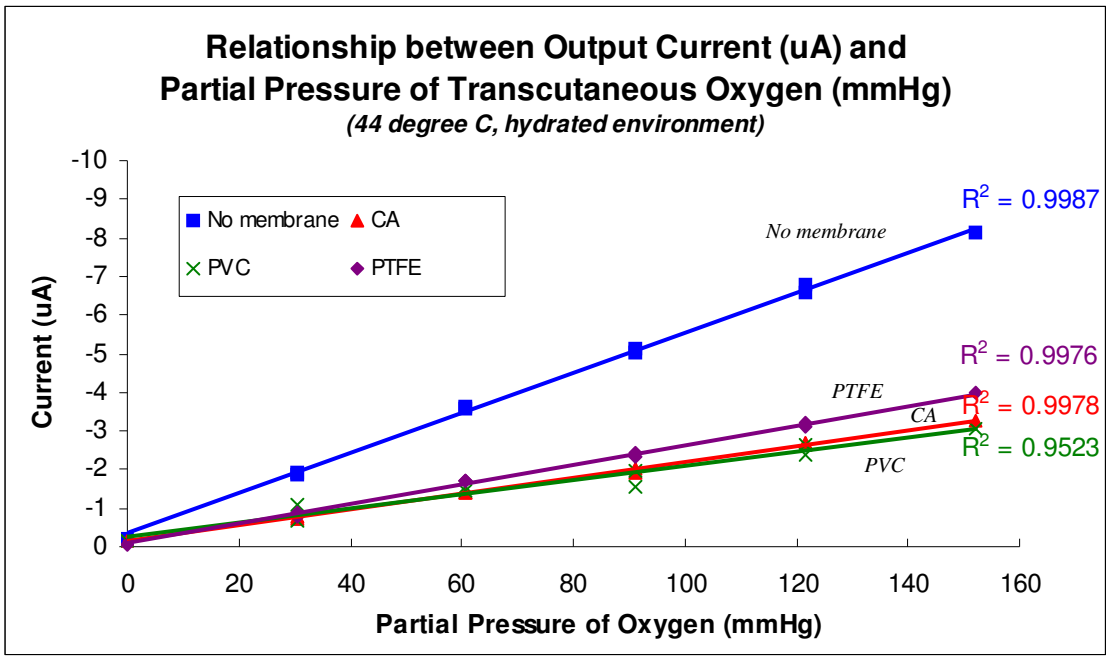

Figure 6.13: Establishing the Relationship between Output Current Measurement with Transcutaneous Partial Pressure of Oxygen

The results illustrated in Figure 6.13 average the data obtained from Figure 6.12 to correlate the percentage of oxygen level to its respective partial pressure equivalent in mmHg by multiplying by a conversion factor of 7.6. The conversion factor is derived by considering the

ideal situation where normal atmospheric pressure is given by 760 mmHg with 100% oxygen content occupying only 20% of the total atmospheric pressure.

It was found that all the sensor prototypes regressed to a linear relationship between the output current and partial pressure of transcutaneous oxygen. The gradient of the regressed results from the sensor without a membrane reflected effective correlation between the two parameters. Although the other three types of sensors produced linear regressions with gentler gradients, the corresponding oxygen level could still be easily found from the calibration graphs.

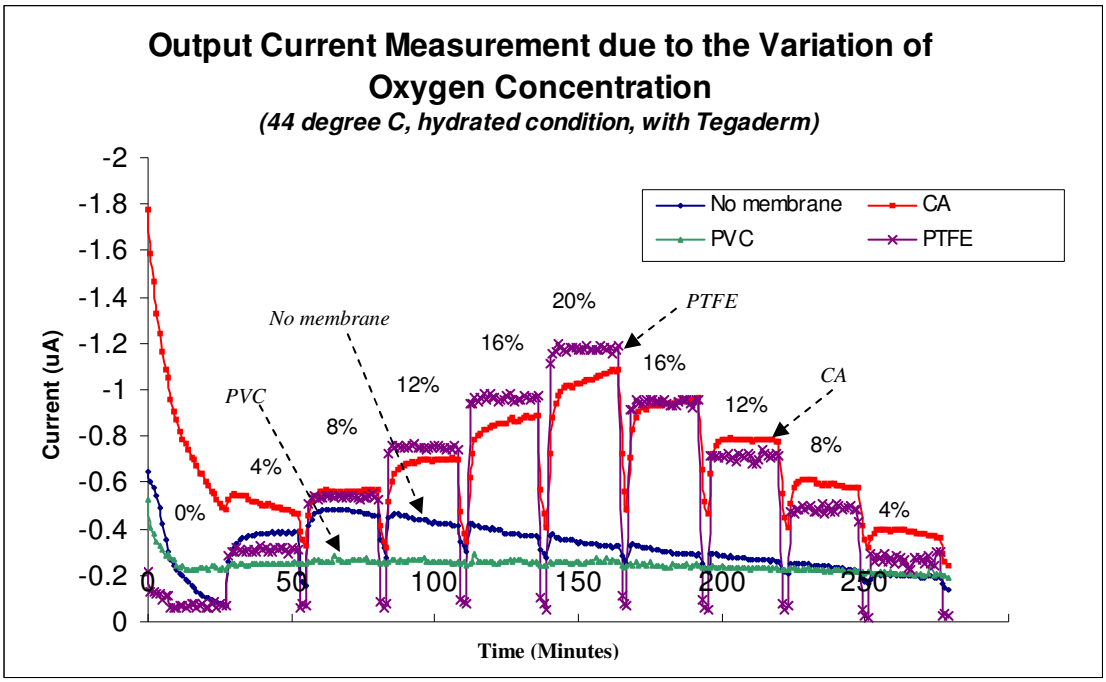

Figure 6.14: Measurement Made from Varying Oxygen Levels at 44 ℃ with the Use of Tegaderm

In order to create a practical situation for transcutaneous measurement, Tegaderm was introduced between the sensor membrane and gas phase. Figure 6.14 depicts the graphs resulting from the continuous monitoring of varying oxygen levels at the transcutaneous measuring temperature and depicts the effects of the attached Tegaderm layer. The most obvious difference was that the overall output current magnitudes were decreased by as much as 70% in comparison to the case of not having Tegaderm. In the beginning of the experiments, all sensors required at least 20 minutes to initialize themselves from the normal

atmospheric conditions to detect a 0% oxygen level. The delays in responses suggested that diffusion through the additional layer of Tegaderm was not instantaneous.

The sensor with a PTFE membrane appeared to maintain its effectiveness under this new condition with the exception of having smaller current outputs and poorer repeatability. The current magnitude was also reduced to approximately -1.5 μA at 20% oxygen. Further, the current measured at each brief re-initialization instance of 0% oxygen did not return to the same value. The CA-membrane sensor experienced more response delays during the transient changes of oxygen levels as shown by the apparent slow rise time of the curve in the graph. The sensor with PVC as the membrane failed to perform by recording an unchanged and noisy output current of approximately -0.2 μA throughout the whole measurement. An interesting finding arose for the sensor without a membrane. For the first three cycles of measuring 0% to 8% oxygen, it appeared to function normally. After this time, a gradual decrease was observed in each measurement stage even though there were no changes in the test conditions. Nonetheless, the sensor was still able to identify the brief moments of 0% oxygen re-initialization.

6.2.4.3 Conclusions on the Relationship between Output Current and Transcutaneous Oxygen Level for Each Nafion-based Sensor Prototype

The main objective of this research topic can only be achieved by performing experiments to correlate current with different oxygen levels. It was found that all sensors were able to track the changes in oxygen levels faithfully with fairly short delays in response time. This was ideal for continuous measurement where sudden variations could be detected almost instantaneously. The repeatability of measuring each oxygen level was also shown to be well within acceptable deviations of approximately ±2.5%, ±5% and ±2% for the sensors with no membrane, PTFE and CA membranes respectively. Unfortunately, the measurements made from the PVC-membrane sensor gave a large deviation of ±17.5%, hence inferring poor ability to reproduce similar current outputs at the same oxygen levels.

Figure 6.13 describes the linear regression plot of the average current obtained at each oxygen level interval. The relationship between the current (I in μA) and the partial pressure of oxygen (PO_2 in mmHg) for each type of sensor is summarized in Table 6.4.

Membrane Material Used	**Current (*I in μA*)**	**Regression coefficient (R^2)**
No membrane	$I = -0.052PO_2 - 0.339$	0.9987
CA	$I = -0.021PO_2 - 0.142$	0.9978
PTFE	$I = -0.025PO_2 - 0.085$	0.9976
PVC	$I = -0.018PO_2 - 0.266$	0.9523

Table 6.4: Relationship Between Output Current and Partial Pressure of Oxygen

The sensor with no membrane gave the highest sensitivity of -0.052 μA/mmHg, followed by the sensors with PTFE, CA and PVC membranes in descending order. The measurements at 0% oxygen did not give zero output current in all cases and the linear regression from the data obtained introduced estimations towards the y-axis intercept value, which was equivalent to the initial offset of individual sensors.

Full hydration increased the conductivity of the prototype employing Nafion polyelectrolyte without a membrane by about 60% during the conductivity relaxation process. With such an improvement in ionic conductivity and having no additional diffusion membrane layer, the sensor appeared to perform with high standards of accuracy and effectiveness. However, one possible disadvantage that might be more obvious in actual applications could be the limited functional life span of this type of sensor. Since there was no protective membrane layer, the sensor would be more susceptible to environmental aggravation and deformation from long-term usage.

The sensor with PTFE as its membrane also produced encouraging responses with good sensitivity and a low y-axis intercept value, thus favouring it as a suitable candidate for transcutaneous measurements. Although screen-printed CA membranes did not perform as well as the former two sensors in terms of current magnitudes, good repeatability and stability during operation was distinctly observed. CA became very porous in the presence of water and this allowed easy gas diffusion. Given the facts that the PVC membrane was not porous to many different kinds of gases and possessed high selectivity for oxygen diffusion when its gas-membrane interface was adjoined with water deposits, the lack of repeatability

and noisy outputs were anticipated. Despite such disadvantages, PVC may demonstrate prospects of being the most accurate and effective pure oxygen sensor.

In the final attempt to realize the whole laboratory setup to match the practical situation, Tegaderm was affixed in front of the Nafion-based sensors to simulate the presence of skin. The sensors with PTFE and CA membranes were found to achieve acceptable levels of current measurements. However, the repeatability worsened at transcutaneous measuring temperature and the presence of Tegaderm deprived the materials of constant hydration. Response times of the sensors were also seriously affected especially for CA membrane sensors, and distinct changes in oxygen levels could no longer be easily identified. The possible reason for the failure of PVC-membrane prototype could be due to that fact that with the addition of Tegaderm, the gas-PVC membrane interface no longer included water specimens, which enhanced oxygen diffusion.

6.2.5 Overall Conclusions for Nafion-based Sensors

Generally, all experiments were again categorized into two main parts namely the voltammograms and the analyses to establish the relationship between output currents and the respective oxygen levels. These investigations brought about a deeper understanding of different membrane materials employed in screen-printed sensors with Nafion polyelectrolyte. The sensor with a PTFE membrane appeared to be the most promising candidate hence it was selected to perform clinical transcutaneous measurements with the results presented in Section 6.5. It was also found that the measurements made using Nafion as the electrolyte gave similar outcomes and observational trends to that of the KNO_3-based sensor.

Experiments and investigations were carried out under controlled environments in relatively ideal conditions that were well defined. However in a practical application, external conditions usually vary and often introduce offsets towards the final current measurement. Two such parameters namely the pH level of surrounding fluid and the level of salt concentration were thoroughly studied so that in the event of significant influences, appropriate compensation could then be done to obtain more accurate results.

6.3 Effects of Changing pH Level on Sensor Prototype

When the sensor was undergoing redox reactions on its electrodes during the different experiments, there would be generation of other chemical products, which may alter the characteristics of the surrounding conditions. At the working electrode, oxidation occurred and hydroxide ions (OH^-) evolved from the reaction as discussed in Chapter 2. Although equilibrium was maintained within the whole electrochemical system, excess OH^- ions might infiltrate into the surrounding de-ionized water. This occurrence would affect the pH levels hence the study of its effects on the sensors' performance was investigated.

6.3.1 Experimental Setup and Procedure

Figure 6.15 depicts the typical experimental setup for carrying out current measurements over a period of time.

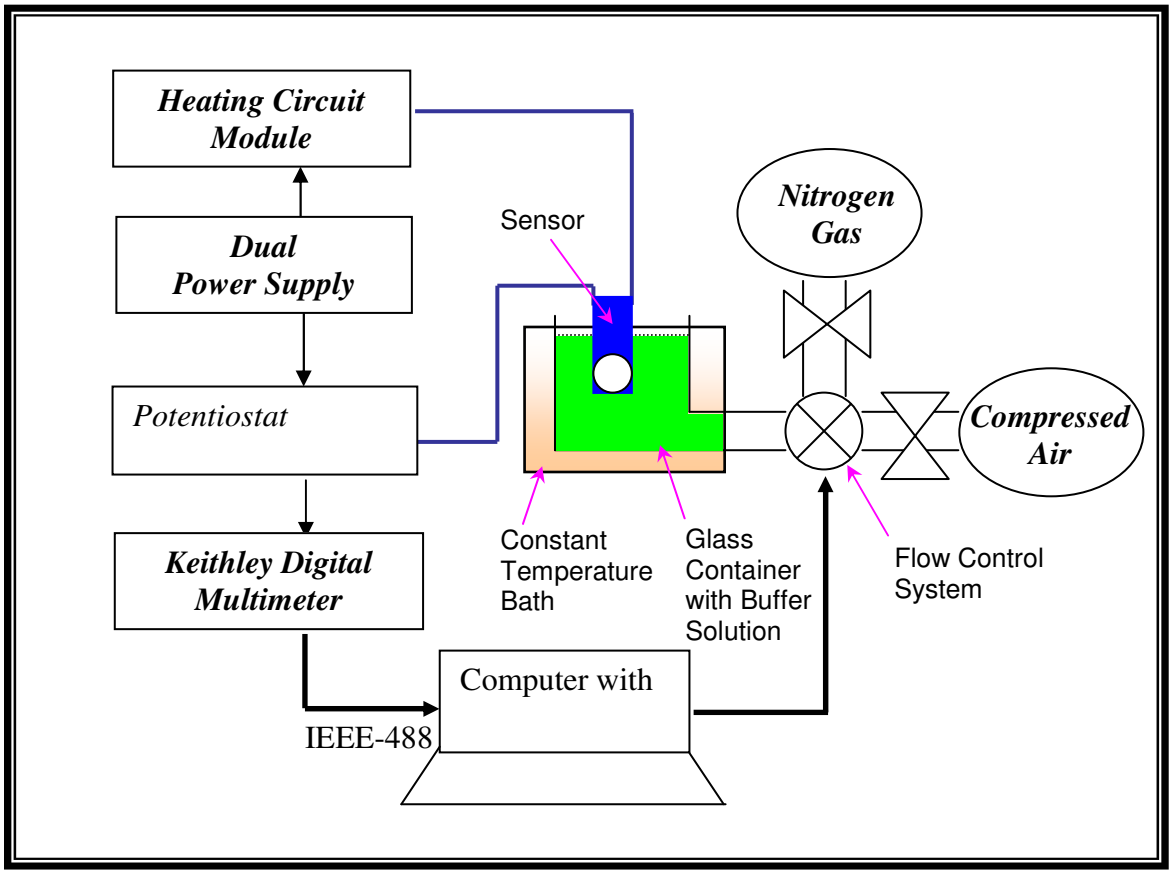

Figure 6.15: Experimental Setup for Current Measurement under the Influence of Varying pH Levels

The sensors have both the heater and oxygen-sensing module printed on opposite sides of the substrate. The temperature of the heater element was controlled by the heating circuit (reference to Chapter 5.2). The oxygen-sensing module was connected to the potentiostat

(reference to Chapter 3.2) and measurements were made via the Keithley 2001 multimeter. Each sensor was placed in the beaker where the concentration of oxygen was regulated at alternating 0% and 20% levels using the Gossen flow controller system (Model 5878). Control was carried out by a TESTPOINT program with the Clifton constant temperature bath maintained at approximately 37 °C. At each concentration level, the corresponding currents were recorded every 40 seconds over a 10-minute period. Initially, a pH4 (phthalate) buffer solution from Fisher Chemicals was placed in the glass beaker and the oxygen or nitrogen was bubbled into the solution via the inlet that was controlled by the flow system. When 4 cycles of alternating 0% and 20% oxygen were completed, the glass beaker was emptied and the next buffer solution (pH7 - phosphate) was used. It then experienced the whole procedure again. Lastly, a pH10 buffer solution (borate) replaced the pH7 solution and the respective measurements were performed to obtain the final set of results. Although only 3 different types of pH solution were available for the test, various sets of sensor samples were subjected to a minimum of 100 test cycles. The results showed high levels of repeatability. Hence, analyses on data regression for the measured results were still carried out to estimate and quantify the possible effects of pH levels on oxygen measurements.

For this experiment, only sensors with KNO_3 electrolyte and PVC or PTFE membranes were used. From previous studies, it was concluded that sensors with PTFE membranes were favoured over others for the fact that it gave high output current levels and remained stable over a long period of time. PVC-membrane sensors were chosen for comparison purposes since it revealed the prospects of high oxygen selectivity. The aim of choosing KNO_3 as the electrolyte was due to the hypothesis that KNO_3 being an aqueous salt electrolyte would encounter higher possibilities of ionic migration compared to Nafion, which was based on producing a free H^+ proton to hop between fixed SO_3^- sites on the Nafion backbone. The working principle of KNO_3 was to allow the substitution of hydroxyl ions (OH^-) resulting from the cathodic reaction with the nitrate ions within the electrolyte. Ionic conduction through the electrochemical cell would be carried out by these nitrate ions. There might be the case where an excess of hydroxyl ions may occur and unwittingly cause a change in pH level in the surrounding environment.

6.3.2 Results and Discussion

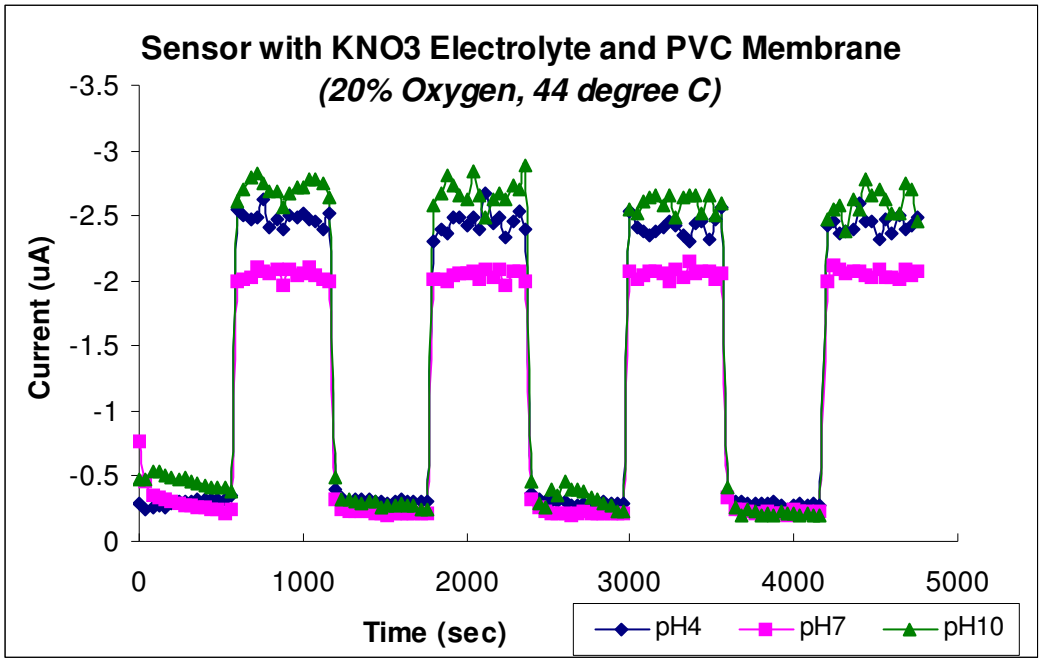

Figure 6.16: Repetitive Oxygen Measurements at Different pH Levels for KNO_3-based Sensors with PVC membrane

Figure 6.16 shows the results of the KNO_3-based sensor with a PVC membrane immersed in buffer solutions with different pH levels. It was found that at the neutral condition of pH 7, the output current measured presented lower magnitudes of approximately -2 μA as compared to the acidic (pH 4) or alkaline (pH 10) situation. For the alkaline case, the possible reason for such an observation may be due to the fact that the overall ionic conduction was actively enhanced by the presence of more mobile OH^- ions (alkaline) in the buffer solution. Conversely for acidic solutions, more H^+ ions may diffuse through the membrane and encouraged the following 4-electron reaction equation at the working electrode [75], which would eventually affect the output current.

$$O_2 + 4H^+ + 4e^- \rightarrow 2H_2O \tag{6.4}$$

Throughout the 10-minute recording period, the sensor appeared to be more stable with a negligible 3% deviation from its mean value at the neutral level. 5.88% and 7.69% error bars were noted for the results obtained at pH 4 and pH 10 levels respectively. Generally, the

sensor performed with fast response and had good repeatability of output current for all three conditions.

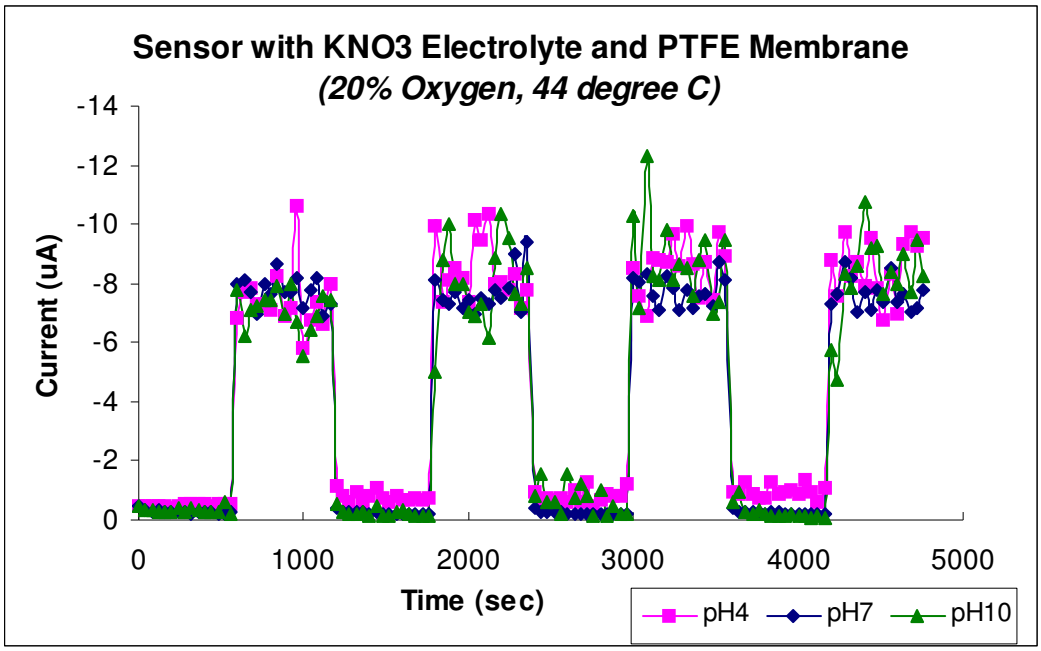

Figure 6.17: Repetitive Oxygen Measurements at Different pH Levels for KNO_3-based Sensors with PTFE membrane

Figure 6.17 illustrates the results obtained from the sensor with a PTFE membrane. The most obvious difference between the PVC-membrane and PTFE-membrane sensors was the magnitude of the output current. PTFE was found by previous studies to be more permeable to gases and hence account for the larger average current of approximately -8 µA. It was also noted that the PTFE-membrane sensor experienced more fluctuations in measurements to give 8.28%, 21.21% and 25% deviations off the average output current for the pH 7, pH 4 and pH 10 conditions respectively. The repeatability of the sensor was seen to be relatively consistent. For the similar reasons as previously discussed, there was an increase in current measured for the test employing acidic and alkaline buffer solutions.

For a more comprehensive illustration on the effects of varying pH levels, Figure 6.18 elaborates on the averaged output current for the sensors with KNO_3 electrolyte and PTFE or PVC as its membrane at 0% oxygen as well as 20% oxygen levels.

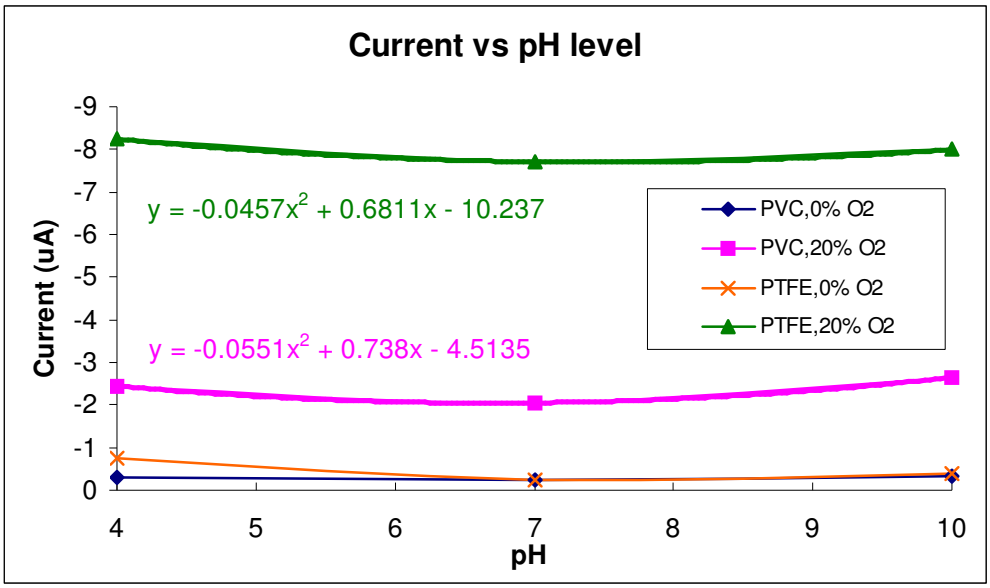

Figure 6.18: Graph of Current vs pH Level at 0% and 20% Oxygen Levels

It can be seen from Figure 6.18 that the sensors experience minor decreases in output current magnitude at pH 7. Due to the lack of available resources, a wider range of measurements on different pH levels could not be carried out. However, based on the 3 measured levels, a general estimated relationship could be established for each of the sensors using a second order polynomial regression.

6.3.3 Conclusions on the Effects of pH Levels

The study of the effects of varying pH levels on output current was carried out to establish quantifiable relationships. From the experiments, it was found that the sensor with KNO_3 electrolyte and a PVC membrane was more stable than the sensor with a PTFE membrane. On the other hand, the latter produced higher output current magnitudes. It was also noted that the output current magnitude was lower at the neutral condition than that in an acidic or alkaline situation. It was observed that if the sensor was immersed in a small amount of buffer solution, the pH 4 buffer solution changed from its original red to yellowish orange at the end of the measurement. The pH 7 buffer solution also tended to result in a greenish blue colouration. This could be due to the introduction of excess OH^- ions, which made the overall solution more basic.

From Figure 6.18, the second order polynomial regression on the current data at 20% oxygen for the sensors was performed in order to obtain mathematical representation for statistical evaluation for the possible effects of pH changes. From the graph of the KNO_3-based sensor, the regression was approximated to:

$$I = -0.0457 \times (\text{pH})^2 + 0.6811 \times (\text{pH}) - 10.237 \tag{6.5}$$

The change of output current (I) due to a change in pH level as shown in Equation (6.6) would be able to indicate the influence of pH value on the final output current measured.

$$\frac{\Delta I}{\Delta \text{pH}} = -0.0914 \times (\text{pH}) + 0.6811 \tag{6.6}$$

Hence, the relative change of current is given by Equation (6.7):

$$\frac{\Delta I}{I} = \frac{-0.0914 \times (\text{pH}) \times (\Delta \text{pH}) + 0.6811 \times (\Delta \text{pH})}{-0.0457 \times (\text{pH})^2 + 0.6811 \times (\text{pH}) - 10.237} \tag{6.7}$$

where ΔI is the change of output current. Substituting the (pH) variable with the average value of 7.4 as well as the (ΔpH) variable, being the difference between the maximum and minimum allowable level that equated to 0.1 or ± 0.05 into Equation (6.7) would simplify to:

$$\frac{\Delta I}{I} = \frac{-0.0914 \times (7.4) \times (\pm 0.05) + 0.6811 \times (\pm 0.05)}{-0.0457 \times (7.4)^2 + 0.6811 \times (7.4) - 10.237} \times 100\% = \mu 0.0031\% \tag{6.8}$$

From Equation (6.8), it can be shown that the percentage change of output current due to ± 0.05 change in pH value amounted to approximately $\pm 0.0031\%$. This indicated that if the pH value changes by 0.01, the final output current obtained would change by only -6.16×10^{-6} of the current, I. Hence, statistically the variation in pH value could be considered negligible or insignificant towards the output current function. In addition, the study on the sensors with a nafion membrane was not carried out due to the hypothesis that KNO_3 would be affected relatively more as compared to nafion under the influence of changing pH levels.

6.4 Effects of Changing Concentration of Salt Levels on Sensor Prototype

In the actual transcutaneous measurement, the sensor would be heated at approximately 44 °C and placing the device on the skin surface would cause sweating of the skin over a long period of time. The main elements of sweat for normal healthy humans consist of water (H_2O) and salts such as potassium chloride (KCl) and sodium chloride (NaCl). There was a need to investigate the effects of different salt concentrations on the sensors' performance. The presence of impurities was not taken into consideration for this study.

6.4.1 Experimental Setup and Procedure

Initially, the screen-printed sensors with KNO_3 electrolyte covered with PVC or PTFE membranes were connected to the heating control circuit and the potentiostat. The typical experimental setup as shown in Figure 6.15 was employed to carry out current measurement over time under the influence of varying salt concentration. The sensors were placed in a glass container, which was immersed into the 8-litre Clifton constant temperature bath. In place of the buffer solutions, solutions with different amounts of salt (KCl or NaCl) were added into the glass container. In order to obtain a salt concentration of 0.01 mol/L (MOL), 0.746g of KCl or 0.585g of NaCl was dissolved in 1 liter of de-ionized water. Applying direct proportioning, 0.1 mol/L or 1 mol/L were obtained by having 7.46g of KCl or 5.848g of NaCl and 74.6g of KCl or 58.49g of NaCl respectively.

The salt solution in the glass beaker was regulated at 0% and 20% oxygen levels by the TESTPOINT program, which controlled the Gossen flow system controller (Model 5878). The constant temperature bath was maintained at a temperature of approximately 37 °C. At each concentration level, the corresponding currents were recorded every 40 seconds over a 10-minute period using the Keithley 2001 multimeter. Initially, the test was carried out whilst subjecting the sensor to the 0.01 mol/L salt solution. When 2 cycles of alternating 0% and 20% oxygen were completed, the glass beaker was emptied and replaced with the 0.1mol/L mixture and the whole procedure was repeated. Finally, the 1mol/L mixture was employed and the respective measurements were performed.

6.4.2 Results and Discussion

Figure 6.19 shows the responses of the KNO_3-based sensor with PVC membrane under the effect of 0.01 mol/L, 0.1 mol/L and 1 mol/L NaCl mixtures.

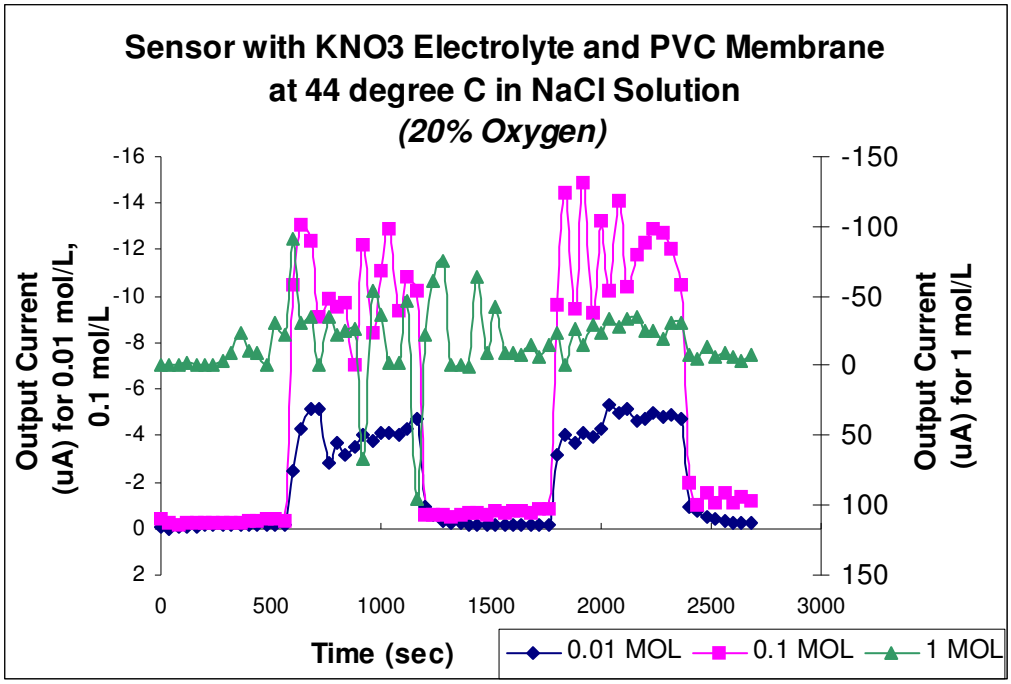

Figure 6.19: Output Current for Sensors with KNO_3 Electrolyte and PVC Membrane in Different Salt Concentration of NaCl Solution

It can be observed that at the lowest salt concentration, the output current also took on the smallest magnitudes averaging -4.5 µA. Having higher salt concentrations would bring about a larger output current due to the fact that there would be more readily available ions for ionic conduction. However as the salt concentration level increased, the amount of fluctuation at 20% oxygen also became more obvious. At the 1 mol/L NaCl mixture, the sensor could no longer perform properly. It could only give unstable measurements as well as poor repeatability. This extreme case was included to enable the establishment of a relationship between output current and salt concentration. Practically, such a situation would not occur during a clinical transcutaneous test since the normal level of sodium chloride in human sweat is approximately 0.055 mol/L [76] and the NaCl level in human blood should not exceed 0.2 mol/L [77], else this would prove to be fatal.

Figure 6.20 illustrates the performance of the sensor with a PTFE membrane, which was subjected to the same experimental procedure. In general, the observations made in Figure 6.20 are similar to that of the sensor with a PVC membrane. The main difference would be the output current magnitude of the PTFE-membrane sensor, which was recorded at approximately -5 µA, which was slightly larger than that of the PVC-membrane sample. It was also observed that at 1 mol/L, the PTFE-membrane sensor also suffered major instability.

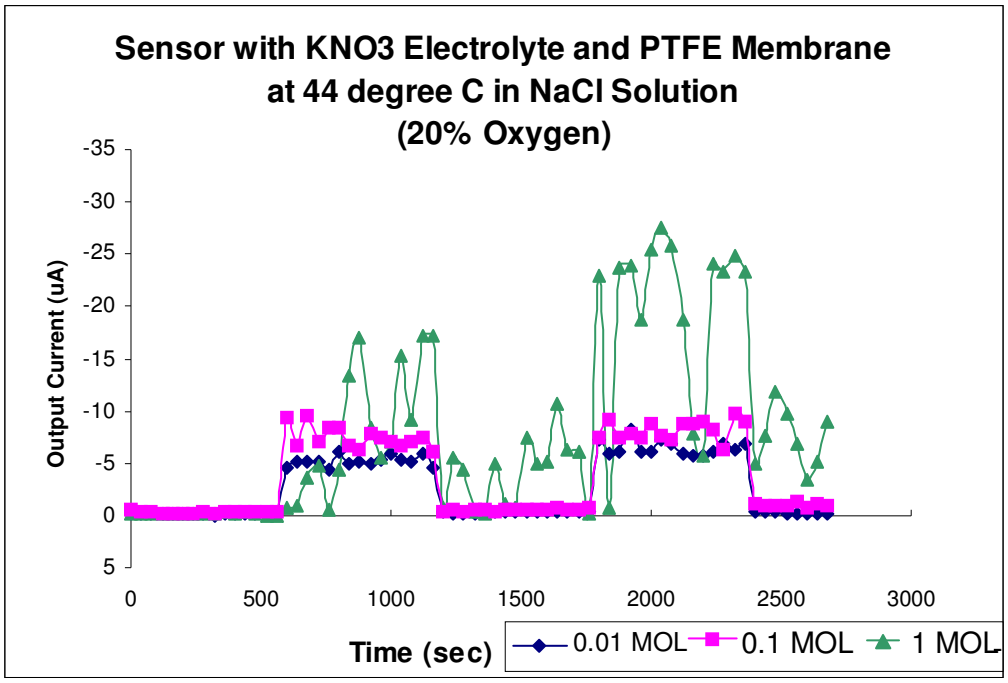

Figure 6.20: Output Current for Sensors with KNO_3 Electrolyte and PTFE Membrane in Different Salt Concentration of NaCl Solution

To establish the relationship between the average output currents and the different levels of salt concentration, the average values were plotted as shown in Figure 6.21 and subjected to linear regressions. Using the Cottrell equation [78], it can be assumed that when the diffusion coefficients and oxygen levels were fixed, current would be directly proportional to the number of moles involved in the electrochemical activity [79]. This assumption would validate that using three data points would be sufficient for the linear approximation.

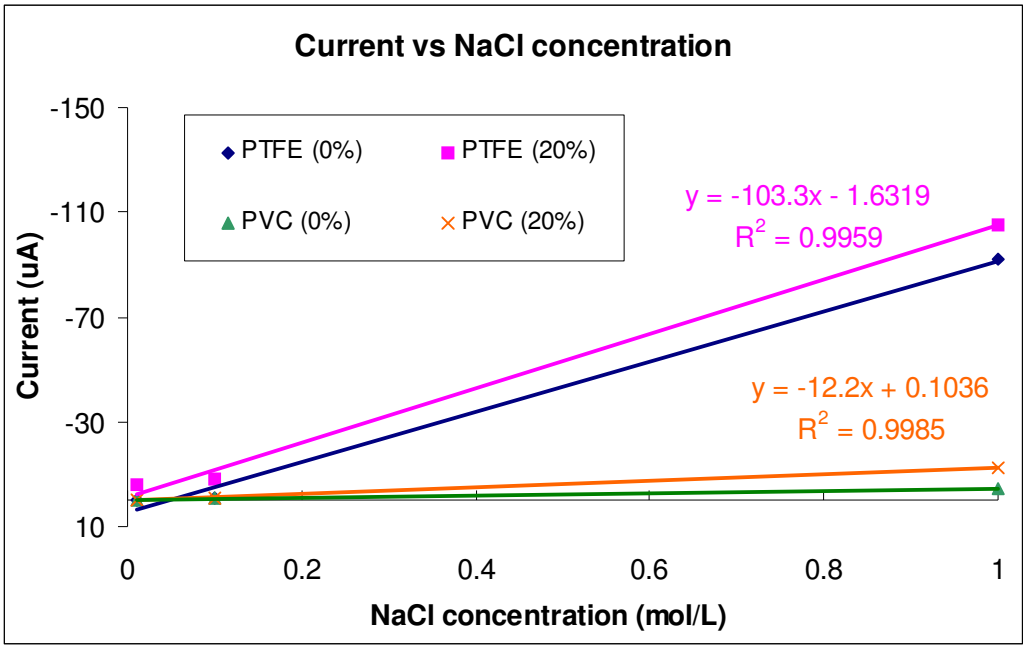

Figure 6.21: Graph of Current vs NaCl Concentration

Figures 6.22 and 6.23 describe the responses of the sensors with PVC and PTFE membranes respectively in the presence of different potassium chloride (KCl) concentration levels. It was found that the trends in terms of stability and repeatability were similar for the sensors in NaCl and KCl solutions. One distinctive difference was that the output current magnitude measured in 0.01 mol/L of KCl gave approximately -8 µA and -10 µA for using PVC and PTFE membranes respectively. Potassium having a larger ionic structure than sodium [80] might enhance the amount of surface interaction for ionic conduction and this may subsequently account for the observed larger current magnitudes. At a salt concentration of 1 mol/L, the responses of both sensors indicated that 0% oxygen could no longer be detected. The output could be influenced and subsequently dominated by drifts, as depicted by the inclining offsets after 1250 seconds of the experimental measurement.

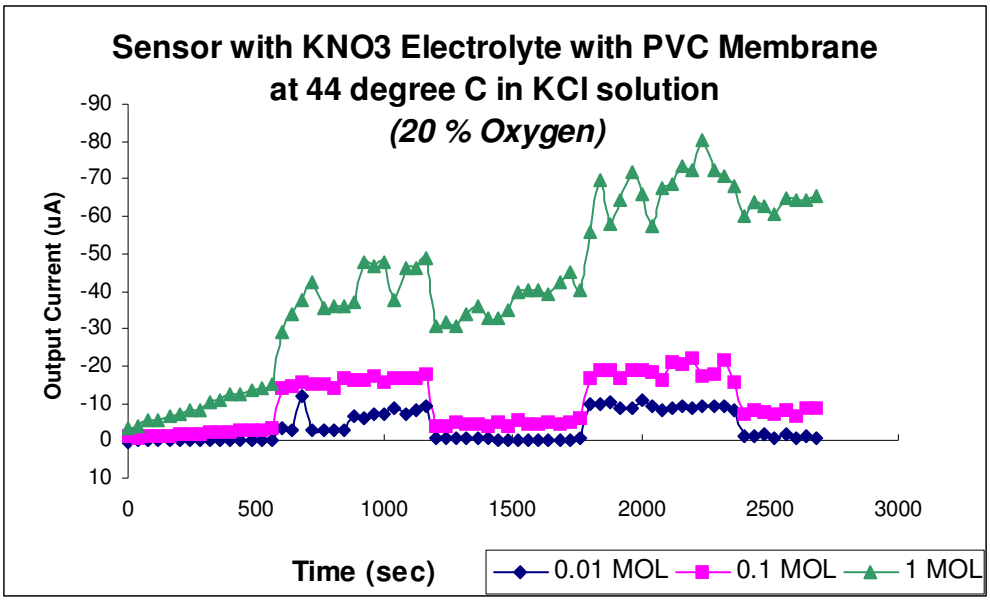

Figure 6.22: Output Current for Sensors with KNO_3 Electrolyte and PVC Membrane in Different Salt Concentration of KCl Solution

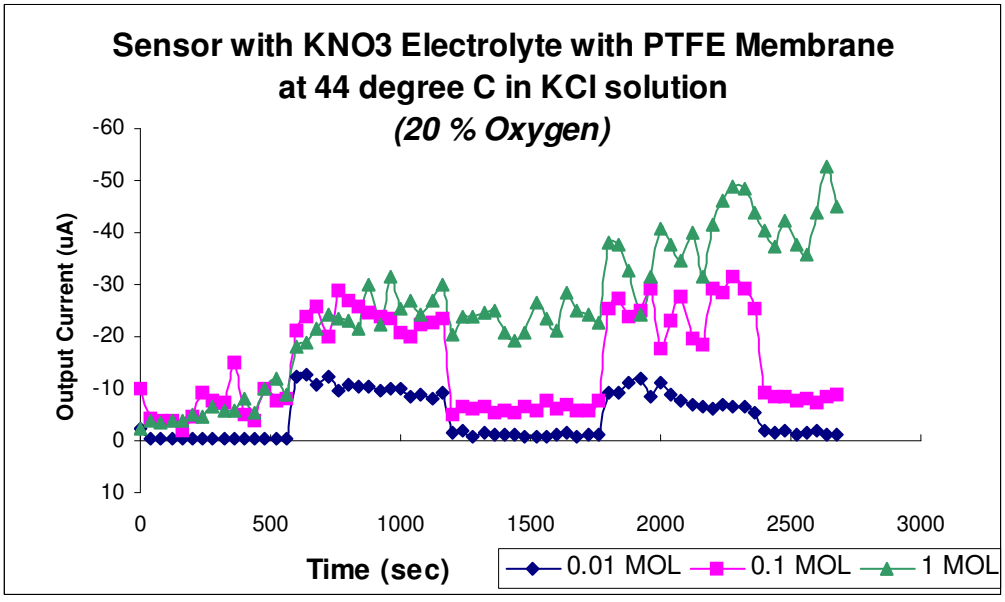

Figure 6.23: Output Current for Sensors with KNO_3 Electrolyte and PTFE Membrane in Different Salt Concentration of KCl Solution

Figure 6.24 summarizes the relationship between output current and KCl concentration for both sensors under different conditions.

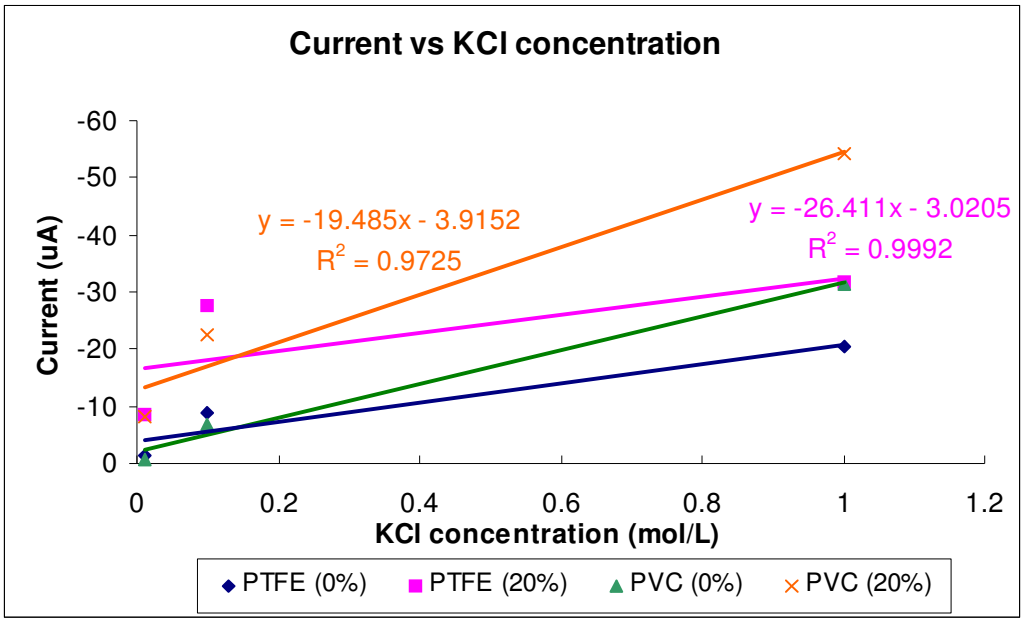

Figure 6.24: Graph of Current vs KCl Concentration

6.4.3 Conclusions on the Effects of Salt Concentration Levels

The study of the relationship between varying salt concentration levels and output current was carried out. From the experiments, it was found that higher salt concentrations led to less stable output currents. Table 6.5 states the linear regression equation and its corresponding coefficient (R^2) for measuring 20% oxygen level.

Membrane	***NaCl Solution***		***KCl Solution***	
	Regression Equation	R^2	Regression Equation	R^2
PVC	$I = -12.2(NaCl) + 0.1036$	0.9985	$I = -19.485(KCl) - 3.9152$	0.9725
PTFE	$I = -103.3(NaCl) + 1.632$	0.9959	$I = -26.411(KCl) - 3.0205$	0.9992

Table 6.5: Regression Information for Establishing Relationship between Output Currents and Salt Concentration Levels

In general, the regression coefficients of both sensors converged close to 1 and this represented the linearity of the relationship. Typically, normal sweat contains 55 mmol/L of

NaCl [76] and non-quantified traces of KCl. Therefore for numerical evaluation purposes, only the case for NaCl was taken into further consideration.

The change of output current (I) due to the variation in salt concentration level would be able to indicate the influence of (NaCl) value on the final output current measured. Hence, the relative change of current for the sensor with PVC membrane is depicted by Equation (6.9):

$$\frac{\Delta I}{I} = \frac{-12.2\times(\Delta\mathrm{NaCl})}{-12.2\times(\mathrm{NaCl})+0.1036} \tag{6.9}$$

where ΔI is the change of output current. Substituting the (NaCl) variable with the average value of 0.055 mol/L and the change of NaCl (ΔNaCl) at ±0.005 mol/L from the typical equivocal range of 0.05mol/L to 0.06 mol/L [76] into Equation (6.9) would simplify to give:

$$\frac{\Delta I}{I} = \frac{-12.2\times(\pm 0.005)}{-12.2\times(0.055)+0.1036}\times 100\% = \pm 10.75\% \tag{6.10}$$

The relative change of current for the sensor with PTFE membrane is shown in Equation (6.11):

$$\frac{\Delta I}{I} = \frac{-103.3\times(\Delta\mathrm{NaCl})}{-103.3\times(\mathrm{NaCl})+1.632} \tag{6.11}$$

Substituting the corresponding variables with the absolute values into Equation (6.11), it reduced to Equation (6.12):

$$\frac{\Delta I}{I} = \frac{-103.3\times(\pm 0.005)}{-103.3\times(0.055)+1.632}\times 100\% = \pm 12.75\% \tag{6.12}$$

From Equations (6.10) and (6.12), it can be shown that the percentage change of output current due to a ±0.005 mol/L change in (NaCl) value for PVC- and PTFE-membrane sensors amounted to approximately ±10.75% and ±12.75% respectively. For a normal healthy human subject, the salt concentration level of sweat should not exceed 0.07 mol/L [76] and should deviate only slightly from the typical value. Hence, for an extreme change of 0.015 mol/L (ΔNaCl) from the typical NaCl value of 0.055 mol/L, the final output current (I) would alter

by approximately 32.3% for the sensor with a PVC membrane and 38.3% for the PTFE equivalent. With these results, the variations in NaCl values ought to be considered and compensated towards the overall output current function, which is in the microampere range. In practice, one possible compensation method could be achieved by using known levels of NaCl concentration and software means. This could be carried by firstly employing a blood gas analyzer to determine the estimated NaCl levels periodically throughout the transcutaneous measurement. In other words, the change of NaCl level would be known. The value would then be presented to the compensating equation, similar to Equation (6.9) or (6.11), where the change in current could be calculated and subsequently be used to offset the current recorded during transcutaneous oxygen measurement. This way, the software compensated current would correspond to a more accurate value of $P_{tc}O_2$.

An experiment was also carried out to investigate the effects of NaCl levels on sensors with a Nafion membrane. Wnek *et al.* [81] found that NaCl concentration was directly proportional to the conductivity of Nafion membrane. Hence, under the influence of a constant voltage potential, a linear regressing relationship between current and NaCl level could be established as shown in Figure 6.25.

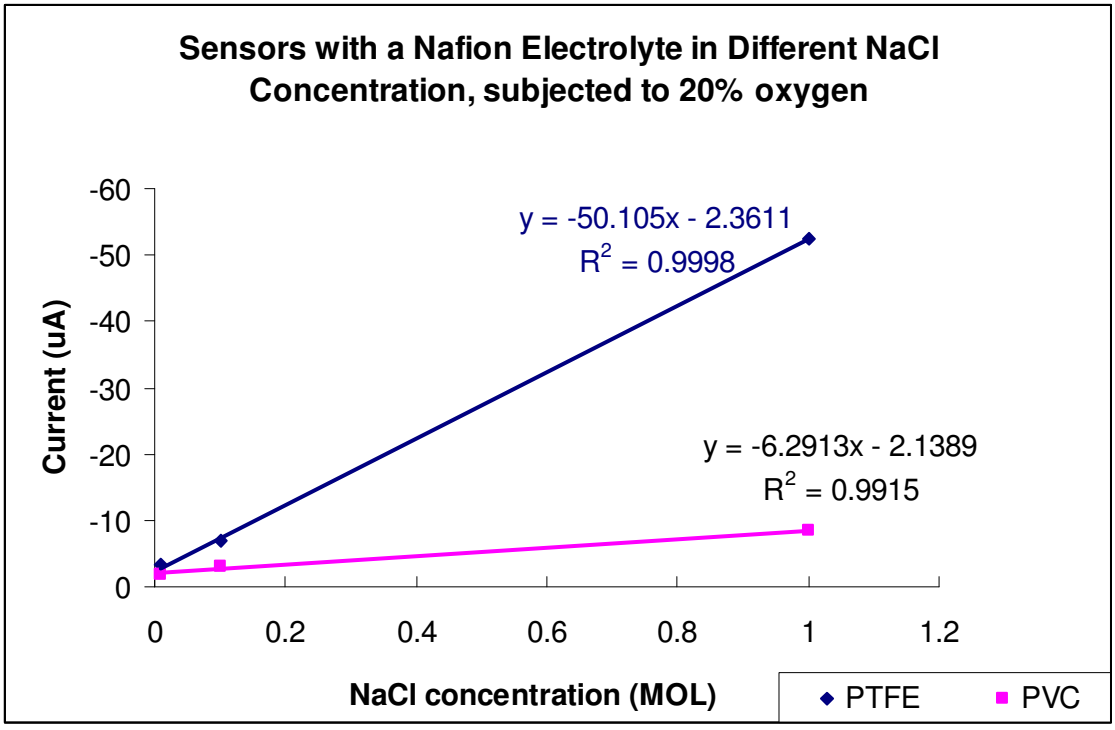

Figure 6.25: Graph of Current vs NaCl Concentration for Sensors with a Nafion Membrane

The relative change of current for the sensor with a Nafion electrolyte and a PVC membrane is depicted by Equation (6.13):

$$\frac{\Delta I}{I} = \frac{-6.2913 \times (\Delta \mathrm{NaCl})}{-6.2913 \times (\mathrm{NaCl}) - 2.1389} \tag{6.13}$$

where ΔI is the change of output current. Substituting the (NaCl) variable with the average value of 0.055 mol/L and the change of NaCl (ΔNaCl) at ±0.005 mol/L into Equation (6.13) would simplify to give:

$$\frac{\Delta I}{I} = \frac{-6.2913 \times (\pm 0.005)}{-6.2913 \times (0.055) - 2.1389} \times 100\% = \pm 1.27\% \tag{6.14}$$

The relative change of current for the sensor with PTFE membrane is shown in Equation (6.15):

$$\frac{\Delta I}{I} = \frac{-50.105 \times (\Delta \mathrm{NaCl})}{-50.105 \times (\mathrm{NaCl}) - 2.3611} \tag{6.15}$$

Substituting the corresponding variables with the absolute values into Equation (6.15), it reduced to Equation (6.16):

$$\frac{\Delta I}{I} = \frac{-50.105 \times (\pm 0.005)}{-50.105 \times (0.055) - 2.3611} \times 100\% = \pm 4.89\% \tag{6.16}$$

From Equations (6.14) and (6.16), it can be shown that the percentage change of output current for the Nafion-based sensors with a PVC and PTFE membrane are ±1.27% and ±4.89% respectively. These effects are considerably lower than that of the KNO_3-based sensors. Hence, this further supports the improvement made to the optimum sensor design by using Nafion as a suitable electrolyte.

6.5 Practical Transcutaneous Oxygen Measurement in a Pilot Hospital Trial

The ultimate objective to verify the viability of the transcutaneous oxygen sensor design ought to be carried out in a practical situation on an actual human being. Due to the extensive administrative restrictions on ethical rights for performing clinical trials on actual patients in a hospital, the pilot measurement was executed on a full grown adult volunteer (the author) instead of the intended neonatal subject under critical care conditions. The sensor prototypes were correlated with a commercial transcutaneous system (TCM-3) from Radiometer that was kindly borrowed from Princess Anne's Hospital, Neonatal Critical Care Unit throughout the whole trial.

Figure 6.26: Commercial Transcutaneous Oxygen System (TCM-3)

The TCM-3 system consisted of a gas calibration unit (on the left in Figure 6.26) and the actual measurement unit (on the right). This unit is an early model that could display the ongoing continuous measurement of partial pressure of transcutaneous oxygen. It requires about 3 minutes of self-calibration at the beginning upon powering up. This commercial unit includes alarms, which could be enabled to alert the medical staff in the event of any measurements falling beyond the preset ranges. It is compact, portable, sensitive and relatively accurate.

6.5.1 Trial Setup and Procedure

As a stand-alone unit for the sensor prototype was not ready for the hospital trial, external equipment such as the Thurbly PL320 dual power supply and the Keithley 2001 multimeter

were employed to facilitate the measurement. The sensor prototypes for this trial focused on the polyelectrolyte, Nafion with an overlying PTFE membrane. PTFE was chosen based on previous positive results as elaborated on in Chapters 5 and 6, containing experiments that investigated different aspects and factors affecting the performance of the samples. Figure 6.27 illustrates the experimental setup for the trial using the Nafion-based sensor, which was connected to the heating control circuit and potentiostat to facilitate transcutaneous measurement. It was attached onto the skin surface along the arm via waterproof adhesive tape as shown in Figure 6.28. This was the simplest and cheapest method available for the primary trial since a self-adhesive alternative was not available. The main aim was to verify that the sensor could work in a practical situation. The thick film transcutaneous sensor was placed on a slightly damped skin surface using de-ionized water. There was no need to apply any KCl conductive gel between the sensor and the skin as normally carried out for other electrode attachment in other biomedical measurements such as electrocardiogram (ECG).

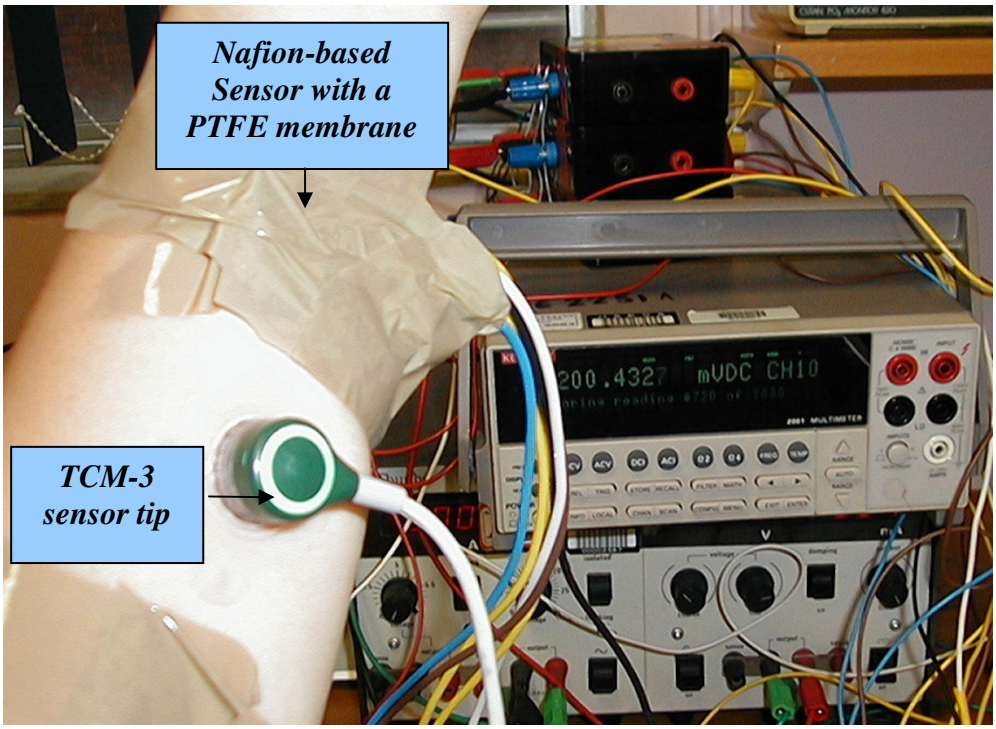

Figure 6.27: Clinical Setup for Nafion-based Sensor with PTFE membrane

The sensor tip would usually be placed along the arm or near the abdomen of the patient. Although the skin would not be thinnest at those locations, relatively accurate transcutaneous

oxygen measurements could be made without subjecting the patient to any major discomfort at the operating temperature of 44 °C.

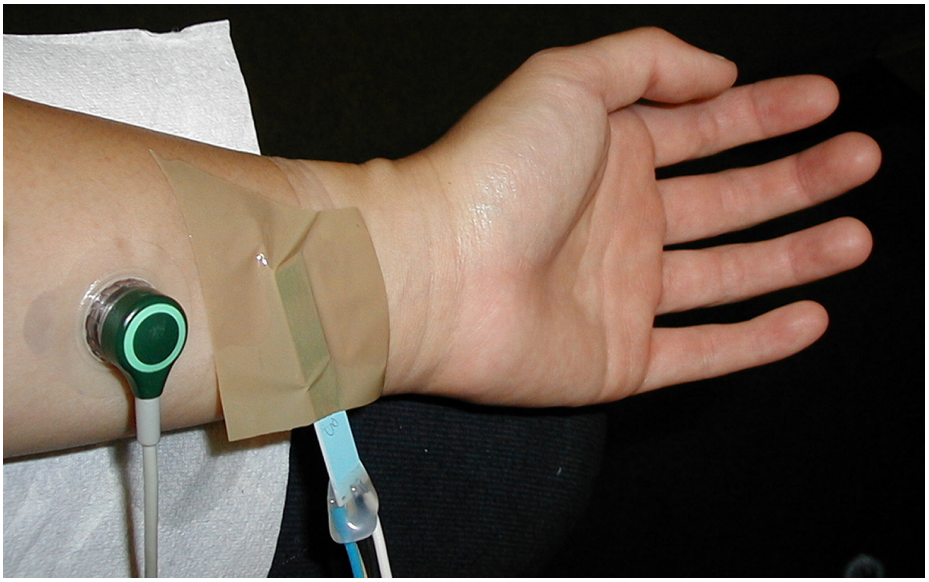

Figure 6.28: Commercial Sensor and In-house Prototype

Figure 6.29 shows the sensor tip of the TCM-3 system. It is also based on the three-electrode configuration and included a heating element. KCl solution was added to the cell and covered with a membrane prior to usage. The skin surface of the patient was cleaned with alcohol and a layer of KCl conductive gel was applied for better conducting contact. The tip was then attached onto the skin surface via a self adhesive ring tape provided.

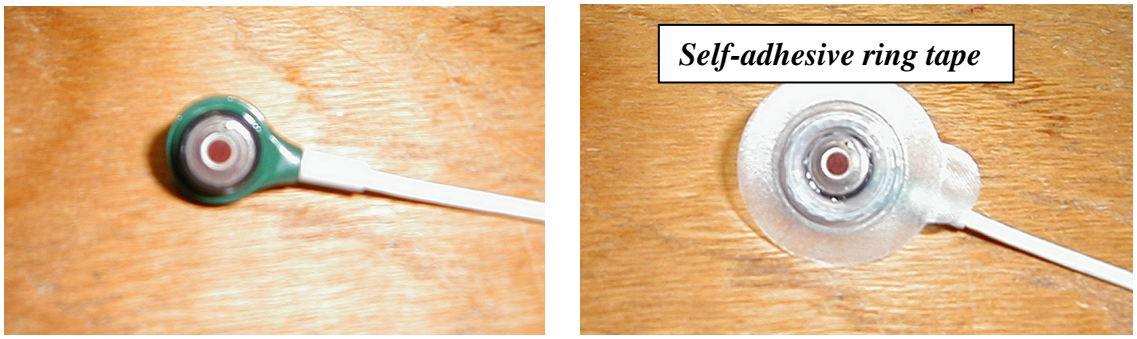

Figure 6.29: Commercial Sensor Tip (TCM-3)

The whole experiment was carried out simultaneously for both types of sensor in order to record correlation data. Figure 6.30 shows the setup for the TCM-3 system.

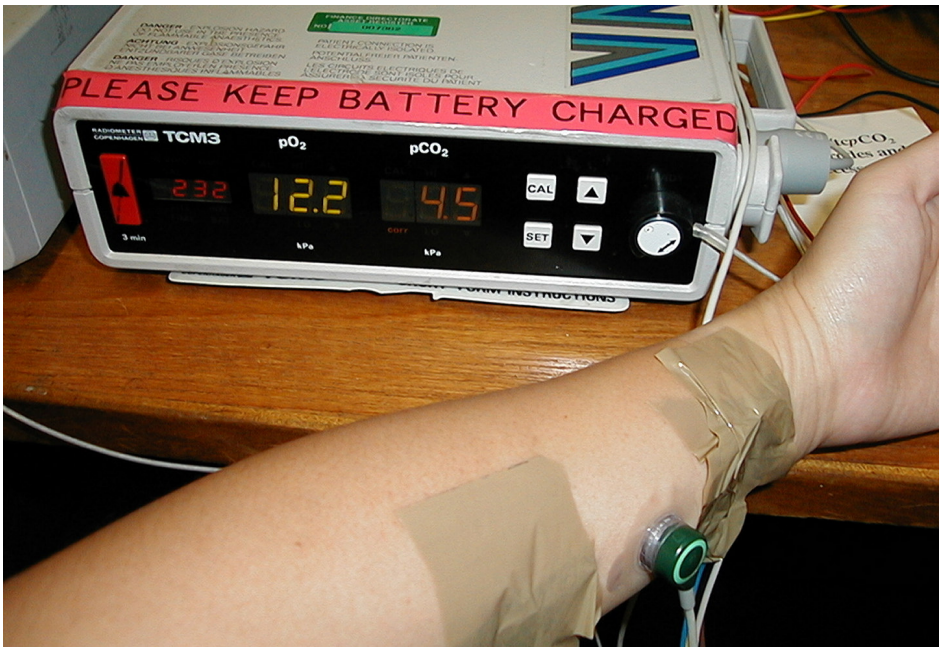

Figure 6.30: Commercial System (TCM-3) Experimental Setup

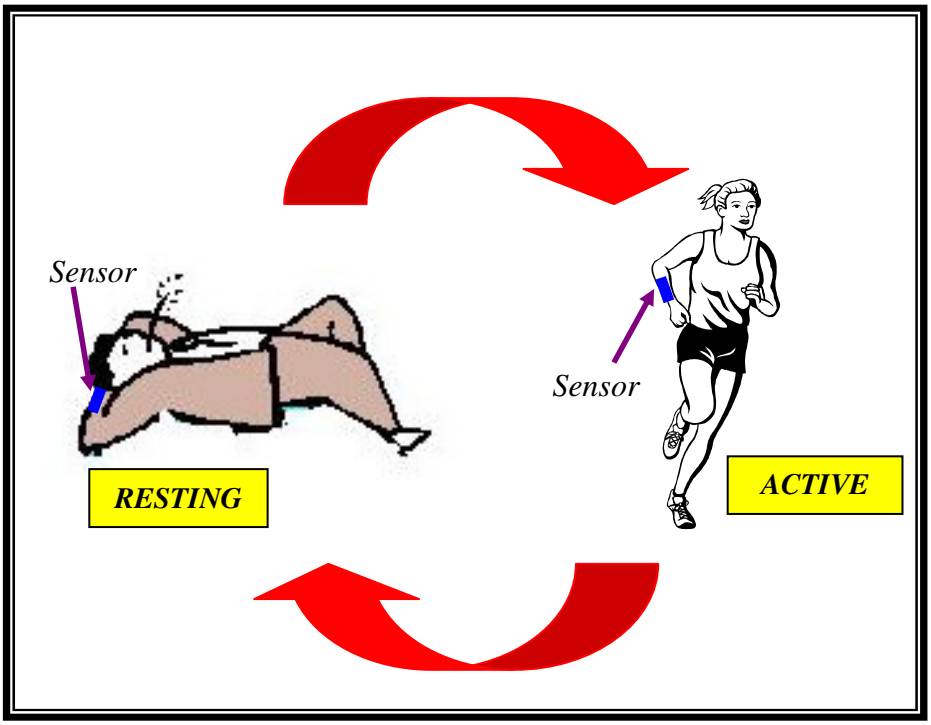

Figure 6.31: Hospital Trial Cycle

Measurements were taken at 10-second intervals for both systems while the subject engaged in a routine which encompassed a 20-minute rest (sitting) position followed by a 20-minute active event as illustrated in Figure 6.31. Immediately after this, the routine was repeated again to evaluate the repeatability of the measurements.

6.5.2 Results and Discussion

Figure 6.32 depicts a linear correlation graph for the tested sensor that regressed to give a current function of $I(\mu A) = -0.0106 \times PO_2(\text{mmHg}) + 0.47$ with respect to the commercial equivalent. The corresponding regression coefficient was 0.9351. It was noted that the current magnitudes were much lower than those of the laboratory experiments. The reasons could be due to the losses and variations in measurements when gas diffused through the human skin. Contact pressure and area also played an important part in the attenuation of output signals.

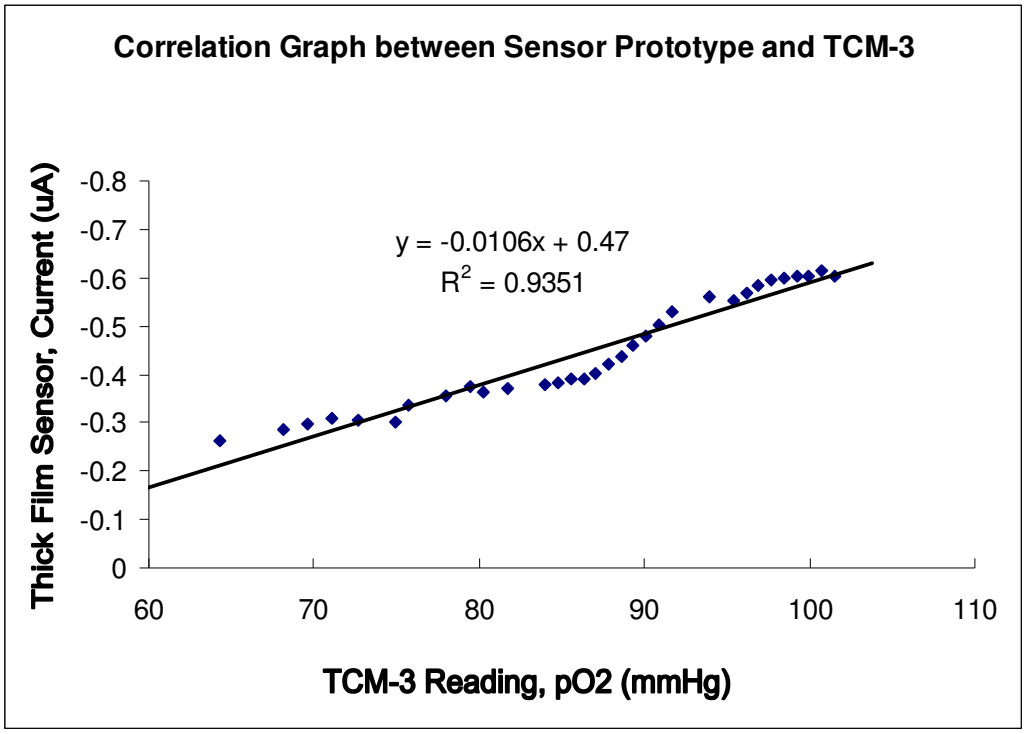

Figure 6.32: Correlation Graph between Thick Film Transcutaneous Oxygen Sensor and Commercial System from Radiometer (TCM-3)

The range of transcutaneous partial pressure was limited for this trial as the subject was a healthy person. In order to widen this range, the test cycle was designed in a way to include alternating activities so as to increase the intake of oxygen. By applying regression functions to the obtained data, correlated values could also be estimated easily for extreme cases of hyperoxia or hypoxia. It was important to note that the operating range for the output measurements of the Nafion-based sensor was found to cover from 0 mmHg up to 160 mmHg, which was equivalent to 21% of 760 mmHg atmospheric pressure.

6.5.3 Conclusions on the Clinical trial

Although the sensor prototype was not packaged in a commercial manner, this trial was carried out to evaluate its effectiveness and viability to measure transcutaneous oxygen. Several advantages could be observed in this trial for employing the Nafion-based sensor with PTFE membrane. The skin surface did not require a layer of conductive gel. As the prototype was developed using a multi-channel multimeter, several sensors could be placed at different positions on the body to measure the oxygen levels all at the same time. The maintenance of the sensor would be kept to the minimum since it was meant to be disposable after approximately 2 days of continuous usage. Conversely, disadvantages were also noted during the experiments. A constant drip of fluid, preferably de-ionized water was required to hydrate the electrolyte of the prototype sample at approximately 5-minute intervals. This was to maintain the ionic conduction paths in the electrochemical sensor. Due to the current design structure of the existing sample, the hard and sharp edges of the ceramic substrate posed some discomfort to the patient.

Despite the pros and cons presented by the prototype, the correlation between the measured output current was found to be linearly proportional to the partial pressure of oxygen recorded by a commercial system. This strongly indicated positive prospects and potential of developing a disposable thick-film transcutaneous oxygen sensor.

Chapter 7 Conclusions

7.1 General Summary and Conclusions

In this research project, literature review was carried out to understand the fundamentals behind the different aspects of a transcutaneous oxygen sensor as well as its application and importance as a medical instrument. In order to achieve the objectives of developing a viable oxygen sensor for clinical tests, thick film fabrication techniques and the chemical aspects of the materials for the construction of the sensor were thoroughly investigated. Although the final aim of this sensor design was geared towards a practical application in hospitals and clinics, all tests and experiments were initially performed under laboratory conditions with several assumptions involved. In many cases, approximate simulations were necessary to study the sensors more closely. Upon the completion of the primary prototype, a simple clinical trial at the hospital was also carried out to correlate its results with an existing commercial system. Fundamental specifications such as non-biohazardousness, low cost and user friendliness of the sensors were constantly maintained in the course of designing each type of sensor. Considerable activity was dedicated to supporting circuitry such as the potentiostat and heating circuit module as they played essential roles for the development as a whole. The main concerns for the circuits were their reliability and stability as the measurements depend greatly on them for proper analysis. The designs also needed to be sufficiently flexible for the different parameters that varied in the course of fabrication.

The sensor design was categorized into two major modules namely the heating element and the oxygen sensor. They were fabricated in-house and experiments were conducted to study these sensors. Firstly, the platinum heating element was calibrated so that measurements could be carried out at the appropriate temperature. Several experiments determined the stability and response time of the heating element with its supporting temperature control circuit based on a one heating element closed loop system. It was found that the temperature distribution over the whole substrate was relatively even and the transcutaneous temperature could be maintained despite changes in environmental conditions.

For the oxygen sensing module, the electrode layout of the sensor was adopted from the typical dissolved oxygen sensor prototype [69]. The advantages included the overall low cost incurred since new screens for the thick film printing process were not necessary until the final design was confirmed. The final outlook of the sensor would take into consideration several issues such as size, material and packaging so as to achieve an optimum design. The dissolved oxygen sensor layout was suitable for transcutaneous measurement as the separation distances and geometry of the working, counter and reference electrodes conformed to a general set of specifications, hence falling well within the requirements. With this, the sensors were ready to undergo different tests for the investigations of suitable materials for the electrolyte and membrane.

The sensors with potassium nitrate (KNO_3) as the aqueous salt electrolyte were covered with membranes of cellulose acetate (CA), polytetrafluoroethylene (PTFE) or polyvinyl chloride (PVC). They were then subjected to voltammetric tests where the relationship between the output current and input biasing voltage was established under different conditions for varying temperature and humidity. It was found that the diffusion limit plateaus for all three types of sensor were in the input biasing voltage range of -0.5V to approximately -1V. Hence, a convenient value of -0.6V was chosen for the biasing potential across the working electrode and counter electrode. Another study was carried out on the effect of the sweeping rate on the input biasing voltage. At a lower rate, a two step two-electron ionization process dominated the electrochemical reaction. Meanwhile, a four-electron ionization process was only observed at higher sweep rates of input biasing voltages.

Several experiments were done to determine the effectiveness of the sensor on the detection of oxygen levels within an enclosed beaker. It was initially performed in dry conditions followed by a hydrated environment for comparison purposes. In dry conditions, PTFE membranes appeared to be most promising but failed to maintain its effectiveness at an elevated temperature of 44 °C. The main cause for the poor response was most probably due to the dehydration of the electrolytes, which would eventually lead to a decrease in the ionization process. With fewer ions available for conduction, the sensor could not be of effective use.

In a more practical and realistic scenario, the sensor was placed on a skin-like membrane known as Tegaderm and the tests were repeated to obtain a more thorough study. However,

the results did not satisfy the requirements for transcutaneous measurements as the relationship between different oxygen concentration and measured output currents were not repeatable.

In view of this, there was a need to pursue the subject in the direction of alternative materials for the electrolyte and membrane. As the field of materials engineering was focusing towards polymers, there was a tendency to adopt polymer electrolytes for the new sensor design. The polymer electrolyte chosen should possess characteristics that fulfilled the requirements for oxygen detection. Furthermore, it must be non-toxic as eventually, the application was meant for a biomedical purpose. It should also give better responses at elevated temperature. Ideally, the conduction and diffusion occurring in the electrolyte should be independent of the hydration limitation as seen for the aqueous salt electrolyte. The choice was then narrowed down to Nafion, which is a popular choice as a polyelectrolyte for fuel cell applications. The voltammetric tests and correlation tests similar to that of the KNO_3-based sensors were then carried out to evaluate their candidature. It was found that the Nafion-based sensors were able to track the changes in oxygen levels faithfully with fairly short delays in response time. This was ideal for continuous measurement where sudden variations could be detected almost instantaneously. The repeatability of measuring each oxygen level was also shown to be well within acceptable deviations for all sensors, with the exception of the PVC-membrane sensor, which gave a large error of ±17.5%, hence inferring poor ability to reproduce similar current outputs at the same oxygen level. These investigations brought about a deeper understanding of different membrane materials employed in screen-printed sensors with Nafion polyelectrolyte. The sensor with a PTFE membrane appeared to be most promising hence it was selected to perform the clinical transcutaneous measurements.

Considering the theoretical aspect of the research, the transient response was simulated by evaluating a one-dimensional diffusion model based on a planar working electrode as elaborated on in Chapter 4. The settling time and steady state outputs were compared to the experimental equivalent. It was found that the trends of the results were similar and this method could be used for future designs to predetermine the responses of the sensors via calculation. This cost saving technique would improve efficiency as well as simplify the procedures for choosing and experimenting with new materials.

Figure 7.1 briefly illustrates the development stages involved in this research project. In the midst of all the investigations, several problems were encountered that led to slow overall progress. Many of the new materials had to be created using trial and error methods, as there was no recommendation available from commercial manufacturers. However, this time consuming technique was indispensable. Furthermore, criteria such as low cost, thick film applicability and being non-biohazardous restricted the choices for the different aspects of the sensor design. Through these pain-staking investigation processes, many new concepts and understandings were established to provide directions and guides toward the subsequent steps of the project.

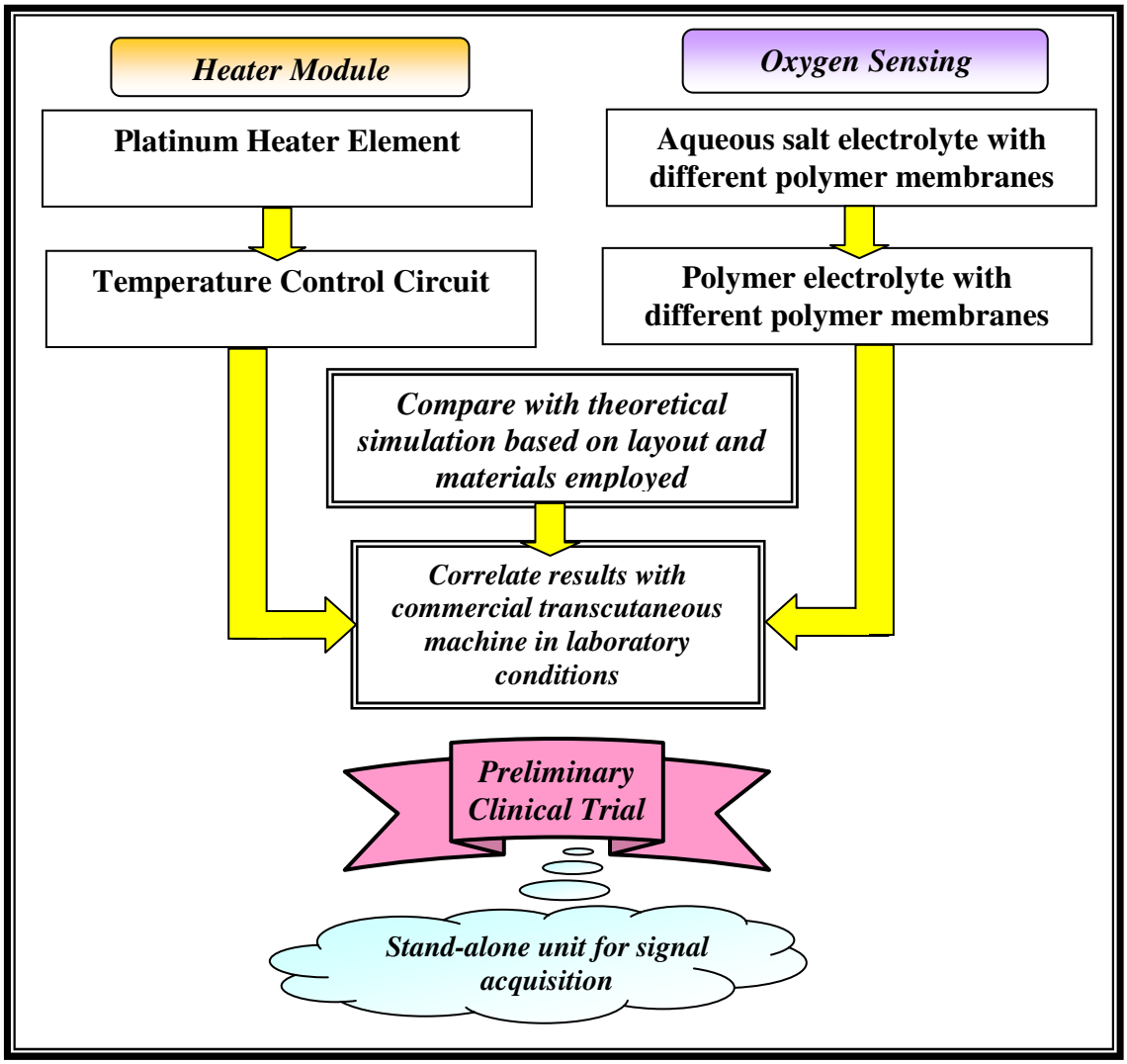

Figure 7.1: Overall Flow Diagram of Stages Involved in Sensor Development

Finally, a preliminary clinical trial was carried out to complete the investigations of the transcutaneous oxygen sensor. A linear correlation was established when compared to a commercial system.

The novel contributions towards this research work were categorized into two major modules. Firstly in the heating module, the innovative aspect was focused on the wheatstone bridge circuit configuration, which involved only a single element taking both the roles of a heating element and a feedback temperature sensor. Secondly, the highlight of the oxygen sensing module was on the effectiveness of using Nafion polyelectrolytes to achieve amperometric measurements for transcutaneous oxygen monitoring. Based on the extensive experimentations and investigations carried out on this project, the most desirable choice for the thick film transcutaneous oxygen sensor was the prototype with Nafion as the electrolyte and PTFE as the membrane. The prototype produced results achieving the following specifications.

(a) *Low cost*

Each printed prototype cost approximately £1 for a batch of 100 sensors. This is a reasonably low-priced piece of equipment for medical application.

(b) *Use for longer period of time*

The prototype was capable of making continuous measurements for up to 46 hours of stable and reproducible measurements. This proved to be a significant improvement from the existing sensors which could only support several hours of continuous usage.

(c) *Power consumption*

At the moment, the power supply of the electronic modules of the sensor design was supported by external d.c. power supply of ±12V. The data acquisitions were made using digital multimeter which was connected to the computer for automation purposes. The project did not concentrate on the improvement of power consumption.

(d) *Portable / Light weight*

The sensor was printed on an Alumina substrate of approximately 50mm by 12mm. In order to keep the overall cost of the project low, it was decided that

further miniaturization was not carried out. Hence, the sensors were manufactured based on existing screens. Although the optimum design was not achieved, the sensors proved to be essentially portable and light weight.

(e) *Compact*

The artwork for the sensor was confined to a reasonably compact area of 10mm by 10mm, even though it was printed on the relatively larger substrate.

(f) *Disposable*

The sensors were made disposable and could also be easily reworked or recycled for future use while maintaining a high standard of hygiene within the hospital environment.

(g) *Non-biohazardous*

The chemicals used for developing the sensors were chosen primarily due to the non-biohazardous feature. There were also no traces of biohazardous electrochemical by-products during the reactions.

(h) *Accurate*

Each sensor type usually produced a unique and calibrated set of readings. Hence, initial calibration employing known levels of oxygen was required in order to obtain the corresponding relationship between current and partial pressure of transcutaneous oxygen ($P_{tc}O_2$). This calibration procedure was performed on the sensors involved in the clinical pilot trial. The sensitivity magnitude of the sensors were approximately 0.025 μA / mmHg. The relative changes in partial pressure of oxygen in the arterial blood were measured with relatively high degrees of accuracy and different oxygen levels were identified easily. The measurement was highly reproducible for the same level of oxygen, giving a maximum deviation of 3%.

(i) *Quick response*

The average response time of the sensors to detect the variations in oxygen levels was 20 seconds, which was far from the ideal steady state measurements of 1

second. Although improvements on this aspect have to be carried out, the response time was sufficient to trace and identify the changes of partial pressure of oxygen during the clinical pilot trial.

(j) *User-friendly*

The current design was considerably user-friendly. The sensor was easily connected to the potentiostat by plugging in 4 wires with proper plug terminators. However, as the sensor required external power supplies and computer link, the overall setup was not favourable towards this specification.

(k) *Easy to integrate and implement*

The sensor proved to be compatible for future upgrading as the basic design was able to be modified on several occasions to test different aspects for transcutaneous measurements.

With more than 70% of the specifications being met, the positive results had confirmed and concluded a successful design for the fundamental version of the disposable transcutaneous oxygen sensor employing thick film fabrication processes.

7.2 Estimation of Cost

As mentioned throughout the whole thesis, lost cost materials and methods were one of the main criteria for developing the transcutaneous oxygen sensor. In general, a basic commercial system would be priced at approximately £20,000 to £30,000. Daily consumables required to maintain the system under a hospital environment averaged an estimated value of a few hundred pounds sterling, depending on the amount of use.

Item	***Cost***	***Fixed***	***Variable***
Screens for Printing Purpose	£60 per screen	✓	

Substrate for 100 pcs	£6		✓
Ink of electrodes for 100 pcs	£30		✓
Electrolyte for 100 pcs	£8		✓
Dielectric Layer for 1 pcs	£0.10		✓
Wires	£0.20		✓
Potentiostat (1 set)	£1.50	✓	
Temperature Control Unit	£2	✓	
Data Acquisition Unit per set	< £2000	✓	

Table 7.1: Estimated Cost of Transcutaneous Oxygen Sensor and its System

For the desired thick film sensor, a breakdown of the costs involved is presented in Table 7.1. The overall budget would be based on 2 major categories, namely a one-time fixed amount and a variable cost, which depended on the output demand for the sensor fabrication. The costs of the thick film equipment such as the printer, the dryer and the furnace were not included since this equipment was not solely dedicated to this purpose.

A conservative price estimation of each disposable sensor, fabricated as a batch of 100 pieces would be approximately £1 including all consumables. If the production volume were to increase, the effective cost per sensor would reduce significantly since thick film techniques were employed. The measuring unit that consisted of the data acquisition module and the different circuitry would cost less than £2000. The maintenance cost would be below £100 per year. Although each sensor tip is disposable, the rugged properties would project high success rates of recycling. Therefore, the desired thick film transcutaneous oxygen sensor system presents a more cost effective alternative or solution to the existing commercial systems. In the long run, the advantages presented by the new sensor system would become more evident.

7.3 Future Work

The acquisition of measurements was performed via multimeters and the results were compiled through data entry into the computer. It would be more desirable if the sensor were to be connected to a stand-alone supporting unit for data acquisition and signal processing. The unit should possess basic features such as measurement displays, recordable memory and hardcopy printouts. It should also have a digital signal processing module where the data could be analyzed and manipulated for offset compensations. However, the outcome of this module could not be realised in time and would only contribute minimally in terms of research novelty. Hence, it was not the most vital aspect of this research since many other standard alternatives for the design of the stand-alone unit could be easily available.

One possible area of future work could involve the integration of the sensor with personal digital assistants (PDAs). C-Cubed Limited has developed a multi-functional data acquisition interface card for the compact flash standard [82]. This enables many hand held computers and PDAs now available to be used as sophisticated data collection and analysis tools. Currently, it is used in the monitoring of bolt forces but this could easily be expanded to include different types of applications. Many medical professionals have PDAs, which they often carry in the course of their work. The portability and convenience of PDAs suggest that they would be suitable choices for developing cost effective supporting units for data acquisition and signal processing in the field of biomedical instrumentation. Hence, the possibility of realising a stand-alone unit using PDAs for transcutaneous measurement could lead to new avenues for research and development.

The projected sensor design would appreciate a reduction in size of the substrate and also the packaging of the sensor tip could be improved to be more desirable. The ideal size of the sensor tip should be not more than 10 mm in diameter whilst maintaining sufficient contact area. Self-adhesive tapes could also be included in the future design to make the attachment of the sensor more user-friendly. Figure 7.2 hypothesizes a possible outlook for such a disposable, thick film transcutaneous oxygen sensor. The thick film sensor tip should be encapsulated within a plastic case fitted to expose the electrode surface to the skin. One essential contribution towards the current design would be developing an electrolyte that could fulfil the role without the need for any hydration at the elevated temperature of 44 °C. Possible methods such as incorporating sol-gel materials or doping adsorbent particles into the electrolyte could be further explored.

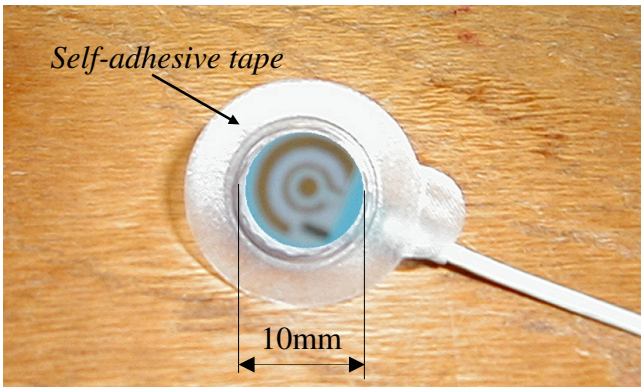

Figure 7.2: Outlook of Improved Transcutaneous Oxygen Sensor

On the whole, the measuring system should possess the following entities to allow multiple functions as depicted in Figure 7.3:

- multiple channels for sensors to perform simultaneous measurements
- touch screen menu for high degree of user-friendliness
- portability
- self calibration of oxygen level in order to compensate for any offsets
- maximum storage for data acquisition
- easy integration with external peripherals such as printer and other instruments
- upward compatibility for future improvement

Figure 7.3: Outlook of Improved Transcutaneous Oxygen Measuring System

Further tests investigating the effects of external parameters such as contact pressure on the output measurements from the sensors should also be carried out. In addition, extensive studies on the effects of pH levels should also be continued in order to establish more

comprehensive statistical representations. If the effects were found to be significant, proper compensation should be performed.

Figure 7.4: Multi-purpose Applications

For the time being, the aim of the final sensor system would be targeted at premature neonatal patients who require ongoing, continuous monitoring of partial pressure of oxygen. Ultimately, the vision for this research topic propagates beyond this application to include gas monitoring namely oxygen and carbon dioxide as well as nitric oxide for both babies and full-grown adults in at the most cost effective manner.

REFERENCES

[1] Application Notes from Radiometer and Hewlett Packard, *"Transcutaneous pO_2 / pCO_2 Monitoring in Neonatology"*, 1994.

[2] S. Niijima, D.B. Shortland, M. I. Levene, D. H. Evans, *"Transient Hyperoxia and Cerebral Blood Flow Velocity in Infants Born Prematurely and at Full Term"*, Arch. Dis. Child, 63, pp. 1126-1130, 1988.

[3] L. J. Graziani, A. R. Spitzer, D. G. Mitchell, D. A. Merton, C. Stanley, N. Robinson, L. McKee, *"Mechanical Ventilation in Preterm Infants: Neurosonographic and Developmental Studies"*, Pediatrics, 90, pp. 515-522, 1992.

[4] Application Notes from Hewlett Packard, *"Pulse Oximetry - A Primer"*, 1990.

[5] Nomura, Hiramoto, Yoneda, Yotsuya, *"Tanscutaneous Oxygen Monitor"*, The 2nd Symposium of Medical Precision Engineering, pp. 151-155, 1983. (Japanese)

[6] M. L. Topfer, *"Thick-Film Microelectronics - Fabrication, Design and Application"*, Litton Educational Publishing Inc., ISBN: 0442285647 m, 1971.

[7] L.C. Clark, *"Monitor and Control of Blood and Tissue Oxygen Tension"*, Trans. Am. Soc. Art. Int. Org. **2,** pp. 41–52, 1956.

[8] V. Linek, V. Vacek, J. Sinkule, P. Benes, *"Measurement of Dissolved Oxygen by Membrane-Covered Probes"*, Ellis Horwood Ltd, Ch 5, pp. 87-99, ISBN: 0470210613 v, 1988.

[9] S. Keston, Kenneth R. Chapman, Anthony S. Rebuck, *"Response Characteristics of a Dual Transcutaneous Oxygen/Carbon Dioxide Monitoring System"*, Chest, 99, pp. 1211-1215, 1991.

[10] W.H. Hoffman, J.P. Locksmith, E.M. Burton, E. Hobbs, G.G. Passmore and A.L. Pearson-Shaver, *"Interstitial Pulmonary Edema in Children and Adolescents with Diabetic Ketoacidosis"*, J. Diabetes Complications 12, pp. 314–320, 1998.

[11] A. M. Macarthur, *"Treatment of Tension Pneumothorax"***,** The Lancet, Volume 277, Issue 7169, pp. 173, 21 January 1961.

[12] M. Yamakage, Y. Kamada, M. Toriyabe, Y. Honma, A. Namiki, *"Changes in Respiratory Pattern and Arterial Blood Gases during Sedation with Propofol or Midazolam in Spinal Anesthesia"***,** Journal of Clinical Anesthesia, Volume 11, Issue 5, pp. 375-379, August 1999.

[13] CIBA – CORNING Operator Manual, 800 series, August 1995.

[14] J. W. Severinghaus, Y. Honda, *"History of Blood Gas Analysis. VII Pulse Oximetry"*, Journal of Clinic Monitoring, 3, pp. 135-138, 1987.

[15] R. A. Wolthuis, D. McCrae, J. C. Hartl, E. Saaski, G. L. Mitchell, K. Garcin, R. Willard, *"Development of a Medical Fiber-Optic Oxygen Sensor Based on Optical Absorption Change"*, IEEE Transactions on Biomedical Engineering, 39 (2), pp. 185-193, 1992.

[16] D. W. Lubbers, *"Theoretical Basis of the Transcutaneous Blood Gas Measurements"*, Critical Care Medicine, 9 (10), pp. 721-733, 1981.

[17] O. Lofgren, L. Jacobson, *"The Influence of Different Electrode Temperatures on the Recorded Transcutaneous PO_2 Level"*, Pediatrics, 64 (6), pp. 892-897, 1979.

[18] Radiometer Non-invasive Blood Gas Monitoring Product Manuals, 1976.

[19] F. Manaco, B. G. Nickerson, J. C. McQuitty, *"Continuous Transcutaneous Oxygen and Carbon Dioxide Monitoring in the Pediatric ICU"*, Critical Care Medicine, 10 (11), pp. 765-766, 1982.

[20] D. W. Lubbers, *"Theoretical Basis of the Transcutaneous Blood Gas Measurement"*, Critical Care Medicine, 9 (10), pp. 721-733, 1981.

[21] J. A. Milne, *"An Introduction to the Diagnostic Histopathology of the Skin"*, London: Edward Arnold, ISBN: 0713141921, 1972.

[22] A. Fenner, R. Muller, H. G. Busse, M. Junge, J. Wolfsdorf, *"Transcutaneous Determination of Arterial Oxygen Tension"*, Pediatrics, 55 (2), pp. 224-231, 1975.

[23] A. Bidani, R. W. Flumerfelt and E. D. Crandal, *"Analysis of the Effects of Pulsatile Capillary Blood Flow and Volume on Gas Exchange"***,** Respiration Physiology, 35, Issue 1, pp. 27-42, October 1978.

[24] Kevin C. Elhers, Kenneth C. Mylrea, Charles K. Waterson and Jerry M. Calkins, *"Cardiac Output Measurements. A Review of Current Techniques and Research"*, Annuals of Biomedical Engineering, 14, pp. 219-239, 1986.

[25] Maria L. Urso and Priscilla M. Clarkson, *"Oxidative Stress, Exercise, and Antioxidant Supplementation"***,** Toxicology, Volume 189, Issues 1-2, pp. 41-54, 15 July 2003.

[26] K. Kogo, K. Kuwa, Y. Miyagawa, K. Yoneda, K. Yotsuya, T. Kitazaki, K. Taniguchi, *"PO-550 Transcutaneous Blood Gas Monitor with a Combined O_2/CO_2 Sensor"*, Sumitomo Electric Technical Review, 28, 1989.

[27] L.C. Clark, Electrochemical device for chemical analysis, US Patent 2913386, 1959.

[28] Southampton Electrochemistry Group, *"Instrumental Methods in Electrochemistry"*, Ellis Horwood Ltd, Ch 5, pp.149-177, ISBN: 0134720938 pbk, 1985.

[29] D. Pletcher, *"A First Course in Electrode Processes"*, Alfresford Press Ltd, Ch 3-4, pp.77-106, ISBN: 0951730703, 1991.

[30] D. J. G. Ives, *"Reference Electrodes. Theory and Practice"*, Academic Press, 1961.

[31] Lide, David R., *"CRC Handbook of Chemistry and Physics 2000-2001: A Ready Reference Book of Chemical and Physical Data",* CRC Press, ISBN: 0849304814 2000.

[32] G. Bianchi, F. Mazza and T. Mussini, *"Oxygen and Hydrogen-peroxide Processes on Gold Electrodes in Acid Solutions"*, Electrochimica Acta, Volume 11, Issue 10, pp. 1509-1523, October 1966.

[33] N. P. C. Stevens and Alan M. Bond, *"The influence of migration on cyclic and rotating disk voltammograms"*, Journal of Electroanalytical Chemistry, Volumes 538-539, pp. 25-33, 13 December 2002.

[34] A. J. Bard, L. R. Faulkner, *"Electrochemical Methods"*, New York: Wiley, ISBN: 0471055425, 1980.

[35] V. Karagounis, L. Liu, C. C. Liu, *"A Thick -Film Multiple Component Cathode Three-Electrode Oxygen Sensor"*, IEEE Transactions on Biomedical Engineering, BME-33 (2), pp. 108-112, 1986.

[36] O. Fumio, *"Polyelectrolytes"*, New York: M. Dekker, ISBN: 0824715055, 1971.

[37] J. R. MacCallum, C. A. Vincent, *"Polymer Electrolyte Reviews"*, London: Elsevier Applied Science, ISBN: 1851663487, 1989.

[38] DuPont™ Nafion® PFSA Membranes N-117 Perfluorosulfonic Acid Polymer product information, NAE101, November 2002.

[39] M. Rikukawa, K. Sanui, *"Proton-conducting Polymer Electrolyte Membranes Based on Hydrocarbon Polymers"*, Progress in Polymer Science, 25, pp. 1463-1502, 2000.

[40] Eastman Chemical Company, *"EASTMAN AQ 55S Polymer Technical data sheet"*, 2003.

[41] M. L. Miller, *"The Structure of Polymers"*, New York: Reinhold Publishing Corporation, pp. 580-656, 1966.

[42] Roberts, Royston M., "*Serendipity: Accidental Discoveries in Science",* John Wiley and Sons; New York, ISBN: 0471602035, 1989**.**

[43] Fenichell, Stephen, *"Plastic: The Making of a Synthetic Century"*, HarperCollins, New York, ISBN: 0887308627, 1996.

[44] Keith E. G. Pitt, *"Introduction to Thick Film - Component Technology"*, Mackintosh Publications Ltd., Ch. 2, pp. 16-22, ISBN: 0904705374, 1981.

[45] M. Prudenziati, *"Thick Film Sensors"*, Elsevier Science B.V., ISBN: 0444897232, 1994.

[46] P. L. Fleischner, *"Beryllia Ceramics in microelectronic applications"*, Solid St. Technol. p. 25, Microelectronics and Reliability, Volume 16, Issue 2, p. 116, 1977.

[47] P. J. Holmes, R. G. Loasby, *"Handbook of Thick Film Technology"*, Electrochemical Publications Limited, ISBN: 0901150053, 1976.

[48] M. L. Hitchman, *"Measurement of Dissolved Oxygen"*, Wiley Interscience, Ch 5, pp. 71-123, ISBN: 0471038857, 1978.

[49] K. Grasshoff, *"The Electrochemical Determination of Dissolved Oxygen"*, Marine Electrochemistry, Wiley, Ch 9, pp. 329-405, 1981.

[50] J. Koryta, J. Dvorak, L. Kavan, *"Principles of Electrochemistry"*, John Wiley & Sons Ltd., Ch 4, pp. 198-235, ISBN: 0471938386, 1993.

[51] J. Bilek, *"Thick Film Heating Element and Design of Temperature Control Circuit"*, Diploma Thesis, Brno University of Technology, 2001.

[52] Electro-Science Laboratories Inc., Cermet Pltainum Conductor ESL-5545 Data Sheet.

[53] A. Cranny, J. Atkinson, *"Thick Film Silver-Silver Chloride Reference Electrode"*, Meas. Sci. Technol., 9, pp. 1-7, 1998.

[54] V. Linek, V. Vacek, J. Sinkule, P. Benes, *"Measurement of Dissolved Oxygen by Membrane-Covered Probes"*, Ellis Horwood Ltd, Ch 3, pp. 28-40, ISBN: 0470210613 v,1988.

[55] N. V. Krylov, *"Introduction to the Theory of Diffusion Process"*, Transl. Math, Monongraphs, Vol. 142, Providence RI, ISBN: 0821846000, 1995.

[56] J. C. Jaeger, Quarterly of Applied Mathematics, 8, pp. 1987, 1950.

[57] Stephen Wolfram, *"The Mathematica Book, 4th edition"*, Cambridge University Press and Wolfram Media, Wolfram, ISBN: 1579550045, 1999.

[58] V. Linek, V. Vacek, J. Sinkule, P. Benes, *"Measurement of Dissolved Oxygen by Membrane-Covered Probes"*, Ellis Horwood Ltd, Table 5, pp. 313, ISBN: 0470210613 v,1988.

[59] A. Pinotto, N. Graiver, A. Califano, N. Zaritzky, *"Effective Diffusion Coefficients of Sodium Nitrite and Potassium Nitrate in Pork Tissue"*, 2001 IFT Annual Meeting, Food Engineering: Transport Processes and Kinetics, p. 73C, 2001.

[60] Y. Hirata, Y. Miura, T. Nakagawa, *"Oxygen Permeability and the State of Water in Nafion® Membranes with Alkali metal and Amino Sugar Counterions"*, Journal of Membrane Science, Volume 163, Issue 2, pp. 357-366, 1999.

[61] N. Grossi, E. Espuche, M. Escoubes, *"Transport Properties of Nafion®/cyclodextrin Membranes"*, Separation and Purification Technology, Volumes 22-23, pp. 255-267, March 2001.

[62] A. Talbot, M. R. Neuman, G. M. Saidel, E. Jacobsen, *"Dynamic Model of Oxygen Transport for Transcutaneous PO_2 Analysis"*, Annals of Biomedical Engineering, 24, 2, pp. 294-304, 1996.

[63] PRC100 Resistive Temperature sensor Data Sheet, RS Catalogue, 1997.

[64] Stress Photonics Inc., DeltaTherm 1300 Data sheet, 2000. Also available at http://www.stressphotonics.com/TSA/TSA_Intro.html

[65] Dee Livingstone-Bridge, Jan C. Myland, Keith B. Oldham, *"A Model of Ionic Current Densities in the Vicinity of a Corroding Disk-shaped Region"*, Electrochemistry Communications, Vol. 3, Issue 8, pp. 384-389, August 2001.

[66] Model 264A, Polarographic Analyzer Stripping Voltmeter Operational Manual, 1988.

[67] CEC TESTPOINT Operational Manual, Capital Equipment Corporation, Massachusetts, 1998.

[68] L. Pataki, *"Basic Analytical Chemistry"*, Oxford: Pergamon, ISBN: 0080238505 1980.

[69] Instruction Manual for BAS Epilson for Electrochemistry Ver 1.10.54, Bioanalytical Systems Inc., 2000-2001.

[70] W. V. Glasspool, *"An Investigation of the Characteristic of Thick Film Amperometric Dissolved Oxygen Sensors"*, Ph. D. Thesis, University of Southampton, 1998.

[71] 3M™ Tegaderm™ Transparent Dressings - Picture Frame Style Product Specification Sheet, 2003.

[72] Andrea Saltelli, Karen Chan, E. Marian Scott, *"Sensitivity Analysis"*, Edition 1, Chichester: Wiley, c2000, Wiley series in probability and statistics, ISBN: 0471998923, 2000.

[73] M. Cappadonia, J. Wilhelm Erning, Seyedeh M. Saberi Niaki, Ulrich Stimming, *"Conductance of Nafion 117 Membranes as Function of Temperature and Water Content"*, Solid State Ion., 77, pp. 65–69, 1995.

[74] M.C. Wintersgill and J.J. Fontanella, *"Complex Impedance Measurements on Nafion"*, Electrochim. Acta 43 10–11, pp. 1533–1538, 1998.

[75] Kirsi Wallgren and Sotiris Sotiropoulos, *"Oxygen Sensors based on a New Design Concept for Amperometric Solid State Devices"*, Sensors and Actuators B: Chemical, Volume 60, Issues 2-3, pp. 174-183, November 1999.

[76] H. Shwachman, A. Mahmoodian and R.K. Neff, *"The Sweat Test: Sodium and Chloride Values*", J Pediatr, 98, pp. 576–578, 1981.

[77] B. Ekwall, C. Clemedson, *"Time-related Lethal Blood Concentration from Acute Human Poisoning of Chemicals (Part 2 - The Monographs), No.13 - Sodium Chloride"*, First Internet Edition, CTLU, 1997. Also available at: http://www.cctoxconsulting.a.se/46_Oxalate.pdf

[78] F.G.Cottrell, Z.Physik.Chem., 42, pp. 385, 1902.

[79] E. Y. Choi, J. H. Choi, S. H. Moon, *"An Electrodialysis Model for Determination of the Optimal Current Density"*, Desalination, Elsevier Science, 153, pp.399-404, 2002.

[80] Puddephatt, R. J. Richard John, "The Periodic Table of the Elements", 2nd Edition, Oxford : Clarendon, ISBN: 0198555164 v pbk, 1986.

[81] G. E. Wnek, J. N. Rider, J. M. Serpico, A. G. Einset, S. G. Ehrenberg and L. Raboin, *"New Hydrocarbon Proton Exchange Membranes Based on Sulfonated Styrene-Ethylene/Butylene- Styrene Triblock Copolymers,"* Proc. First Int'l Symposium on Proton Conducting Membrane Fuel Cells, Electrochemical Society Proc. Vol. 95-23, p. 247, 1995.

[82] C-cubed Limited, *"Portable data acquisition – a pocket revolution?"*, Instrumentation, February 2002.

APPENDICES

APPENDIX A

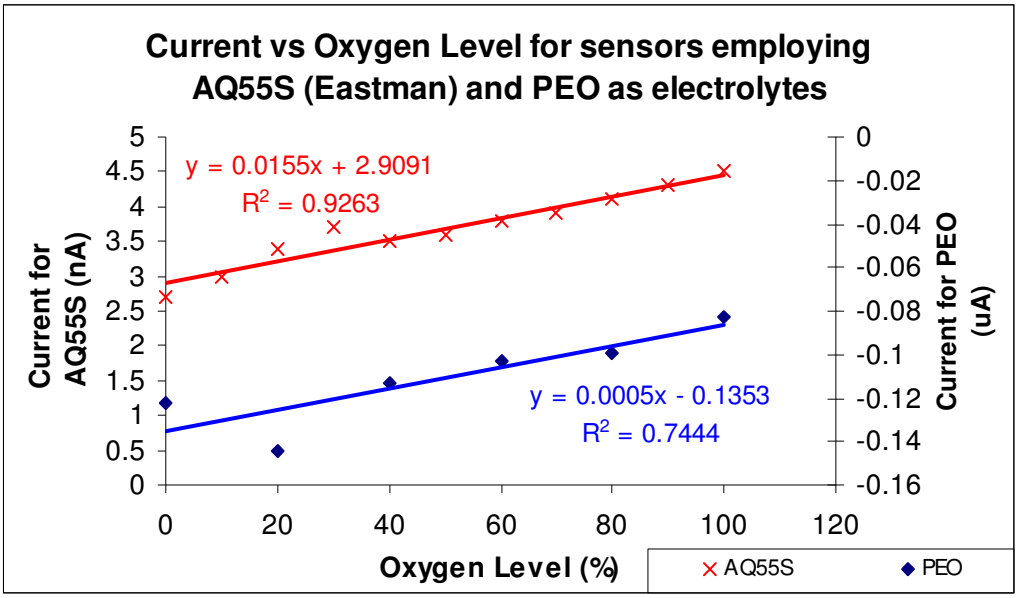

From the graph, it can be seen that the current values measured for the sensor covered with AQ55S (from Eastman Chemical Company) as the electrolyte are in the range of nanoamperes. This observation suggests that the currents are comparable to the noise levels, which are also in nanoamperes. This is undesirable as it would be difficult to identify signal from noise during the measurements. It is also noted that AQ55S-based sensors have output currents which have positive polarity with respect to the output of the inverting amplifier 4 in the potentiostat (Refer to Figure 3.5). This indicates that the potentiostat might be delivering a very high current at the counter electrode or experiencing a large impedance across the counter and reference electrode.

The sensor employing saturated PEO as its membrane gives unstable measurements at fixed levels of oxygen with considerable errors of approximately ±17%. An averaged value was then calculated over the unstable measurements to plot against each corresponding oxygen level. From the averaged results obtained, it was found that as the oxygen level increased, the current magnitude decreased. The graph for the PEO sensor is not a good representation of a working device. The results are not reliable and could not be repeated.

In other words, both types of sensors were not suitable for further investigations to achieve a screen-printed transcutaneous oxygen sensor.

APPENDIX B: *Screen Artwork*

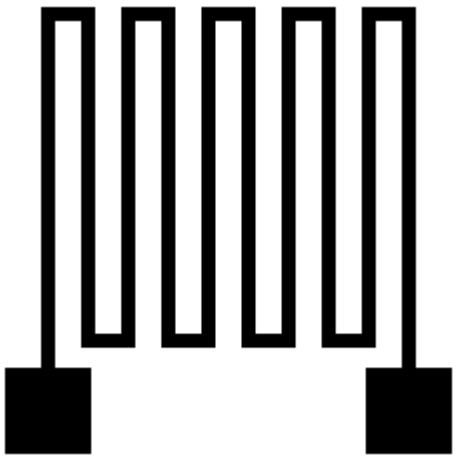

Artwork of Heating Element

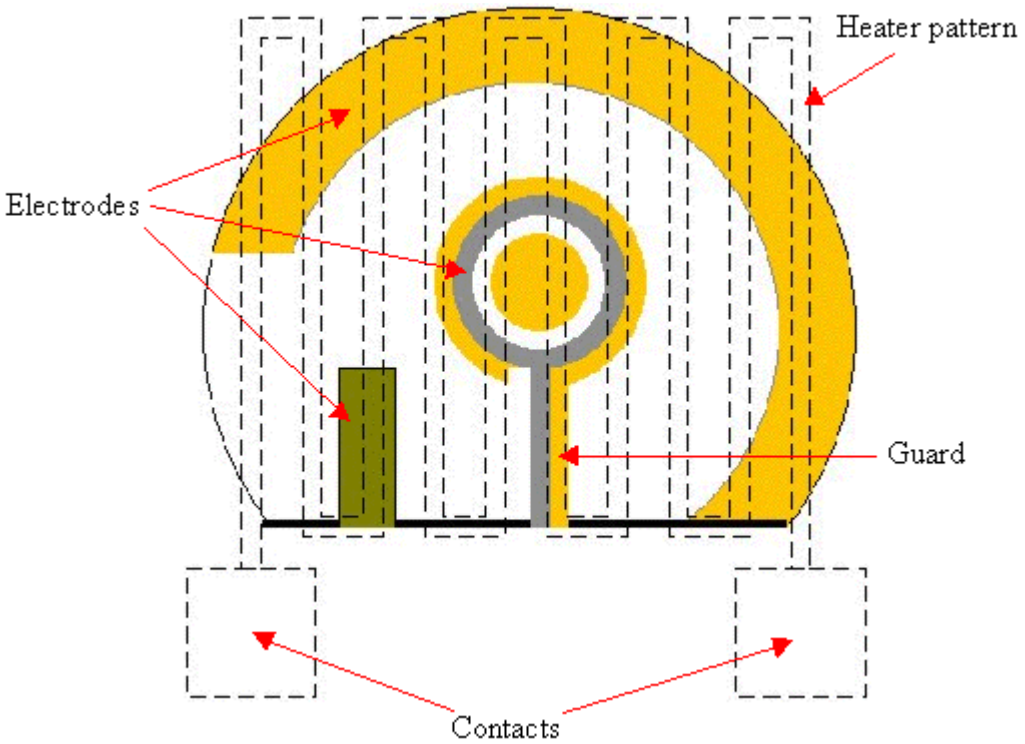

Artwork of Oxygen Sensing Module

APPENDIX C

Sensor Prototype with KNO_3 Electrolyte and PTFE Membrane

Calculating the Steady-state Oxygen Flux

In[1]:

$$p_{S(KNO_3)} = 13 \times 10^3;$$
$$R_M = 6.84932 \times 10^9;$$
$$L_{E(KNO_3)} = 0.1095;$$
$$N_{S(KNO_3)} = \frac{p_{S(KNO_3)}}{R_M \times (1 + L_{E(KNO_3)})}$$

Out[1]:

$$1.71068 \times 10^{-6}$$

Calculating the Positive Roots of Equation (4.12)

In[2]:

$$S_{E(KNO_3)} = 2.61173;$$
$$A_{E(KNO_3)} = 0.0419263;$$
$$K_M = 0.03125;$$
$$\text{Plot}[y = (S_{E(KNO_3)} \times \text{Cos}[\alpha] \times \text{Sin}[A_{E(KNO_3)} \times \alpha]) + (\text{Sin}[\alpha] \times \text{Cos}[A_{E(KNO_3)} \times \alpha]), \{\alpha, 0, 200\}]$$

Out[2]:

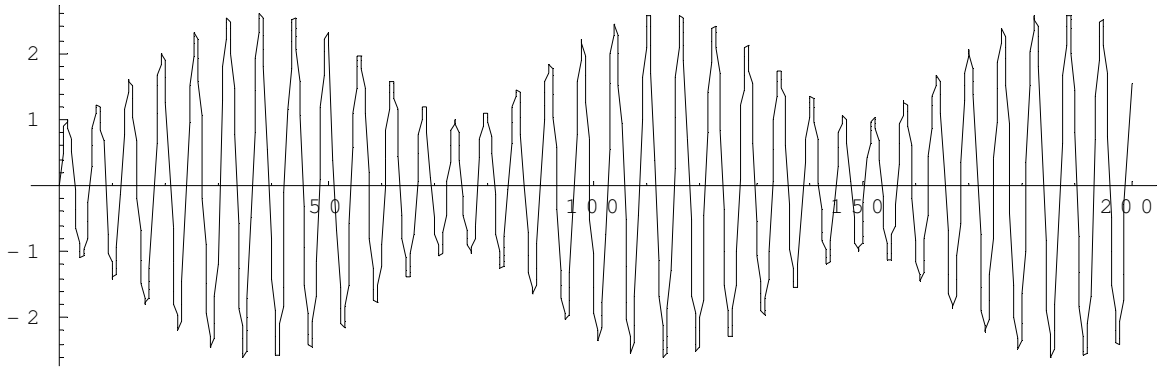

- Graphics -

Calculating the Positive Roots of Equation (4.12)

In[3]:

```
Array[r, 20 × 10^0];
Array[q, 20 × 10^0];
For[i = 0; α = 2.84, i < 20 × 10^0, i++;
 q[i] = (1 + L_E(KNO3)) × Cos[α] × Cos[A_E(KNO3) × α] -
    (A_E(KNO3) + S_E(KNO3)) × Sin[α] × Sin[A_E(KNO3) × α];
 r[i] = α; α += 3]
```

Plotting the H(t) *Function*

In[4]:

$$\texttt{Plot}\left[\texttt{y} = 1 + 2 \times (1 + L_{E(KNO_3)}) \sum_{n=1}^{20\times 10^0} \frac{\texttt{Exp}[-K_M \times \texttt{r}[\texttt{n}]^2 \times \texttt{t}]}{\texttt{q}[\texttt{n}]},\ \{\texttt{t}, 0, 50 \times 10^0\},\ \texttt{PlotRange} \to \{0, 1.25\}\right]$$

Out[4]:

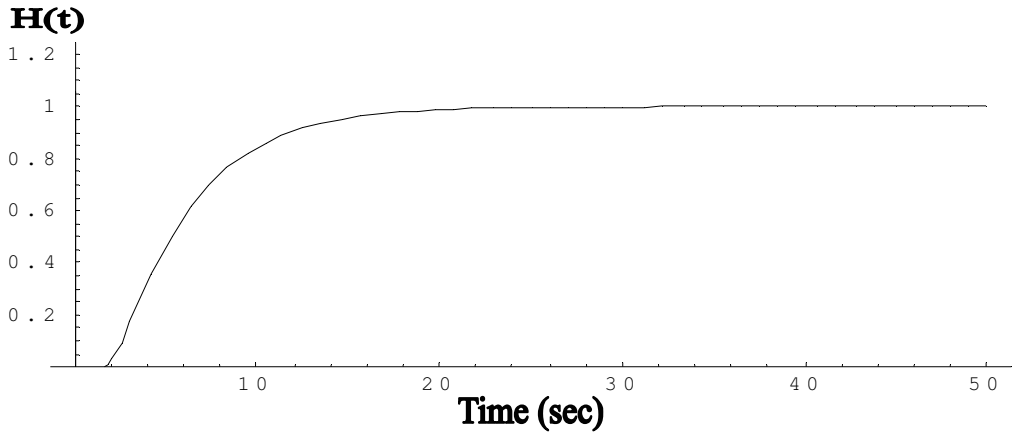

- Graphics -

Plotting the (1-H(t)) *Function*

In[5]:

$$\texttt{Plot}\left[\texttt{y} = 1 - \left(1 + 2 \times (1 + L_{E\,(KNO_3)}) \sum_{n=1}^{20\times 10^0} \frac{\texttt{Exp}[-K_M \times \texttt{r[n]}^2 \times \texttt{t}]}{\texttt{q[n]}}\right),\ \{\texttt{t}, 0, 50 \times 10^0\},\ \texttt{PlotRange} \rightarrow \{-0.2, 1.25\}\right]$$

Out[5]:

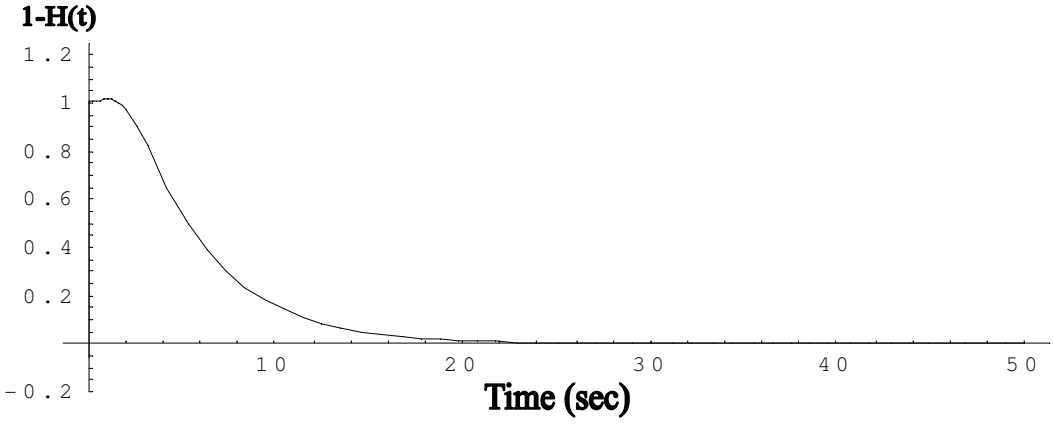

- Graphics -

APPENDIX C

Sensor Prototype with Nafion Electrolyte and PTFE Membrane

Calculating the Steady-state Oxygen Flux

In[1]:

$$p_{S\,(NAFION)} = 13 \times 10^{3};$$
$$R_M = 6.84932 \times 10^{9};$$
$$L_{E\,(NAFION)} = 0.4593;$$
$$N_{S\,(NAFION)} = \frac{p_{S\,(NAFION)}}{R_M \times (1 + L_{E\,(NAFION)})}$$

Out[1]:

$$1.30062 \times 10^{-6}$$

Calculating the Positive Roots of Equation (4.12)

In[2]:

$$S_{E\,(NAFION)} = 5.2491;$$
$$A_{E\,(NAFION)} = 0.0875;$$
$$K_M = 0.03125;$$
$$\text{Plot}[y = (S_{E\,(NAFION)} \times \text{Cos}[\alpha] \times \text{Sin}[A_{E\,(NAFION)} \times \alpha]) + (\text{Sin}[\alpha] \times \text{Cos}[A_{E\,(NAFION)} \times \alpha]), \{\alpha, 0, 100\}]$$

Out[2]:

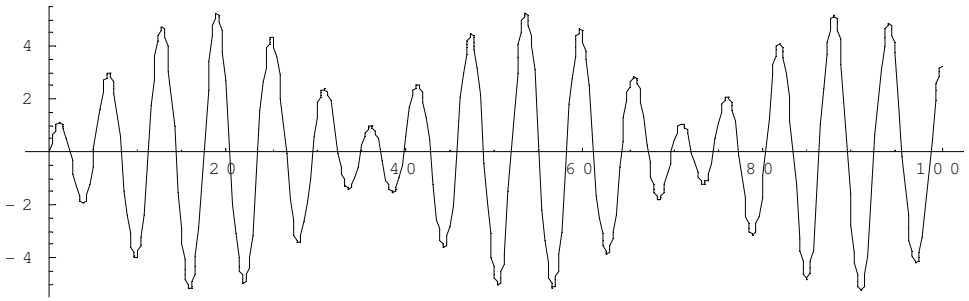

- Graphics -

Calculating the Positive Roots of Equation (4.12)

In[3]:

```
Array[r, 50 × 10^0];
Array[q, 50 × 10^0];
r[1] = 2.31799;

q[1] = (1 + L_E (NAFION)) × Cos[r[1]] × Cos[A_E (NAFION) × r[1]] -
   (A_E (NAFION) + S_E (NAFION)) × Sin[r[1]] × Sin[A_E (NAFION) × r[1]];
For[i = 1; α = 5.09196, i < 50 × 10^0, i++;
 q[i] = (1 + L_E (NAFION)) × Cos[α] × Cos[A_E (NAFION) × α] -
    (A_E (NAFION) + S_E (NAFION)) × Sin[α] × Sin[A_E (NAFION) × α];
 r[i] = α; α += 3]
```

Plotting the H(t) *Function*

In[4]:

$$\texttt{Plot}\left[\texttt{y} = 1 + 2 \times (1 + L_{E\,(NAFION)}) \sum_{n=1}^{50\times 10^0} \frac{\texttt{Exp}[-K_M \times \texttt{r}[\texttt{n}]^2 \times \texttt{t}]}{\texttt{q}[\texttt{n}]},\ \{\texttt{t}, 0, 100 \times 10^0\},\ \texttt{PlotRange} \to \{0, 1.25\}\right]$$

Out[4]:

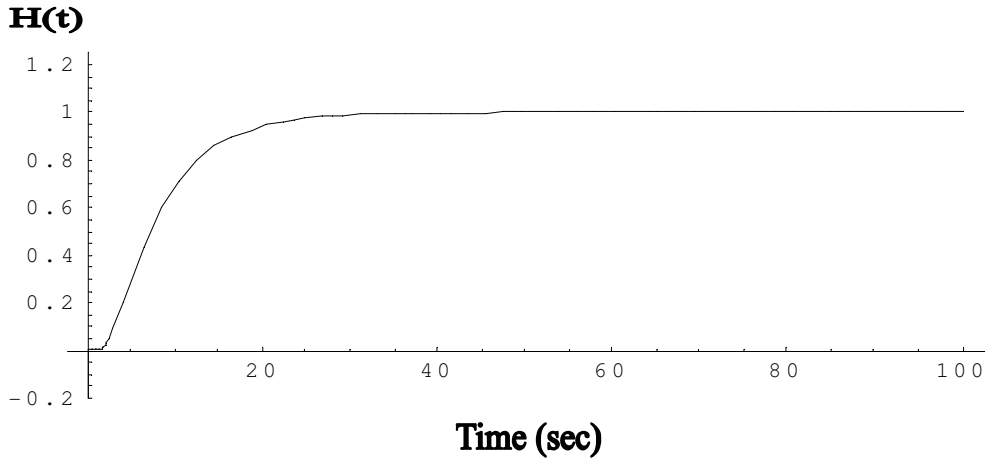

- Graphics -

Plotting the (1-H(t)) *Function*

In[5]:

$$\text{Plot}\left[y = 1 - \left(1 + 2 \times (1 + L_{E(KNO_3)}) \sum_{n=1}^{50\times10^{0}} \frac{\text{Exp}[-K_M \times r[n]^2 \times t]}{q[n]}\right),\right.$$
$$\left.\{t, 0, 100\times10^{0}\}, \text{PlotRange} \rightarrow \{-0.2, 1.25\}\right]$$

Out[5]:

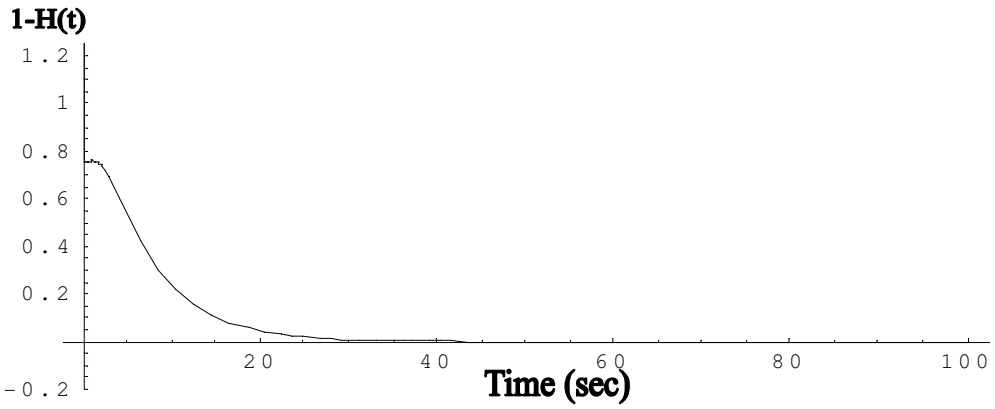

- Graphics -

APPENDIX D

TESTPOINT Voltammogram Program Listing

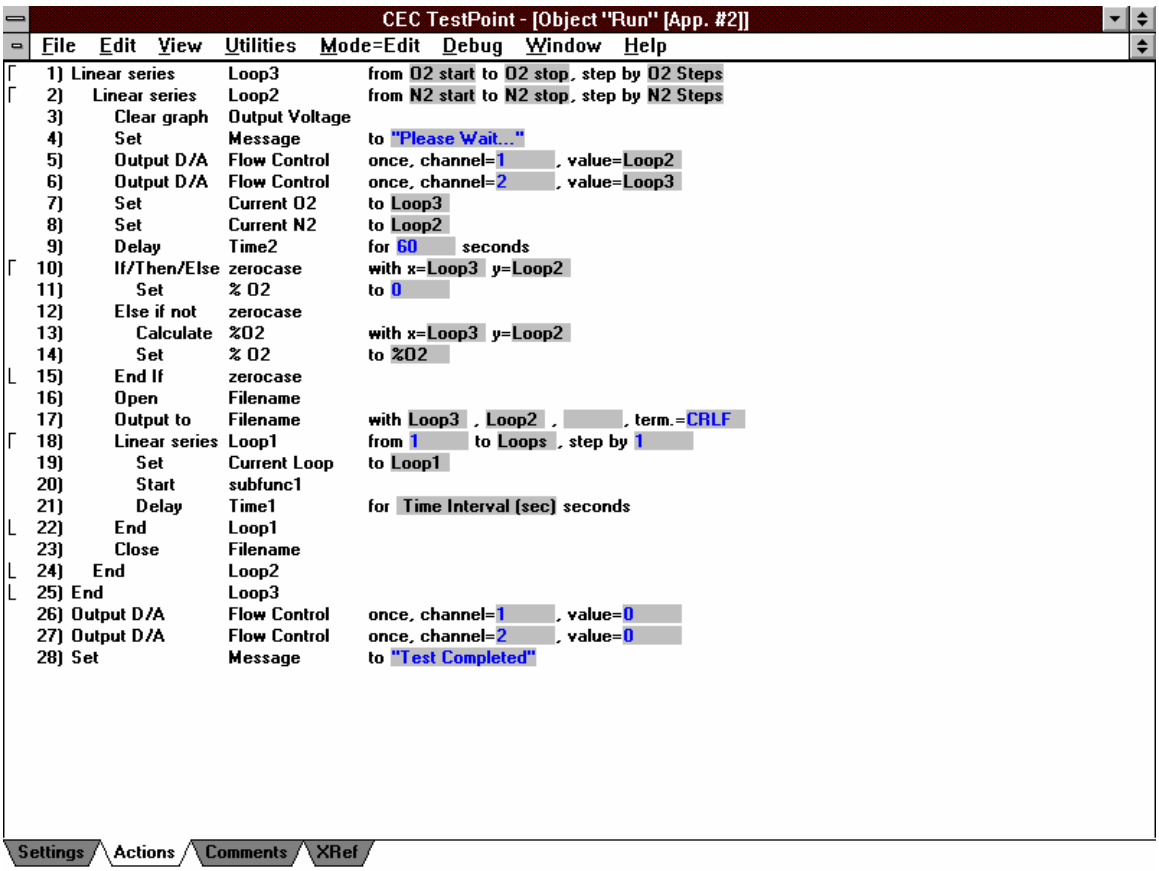

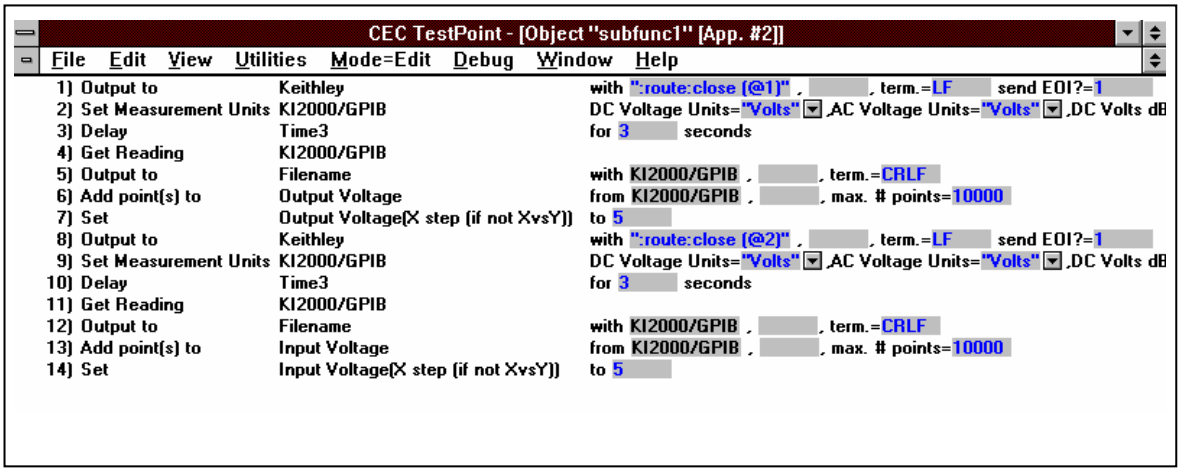

TESTPOINT Static Test Program Listing

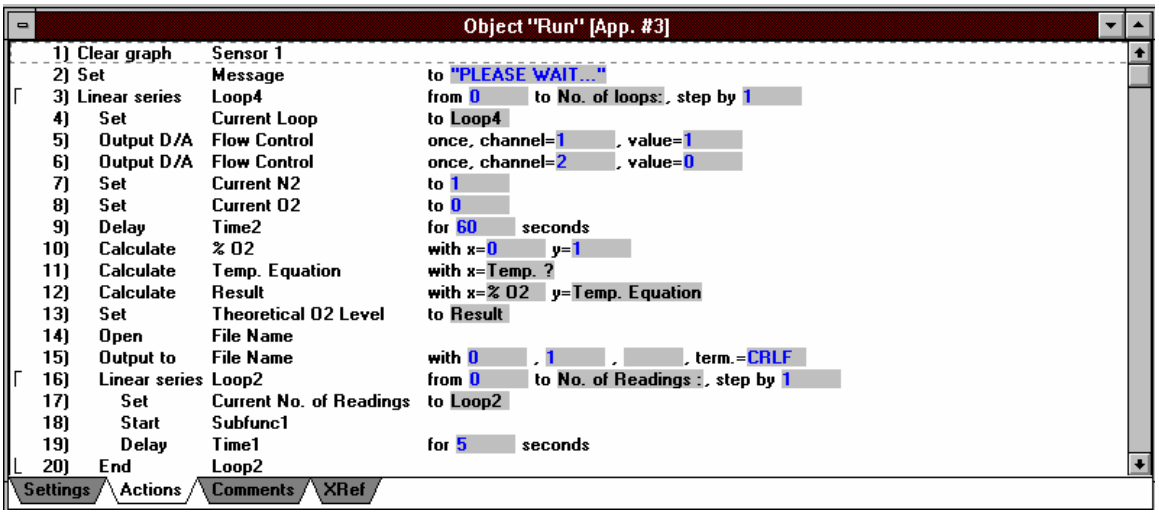

Object "Run" [App. #3]

1)	Clear graph	Sensor 1	
2)	Set	Message	to "PLEASE WAIT..."
3)	Linear series	Loop4	from 0 to No. of loops:, step by 1
4)	Set	Current Loop	to Loop4
5)	Output D/A	Flow Control	once, channel=1 , value=1
6)	Output D/A	Flow Control	once, channel=2 , value=0
7)	Set	Current N2	to 1
8)	Set	Current O2	to 0
9)	Delay	Time2	for 60 seconds
10)	Calculate	% O2	with x=0 y=1
11)	Calculate	Temp. Equation	with x=Temp. ?
12)	Calculate	Result	with x=% O2 y=Temp. Equation
13)	Set	Theoretical O2 Level	to Result
14)	Open	File Name	
15)	Output to	File Name	with 0 , 1 , , term.=CRLF
16)	Linear series	Loop2	from 0 to No. of Readings :, step by 1
17)	Set	Current No. of Readings	to Loop2
18)	Start	Subfunc1	
19)	Delay	Time1	for 5 seconds
20)	End	Loop2	

Settings | Actions | Comments | XRef

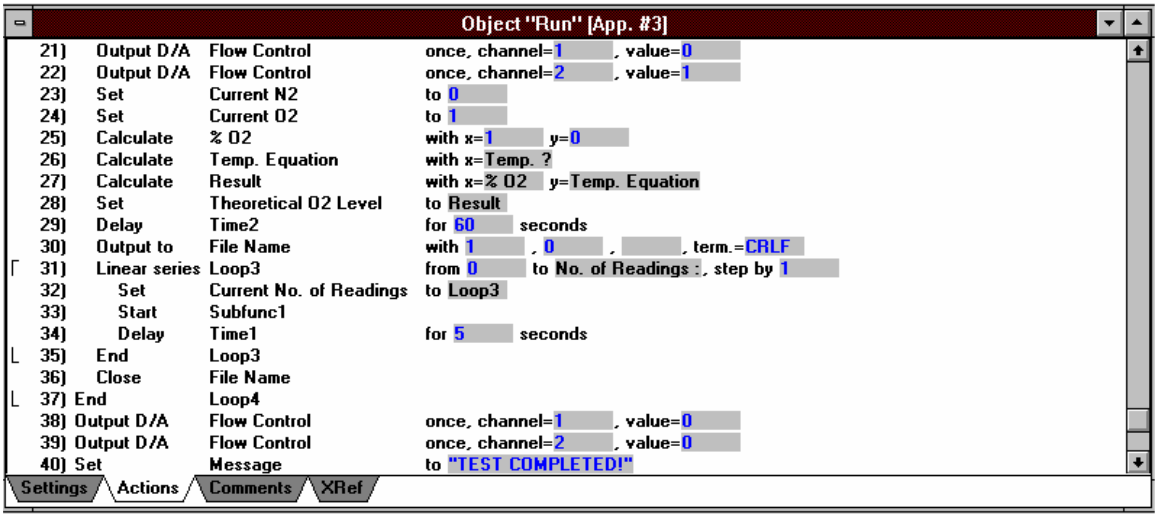

Object "Run" [App. #3]

21)	Output D/A	Flow Control	once, channel=1 , value=0
22)	Output D/A	Flow Control	once, channel=2 , value=1
23)	Set	Current N2	to 0
24)	Set	Current O2	to 1
25)	Calculate	% O2	with x=1 y=0
26)	Calculate	Temp. Equation	with x=Temp. ?
27)	Calculate	Result	with x=% O2 y=Temp. Equation
28)	Set	Theoretical O2 Level	to Result
29)	Delay	Time2	for 60 seconds
30)	Output to	File Name	with 1 , 0 , , term.=CRLF
31)	Linear series	Loop3	from 0 to No. of Readings :, step by 1
32)	Set	Current No. of Readings	to Loop3
33)	Start	Subfunc1	
34)	Delay	Time1	for 5 seconds
35)	End	Loop3	
36)	Close	File Name	
37)	End	Loop4	
38)	Output D/A	Flow Control	once, channel=1 , value=0
39)	Output D/A	Flow Control	once, channel=2 , value=0
40)	Set	Message	to "TEST COMPLETED!"

Settings | Actions | Comments | XRef

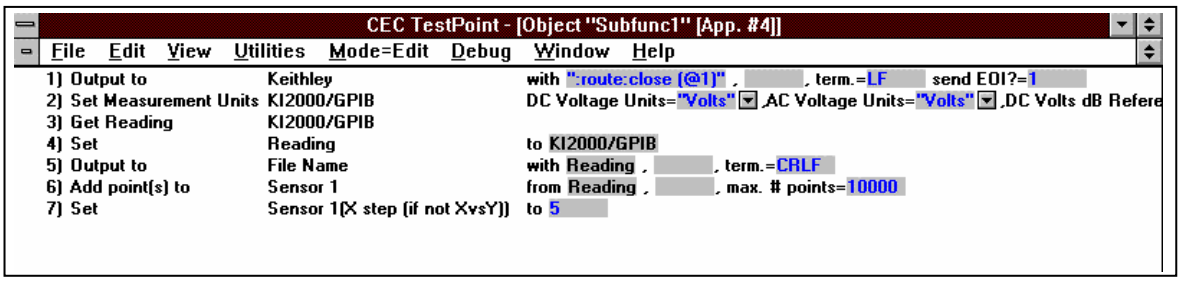

CEC TestPoint - [Object "Subfunc1" [App. #4]]

File Edit View Utilities Mode=Edit Debug Window Help

1) Output to	Keithley	with ":route:close (@1)" , , term.=LF send EOI?=1
2) Set Measurement Units	KI2000/GPIB	DC Voltage Units="Volts" ,AC Voltage Units="Volts" ,DC Volts dB Refere
3) Get Reading	KI2000/GPIB	
4) Set	Reading	to KI2000/GPIB
5) Output to	File Name	with Reading , , term.=CRLF
6) Add point(s) to	Sensor 1	from Reading , , max. # points=10000
7) Set	Sensor 1(X step (if not XvsY))	to 5